Improved methods for estimating spatial and temporal trends from point transect survey data

Richard Joseph Camp

A thesis submitted for the degree of PhD
at the
University of St Andrews

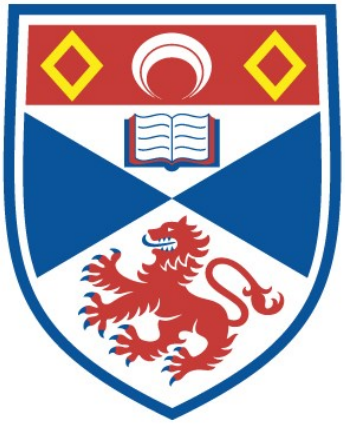

2021

Abstract

This thesis is about methods for improving estimates of abundance and trends from distance sampling surveys. My particular focus is on point transect surveys of endemic Hawaiian songbirds. When critical assumptions are met, design-based distance sampling provides unbiased abundance estimates; however, for rare endangered Hawaiian forest birds, the estimates can have high variance, hindering their use in assessing conservation efforts.

One approach to improve precision is to use spatial models instead of design-based methods. I fitted density surface models (DSMs), accounting for spatial and temporal correlation, using a two-stage approach that separated modelling of detection probability from modelling spatio-temporal patterns in density using generalized additive models (GAMs). Precision was improved and maps depicted spatio-temporal patterns in densities.

I compared the model that I fitted for a single year to two alternative approaches: spatial point-process model based on a log-Gaussian Cox process with a Matérn covariance (LGCP) and a soap-film smoother. The GAM-based DSMs and LGCP approaches produced better precision than the design-based method but varied in how they captured pattern in the data. I also implemented a GAM that used a smoother which took into account the study area boundary (a soap-film smoother) and found this produced better extrapolations into parts of the study area not surveyed.

Including biological realism is another approach to improve modelling of population change over time is to link design-based abundance estimates to an underlying population dynamics model, using a state-space modelling framework. This constrains population changes to be biologically realistic, as I demonstrate with a set of models that make different assumptions about the demographic parameters driving population changes.

Overall, I demonstrate that spatial, spatio-temporal and population dynamics modelling procedures reduced the variance in density estimates in single- and multi-year abundance data compared to design-based methods, thus better informing management and conservation decisions.

Dedication

To the Hawaiian forest bird conservation community

Candidate's declaration

I, Richard Joseph Camp, do hereby certify that this thesis, submitted for the degree of PhD, which is approximately 39,300 words in length, has been written by me, and that it is the record of work carried out by me, or principally by myself in collaboration with others as acknowledged, and that it has not been submitted in any previous application for any degree.

I was admitted as a research student at the University of St Andrews in February 2017.

I received funding from an organisation or institution and have acknowledged the funder(s) in the full text of my thesis.

Date 26th August 2020 Signature of candidate

Supervisor's declaration

I hereby certify that the candidate has fulfilled the conditions of the Resolution and Regulations appropriate for the degree of PhD in the University of St Andrews and that the candidate is qualified to submit this thesis in application for that degree.

Date 26th August 2020 Signature of supervisor

Permission for publication

In submitting this thesis to the University of St Andrews we understand that we are giving permission for it to be made available for use in accordance with the regulations of the University Library for the time being in force, subject to any copyright vested in the work not being affected thereby. We also understand, unless exempt by an award of an embargo as requested below, that the title and the abstract will be published, and that a copy of the work may be made and supplied to any bona fide library or research worker, that this thesis will be electronically accessible for personal or research use and that the library has the right to migrate this thesis into new electronic forms as required to ensure continued access to the thesis.

I, Richard Joseph Camp, confirm that my thesis does not contain any third-party material that requires copyright clearance.

The following is an agreed request by candidate and supervisor regarding the publication of this thesis:

Printed copy

Embargo on all of print copy for a period of 2 years on the following ground(s):

- Publication would preclude future publication

Supporting statement for printed embargo request

We would like to request an embargo for both the printed and electronic versions of this thesis, for an initial period of two years. This thesis makes contributions to a fast-moving, highly competitive research discipline, and premature disclosure of analyses and findings would provide other research groups with a competitive advantage, potentially affecting the candidate's ability to publish his results in scientific journals.

Electronic copy

Embargo on all of electronic copy for a period of 2 years on the following ground(s):

- Publication would preclude future publication

Supporting statement for electronic embargo request

We would like to request an embargo for both the printed and electronic versions of this thesis, for an initial period of two years. This thesis makes contributions to a fast-moving, highly competitive research discipline, and premature disclosure of analyses and findings would provide other research groups with a competitive advantage, potentially affecting the candidate's ability to publish his results in scientific journals.

Title and Abstract

- I agree to the title and abstract being published.

Date 26th August 2020 Signature of candidate

Date 26th August 2020 Signature of supervisor

Underpinning Research Data or Digital Outputs

Candidate's declaration

I, Richard Joseph Camp, hereby certify that no requirements to deposit original research data or digital outputs apply to this thesis and that, where appropriate, secondary data used have been referenced in the full text of my thesis.

Date 26th August 2020 Signature of candidate

Contributions from collaborators

The groundwork for this thesis was laid before I became a PhD student at the University of St Andrews, while working full-time at the United States Geological Survey (USGS); in addition, some parts of the thesis work have been undertaken collaboratively. The purpose of this section, therefore, is to clarify my PhD research contributions.

Before coming to St Andrews, I developed the Hawaiian forest bird monitoring database, populating it with point-transect distance sampling survey data. A subset of these data are used in the research undertaken for this thesis. This included the 'ākepa survey data collected at Hakalau Forest National Wildlife Refuge, Hawai'i Island.

Chapter 3 contains joint work with Mr. Andrew Seaton, a fellow PhD student at St Andrews. In that chapter, I identified the survey that provided sufficient spatial coverage and adequate numbers of 'ākepa detections to reliably estimate densities and supplied the data to Mr. Seaton. Mr. Seaton conducted a one-stage model-based approach to model PTDS data using point-process, spatial-analysis methods through iterated integrated nested Laplace approximations and provided me with the estimates. I conducted the companion analysis using a two-stage modelling approach and evaluated the similarities and differences in parameter estimates between the one- and two-stage analyses. These analyses are detailed in Chapter 3, corresponding parts of Mr. Seaton's thesis, and two accompanying manuscripts to be submitted to Royal Statistical Society, Series C where Mr. Seaton is the lead author and Ecological Modelling of which I am the lead author.

Acknowledgements

I thank my advisory team Len Thomas, Supervisor, Steve Buckland and David Miller, Co-supervisors, for their guidance, encouragement and support. Without their help and input my thesis would not have been possible. I asked a question about accounting for variances in densities at the 2002 distance sampling workshop. Len's response propelled me to try to better understand the sources of variance and explore how to better account for those sources.

Many people helped me prior to embarking on a PhD and for their help I am grateful. Jerry Freilich inspired me to view quantitative ecology as a tool to help land managers better manage resources. Thane Pratt imparted a deep appreciation and understanding of Hawaiian forest bird ecology, and Bethany Woodworth made much of my research possible when in 1999 she brought me out to Hawai'i for a one-year project to establish the Hawaiian Forest Bird Interagency Database. I thank Kevin Brinck and Marcos Gorresen for many long discussions on how to better estimate Hawaiian forest bird numbers and their collaboration on several papers that helped lay the foundation of my thesis objective - reduce estimator uncertainty.

Sharon Ziegler-Chong and Gordon Tribble employed me and in the process helped me formulate, refine and transcribe my ideas and thoughts from obtuse concepts into a (hopefully) coherent product. Brian Wissman was my maths advisor at University of Hawai'i at Hilo and helped me focus on coursework necessary for statistics. Erica Bernstein was my mathematical statistics instructor and who at my request (and fellow students mortification) devoted 2 weeks to Bayesian analyses. Vanessa Aguirre and I commiserated through calculus, statistics and mathematical statistics courses at University of Hawai'i at Hilo. Discussions with Claire Horwell and Rebecca Montgomery helped me clarify what it means to be a PhD student and develop potential strategies for a PhD that made returning to school a possibility.

I thank my good friends Chris Collins and Jeff Duda who over the years have inspired and motivated me. Moreover, they made sure I got out of the office on adventures and back into nature to explore.

While at University of St Andrews Gui Bortolotto was my first officemate and became a good friend who listened and provided essential support. Jeremy Greenwood was another officemate with whom discussions ranged far and wide, spanned historical to current events, and he made sure I got into the field to ring a few Scottish birds. Sophie Smout

was an early officemate who asked questions that got me thinking about the broader applications of statistics in ecology and resource management, and the philosophical underpinnings of education. Richard Glennie provided R script, and more importantly explained and described (often repeatedly) the code structure and how it works. I also thank the St Andrews statistics cohort Fanny Empacher, Wei Jing, Andy Seaton, Filippo Franchini and Nseobong Uto for support and encouragement, and the greater UK statistics cohort who made APTS training sessions educational and fun.

To Rhona Rodger, Phil La Feuvre and Pam Eddie who took care of all the administration, IT and estates tasks that often get overlooked and under appreciated. Your help and smiles made my days much easier and more enjoyable.

While in Scotland, my family and I were welcomed and supported by Claudia Faustino, Cornelia Oedekoven, Charles Paxton and Valentin Popov. Pints and pedalling got us across Scotland, over highland roads and along lochs. In addition, we met a great family while at a local playground. Thank you to Richard, Nicola, Ellie, Bea and Brodie Hearnden for outings, running, biking, camping and time spent together.

My time in St Andrews was made possible by several friends in Hawai'i. Mel Dean and Jesse Eiben housed many boxes and household items, and a very special thank you to Colleen, Ian, Finn and Milo Cole for watching Phoebe.

There are many boundaries to understanding, but human creativity can push each and every one of those boundaries. In that process, new frontiers are discovered. It is unlikely that I have actually broken any boundaries to push statistics forward. Instead, I have had the opportunity to spend a fair amount of time learning and thinking about those boundaries, exploring frontiers of using statistics to better understand population processes, and striving to better understand ecological patterns in space and time. A slow and ponderous process when looking at complex issues and their interactions. For providing me that opportunity and supporting me along the way thank you to my family: Kiko and Isabel.

Data acknowledgements

Hawai'i 'ākepa (*Loxops coccineus*) point-transect distance sampling data were provided by U.S. Fish and Wildlife Service, Hakalau Forest National Wildlife Refuge. Research data underpinning this thesis for the Hawai'i 'ākepa data from 1987–2017 are available from USGS (Camp 2019) at https://doi.org/10.5066/P98IO297 and the expanded 2002 data are available from USGS (Camp 2020) at https://doi.org/10.5066/P9Q9UXMZ.

Institutional funding acknowledgements

Funding to support my research and write my thesis was partially provided through a studentship from Centre for Research into Ecological & Environmental Modelling, University of St Andrews and partially provided by the U.S. Geological Survey.

Abbreviations and Notations

Abbreviations

Name	Description
1D	one dimension
2D	two dimension
AIC	Akaike's information criterion
asl	above sea level
CAR	conditionally autoregressive model
CI	confidence interval
CIW_{DB}	confidence interval width design-based estimate
CIW_{DM}	confidence interval width delta method
CIW_{VP}	confidence interval width variance propagation method
CrI	credible interval
DSM	density surface model
EAS	effective area searched
EDF	effective degrees of freedom
GAM	generalized additive model
GCV	generalized cross validation score
GLM	generalized linear model
HFBS	Hawaii forest bird survey
Mya	Million years ago
PDM	population dynamic model
PTDS	point-transect distance sampling
QQ	quantile-quantile
REML	restricted maximum likelihood
SE	standard error
TPRS	thin plate regression spline
UTM	Universal Transverse Mercator

Notations

Name	Description
a	hazard rate scale parameter
b	hazard rate shape parameter
β_0	intercept
β_1	slope
δ	hazard rate covariate for year
ϵ	error term
η	linear predictor
$f()$	smoothing function
g	the link function in GLMs and GAMs
k	sampling points
λ	Chapters 2 – 4: mean of Poisson distribution; smoothing penalty term or penalty parameter; Chapter 5: recruitment rate
μ	mean
n	numbers of birds counted or detected; sample size
N	true population size
$\hat{N}$	estimated population size
ν	effective area searched
p	detection probability
π	priors and hyperpriors pdf
ϕ	Chapters 2 – 4: dispersion parameter of the negative binomial distribution Chapter 5: survival rate
q	dispersion parameter of the Tweedie distribution
r	Chapters 1 – 4: radius from point centre to detected bird; Chapter 5: growth rate
R	number of recruits
S	number of adults surviving
$s()$	1D isotropic TPRS smooth function
s^2	estimate of variance σ^2
σ^2	variance
$ti()$	2D or higher interaction TPRS smooth function
w	truncation width or truncation distance
x	predictor variable
y	response variable
z	hazard rate covariate

Contents

List of Figures

List of Tables

Chapter 1

Introduction

The research in my thesis is motivated by the need to have precisely estimated bird densities. Species management, particularly the conservation of rare species, is costly, requiring funding, personnel and time that are increasingly limited. Conservation planning focuses on the proposed benefits returned from management actions, the costs of implementing actions, and the likely outcome of actions (Walls 2018). Evaluating trends of Hawaiian forest birds however is hampered by imprecise estimates yielding inconclusive results (Camp et al. 2009).

The remainder of Chapter 1 of my thesis is organized as follows: I describe Hawaiian avifauna and monitoring in Section 1.1. In Section 1.2 I describe the study area from which the data are collected and provide a description of the species used in the analyses. The sampling methods and data collected are detailed in Section 1.3. Distance sampling methods are presented in Section 1.4, including the theory and general principles, model assumptions and likelihoods. In this section I apply distance sampling methods to estimate bird densities and estimator uncertainty; these estimates serve as a baseline and are compared against analyses conducted in the subsequent chapters. In Section 1.5 I provide a road map outlining and describing the analyses in the remaining chapters of my thesis.

1.1 Background

Situated near the middle of the Pacific Ocean, the Hawaiian Islands are the most remote archipelago in the world. Being more than 4,000 km distant from North and South America, eastern Asia and islands in the South Pacific, the Hawaiian Islands are well beyond the distance non-migratory land birds are expected to traverse. Unique among the 23 or more founder land bird species to reach and establish on the Hawaiian Islands was a cardueline finch (Fringillidae; Pratt 2009). Arriving some 5–6 Mya, the colonizing species found a new environment with tropical forests and shrublands, and was released from limiting factors such as competitors, predators, and diseases and their vectors. In the absence of many limiting factors and given sufficient time, evolutionary divergence of the founder species led to the largest adaptive radiation of oceanic archipelago birds worldwide resulting in new trophic morphologies and life histories. The derived Hawaiian Honeycreepers (Drepanidinae) differentiated into 21 genera and more than 50 species gen-

erally grouped according to feeding niches with many species and subspecies being island endemics. While variation in bill morphology and feeding behaviours were advantageous, honeycreepers, like most insular bird species, also evolved a variety of traits that may be deleterious should the environment change. These traits include greater longevity, delayed maturation, decreased clutch size, reduced dispersal abilities, and loss or reduction of defences against predators and diseases (Woodworth and Pratt 2009).

The loss of defensive adaptations made the honeycreepers particularly vulnerable to humans and the changes they brought. When Polynesian peoples arrived 700-800 years ago (Wilmshurst et al. 2011) they profoundly transformed the Hawaiian environment making it more suitable for human habitation, and brought competitors and predators. Western contact further exacerbated these effects including introducing diseases and their vectors, and ungulates that destroy and degrade forest habitats. As a result, more than half of the honeycreeper species are now extinct, with 17 lost since Western contact a mere 240 years ago (Banko and Banko 2009). The remaining 23 species persist in restricted fragments of their original ranges, usually in sub-optimal habitat, and in small numbers. Most of these remnant populations are in serious trouble: 21 species have been categorized as critically endangered, endangered or vulnerable under the IUCN Red List of Threatened Species, while only two species are categorized as least concern (IUCN 2018).

Over the last half century the limiting factors and vulnerabilities of Hawaiian forest birds have been identified. Government and non-government organizations have used this information to recover and protect native forest birds and their habitat at community- and species-level scales. In many cases, because of the restricted distribution of species, the population- and species-level scales are synonymous. Hereafter I use the more general species-level scale when referring to either population- or species-level management and conservation. Restricted to high-elevation, native-dominated vegetation most forest birds are concentrated into geographically limited areas. These areas are geographic hotspots of biodiversity where five or more native forest bird ranges overlap (see Gorresen et al. 2009). Community-level conservation focuses on ecosystem management. At these locations, conservation partners are recovering habitat through understory planting, conducting ungulate and predator control through removal and fencing, and chemical and mechanical weed control. In addition, restoration and reforestation of upland pastures are being conducted on Hawai'i and Maui islands through out-planting of native tree species. Monitoring population responses to management actions are needed to evaluate management effectiveness.

Species-level programs include the ecosystem management, as well as species-specific strategic actions. Species-level programs include demographic studies to estimate vital rates of survival and fecundity. Demographic studies may be used to identify class- or group-specific threats such as depredation of nesting females, and determine management actions needed to alleviate threats. Management actions typically include fencing to exclude ungulates and ungulate removal, predator control and habitat restoration. When combined with ecological studies, such as investigating competition, food-web disruption and habitat fragmentation, species-level research provides insight into interactions among

agents of decline and population trajectories. Monitoring is required at both community- and species-level programs to track populations, evaluate management actions and assess conservation priorities.

Much of our understanding of how forest birds are responding to management and recovery actions has been gained through abundance monitoring. Between 1976 and 1983 the U.S. Fish and Wildlife Service conducted surveys to determine forest bird distribution and status, and assess the state of forest bird habitat (Scott et al. 1986). Termed the Hawai'i Forest Bird Survey (HFBS), these surveys have been used for recovery plans, to identify geographic hotspots of biodiversity and serve as a baseline to evaluate population trends, among other conservation priorities (Camp et al. 2009). The HFBS employed point-transect distance sampling (PTDS) methods, a form of distance sampling (Buckland et al. 2015), to survey birds at points along transects that traversed native-dominated forests. Over the subsequent four decades PTDS has became the standard for surveying Hawaiian forest birds, and more than 700 forest bird surveys have been conducted, transcribed and included in the Hawai'i Forest Bird Monitoring Database (Camp and Genz 2017). Both species-specific and multi-species PTDS surveys are included in the database on all main Hawaiian Islands and have been used to estimate bird status and evaluate trends (e.g., Gorresen et al. 2009; Camp et al. 2016; Paxton et al. 2016). A detailed description of PTDS methods is provided below.

Recovery programs require tracking populations as they respond to conservation and management actions. Density, or population size, is a fundamental metric of recovery programs. Surveys conducted over time are useful for evaluating trends. I define trend as the long-term, overall directional change in densities over time. With this definition assessing trends requires evaluating the pattern of a density time series. There are many methods for analysing time series (Thomas 1996), but generally they rely on either linear or non-linear regression methods. For either method, however, variances of bird density estimates are generally quite large (Gibbs 2000). I assume that the bird density estimator is unbiased; therefore, I consider the primary objective of the HFBS is to produce unbiased density estimates that are precise. A lack of estimator precision is problematic because change can occur without detection and management actions cannot be evaluated. Imprecise estimates further hamper species conservation and recovery planning.

1.2 Study areas & study species

1.2.1 Study areas

Established in 1985 on the island of Hawai'i, Hakalau Forest National Wildlife Refuge (hereafter Hakalau; 19° 51'N, 155° 18'W) is actively managed to preserve native forest birds, rainforest plants and their habitats. The 15,390-ha montane forest is dominated by native 'ōhi'a (*Metrosideros polymorpha*) and koa (*Acacia koa*) with a mixture of native and non-native understory plants. Temperature averages 15° C with annual variation <5° C, and annual precipitation averages 2,500 mm with a maximum of 6,100 mm (Juvik and Juvik 1998).

Following the creation of Hakalau, in 1987 refuge staff initiated an annual abundance monitoring program by establishing 350 point samplers (hereafter, points) on 14 transect lines following a systematic random design spanning the upper elevations of Hakalau. The distance among points is approximately 150-m with transects being either 500 or 1,000 m apart (Fig. 1.1). Research in Chapters 2 and 5 focus on the 3,061 ha open-forest stratum at an elevation between 1,400 and 1,920 m (Fig. 1.1). Previously heavily grazed, regeneration in the open-forest stratum is proceeding naturally since the removal of cattle in 1988 (Maxfield 1998). My research in Chapters 3 and 4 includes the reforested pasture and closed-forest strata. The pasture stratum extends from the western edge of the open-forest stratum out to the Hakalau boundary, elevation between 1,650 and 2,000 m and an area of 1,271 ha (Fig. 1.1). The pasture was intensely grazed through the mid-1980s and is being gradually reforested through outplanting koa. The closed-forest stratum extends down slope from the eastern edge of the open-canopy stratum between 1,400 and 1,700 m. The closed-forest stratum was least modified by grazing and surveys commenced in 1999 covering an area of 1,541 ha. I modified the strata polygons from Camp et al. (2010) to exclude the southern, unsampled portion of their study area. Scott et al. (1986) provides a more detailed description of the region and Camp et al. (2010) describes Hakalau and the study area in more detail.

Chapter 5 of my thesis explores the use of population dynamics modelling as a way to estimate population trends of Hawai'i 'ākepa (*Loxops coccineus*; nomenclature according to Chesser et al. 2018 and Gill and Donsker 2019; hereafter 'ākepa). This requires information about 'ākepa demography. In the 1970s and 1980s, 'ākepa demography was studied in four areas on the eastern, windward, side of Hawai'i Island: Kau Forest Reserve (19° 13'N, 155° 39'W, 1,750 m), Kilauea Forest (19° 31'N, 155° 19'W, 1,600 m), Keauhou Ranch (19° 30'N, 155° 20'W, 1,800 m) and Hamakua (19° 47'N, 155° 20'W, 1,770 m) (Ralph and Fancy 1994) (Fig. 1.1). The Kau Forest Reserve and Kilauea Forest study sites occurred in ungrazed, closed canopy 'ōhi'a forests, with koa also in Kilauea. Cattle grazing and logging occurred at the Keauhou Ranch study site resulting in a discontinuous, open 'ōhi'a and naio (*Myoporum sandwicense*) forest. In the 1990s and 2000s, demographic data were collected at three study sites within Hakalau. From south to north they are Pua 'Ākala, Nāuhi, and Maulua and range in elevation between 1,500 m and 1,640 m (Fig. 1.1). See Woodworth et al. (2001) for detailed description of the demographic research study sites. The Pua 'Ākala site at which Hart (2001) sampled is slightly up-slope at 1,850 m from the Woodworth et al. (2001) site of the same name, and coincides with the Hamakua study area sampled by Ralph and Fancy (1994). The Pedro site sampled by Hart (2001) is further north and down-slope from Nāuhi. These appear to be the same sites sampled by Lepson and Freed (1995), Freed et al. (2008) and references therein, although detailed location information is lacking. Data from the Maulua site are not used in my thesis because 'ākepa were not captured at this site.

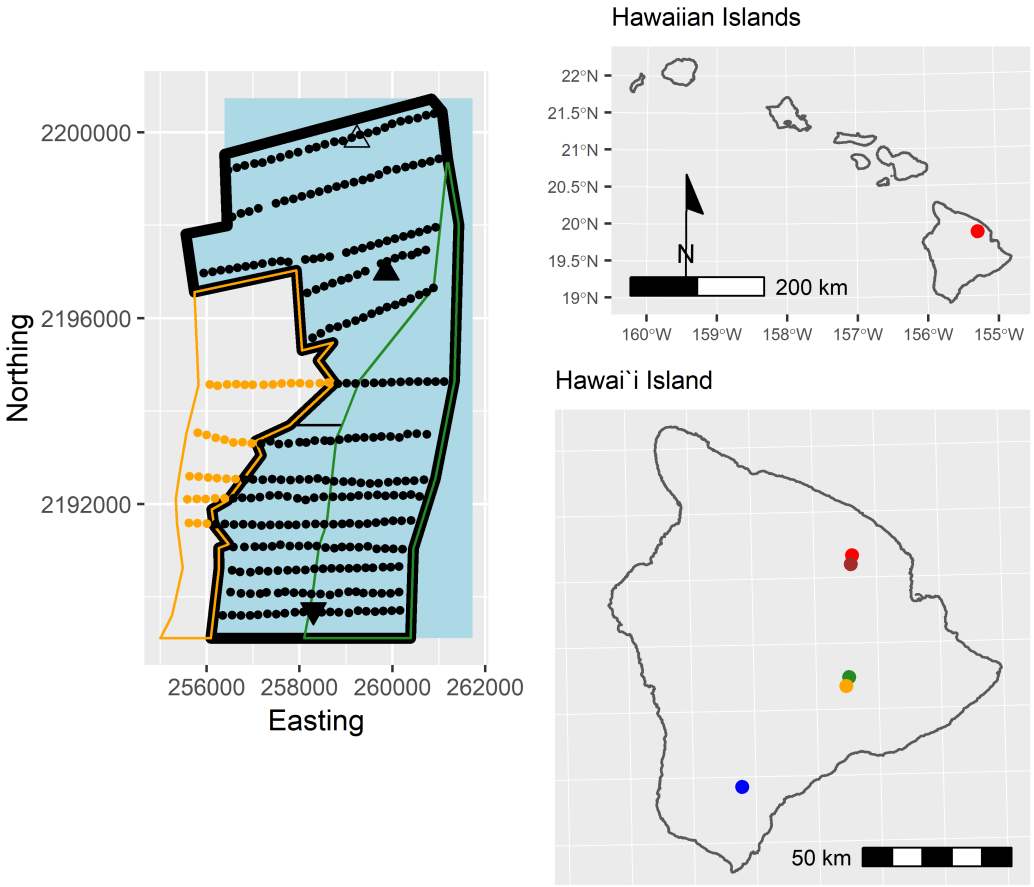

Figure 1.1: Left panel: study areas showing survey points (black dots) in the open- and closed-forest stratum (heavy black polygon), and reforested pasture stratum (orange dots in orange polygon). Forest strata demarcated as open-forest (light black polygon) and closed-forest (green polygon) stratum. The open-forest stratum is separated into north and south strata (black polygons). Blue polygon represents the expanded forest study area. Demographic research areas are Pua 'Ākala (filled downward triangle), Nāuhi (filled upward triangle), and Maulua (open upward triangle). Right panels: the location (red dot) of Hakalau Forest National Wildlife Refuge (Hakalau) is shown on the Hawaiian Islands (top panel), and on Hawai'i Island (bottom panel). Demographic study areas on the Hawai'i Island are Kau Forest Reserve (blue dot), Kilauea Forest (green dot), Keauhou Ranch (orange dot) and Hamakua (brown dot). Base map from World Geodetic System 1984 (WGS84) zone 5; coastline from U.S. Geological Survey's National Elevation Dataset (USGS, U.S. Geological Survey 2014).

Figure 1.2: Photo of Hawai'i 'ākepa. Photo credit: Jack Jeffrey.

1.2.2 Study species

The focal species for my thesis is the 'ākepa. The 'ākepa (Fig. 1.2) is an internationally and federally endangered Hawaiian honeycreeper (Drepanidinae; USFWS, U.S. Fish and Wildlife Service 1970, BirdLife International 2016) endemic to Hawai'i Island, USA. The 'ākepa is a diet specialist honeycreeper that forages for spiders, insects and psyllids by probing terminal leaf clusters, but it also consumes nectar. The species declined dramatically during the 20th century due to mosquito-transmitted avian diseases (Pratt 1994, Atkinson et al. 1995), habitat modification (Scott et al. 1986, Pratt 1994), introduced predators (Lepson and Freed 1997), and food resource competitors (Lepson and Freed 1997). 'Ākepa are now restricted to five spatially distinct populations, with a global abundance of 16,248 (95%CI 10,074–25,198) birds (Judge et al. 2018). The largest population, estimated in 2012 at more than 11,000 birds (Camp et al. 2016), occurs in Hakalau (Judge et al. 2018).

Refuge-wide distance sampling monitoring reveals that 'ākepa are stable to increasing (Camp et al. 2016, Rozek et al. 2017), and that the population is expanding into the adjacent reforested pasture (Paxton et al. 2018). 'Ākepa densities, however, vary geographically (Reding et al. 2010) and localized populations may be declining despite widespread increases (Freed and Cann 2010). Modelling the spatio-temporal distribution in the 'ākepa population can help reveal patterns in its distribution and abundance, as well as estimate densities for any defined sub-area within the study area and increased

precision by modelling spatio-temporal covariance.

1.3 Sampling methods & data collected

In order to avoid redundancy by repeating a description of the sampling methods in each chapter, I present here a detailed description of the methods employed in Hawaiian abundance monitoring and demography sampling. I start by describing the methods used to monitor forest bird abundance. The density estimates are then used in the analyses in Chapters 2–5 where they are compared with spatio-temporal, point process, soap-film smoother and population dynamics modelling. The spatio-temporal and point process modelling relies entirely on the distance sampling survey data; however, additional information is required for the population dynamics analyses. Below I describe the sampling methods used to collect 'ākepa biological traits and demographic vital rates. This information is mostly gathered from study sites in Hakalau, but also includes data collected in the Kau Forest Reserve, Hawai'i Island, in which the second largest 'ākepa population inhabits.

1.3.1 Abundance monitoring

Abundance monitoring via the HFBS is the focus of Chapters 2–5. Since 1987, 'ākepa, along with other forest bird species, are monitored at Hakalau. Annual surveys have been conducted, usually in April, through 2017 (except in 2009) employing PTDS methods to produce abundance estimates (see Camp et al. (2010, 2016) for details). Following a standard protocol, trained and calibrated observers recorded the horizontal distance from the centre-point to birds detected during an 8-min count. Birds are detected as individuals and their locations estimated and recorded as exact distances rounded to the nearest meter. The sampling conditions cloud cover, rain, wind strength, gust strength, and time of day each point is surveyed are also recorded. Sampling commenced at dawn and continued until 11:00 (Best 1981), and occurred only during favourable conditions (halting when conditions exceeded light rain and wind level 3 on the Beaufort scale). The Hawai'i 'ākepa data from 1987–2017 are available from USGS: https://doi.org/10.5066/P98IO297 (Camp 2019)[1] and the expanded 2002 data are available from USGS: https://doi.org/10.5066/P9Q9UXMZ (Camp 2020)[2].

1.3.2 Demography sampling

'Ākepa demography data is combined with population monitoring data in Chapter 5. I conducted a literature search for estimates of 'ākepa vital rates instead of analysing raw banding and resight data. Newman et al. (2014) states that it can be better to use estimates from summarized data as estimates are easier to model and give similar results to modelling the raw data. Density and vital rate parameters are often estimated from sophisticated software that is specialized for the analysis of relevant data (e.g., distance

[1] Data release as part of my thesis research.
[2] Data release as part of my thesis research.

sampling and mark-recapture data). Detailed descriptions of the mist netting, banding, resighting and nest searching methods are provided in Ralph and Fancy (1994), Lepson and Freed (1995), Hart (2001), and Woodworth et al. (2001). A fair amount of demographic information is available on 'ākepa, which is summarized in Lepson and Freed (1997) and Woodworth and Pratt (2009). Since 2008, there have been few studies providing additional information of 'ākepa traits and vital rates. Recent papers provide additional insights on juvenile survival by time period (1987-2000 vs 2001-2006; Freed and Cann 2009); juvenile survival based on fledging mass (Medeiros and Freed 2009); nest success and productivity (Cummins et al. 2014); and adult survival, recruitment and population growth rate (Guillaumet et al. 2016). There is also an on-going demographic research study at Hakalau being coordinated by Eben Paxton, U.S. Geological Survey, but vital rate information is not yet published. In Chapter 5 I summarize the demographic information following the format by Woodworth and Pratt (2009), paying particular attention to the traits relevant to 'ākepa population dynamics modelling. This information is gathered from the study areas described above.

1.4 Analyses and statistics

Many bird survey programs track counts as an index, where all birds are assumed detected out to a distance w (Hutto 2016). In most, if not all, cases simple counts of birds are unreliable measures of actual bird numbers as the index does not track the true abundance, nor do index-based counts provide measures of uncertainty (Anderson 2001, Diefenbach et al. 2003, Norvell et al. 2003, Marques et al. 2017, Williamson et al. 2018). Therefore, I employ only methods that provide the necessary information to compute a detection probability such as distance sampling (Buckland et al. 2015). Moreover, while all bird species are recorded during Hawaiian PTDS surveys, the distance sampling analyses conducted here are restricted to 'ākepa.

1.4.1 Point-transect distance sampling

An intuitive description of PTDS entails observers traversing through a study area and stopping at predetermined locations, points, to conduct bird counts for a prescribed length of time. These points along transects constitute PTDS. An important piece of information the counter (also called an observer) collects is that for each detection they estimate the horizontal distance from the bird to the centre of the point. A detection probability is estimated by fitting a detection function to the distance measurements, which is then used to compute absolute density of birds (see Section 1.4.2 below for details). Distance sampling is based on well developed theory with several books (Buckland et al. 2001, 2004, 2015) to help with the design, analysis and interpretation. To facilitate design and analysis free software has been developed and is available as stand-alone software Distance for Windows (Thomas et al. 2010; distancesampling.org) or as the R (R Core Team 2017) package `Distance` (Miller 2017, Miller et al. 2019) and other packages. There are several advantages to conducting PTDS relative to line transect distance sampling. PTDS is useful

in rough terrain where it is difficult to traverse while concentrating on detecting birds and maintaining the location of a transect centreline. In the tall stature, tropical forests of Hawai'i PTDS method allows observers to stop, stage and more thoroughly observe birds that are close to the point and high overhead in tree canopy. As with all sampling techniques, there are disadvantages in that there can be substantial non-sampling time when traversing between points (Buckland 2006), and the estimator can be strongly biased if birds move in response to observers, or display independent, non-responsive movement (Marques 2007, Buckland et al. 2015, Glennie et al. 2020) or if there are errors in the distance measures (Marques 2007, Buckland et al. 2015).

Based on theory and simulations, PTDS provides unbiased estimates of population size when critical assumptions are met (Buckland et al. 2001, 2015). A critical assumption about bird distribution is that it is random with respect to point locations, which is ensured by randomly locating points. Critical assumptions about the survey method are that (1) all birds are detected with certainty at the station centre point (this is commonly referred to as the $g(0) = 1$ assumption) and the probability of detecting a bird decreases with distance from the centre point, (2) birds are detected prior to any responsive and non-responsive movement, and (3) distances are measured without error. It is likely that there are moderate violations to these assumptions. Observers participate in calibration and training prior to each survey. This not only standardizes differences among observers, but it helps ensure that distances are estimated accurately. To these ends, observers continue calibration until deviations from the true distance are less than 10%, and all birds near the centre point are measured to the meter without error (Camp 2007). Furthermore, observers are advised that if they cannot accurately estimate the distance to a bird they should not record the detection, as long as all birds in proximity to the sample point are detected, accurately measured and recorded. During mock counts an emphasis is placed on detecting all birds near the sample point, thus ensuring that the $g(0) = 1$ assumption is met. Detections from observers are compared which helps identify birds that may have been missed. Meeting the $g(0) = 1$ assumption is facilitated by most Hawaiian birds being very vocal so that birds high above in the canopy are readily detected. Finally, anecdotal observations indicate that 'ākepa are not known to respond to observers, minimizing the influence of responsive movement prior to birds being detected. Equally important, particularly for PTDS, is a lack of non-responsive movement, independent of the counter (Marques 2007, Glennie et al. 2020). Ideally counts should be instantaneous to minimize animal movement (Buckland 2006). The 8-min counts are relatively long thus bird movement may be an issue. Inspection of the probability density plots from previous analyses does not show any evidence of evasive movement, but this may be difficult to detect (Glennie et al. 2020).

Fitting the detection function assumes that observations are independent; however, the methods are robust to failures of this assumption but variance may be underestimated (Buckland et al. 2015). There are two additional requirements for reliable estimation. For PTDS analyses the derivative of the probability density function (pdf) of the detection function is evaluated at the distance $r = 0$, thus it is important that there is a shoulder

on the detection function (Buckland et al. 2015). I assume the detection function has a fairly broad shoulder for the 'ākepa data, as evidenced from previous analyses (Camp et al. 2010, 2016). There also needs to be sufficient numbers of detections to reliably model the detection function. Buckland et al. (2015) recommends 75–100 detections for PTDS. Annual 'ākepa detections ranged from 41 to 188 with 23 of the 30 surveys having >75 detections (see Section 1.4.5). The assumptions and additional requirements are typically met in the 'ākepa data.

1.4.2 Conventional distance sampling

Distance sampling combines model- and design-based methods (Buckland et al. 2016). In the first stage model-based methods are used to estimate a detection probability. In the second stage the estimated detection probability is combined with counts using a design-based method to estimate densities (Buckland et al. 2015, 2016). Density $\hat{D}$ is the number of birds n detected within distance w of all points in the study area A divided by the total area surveyed $a = K\pi w^2$ where K is the number of points (i.e., point-transect survey points; these are commonly referred to as samplers in the statistical literature or stations in the sampling literature). Thus density is

$$\hat{D} = \frac{n}{K\pi w^2} \tag{1.1}$$

assuming all birds within distance w are detected. The ability to detect birds decreases with increasing distance; thus, detection probability may be <1 within the surveyed area a. Conventional distance sampling (CDS) methods are commonly used to estimate absolute abundance by accounting for birds that are present but missed, i.e., incomplete detection (Buckland et al. 2001, 2015). The expected proportion of birds counted p_a is $0 \leq p_a \leq 1$. p_a can be estimated from recorded distances to produce $\hat{p}_a$ and the estimate of density correcting for incomplete detection is

$$\hat{D} = \frac{n}{K\pi w^2 \hat{p}_a}. \tag{1.2}$$

Estimating $\hat{p}_a$ can be accomplished by fitting a *pdf*, $f(r)$, to the observed distances to detections where $f(r)$ is dependent only on distance r from the point ($0 \leq r \leq w$). The form of the *pdf* can then be modelled with a specified detection function, $g(r)$, which represents the probability of detecting a bird given that it is at distance r. The distribution of all birds with distance from the point, whether detected or not, is denoted $\pi(r)$. For PTDS, given random placement of sample points, $\pi(r)$ has a triangular shape, meaning that the number of birds increases linearly with increasing distance, taking the form $\pi(r) = \frac{2r}{w^2}$ for $0 \leq r \leq w$. This accounts for the increasing area of a thin annulus (circular strip or donut) of fixed width as distance increases. The first derivative of $f(r)$ with respect to r evaluated at $r = 0$ is a diagonal, tangent line with slope $h(0)$ (Fig. 1.3, top left panel).

The function $f(r)$ increases following the slope of $h(0)$ and continues to increase after first separating from the line of perfect detection before reaching a maximum and decreasing toward distance w (Fig. 1.3, top right panel). Thus $f(r)$ is proportional to $\pi(r)g(r)$

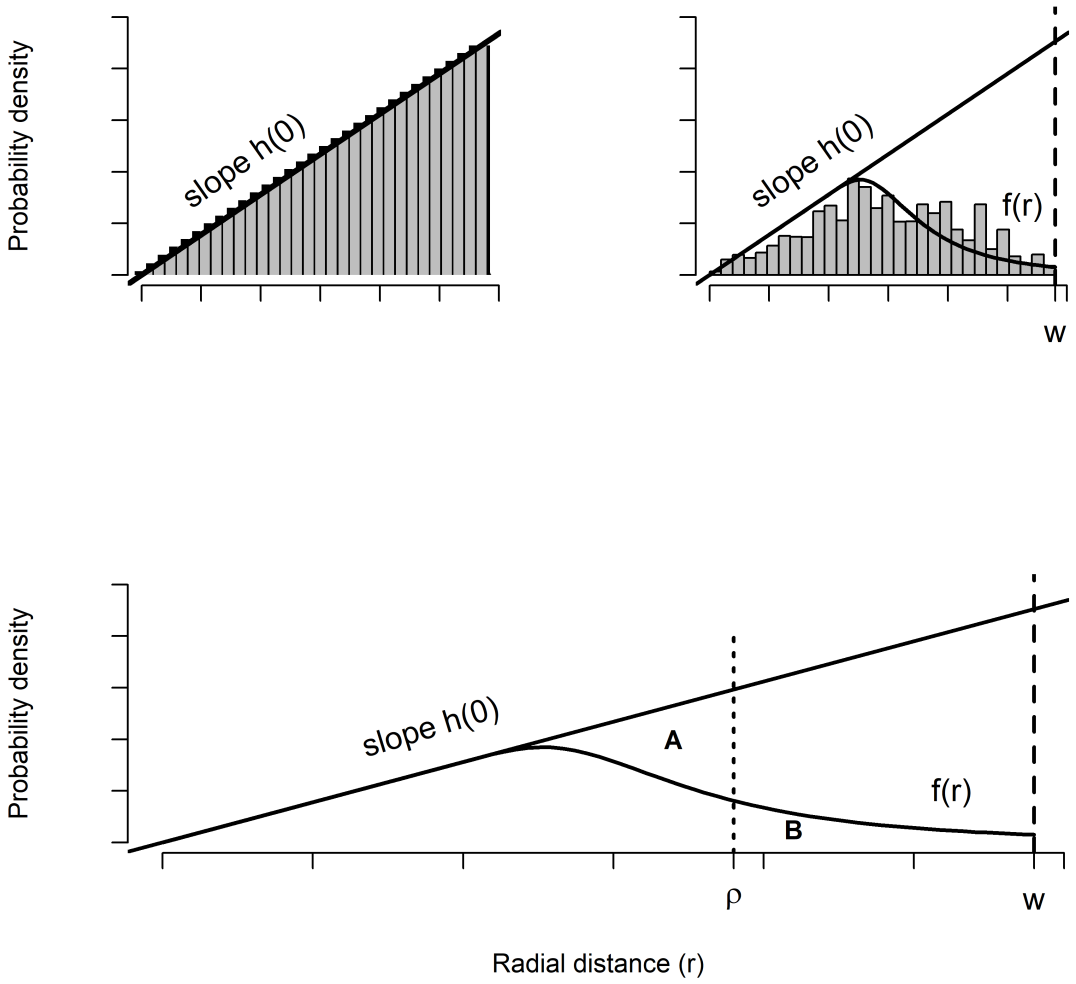

Figure 1.3: The relationship between bird detection with increasing radial distance from the centre point r and the probability density function of observed distances $f(r)$. If all birds are detected then the relationship has a triangular shape with a slope $h(0)$ computed as the first derivative of $f(r)$ evaluated at $r = 0$ (top left panel). Bird detection decreases with distance and the detection function $f(r)$ increases along $h(0)$ before decreasing to distance w (top right panel). The top right panel shows the detection function fitted to the 'ākepa histogram data. ρ is the radius where the numbers of birds missed **A** is equal to the numbers of birds detected **B** (bottom panel). The detection probability can then be calculated as $\hat{p} = \frac{\hat{\rho}^2}{w^2}$.

as

$$f(r) = \frac{\pi(r)g(r)}{\int_0^w \pi(r)g(r)dr} = \frac{rg(r)}{\int_0^w rg(r)dr}. \tag{1.3}$$

It can be seen in the top right panel of Fig. 1.3 that birds in the area between the slope $h(0)$ and $f(r)$ are missed. The radius ρ in Fig. 1.3, bottom panel, is the distance at which the number of birds missed between $0 \leq r \leq \rho$ (area labelled **A**) is equal to the number of birds detected between $\rho < r \leq w$ (area labelled **B**). In the distance sampling literature ρ is termed the "effective radius." It is convenient to define the effective area surveyed per point as $\nu = 2\pi \int_0^w rg(r)dr = \pi w^2 p_a$ such that $f(r)$ can be written as

$$f(r) = \frac{2\pi r g(r)}{\nu}. \tag{1.4}$$

The area of a circle with radius ρ is $\pi\rho^2$, from which the detection probability can be calculated as $\hat{p} = \frac{\hat{\rho}^2}{w^2}$. Understanding how ρ relates to the *pdf* of detected distances is useful. That is, the detection probability is

$$\hat{p} = \int_0^w \hat{g}(r)\frac{2r}{w^2}dr = \frac{\hat{\nu}}{\pi w^2} = \frac{\hat{\rho}^2}{w^2} \tag{1.5}$$

where the quantity ρ relates to ν such that $\nu = \pi\rho^2$ where ν is the "effective area surveyed per point," and the total effective area surveyed is then νK. With this information the likelihood can be formulated. Distances from the points of the n detected birds can be denoted by $r_1, r_2, \ldots, r_n$, where the likelihood (conditional on n) using the model for $f(r)$ from Eqn. 1.4 is

$$\mathscr{L}_r = \prod_{i=1}^{n} f(r_i) = \left[\frac{2\pi}{\nu}\right]^n \prod_{i=1}^{n} r_i g(r_i). \tag{1.6}$$

Buckland et al. (2001) recommends the key function $g(r_i)$ for PTDS is either the half-normal model

$$g(r_i) = \exp\left[\frac{-r_i^2}{2\sigma^2}\right], \tag{1.7}$$

or the hazard-rate model

$$g(r_i) = 1 - \exp\left[\left(\frac{-r_i}{\sigma}\right)^{-b}\right] \tag{1.8}$$

where σ is the scale parameter and b is a shape parameter, and for $r(0 \leq r \leq w)$. The fit of key functions can be improved by including adjustment terms where the half-normal can be paired with cosine and Hermite polynomial adjustment series, and hazard-rate can be paired with cosine and simple polynomial series (Buckland et al. 2001, pgs. 361 & 365). To limit over-fitting, the number of adjustment terms are added using a forward selection algorithm that is stopped when no additional terms produce a decrease in Akaike's information criterion (AIC).

1.4.3 PTDS variance

There is a well-established adage "An estimator is only useful if it possesses a measure of uncertainty." Expanding upon this adage, an estimator is only useful if its uncertainty is sufficiently small as to evaluate its biological relevance, as well as its relevance to assessing management and conservation effectiveness. In PTDS the delta method is used to estimate variance (Buckland et al. 2001). The basic formula for estimating density variance is

$$\widehat{\text{var}}(\hat{D}) = \hat{D}^2 \left[\frac{\widehat{\text{var}}(n)}{n^2} + \frac{\widehat{\text{var}}\left[\hat{h}(0)\right]}{\left[\hat{h}(0)\right]^2} \right] \tag{1.9}$$

Eqn. 1.9 might also include terms for uncertain detection at the centre point and group size variance, if these are present.

The first variance component in Eqn. 1.9, $\widehat{\text{var}}(n)$, is computed from variability in n between points. For PTDS the empirical estimate of $\text{var}(n)$ is computed as the observed variation among points. It is convenient to quantify the encounter rate variance, $\text{var}\left(\frac{n}{K}\right)$, instead of the variation in n (Buckland et al. 2015, pg 106). The encounter rate variance typically dominates the component percentages of $\widehat{\text{var}}(\hat{D})$ when estimating Hawaiian forest bird densities from PTDS data (Camp et al. 2009). Thus, I focus on reducing the substantial encounter rate variance through density surface modelling (Chapter 2), point process modelling (Chapter 3) and soap-film smoother modelling (Chapter 4).

The variance of $\hat{h}(0)$ in Eqn. 1.9 is a measure of the uncertainty in the estimate of the detection probability. Distance sampling employs maximum likelihood methods thus the variance of $\hat{h}(0)$ is estimated from the Hessian of the likelihood with respect to the parameters (Buckland et al. 2015). From this, the standard error of $\hat{\nu}$ and the standard error of the detection probability $\hat{p}_a$ are estimated using $\text{cv}[\hat{f}(0)] = \text{cv}(\hat{\nu}) = \text{cv}(\hat{p}_a)$.

1.4.4 Multiple-covariate distance sampling

Distance sampling methods are commonly used to estimate absolute abundance by accounting for birds that were present but missed, i.e., incomplete detection (Buckland et al. 2001, 2015). Previous analyses of Hawaiian forest birds (Camp et al. 2009) showed that the probability of detection was affected not only by distance but also by covariates such as observer, sampling conditions, habitat, etc. The likelihood from CDS can be extended to multiple-covariate distance sampling (MCDS) where detectability is conditional on n and covariates (Marques and Buckland 2004, Buckland et al. 2015). The key detection functions half-normal and hazard-rate each have a scale parameter σ. In MCDS, the scale parameter is modelled as a function of the vector of covariates such that $\sigma(\mathbf{z}_i) = \exp\left(\alpha + \sum_{q=1}^{Q} \beta_q z_{iq}\right)$ for $\mathbf{z}_i = (z_{i1}, z_{i2}, \ldots, z_{iQ})'$. For each detection there is an associated vector of covariate values, and the coefficients α and β_q are estimated. (This assumes numerical covariates; factor covariates are coded in the usual way through a series of dummy variables assigned a value of 1 or 0 with one level of the factor being assigned

to the intercept.) The key function $g\left(r_i, \mathbf{z}_i\right)$ is either the half-normal model

$$g\left(r_i, \mathbf{z}_i\right) = \exp\left[\frac{-r_i^2}{2\sigma^2\left(\mathbf{z}_i\right)}\right], \tag{1.10}$$

or the hazard-rate model

$$g\left(r_i, \mathbf{z}_i\right) = 1 - \exp\left[\left(\frac{-r_i}{\sigma\left(\mathbf{z}_i\right)}\right)^{-b}\right], \tag{1.11}$$

and assuming that the distribution of covariates is independent of the distribution of distances, then the effective area is

$$\nu(\mathbf{z}_i) = 2\pi \int_0^w g(r, \mathbf{z}_i) dr. \tag{1.12}$$

From the fitted model for $f(r_i|\mathbf{z}_i)$ the estimates $\hat{\nu}(\mathbf{z}_i)$ and $\hat{h}(0|\mathbf{z}_i)$ conditional on $\mathbf{z}_i$ are obtained from the maximum likelihood estimates of the detection function parameters, and $p_a(\mathbf{z}_i)$ is estimated as

$$\hat{p}_a(\mathbf{z}_i) = \frac{\hat{\nu}(\mathbf{z}_i)}{\pi w^2} = \frac{2}{w^2 \hat{h}(0|\mathbf{z}_i)}. \tag{1.13}$$

To avoid the need to specify a distribution on the covariates, a conditional likelihood approach is used (Marques and Buckland 2004):

$$\mathscr{L}_{r|z} = \prod_{i=1}^{n} f_{r|z}(r_i|\mathbf{z}_i) = \prod_{i=1}^{n} \frac{g(r_i, \mathbf{z}_i)}{\nu(\mathbf{z}_i)}. \tag{1.14}$$

Thus, it is assumed that the distribution of distance r for detected and not detected birds is independent of the covariates $\mathbf{z}$, which is achieved by random placement of the points. The Horvitz-Thompson-like abundance estimator is then

$$\hat{N} = \frac{A}{a} \sum_{i=1}^{n} \frac{1}{\hat{p}_a(\mathbf{z}_i)}, \tag{1.15}$$

for birds detected in groups of size 1 and measures of exact distances to individuals, where a is the total area of the K points of radius w, and A is the size of the study area.

Incorporating covariates into conventional distance sampling affects the detection probability variance, $\text{var}\left[\hat{h}(0)\right]$, but not the variance in the counts, $\text{var}(n)$ (Marques and Buckland 2004). Accounting for heterogeneity in the detection probability is beneficial to producing precise density estimates, particularly when stratum-specific densities are needed and sufficient numbers of birds are not detected to reliably model the detection function separately for each stratum, or as I have done here when stratification is required to address differences in sampling effort, see below. However, for Hawaiian forest birds a majority of the component percentages of $\hat{\text{var}}(\hat{D})$ is due to variance in the counts, which is the focus of subsequent chapters of my thesis.

1.4.5 'Ākepa PTDS analysis and results

I present here detailed methods and results of estimating 'ākepa densities using distance sampling methods. These estimates are used in the subsequent chapters and set a baseline against which subsequent precision estimates are compared. Fewster et al. (2009) noted that stratification procedures should be employed to allow for differences in the encounter rate over the study area. This procedure helps reduce the encounter rate variance. In Hawai'i, bird density generally increases with increasing elevation thus transects are oriented perpendicular to elevation contours. There is however a stronger north-south density gradient than elevational gradient at Hakalau with low densities in the northern portion of the study area and substantially larger densities in the southern portion. This issue is further confounded with the intensity of sampling that coincides with the north-south gradient. In the northern portion of the refuge the transects are about 1 km apart while in the southern portion the transects are roughly 500 m apart. Because of the unequal sampling coverage, standard analyses ignoring the higher sampling intensity where densities are higher, would result in overestimated density estimates. Stratification procedures may also be used to reduce variance. Fewster et al. (2009) showed that the default variance estimate approach implemented in Distance for Windows over-estimates variance for populations with a strong density gradient that are sampled using a systematic survey design. However, a systematic survey design provides better spatial coverage and increases estimator certainty (Buckland et al. 2001, Fewster et al. 2009).

To control for varying sampling intensities I partitioned the open-forest stratum study area into two strata that coincide with the distance between transects (i.e., a stratum with roughly 500m separation of lines, and one with 1,000m separation; Fig. 1.1). I delineated the open-forest stratum into internal regions coinciding with the north (2,143 ha) and south (918 ha) strata.

I estimated the 'ākepa detection probability from the PTDS data using Distance for Windows, version 7.1, release 1 (Thomas et al. 2010). Candidate models were restricted to the half-normal and hazard-rate detection functions with up to two adjustment terms (Buckland et al. 2001). Using the `MCDS` engine covariates related to the sampling conditions (e.g., cloud cover), observer and survey year were evaluated. Here I consider only plot-level covariates, eliminating the individual-level covariate detection type from the candidate pool of covariates (Buckland et al. 2016). Individual-level covariates were not collected as it is not possible to distinguish between bird age, sex, maturity (breeders, nonbreeders and failed breeders) or other life history states during Hawaiian PTDS surveys. I used a forward selection algorithm to add covariates, at each step adding the covariate that produced the greatest reduction in AIC and stopped when no additional covariate produced a decrease in AIC. I considered only single-covariate models as there were too few detections to reliably model combinations of covariates (75-100 detections per factor combination; Buckland et al. (2015), pg 23). Covariates were screened for pairwise correlation and qualitatively evaluated for confounding (i.e., factor covariates where only limited combinations were observed together); covariates with strong correlations or confounding were not fitted together. Data were truncated at a distance w where the

estimated detection probability (using a preliminary detection function model) was about 0.1 to facilitate detection function modelling and to avoid over-fitting to distant detections. Visual inspection of diagnostic plots was conducted and model fit evaluated with a Cramér-von Mises test (Buckland et al. 2015).

Using post-stratification procedures Distance for Windows outputs annual regional densities and standard errors. Annual mean densities within the study area and variance estimates are computed from area-weighted estimates (Thomas et al. 2010). For each year, the mean annual density (averaging over the two regions) is computed as $\hat{D} = \left(\hat{D}_{\text{No}}A_{\text{No}} + \hat{D}_{\text{So}}A_{\text{So}}\right)/A_{\text{To}}$ where the density estimate in the northern region is $\hat{D}_{\text{No}}$ and in the southern region is $\hat{D}_{\text{So}}$ while the total study-wide area is the sum of the northern and southern regional areas $A_{\text{To}} = A_{\text{No}} + A_{\text{So}}$.

From Distance for Windows the annual $\hat{p}$ and $\text{var}(\hat{p})$, and annual, stratum-specific encounter rate $\frac{n}{k}$ and encounter rate variance $\text{var}(\frac{n}{k})$ values are output. The encounter rate variance was calculated using the empirical between-sample variation method (Thomas et al. 2010, Distance for Windows User's Guide). Because the survey design involved laying out a set of points along transect lines, points within transect lines are not independent from a design perspective. Hence, in calculating encounter rate variance, points within transect lines were combined, making the transect line the sampling unit.

To compute variance in density, $\widehat{\text{var}}(\hat{D})$, I used the delta method (Seber 1973) assuming independence:

$$\widehat{\text{var}}(\hat{D}) = \hat{D}^2 \left[\frac{\text{var}(\hat{p})}{\hat{p}^2} + \frac{\left(\frac{A_{\text{No}}}{A_{\text{To}}}\right)^2 \text{var}\left(\frac{n_{\text{No}}}{k_{\text{No}}}\right) + \left(\frac{A_{\text{So}}}{A_{\text{To}}}\right)^2 \text{var}\left(\frac{n_{\text{So}}}{k_{\text{So}}}\right)}{\left(\frac{A_{\text{No}}}{A_{\text{To}}}\frac{n_{\text{No}}}{k_{\text{No}}} + \frac{A_{\text{So}}}{A_{\text{To}}}\frac{n_{\text{So}}}{k_{\text{So}}}\right)^2} \right]. \tag{1.16}$$

Note that the above formula assumes that the estimated annual detection probability is the same across both regions; this is the case here because year was the only selected covariate (see Results, below). Had region- or transect-level covariates been selected then an alternative formulation for variance would have been required. To calculate confidence intervals, I assume that $\hat{D}$ are log-normally distributed with independent detection function parameters to compute first order z_α approximate confidence intervals with nominal-level $100(1-2\alpha)\%$ following the method by Burnham et al. (1987; as cited in Buckland et al. 2001, pgs 88-89). The log-normally distributed confidence interval is computed as $(\hat{D}/C, \hat{D}C)$ where $C = \exp\left[z_\alpha \sqrt{\widehat{\text{var}}(\ln\{\hat{D}\})}\right]$. z_α is the upper $\alpha\%$ from the normal$(0,1)$ distribution, and $\widehat{\text{var}}(\ln\{\hat{D}\}) = \ln\left[1 + \frac{\widehat{\text{var}}(\hat{D})}{\hat{D}^2}\right]$.

An alternative approach, which has been shown to have better properties is to use the Satterthwaite method (1946; see Buckland et al. 2001, pg 78), which is based on the t–distribution. However, because of the stratification I employed to account for varying sampling intensity to compute densities, it is not apparent what values to use when computing degrees of freedom for the t–distribution (see Buckland et al. 2001, pgs 89-90).

In addition to computing density and variance using analytic methods described above, I used nonparametric bootstrap procedures, resampling at transects with replacement within strata and year, to estimate strata-specific density and variance estimates (year by

north/south stratum) in Distance for Windows (Buckland et al. 2001, pg 84). For PTDS Buckland et al. (2015) recommend that there are 10–20 replicate transects or points to reliably estimate variance. As noted above, sampling points at Hakalau are correlated and cannot be considered independent. In this situation the 14 transects are considered the sampling unit (six transects in the north stratum and eight transects in the south stratum; see Fig. 1.1). Estimates are produced as the median value within stratum and the nominal-level $100(1-2\alpha)\%$ confidence intervals as the 0.025 and 0.975 quantiles using the algorithm that is approximately median-unbiased regardless of the density distribution. Annual study-area wide density and variance estimates are computed from area-weighted, iteration-wise estimates.

Results

The selected detection function was a hazard-rate model without series expansion (Figs. 1.4 and 1.5). Detection function with adjustment terms were evaluated but not selected using AIC. The covariate `Year` improved model fit by >112 AIC units (Table 1.1; Appendix A Fig. A.1). Correlation and confounding effects were evaluated for combinations of covariates against year. Point coordinates, elevation, and habitat type covariates were confounded with year and their combinations were not evaluated in modelling a detection function. Observer participation varied from 1 to 26 times over the 31-year time series; thus, observer was confounded with year and the combined covariate model was not evaluated. Correlation was large between gust and wind with year and their combinations were excluded (Table 1.2). Inference was made from the hazard-rate key detection function with year-only covariate. The Cramér-von Mises test was not significant at the $\alpha = 0.05$ level (test statistic = 0.15, $p = 0.38$) indicating that the distribution of observed distances did not statistically differ from that predicted under the model. Inspection of the detections revealed that the detection probability was about 0.1 at 58m, which was therefore set as the truncation distance and yielded 2,842 observations from 5,255 points (Table 1.3). The shoulder extends out to 25 m before decaying rapidly. Annual detection probabilities varied from year to year but were relatively precise (CV <12%; Fig. 1.6; Appendix A Table A.1). Encounter rates also varied annually with much higher uncertainty (CV 27.71–69.45%; Appendix A Table A.2).

Differences in the widths of CIs (CIW) between the analytic and bootstrap methods were calculated as the percentage change in CIW as

$$\left(\frac{\text{CIW}_{\text{analytic},i}}{\text{CIW}_{\text{bootstrap},i}} - 1\right) \times 100\%$$

for each year i. The bootstrap method gives on average a CI width that was 7.8% shorter than the CI width of the analytic method (SD=31.5%; Appendix A Fig. A.2). Two issues should be noted with variance estimation. First, although both analytic and bootstrap approaches account for the non-independence of points within lines, both treat the lines as independent between years and hence uncertainty may be underestimated. Second neither approach accounts for the systematic line spacing, and hence uncertainty may be

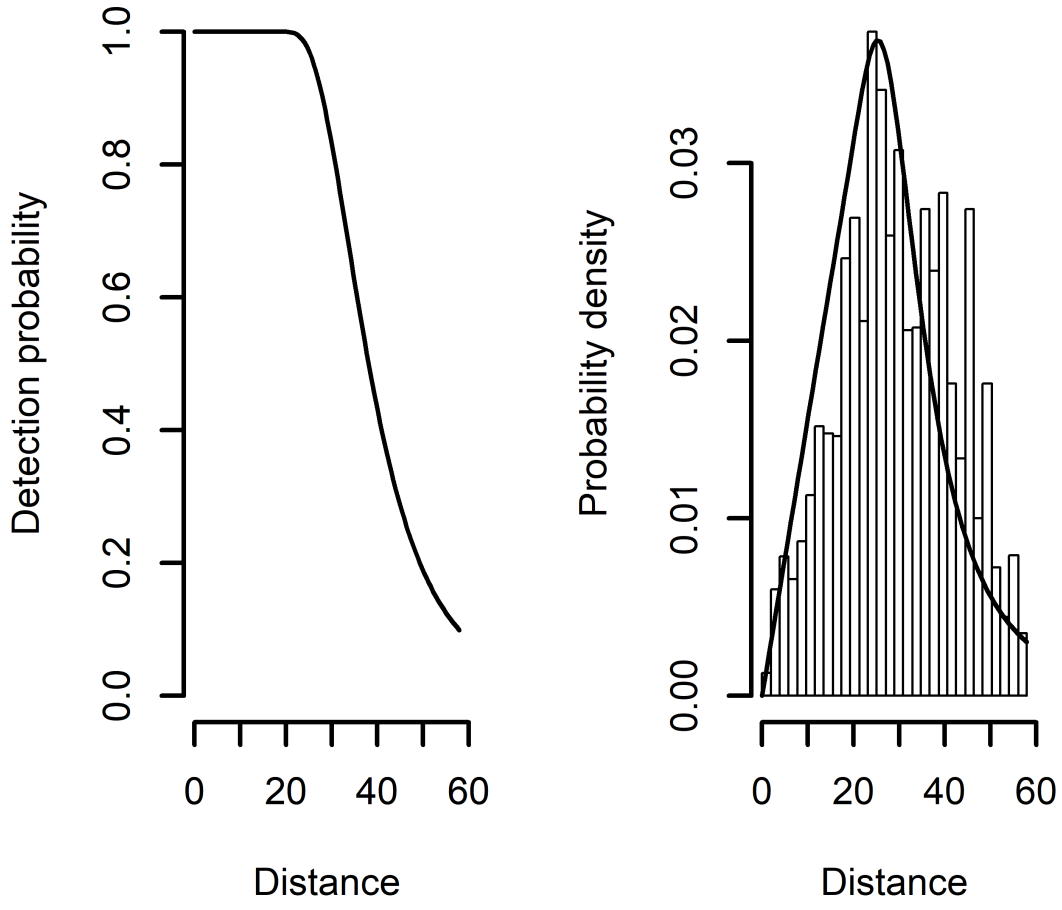

Figure 1.4: Detection function plots for the model selected to estimate 'ākepa detection probability. Plots represent the average detection probability (left panel) and probability density (right panel) for the hazard-rate model without series expansion and with `Year` as a covariate.

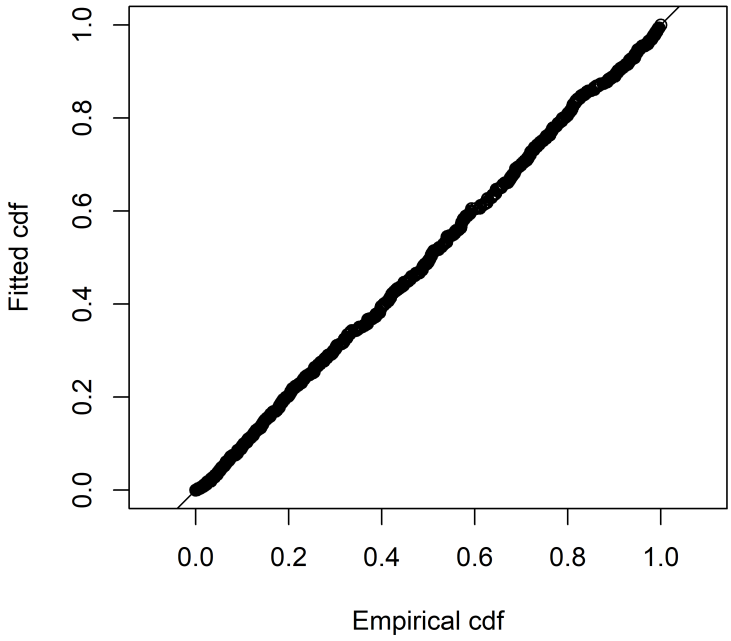

Figure 1.5: Quantile-quantile plot for the detection function model selected to estimate 'ākepa detection probability. The fitted cumulative distribution function (cdf) is plotted against the empirical cdf. The points seem to fall about the straight line, which provides evidence the function fits the data.

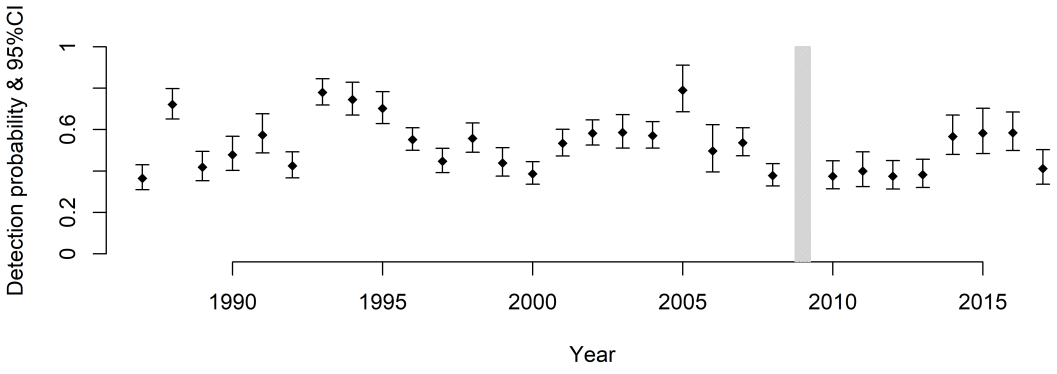

Figure 1.6: Annual detection probability with 95%CI estimates (diamond and whisker bar) from the hazard-rate model without series expansion and with the covariate `Year` produced using Distance for Windows. Surveys were not conducted in 2009 (vertical bar).

Table 1.1: Detection function models used to compute density estimates of Hawai'i 'ākepa from point-transect distance sampling surveys on Hakalau Forest National Wildlife Refuge, Hawai'i, between 1987 and 2017. Base models (Fun) include half-normal (HN) and hazard-rate (HR) key detection functions with cosine (Cos), hermite polynomial (Hpoly) and simple polynomial (Spoly) adjustment terms (AdjTerm). Covariates were incorporated with the highest AIC-ranked base model included rain, wind strength, gust strength, elevation (Elev), habitat type, minutes since survey start (MinSS), observer and year of survey (Yr). All covariates were treated as categorical variables, except minutes since survey start was treated as a continuous variable. Also presented are the number of estimated parameters (Par), negative log-likelihood (-LogLike), AIC values, change in AIC (ΔAIC), and AIC weights (AICw). † Base model selected.

Fun	AdjTerm	Covariate	Par	-LogLike	AIC	ΔAIC	AICw
HR	None	Yr	31	15467.90	30997.80	0	1
HR	None	Obs	13	15525.51	31077.03	79.23	6.243E-18
HR	None	Wind	5	15557.88	31125.76	127.96	1.636E-28
HR	None	Elev	3	15565.44	31136.88	139.08	6.297E-31
HR	None	Hab	3	15566.12	31138.24	140.44	3.190E-31
HR	None	Rain	4	15570.26	31148.52	150.72	1.868E-33
HR	None	Gust	5	15569.90	31149.79	151.99	9.903E-34
HR	None		2	15573.40	31150.81	153.01	5.947E-34
HR	None	MinSS	3	15572.70	31151.40	153.60	4.427E-34
HN	None		1	15609.92	31221.84	224.04	2.240E-49
HN	Cos†						
HN	Hpoly†						
HR	Cos†						
HR	Spoly†						

Table 1.2: Correlation between detection function covariates with `Year` for the point-transect distance sampling surveys on Hakalau Forest National Wildlife Refuge, Hawai'i, between 1987 and 2017. Covariates included rain, wind strength, gust strength and minutes since survey start (MinSS). Spearman correlation was used for all covariates, except the continuous covariate minutes since survey start (MinSS), for which a Kendall rank correlation was used.

Covariate	Correlation
MinSS	0.04
Rain	-0.08
Wind	-0.31
Gust	0.50

Table 1.3: Number of points sampled, 'ākepa detected and 'ākepa detected within the 58m truncation distance by year from point-transect distance sampling surveys on Hakalau Forest National Wildlife Refuge, Hawai'i, between 1987 and 2017. Survey not conducted indicated with a —.

Year	Points	Detections	Detections $\leq$ 58m
1987	194	124	93
1988	194	125	108
1989	198	86	82
1990	197	81	71
1991	197	80	65
1992	197	108	106
1993	194	149	133
1994	194	110	92
1995	195	110	100
1996	198	188	182
1997	193	130	129
1998	197	112	110
1999	195	95	92
2000	198	123	123
2001	196	130	127
2002	195	159	152
2003	199	91	88
2004	198	141	137
2005	166	49	45
2006	162	41	41
2007	147	118	116
2008	145	126	120
2009	—	—	—
2010	136	79	78
2011	139	58	57
2012	139	76	76
2013	139	80	79
2014	136	68	64
2015	139	53	50
2016	139	70	67
2017	139	61	59

overestimated. I therefore take a more conservative approach and use analytic methods to compute density uncertainty.

Densities of Hawai'i 'ākepa have relatively wide confidence intervals and vary temporally across the time series (95%CIs produced using analytic methods; mean of annual CVs = 0.27, SD of annual CVs = 0.10, range of annual CVs 0.16—0.62; Fig. 1.7; Appendix A Table A.3). In the northern portion of the refuge 'ākepa densities remained low but appear to have increased across the time series and were very poorly estimated (mean of annual CVs = 0.93, SD of annual CVs = 0.43, range of annual CVs 0.43—2.24; Fig. 1.7; Appendix A Table A.4). Although 'ākepa were known to occur in the north region throughout the time series, no 'ākepa were detected during 1994, 2000 and 2005 surveys resulting in densities of zero. Densities in the south region were substantially larger than those in the north region, appeared to be driving the overall density patterns observed in the study area, and were better estimated (mean of annual CVs = 0.25, SD of annual CVs = 0.07, range of annual CVs 0.16—0.47; Fig. 1.7; Appendix A Table A.5). In the subsequent chapters I demonstrate that spatio-temporal smoother, point process, soap-film smoother and population dynamics modelling procedures produce more precise density estimates than those generated using standard distance sampling methods.

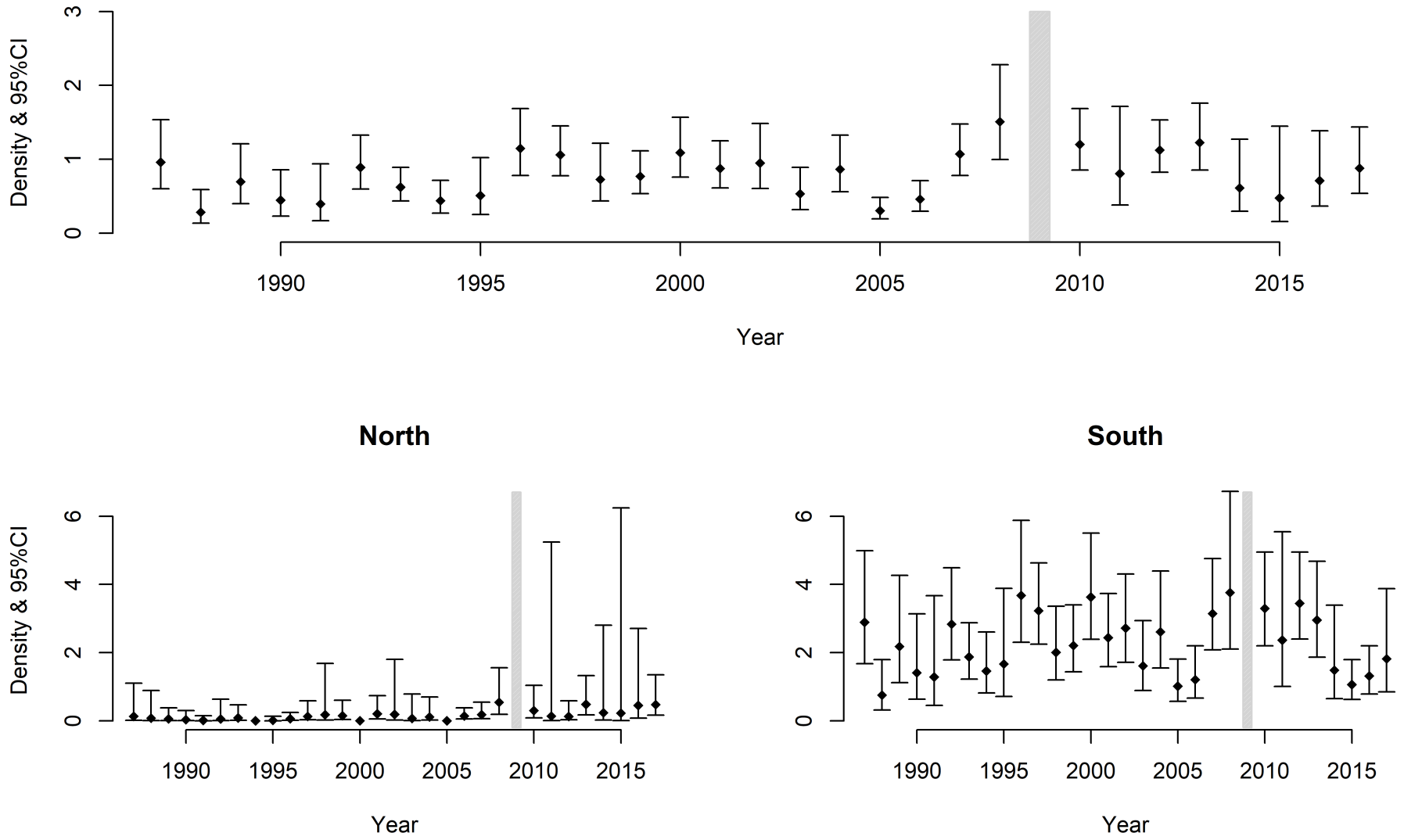

Figure 1.7: Density (birds ha^{-1}) estimate with 95% confidence interval (diamond and whisker bar) computed using standard distance sampling analysis methods for the 'ākepa population across Hakalau (top panel), North (bottom left panel) and South (bottom right panel) strata of Hakalau.

1.5 Subsequent chapters

Understanding how the density, or status, of a population changes through space and time is critical for management and conservation. By approaching the data as a 3D projection, a density surface map of bird distribution and density can be modelled as spatial and temporal processes with peaks of high densities, valleys with low densities and areas absent of bird populations. Underpinning bird distribution and density are geographic, environmental and demographic drivers that influence population change through both space and time. These processes can be formulated through population dynamics models. Modelling a population distribution and density as a 3D projection reduces estimator uncertainty by minimizing the difference between the numbers of bird detected and those expected based on the model. In the following chapters I work through several analytic methods to improve inference in abundance surveys.

In Chapter 2 I apply smoother modelling methods that include covariates of spatial and temporal variables to produce density estimates, thus accounting for both spatial and temporal correlation. Population trends are rarely linear as densities fluctuate in response to biotic and environmental drivers. This can be modelled using smoothing techniques by including smooth functions that introduce "flexibility" into modelling the response variable. I use annual detection probability as an offset to model the spatial and temporal patterns of bird densities using basis-penalty smoothers in a generalized additive model (GAM). In addition to predicting annual spatio-temporal density surfaces from the GAM, I propagate the detection probability uncertainty using the delta method assuming independence (Seber 1973) and using a posterior simulation approach where the detection probability variance is propagated as a random effect (Bravington et al. 2018). I compare the width of confidence intervals to discern model performance. Introduced by Hastie and Tibshirani (1986), GAM theory is well developed and GAMs have been used to evaluate time series of densities; therefore, a formal simulation test is not conducted. My comparison shows the amount of understanding that can be gained from modelling spatio-temporal correlation in an actual dataset.

An alternative approach to modelling a density surface is to employ point process models. PTDS fundamentally involves spatial sampling where points are established systematically throughout a study area and birds detected based on their proximity to the points. In Chapter 3 I apply point-process, spatial-analysis methods to model the spatial correlation of 'ākepa densities. A comparison of the estimates is presented visually where the alignment of densities and their SE indicates similarity. Dissimilarities and their likely causes are identified. I discuss the smoothing effects, underlying assumptions, and conditions for choosing between the two modelling approaches. Again, this is not a simulation test so I evaluate model performance by comparing similarities and dissimilarities.

In Chapter 4 I apply a soap-film smoother to control the boundary behaviour in the basis-penalty smoother to avoid predicting densities into non-suitable habitat, a modelling artefact commonly termed 'leakage'. The soap-film smoother achieves this through two separate but linked bases; one for the boundary and one for the film itself. I evaluate smoother performance by comparing similarities and dissimilarities between a spatial thin

plate regression spline, a modification of the GAM developed in Chapter 2, and the soap-film smooth. While I am not able to assess bias in either the spatial thin plate regression spline or soap-film estimates, I compare these model estimates to those produced using the design-based distance sampling approach assuming that the latter approach is unbiased.

Understanding the patterns of status change through space and time however does not address why densities are changing. Chapter 5 explores potential factors driving population using a state-space model (SSM) framework. SSMs are comprised of a state model and a measurement model. The state model describes the change of the state parameter, population size in this case, and reflects the stochastic sub-processes driving population change. Given the relative lack of information about Hawaiian forest bird population structure I use a single state variable, total population size; however, the state model can be expanded to be age or sex specific. The measurement model (also called an observation model) describes the relationship between the observations, counts corrected for detection probability in this case, and the state parameter. I apply SSMs to abundance time-series data to make inferences about the underlying growth rates. SSMs can be expanded to incorporate demographic data, or derived demographic quantities, to make inferences about states and vital sign parameters. This allows for the formulation of population dynamics models (PDM). I compiled the vital rates as derived quantities from the literature rather than raw data, thus avoiding modelling complex distributional structures. I use Bayesian methods that allow for propagating uncertainty from the various data, estimate missing values and share information among population processes. I compare the width of confidence/credible intervals among abundances generated using Distance for Windows and PDMs to discern increases in precision.

I conclude in Chapter 6 with an overview of the questions I address and highlight how the analyses improve estimator precision. I describe how my research is useful for Hawaiian forest bird management and conservation, and identify how the analyses can be applied to other taxa to aid in global efforts to arrest declines in populations and biodiversity. All research raises more questions than it answers; therefore, I conclude my thesis by identifying some key areas that I anticipate will be the focus of future research.

Chapter 2

Spatio-temporal abundance estimation using smoother models

2.1 Overview

Here I apply smoother-based modelling methods that include spatially- and temporally-referenced covariates to produce abundance estimates, thus accounting for both spatial and temporal correlation to produce more precise density estimates than are available from standard design-based methods. Linear models can be used to describe the overall, long-term trend in the population status; however, two key assumptions of linear models are that the effects are linear and the response is Gaussian. Generalized linear models (GLM) are an extension to linear models to account for non-normal response distributions. Population trends are rarely linear; instead abundances fluctuate in response to biotic and environmental drivers. This results in a non-linear relationship that can be modelled using smoothing techniques which introduce flexibility into modelling the expected response. I use a generalized additive model (GAM), with the annual effective area surveyed per point as an offset, to model the spatial and temporal patterns of bird densities. This approach is sometimes referred to as a density surface model (DSM), particularly in the context of modelling distance sampling survey data. In addition to predicting annual spatio-temporal density surfaces from the GAM, I incorporated detection probability uncertainty using two methods, one that assumes independence of the model components and one that does not assume independence. I compared the uncertainty derived from spatio-temporal models to that from conventional design-based methods. Results from this analysis have been published in Camp et al. (2020)[1]

This chapter is laid out as follows. In Section 2.2 I introduce regression models in the context of trend evaluation, and describe how smoother-based models are extensions of linear and generalized linear models. In Section 2.3 I describe the multi-stage modelling approach to model the detection probability, estimate the density surface and propagate variance that I apply to the 'ākepa data. The results of the smoother and variance propagation are presented in Section 2.4 and compared to estimates generated using program

[1]Paper authored by me as part of my thesis research.

Distance for Windows or `Distance` in `R` from Chapter 1. Section 2.5 gives a discussion of the statistical, biological and management implications of applying smoothers to estimate population status and trend.

2.2 Introduction

In this chapter I apply flexible regression methods to account for non-linear relationships between bird densities with spatially- and temporally-referenced covariates. Spatio-temporal models attempt to capture the distribution of bird density as a function of space and time, and estimate abundance. Spatial modelling can be used to predict spatially restricted regional or local trends and can be more informative than what can be observed at the stratum-wide level. 'Ākepa are strongly philopatric, have relatively small home ranges and there is scant evidence of movement among populations (Ralph and Fancy 1994, Lepson and Freed 1997). There are also good geographical arguments supporting using the spatial predictor variables `Easting` and `Northing`. Traversing from west to east across Hakalau, the habitat progresses from pasture to the pasture-forest edge and into more suitable forest habitat. The substrate underlying Hakalau transitions from relatively fertile, old lava flows (11,000–64,000 years old) in the south to nutrient-limited, new lava flows (5,000–11,000 years old) in the north (Vitousek et al. 2009, USFWS, U.S. Fish and Wildlife Service 2010). Additionally, vegetation in the north-eastern portion of Hakalau has a more complex and denser structure in the canopy, understory and ground cover than in the south-western portion. Differences in the 'ākepa population are undoubtedly a product of the habitat and its interactions with the substrait, nutrients and other environmental factors.

Previous analyses demonstrated that 'ākepa densities and abundances across Hakalau are stable to increasing over time (Camp et al. 2010, 2016). It is likely that these overall trends miss smaller-scale variation in the population, which can be captured by including a smooth of year. This variability may be observed in spatio-temporal maps that depict local trends in bird densities. I summarise trends in densities at two spatial scales: (1) broad-scale trends across Hakalau, and (2) regional-scale trends coinciding with the north and south strata of Hakalau (see Chapter 1 for details).

I use a 2-stage model to estimate spatio-temporal patterns in 'ākepa densities across a 31-year time series. In the first stage, I use point-transect distance sampling (PTDS) to compute the detection probability. In the second stage, I incorporate the detection probability as an offset to model the spatial and temporal patterns in bird densities using a GAM. I combine variance component estimates (detection probability and GAM) using two methods: (1) calculate the combined uncertainty using the delta method that assumes independence between components (Seber 1973), and (2) propagate the uncertainty associated with estimating detection probability into uncertainty in the spatio-temporal model using methods developed in Williams et al. (2011) and described more fully in Bravington et al. (2018) to propagate variances between model stages. This second method does not assume independence between model stages. I compare the uncertainty derived from the spatio-temporal models to conventional design-based distance sampling methods where

change in uncertainty was calculated as the ratio in confidence interval widths.

The design-based detection probability and uncertainty, and associated abundances, are estimated using a frequentist approach (Buckland et al. 2016), while model-based estimates using smoothers use an empirical Bayesian approach (Wood 2017 Sects. 5.8, 6.2.6 & 6.10.3). A common expression of uncertainty is a confidence interval, which is a range of values that includes the true population value with a given level of confidence (e.g., 95%). In frequentist approaches confidence intervals (CIs) can be obtained using asymptotic theory. The design-based CIs are estimated following the method by Burnham et al. (1987; as cited in Buckland et al. 2001, pgs 88-89). In Bayesian approaches uncertainty can be expressed as credible intervals (CrIs) which can be obtained by sampling from the posterior distribution where parameter values were drawn from a prior probability distribution (Gelman et al. 2013). Interval lengths from point process and state-space models in this thesis (which use Bayesian approaches) are credible intervals (Gelman et al. 2013). Interval lengths from spatio-temporal smoothers (which use empirical Bayesian methods) are confidence intervals (Carlin and Gelfand 1990), and thus, interval lengths computed from the spatio-temporal smoothers and detection function models using the delta method assuming independence and the variance propagation method are confidence intervals.

2.2.1 Linear Regression

Precise measures of population abundance and trend are needed for species conservation. Precise measures are most difficult to obtain for rare and rapidly changing populations (Gibbs 2000). It is common for coefficients of variation to exceed 50% and for some species even 100% (Gibbs 2000, Camp et al. 2009). These imprecise estimates preclude drawing conclusions needed for management and conservation actions. There are a large number of methods to assess population trends (Thomas 1996). Generally, most methods typically apply some form of linear regression. These approaches define trend as the long-term, overall directional change in densities over time. Urquhart and Kincaid (1999) suggest this approach to capture the overall increase or decrease in a population. However, the authors note that if the population estimates at the beginning and end of the time series are approximately equal while there is a strong upward or downward cycle in the data or if the time-series is made up of fluctuating shorter trajectories a linear trend model will have high levels of residual deviance resulting in non-statistically significant results and important biological patterns in response to changing environmental conditions may be missed. Model assumptions (see below) should also be met for reliable trend assessment.

The model for linear regression with only one covariate may be written as

$$y = \beta_0 + \beta_1 x + \epsilon \qquad \epsilon \sim \text{normal}\left(0, \sigma^2\right) \tag{2.1}$$

where y is the response variable, x is the covariate, model parameters are the intercept β_0 and slope β_1, and ϵ is the random error, assumed normally distributed with mean zero and variance σ^2. This is termed simple linear regression, as there is only a single covariate.

Multiple linear regression would include additional covariates and slope parameters. The relationship between y and x is assumed to be linear. The primary interest in linear regression in the context of population trend modelling is in estimating the slope, β_1, as it represents the population trend across the time series. Producing reliable estimates of β_1 depends on meeting several model assumptions. A key assumption of linear regression is that the response is normally distributed with constant variance. In the case of 'ākepa, Camp et al. (2010, 2014) show that the application of log-linear regression transformed the skewed distribution of abundances to be approximately normally distributed. While this procedure allowed for analysing the data assuming constant variance on the transformed scale, visual inspection of the time series shows a fluctuating, non-linear trend in the log abundances. Before introducing non-linear models I provide a brief review of linear regression models, focusing on computing variance. This allows me to introduce a number of the main features of regression in a simple context that I then build upon in later sections through the development of GLMs and finally GAMs.

It is useful to rewrite the linear equation (Eqn. 2.1) in matrix-vector notation

$$\mathbf{y} = \mathbf{X}\boldsymbol{\beta} + \boldsymbol{\epsilon} \tag{2.2}$$

where

$$\mathbf{y} = \begin{bmatrix} y_1 \\ y_2 \\ \vdots \\ y_n \end{bmatrix}, \quad \mathbf{X} = \begin{bmatrix} 1 & x_1 \\ 1 & x_2 \\ \vdots & \\ 1 & x_n \end{bmatrix}, \quad \boldsymbol{\beta} = \begin{bmatrix} \beta_0 \\ \beta_1 \end{bmatrix}, \text{and} \quad \epsilon = \begin{bmatrix} \epsilon_1 \\ \epsilon_2 \\ \vdots \\ \epsilon_n \end{bmatrix}.$$

Given that observations are normally distributed with constant variance then the maximum likelihood estimate of $\boldsymbol{\beta}$ is

$$\hat{\boldsymbol{\beta}} = \left(\mathbf{X}^\mathsf{T}\mathbf{X}\right)^{-1}\mathbf{X}^\mathsf{T}\mathbf{y} \tag{2.3}$$

with standard error

$$\text{se}\left(\hat{\boldsymbol{\beta}}\right) = \sqrt{\sigma^2\left(\mathbf{X}^\mathsf{T}\mathbf{X}\right)^{-1}}. \tag{2.4}$$

The usual estimator of the variance σ^2 is $s^2 = \frac{\left(\mathbf{y}-\mathbf{X}\hat{\boldsymbol{\beta}}\right)^\mathsf{T}\left(\mathbf{y}-\mathbf{X}\hat{\boldsymbol{\beta}}\right)}{(n-M)}$ where M is the number of β parameters estimated, $M = 2$ in this formulation (β_0 and β_1). If additional covariates are used, the design matrix is expanded by adding a column for each predictor variable and a corresponding coefficient is estimated as above. Linear regression estimates the intercept and slope such that the sum of squares of the residuals is minimized. The degrees of freedom for linear regression equals the number of parameters to be estimated and is calculated as the trace of the hat matrix

$$\text{df} = \text{tr}\left(\mathbf{H}\right) = \text{tr}\left(\mathbf{X}\left(\mathbf{X}'\mathbf{X}\right)^{-1}\mathbf{X}'\right). \tag{2.5}$$

2.2.2 Generalized Linear Models

Generalized linear models are an extension of linear regression where the response variable is not necessarily normally distributed. The distribution of the response variable belongs to the exponential family, with relevant distributions for count data. Poisson and negative binomial are two potential options (see below). A link function is included in the model equation that links the relationship between the linear predictor and the expectation of the observation. The expectation of the random response $\boldsymbol{Y}$ in a GLM is

$$\mathbb{E}(\boldsymbol{Y}) = \boldsymbol{\mu} = g^{-1}(\mathbf{X}\boldsymbol{\beta}) \tag{2.6}$$

where $\mathbf{X}\boldsymbol{\beta}$ is the linear predictor and g the link function. Within this framework the model is linear on the linear predictor scale but not on the response scale. The coefficients are estimated with maximum likelihood.

The Poisson distribution models the probability of observing n events for any non-negative integer of n, in my case the numbers of birds counted during an 8-min period at a sampling point. The expected value of a Poisson distribution is also its variance.

When the variance is larger than the mean the data are over-dispersed relative to Poisson and this is common for counts (Wood 2017, pg 115). The negative binomial distribution can be used as an alternative to the Poisson distribution for discrete data where the variance exceeds the mean. The negative binomial is a compound probability distribution of a gamma-Poisson mixture distribution. The negative binomial distribution includes an extra scalar parameter ϕ, a dispersion parameter. The negative binomial distribution variance is $\text{var}(\mu) = \text{E}[\mu] + \phi\text{E}[\mu^2]$.

An additional distribution that is useful for count data that is over-dispersed relative to the Poisson is the Tweedie distribution. Like the negative binomial distribution, the Tweedie distribution has a dispersion parameter ϕ along with a power parameter p to account for over-dispersion. The negative binomial and Tweedie distributions are useful for modelling distributions that have a large number of zero observations. The Tweedie distribution is a compound Poisson-gamma distribution with mass at zero but otherwise positive and continuous real numbers (Shono 2008, Foster and Bravington 2012). The Tweedie distribution variance is $\text{var}(\mu) = \phi\mu^p$ for $1 < p < 2$ where the dispersion parameter ϕ and the power parameter p are positive constants. During the fitting procedure in standard statistical software such as `mgcv` (Wood 2016) the ϕ and p parameters are estimated (Wood 2017).

Another distribution that has been used to model count data is the quasi-Poisson. I did not investigate this distribution as its reliability is questionable with low expected counts and a full likelihood is desired (see citations in Wood 2017, pg 355).

2.2.3 Flexible Regression

It is common to model non-linear population trends (Fewster et al. 2000). Non-linear trends can reveal medium-term fluctuation in populations and are useful for monitoring programs with long time spans where the assumption of a constant linear trend is unlikely

to be met (Knape 2016). GAMs are an extension of the GLM framework that allow for flexible, smooth modelling of the covariates, beyond the strict linear relationships dictated by the GLM structure. This is achieved through the use of semi-parametric functions in modelling the response variable (Hastie and Tibshiani 1990).

My interest lies in the geo-referenced relationship of bird data collected across a given area where observations are taken at specific locations that have geographical coordinates. The location of Hawaiian bird data are recorded as Easting and Northing in the Universal Transverse Mercator (UTM) coordinate system. Like linear and generalized linear models, GAMs can allow for modelling multiple spatially and temporally referenced variables. As such, I assume that bird densities vary smoothly across space and over time.

Spatial distance sampling models based on point process models were first proposed by Stoyan (1982) and Högmander (1991). Hedley (2000) and Hedley and Buckland (2004) developed models based on aggregating detections within small segments of transects and using GAMs to model the number of detected objects or groups in each segment, offering a simpler analysis method, leading to what is now termed density surface modelling. Miller et al. (2013) provided software for fitting density surface models, using the two-stage approach proposed by Hedley and Buckland (2004), in which the detection function is modelled in the first stage, and the counts modelled in the second, with an estimated offset to account for detectability. Buckland et al. (2016) provided a more general framework for model-based distance sampling, and reviewed the above approaches. I adopt the density surface modelling approach here. I estimated detection probabilities using standard multiple-covariate distance sampling methods (see Chapter 1 Section 1.4.4; Buckland et al. 2015).

I model spatial and temporal pattern using penalized spline-based smoothing within a generalized additive modelling framework. There is a rich variety of possible smooth functions such as spatio-temporal variations of principal component analysis, canonical correlation analysis, conditionally autoregressive (CAR) models, kriging, kernel density estimation, and hierarchical dynamical spatio-temporal models (see Cressie and Wikle 2015). Wood (2017) recommends using regression splines to fit a smooth curve to model the relationship between the predictor, x, and response variables, y, where the amount of smoothing is controlled by a penalty term (frequentist approach) or prior of the space of functions (Bayesian approach). My preference is to use semi-parametric model fitting procedures such as penalized spline-based smooths. There are several reasons I use GAMs. First, densities of 'ākepa vary relatively smoothly throughout Hakalau. Second, the amount of smoothing is controlled within the GAM framework that prevents overfitting the predictor function. Finally, the well developed software package `mgcv` (Wood 2016) facilitates modelling smoothers including model selection and model checking.

Within this framework a simple form of an additive model is a GAM with identity link given by

$$y_i = f(x_i) + \epsilon_i, \tag{2.7}$$

for samples $i = 1, \ldots, n$ where the response variable y_i and its relationship to the predictor variable x_i is described by a smooth function f plus independent errors ϵ_i. The error term

of this simple additive model is assumed to be normally distributed with mean zero and variance σ^2. As for the GLM described above, the response distribution can be replaced with an exponential family distribution such as Poisson, negative binomial or Tweedie distributions (the Tweedie distribution is only exponential family for fixed values of the power parameter), and thus an additive model becomes a generalized additive model incorporating the link function and linear predictor.

Eqn. 2.7 can be expanded simply by including an additive component for multiple smooths in the model. Each smooth is represented as a function with a penalized basis expansion such that Eqn. 2.7 remains an additive model

$$\begin{aligned} \boldsymbol{y}_i &= \exp\left[\beta_0 + \sum_j f_j\left(x_{ij}\right)\right] + \boldsymbol{\epsilon}_i \\ &\text{and in matrix notation} \\ \boldsymbol{y}_i &= \mathrm{X}\boldsymbol{\beta} + \boldsymbol{\epsilon}_i \end{aligned} \tag{2.8}$$

where the exponent is the inverse of the link function, $f_j(x_i)$ is the smooth function of the x_i variables, and $\boldsymbol{X}$ and $\boldsymbol{\beta}$ as defined above. Then for a single, given smooth f we have the following basis expansion

$$f(x_i) = \sum_{m=1}^{M} \beta_m b_m(x_i). \tag{2.9}$$

Where the β_m are estimated and the b_m are fixed (Wood 2017, pg 162). M is the number of basis functions used for this term and I refer to this as the basis complexity. I further restrict my selection of spline-based smooths to penalized regression splines that can be applied to two-dimensions or higher and are isotropic. For spatial covariates of geographic coordinates isotropy (i.e., rotationally invariance) is important as it is the property where smoothing in the x_1 direction can produce similar wiggliness in the x_2 direction (Wood 2017, Sects. 5.5 & 5.7). That is, the smooth has the same smoothness in the Easting direction as in the Northing direction, which is further supported as the point locations use UTM coordinates that are spatially isotropic. Based on these conditions the following basis functions are eligible: thin plate regression splines (TPRS) and soap-film smoother bases (Wood 2017). I chose the TPRS because it is isotropic and, unlike the soap-film smoother, does not constrain the smoothing at the boundary. For univariate terms the TPRS is used for the spatial and temporal variables. A tensor product is used to produce interaction terms for the two and three-way spatial and temporal variable interactions because space and time measurements are on different scales. The advantage of this approach is that in the computational process the TPRS smooth automatically selects a representative set of knots within the extent of the data. This eliminates subjectivity in knot selection and placement reducing the size of the basis function (Wood 2003).

In smoothing the goal is to fit a function that neither follows the data too closely nor is overly smooth. If the function is very flexible it simply interpolates the data. Thus a very flexible function jumps from datum to datum, which does not provide additional insight

about the spatial distribution than merely inspecting the data. Conversely, a completely smoothed function fails to pick up nuanced patterns in the data and provides no further information than linear regression. For simplicity a univariate case is considered. Parsimony in the function is achieved by adding a penalty to the fitting criterion, commonly called a roughness penalty, to minimise

$$\sum_{i=1}^{n}(y_i - f(x_i))^2 + \lambda \int_a^b \left[f''(x)\right]^2 dx \tag{2.10}$$

for a data set (x_i, y_i) with $a \leq x_i \leq b$. The summation term is the fit to the data and is the residual sum of squares. $f''(x)$ is the second derivative of the smooth function of x. A balance between the fitting and roughness is achieved with the λ parameter. A λ of zero leads to a fully saturated model (one parameter per data point) where the data points are interpolated, whereas a λ of infinity leads to a reduced model that produces a strongly smoothed curve (i.e., a line). The penalization process shrinks the fully saturated model toward the smooth model if not differently supported by the data.

The smoothing parameter λ controls the trade-off between the model goodness of fit and model smoothness. That is, how closely the curve follows the data versus the curve being linear. There are well developed methods for estimating λ, and I use restricted maximum likelihood (REML) methods for estimating smoothing parameters because they (1) are a maximisation method opposed to generalized cross validation (GCV) score; (2) performs well with over-dispersed, low-mean count data (Wood 2017, pg 150); and (3) tends to be more resistant to over-fitting (see Wood 2017, Sect. 6.2.8).

Wood (2017, Sects. 5.8, 6.2.6 & 6.10.3) describes how models fitted using `mgcv` can be interpreted as empirical Bayesian models. Priors for the βs are multivariate normal distributions for which the precision matrices are the penalties. Smoothing parameters are estimated from the data by optimisation that is equivalent to using a uniform prior (Wood 2011). Parameter estimation is via REML methods in all GAMs in my thesis.

In a GAM the degrees of freedom are affected by the amount of smoothing and are called effective degrees of freedom (EDF). The EDF is the trace of the hat matrix similar to Eqn. 2.5 that maps coefficients to predictions but includes the wiggliness penalty coefficient matrix and smoothing parameter (Wood 2017, pg. 211). The number of EDF will decrease the degree of smoothing as the number of smoothing parameters increases. If the penalty goes to zero the model is a GLM with a trace equivalent to Eqn. 2.5.

I refer the interested reader to Hastie and Tibshiani (1990) and Wood (2017) for the technical descriptions and formal proofs. The most common way to fit smoothers is conducted in `R` (R Core Team 2017) through the `mgcv` package (Wood 2016). This package allows for the selection of penalised splines and automatically tunes the smoothing parameter (Wood 2016).

2.3 Smoothing Using GAMs

Since I expect density to vary non-linearly over the study area in space and time, it is reasonable to start modelling with a GAM instead of linear models. I applied spatio-temporal GAMs to a 31-year time series of the endangered Hawai'i 'ākepa in the open-forest stratum (Chapter 1 Fig. 1.1).

2.3.1 Detection probability estimation

In Chapter 1, I detailed the procedures to estimate the 'ākepa detection probability from point-transect data using Distance for Windows (Thomas et al. 2010). The data used in this first-stage analysis were the 31-year, open-forest stratum time series of 'ākepa. A hazard-rate key detection function only with year as a factor-covariate model was selected. The truncation distance w and estimated annual detection probabilities $\hat{p}_i$ were used to compute the effective area searched (EAS) as $\hat{\nu}_i = \pi w^2 \hat{p}_i$ (Buckland et al. 2015). Formally the EAS is computed following Buckland et al. (2015) Eqn. 5.47:

$$\nu_i = 2\pi \int_0^w r g\left(r|\mathbf{z}_i\right) dr, \tag{2.11}$$

where the hazard-rate detection function is

$$g\left(r|\mathbf{z}_i\right) = 1 - \exp\left[\left(-\frac{r}{\sigma(\mathbf{z}_i)}\right)^{-b}\right] \tag{2.12}$$

for distance r, $0 \leq r \leq w$, where b is the hazard-rate shape parameter, and

$$\sigma\left(\mathbf{z}_i\right) = \exp\left[\alpha + \delta_i\right] \tag{2.13}$$

where α is an intercept parameter and δ_{z_i} is the parameter for year z_i. To ensure identifiability, the value of δ in the first year of the time series, δ_{1987}, is set to 0.

The EAS was incorporated as an offset in the second-stage model-based density estimation. This allowed the effective search area to vary depending on the year of the survey.

2.3.2 Model specification

I fitted a GAM with smooths of location variables `Easting` and `Northing`, temporal variable `Year`, their interactions, and offset $\hat{\nu}_i$ on the scale of the link. This model has the form

$$\begin{aligned}\log\{\mathbb{E}(n_{ik})\} =& f_1(\texttt{Easting}_k) + f_2(\texttt{Northing}_k) + f_3(\texttt{Year}_i) \\ &+ f_4(\texttt{Easting}_k, \texttt{Northing}_k) + f_5(\texttt{Easting}_k, \texttt{Year}_i) \\ &+ f_6(\texttt{Northing}_k, \texttt{Year}_i) \\ &+ f_7(\texttt{Easting}_k, \texttt{Northing}_k, \texttt{Year}_i) + \log(\hat{\nu}_i)\end{aligned} \tag{2.14}$$

where n_{ik} is the bird count in the i-th year at the k-th point. Smooths (f_{1-7}) were modelled as thin plate regression splines (TPRS; Wood (2003)). The advantage of the TPRS approach is that knot positions were selected automatically from the data, eliminating knot placement subjectivity. The space-time interactions in f_{5-7} were anisotropic as space and time measurements were on different scales, so interactions with time were generated via tensor products (Wood et al. 2013). For each term, the maximum basis complexity was set and the penalty controlling the degree of smoothing was selected using REML (Wood 2017, pg 185). The model was built in `R` (R Core Team 2017) using the `mgcv` package (Wood 2016).

An advantage of using REML in the `mgcv` package was that the dispersion parameter (ϕ and p) can be automatically selected for the negative binomial and Tweedie distributions, respectively (Wood 2017, pg 356). Moreover, they reduce the tendency to under-smooth which is a concern when using prediction error criteria with selection penalties. In lieu of in-out-style model selection, I used the approach where an extra penalty is added to each term through the linear terms in the model (Marra and Wood 2011). By using the extra penalty method each smooth term is retained in the model permitting parameter uncertainty to be incorporated in total estimates of density uncertainty. This approach is a variable selection process where coefficients for terms that have no effect on the model mean are shrunk to zero.

2.3.3 Model checking

Since the response variable is a discrete, non-negative count, I modelled counts with three response distributions: Poisson, negative binomial and Tweedie distributions, all with a log link function. For the Tweedie distribution I restricted the power parameter to $p = (1.1, 2)$ following recommendations provided in the `mgcv` package help pages. I conducted a linear search to bracket the power parameter between $(1.1, 2)$ and used a method of bisection to approximately identify the maximum. Sensitivity to the choice of response distribution and model assumptions were checked through inspection of the deviance residuals following approaches suggested by Zuur (2012) and Wood (2017). Akaike's information criterion (AIC) was used to select among distributions. I refitted the selected model, with intercept, to the residuals to determine if any residual variance remained following methods by Marra et al. (2012) and Wood (2017). The desired refitted model EDF should be approximately zero with basis complexity (k-index) near one for each term.

2.3.4 Spatial model including habitat

Judge et al. (2018) showed that 'ākepa density varies by habitat type. Spatial models are particularly useful for exploring how densities relate to habitat types, and other variables such as climate and elevation. I identified point-specific habitat type based on the terrestrial ecosystems data from the LANDFIRE classification (USGS, U.S. Geological Survey 2013). Habitat was classified at the formation level describing plant communities of the U.S. National Vegetation Classification (Jennings et al. 2009, and `http://usnvc.org`), and defined by broad combinations of growth forms (e.g., forest trees) with moisture (e.g.,

wet or mesic) and temperature (e.g., montane) conditions.

Exploratory analysis indicated that within the study area there were two habitat types: (1) montane mesic forest; and (2) montane wet forest. Thus, habitat was categorical with 2 levels. Generally there was greater coverage in montane wet forest than montane mesic forest (148 points in wet forest and 52 points in mesic forest; Fig. 2.1). I included the categorical variable `Habitat` in the spatio-temporal smoother model of the form

$$\begin{aligned}\log\{\mathbb{E}(n_{ik})\} =& f_1(\texttt{Easting}_k) + f_2(\texttt{Northing}_k) + f_3(\texttt{Year}_i) \\ &+ f_4(\texttt{Easting}_k, \texttt{Northing}_k) + f_5(\texttt{Easting}_k, \texttt{Year}_i) \\ &+ f_6(\texttt{Northing}_k, \texttt{Year}_i) \\ &+ f_7(\texttt{Easting}_k, \texttt{Northing}_k, \texttt{Year}_i) + \texttt{Habitat}_k + \log(\hat{\nu}_i))\end{aligned} \tag{2.15}$$

where `Habitat` was a two level variable taking values "wet" or "mesic", and the other variables were as above. AIC was used to select between the smoother-only and the smoother-with-habitat models.

2.3.5 Propagating variance

The modelling approach described here potentially achieves propagating variance, relative to the design-based methods of the previous chapter, by attempting to account for spatial and temporal pattern in the data. The two-stage modelling approach first involves estimating the detection probability then modelling the spatio-temporal correlation. Naive approaches fail to incorporate uncertainty from all model terms, specifically detection probability uncertainty. Variance estimation procedures in standard modelling using GAMs account for the spatial and temporal dependence in the data. Without additional analyses, GAMs will not account for detection probability variance. Procedures to account for both sources of variance are: (1) ignore; (2) calculate the total variance using delta method assuming independence between the two variance components; (3) apply bootstrap procedures; and (4) apply methods developed in Williams et al. (2011) and described more fully in Bravington et al. (2018) to propagate variances between model stages using posterior simulation.

Ignore

Many analyses ignore the uncertainty of the offset parameter and treat it as known instead of estimated. Uncertainty in detection probability affects the offset of the GAM in the portion of the model that rescales the linear predictor (Bravington et al. 2018). If this source of variance is ignored it can give false confidence, leading to mis-estimated variances and incorrect inference.

Delta method assuming independence

Ignoring additional sources of variability is inadvisable and fortunately there is a simple way to combine various sources of error via the delta method. The delta method assumes that the estimates of variance are independent thus approximate precision and

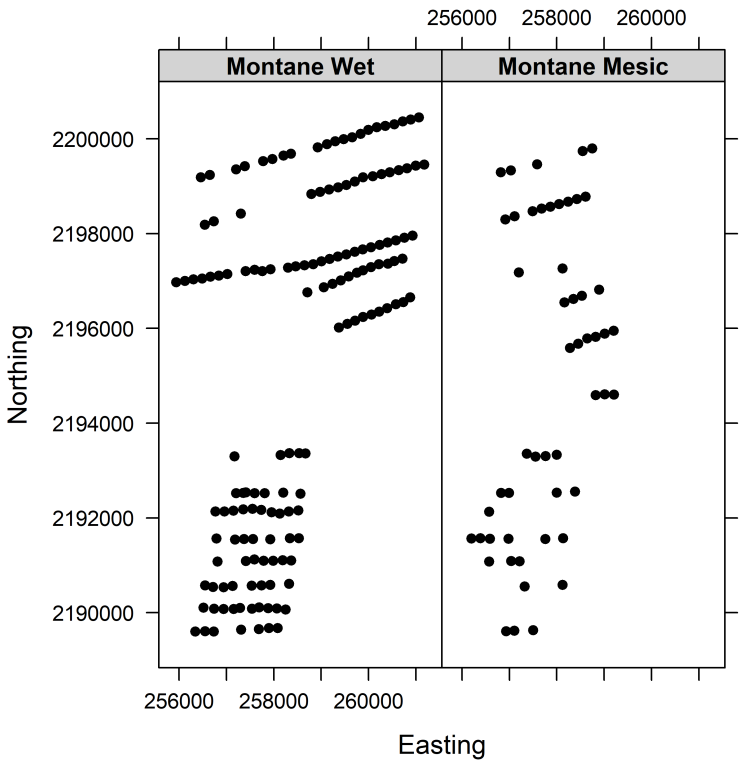

Figure 2.1: Location of points within each habitat type montane wet and montane mesic forest.

confidence intervals of density estimates can be obtained using asymptotic theory (Seber 1973). Using the delta method, the Distance for Windows derived detection probability variance is combined with the GAM density estimate variance to produce total uncertainty in the GAM derived density estimates. Specifically, the annual standard error estimate for year i, $\text{SE}_{\text{tot},i}$, is calculated as $\text{CV}_{\text{tot},i} \times \hat{d}_i$ where the $\text{CV}_{\text{tot},i}$ is computed as $\text{CV}_{\text{tot},i} = \sqrt{\text{CV}^2_{\text{tot},i}} = \sqrt{\text{CV}^2_{\hat{p},i} + \text{CV}^2_{\text{GAM},i}}$ and $\hat{d}_i$ is the ith-year density estimate. My concern with using the delta method is that within a year the estimated detection probability and the density estimate for that year from the GAM are not independent, which violates the assumption of independence for combining variance component estimates (Seber 1973). The delta method is computationally cheap and despite violations of the independence assumption is commonly used to combine variances across models even though variances are overestimated. For illustrative purposes, I computed uncertainty using the delta method and compared the differences in the widths of CIs generated using the design-based log-normal confidence intervals computed with parameter estimates from Distance for Windows (DB; ($\text{CIW}_{\text{DB},i}$)) and from the delta method (DM; ($\text{CIW}_{\text{DM},i}$)). The change in uncertainty was calculated as the percentage change in CIW expressed as $\left(\frac{\text{CIW}_{\text{DM},i}}{\text{CIW}_{\text{DB},i}} - 1\right) \times 100\%$ for each year i.

Bootstrap methods

With many complex models, such as GAMs and spatio-temporal models, independence assumptions are not realistic. Bootstrap methods can in theory combine $\hat{p}$, spatial and temporal error components to produce unbiased estimates of uncertainty in density. An intuitive explanation of the bootstrap method it that by resampling from the data, it attempts to recreate the underlying relationship between the population and the sample. The advantage of this procedure is that while the population is unknown, the sample and resamples are either known or have known distributions allowing for statistical inference (Lahiri 2003). For the cases where the sample and resample distributions are known a parametric bootstrap method is used, otherwise a non-parametric bootstrap method is applied. There are limitations, however, when applying bootstrap methods. Lahiri (2003) showed that bootstrap methods miss-specify first and second moments when the distribution of the count data possesses large numbers of zero counts and the data are highly skewed. These datasets are similar to the endangered 'ākepa surveys that possess many points with zero counts.

A further limitation specific to spatio-temporal modelling is the need to retain the underlying serial correlation during the resampling procedure. The block bootstrap method was developed to address this issue (Lahiri 2003). By block I refer to grouping spatially and/or temporally adjacent samples. Selection of the block shape and size remains an issue specific to my data. Standard block shapes include circles, squares and hexagons, while sizes vary from relatively small to large depending on the correlation distances. There is a mismatch with the sampling unit in the distance sampling portion of the data. For PTDS surveys where points are placed along lines and the distances between points and lines differ, the points are correlated and cannot be considered independent. To estimate the

detection probability and its variance an appropriate form of resampling is to block and resample the lines (Buckland et al. 2001, 2015).

In the case of the 'ākepa analysis there are multiple underlying processes. As noted in Chapter 1, the transect line was the sampling unit and to correctly estimate densities the study area was stratified into north and south regions. This procedure resulted in fewer than 10 transect lines in each strata, which is a small sample size issue when applying bootstrap methods. In addition, the data are pooled across surveys to fit the detection function, and post-stratification procedures are used to estimate geographically survey-specific detection probabilities. To account for temporal differences in the detection probability the covariate survey year is included in the detection function model. The counts require blocking on spatially-explicit grids to account for spatial correlation. Therefore, bootstrap methods, whether out-of-the box or manually-coded, are not the best approach to incorporate the detection probability variance nor capture the underlying serial correlation to estimate first and second moments.

Variance propagation

Sampling unevenly spaced (spatial, temporal or other) data can be problematic. Therefore, I propagated detection probability uncertainty through to the spatio-temporal model using the variance propagation method of Williams et al. (2011) and Bravington et al. (2018). This approach allowed me to capture uncertainty from both the detection and spatio-temporal models without assuming independence between model components.

The `dsm` package (Miller et al. 2018) is a wrapper in `R` (R Core Team 2017) used to model a detection function to estimate the detection probability and its variance. In the `ds` function of `Distance` for R (Miller et al. 2019) I refitted the best detection function model from Distance for Windows (Thomas et al. 2010; see Chapter 1 Table 1.1). The detection probability was then passed to the GAM along with an additional random effect which accounts for the variance in detectability. The additional random effect is assumed a normal distribution with mean zero and variance derived from the detection function. The GAM allows for calculating the posterior covariance $\mathbf{V}_\beta$ matrix of the intercept and smoother terms. This matrix has the structure

$$\mathbf{V}_\beta = \begin{bmatrix} \mathbf{V}_{\text{GAM}} & \text{cov} \\ \text{cov} & \mathbf{V}_{\text{DS}} \end{bmatrix} \tag{2.16}$$

where $\mathbf{V}_{\text{GAM}}$ are the spatio-temporal variances, $\mathbf{V}_{\text{DS}}$ the detection probability variances, and the off-diagonal blocks are the covariances between the spatio-temporal and detection probability parameters.

The GAM uncertainty is estimated as a multivariate normal posterior distribution of the smoother model for the vector of $\boldsymbol{\beta}$s conditional on the data, $\mathbf{y}$, and smoothing parameter, $\boldsymbol{\lambda}$, as $\boldsymbol{\beta} \mid \mathbf{y}, \boldsymbol{\lambda} \sim \text{MVN}\left(\hat{\boldsymbol{\beta}}, \mathbf{V}_{\hat{\beta}}\right)$. This is presented in Marra et al. (2012) and detailed in (Wood 2017, Sect. 6.10). Simulating replicate coefficient vectors, $\hat{\boldsymbol{\beta}}$, a large number of times from the posterior of the parameters then allows for variance to be estimated, and using quantiles, the confidence intervals can be calculated. Thus, the

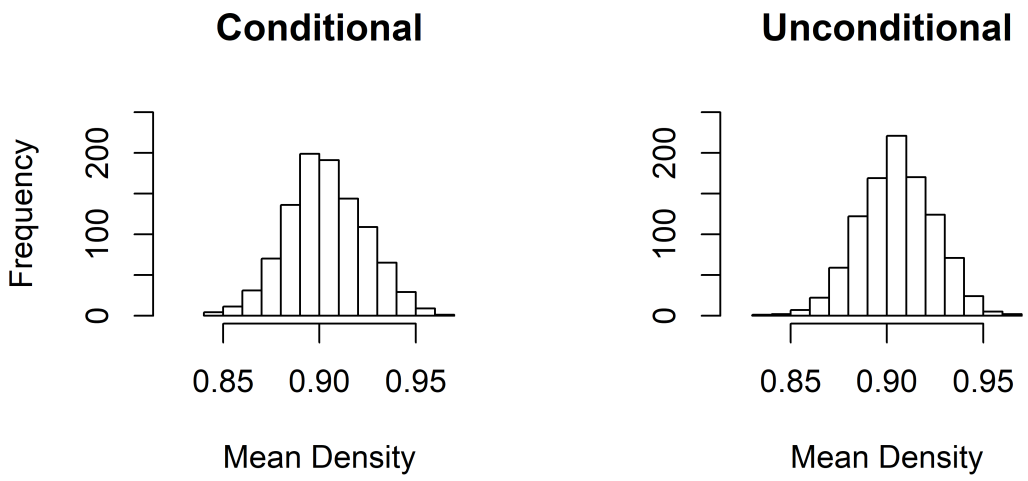

Figure 2.2: Histograms of 1000 replicate parameter sets from the posterior distribution using a covariance matrix conditional (`vcov(m, unconditional=FALSE)`; left panel) and unconditional (`vcov(m, unconditional=TRUE)`; right panel) on the smoothing parameters.

prediction matrix maps the model parameters to the linear predictor, $\hat{\boldsymbol{\eta}}_p$, as $\hat{\boldsymbol{\eta}}_p = \mathbf{X}_p\hat{\boldsymbol{\beta}}$.

The smoothing parameter uncertainty is incorporated in the posterior simulations in the covariance matrix (see pg 302 in Wood 2017). Such simulations are conditional on the estimated smoothing parameters by simulating from the posterior. I compared the conditional distribution to simulations drawn from the desired unconditional distribution for the annual mean densities. In `mgcv` the covariance matrix is computed via `vcov(m, unconditional=TRUE)` when the model is estimated using REML smoothing parameter estimation. I found there to be minor computational costs in computing the unconditional covariance matrix which yielded a slightly wider correction factor (Fig. 2.2). My goal is to account for sources of uncertainty; therefore, I simulated from the unconditional distribution.

The detection probability uncertainty can be estimated by fitting

$$\log\left[\mathbb{E}\left(n_i\right)\right] = \log\left(\mathrm{A}_i\right) + \log\left(\hat{p}_i\right) + \boldsymbol{\beta}_0 + \left.\frac{\partial \log_e\{\hat{p}_i\}}{\partial \boldsymbol{\theta}}\right|_{\boldsymbol{\theta}=\hat{\boldsymbol{\theta}}} \left(\hat{\boldsymbol{\theta}} - \boldsymbol{\theta}_0\right) + s\left(\texttt{Easting}_k, \texttt{Northing}_k, \texttt{Year}_i\right). \tag{2.17}$$

The extra term in Eqn. 2.17 is the Taylor expansion of the detection probability on the log scale. $\left(\hat{\boldsymbol{\theta}} - \boldsymbol{\theta}_0\right)$ is a random effect in the refitted GAM with $\left(\hat{\boldsymbol{\theta}} - \boldsymbol{\theta}_0\right) \sim \mathrm{MVN}\left(0, \mathbf{V}_{\mathrm{DS}}\right)$ distribution. Bravington et al. (2018) provides a detailed description of this process. Uncertainty in the detection probability is then a component in the variance-covariance matrix $\mathbf{V}_\beta$ along with the $\boldsymbol{\beta}$s.

Refitting the spatio-temporal model with a correction to include detection function uncertainty was performed using the `dsm_varprop` function in the R package `dsm` (Miller et al. 2018) (R code provided in Appendix B). I then used posterior simulation (Wood 2017,

Sect. 7.2.7) to generate possible predictions from the model, taking appropriate summaries to give uncertainty estimated. Differences in the widths of the variance propagation CIs (VP; ($\text{CIW}_{\text{VP},i}$)) were calculated and the change in uncertainty was calculated as the percentage change in CIW expressed as $\left(\frac{\text{CIW}_{\text{VP},i}}{\text{CIW}_{\text{DB},i}} - 1\right) \times 100\%$ for each year i.

2.4 Results

2.4.1 Distribution selection

I evaluated the performance of Poisson, negative binomial and Tweedie distributions when applied to the full spatio-temporal model. I used default basis complexity after checking basis size had sufficient flexibility for the smooth terms in the model. Inspection of the diagnostic plots revealed that the Poisson distribution did a moderately acceptable job of handling residual errors (Fig. 2.3). The residuals to fitted values in the first plot possessed bands and there was a decline from positive to negative valued residuals with increasing fitted densities (Fig. 2.3 top left panel). This pattern occurs in data sets with lots of zeros, as seen here in the 'ākepa data set, where the fitted value is zero, than the observed values have to be zero or greater, so the residuals at the left-hand end of this plot cannot be negative. There appeared to be no other un-modelled residual structure. The number of data points obscured heteroscedasticity patterns in the residuals fitted to the `Easting` variable (Fig. 2.3 top right panel), apart from influences in the sampling design of the transects and points (Chapter 1 Fig. 1.1): the geographic layout of points influenced coverage in the west versus east half of the study area with sampling in the west half more than twice that in the east, although there was good spread in the residuals within each half. Observed densities of zero influenced the negative residual values, particularly in the eastern half (Fig. 2.3 top right panel).

Similar patterns of heteroscedasticity occurred for residuals fitted to the `Northing` variable (Fig. 2.3 middle left panel). In the south half of Hakalau the transects run west to east at roughly 500 m apart parallel to the Northing coordinate (see Chapter 1 Fig. 1.1), yielding the banding pattern in the residuals (Fig. 2.3 middle left panel). In the north half the transects run diagonal to the Northing coordinate providing more complete coverage. The spread in the residuals was good within each half, although densities of zero influenced negative residual values more so in the north than south half. Mean residuals by `Year` appeared to decrease and uncertainty increased across the time series, although there was no apparent pattern in the residual outliers (Fig. 2.3 middle right panel). The numbers of points sampled in the south half of the study area halved starting in 2005 with roughly every other transect dropped (Appendix B Fig. B.1). This likely influenced the mean residuals decrease in the latter part of the time series and resulted in the increased uncertainty in these residuals (Fig. 2.3 middle right panel). The histogram of residuals revealed a spike in the number of slightly negative to zero residuals (again the influence of the many zero counts where the fitted values are just slightly above zero with slightly negative residuals), and there was a long right-tail in the numbers of positive residual values (Fig. 2.3 bottom panel). The quantile-quantile (QQ) plot showed that the

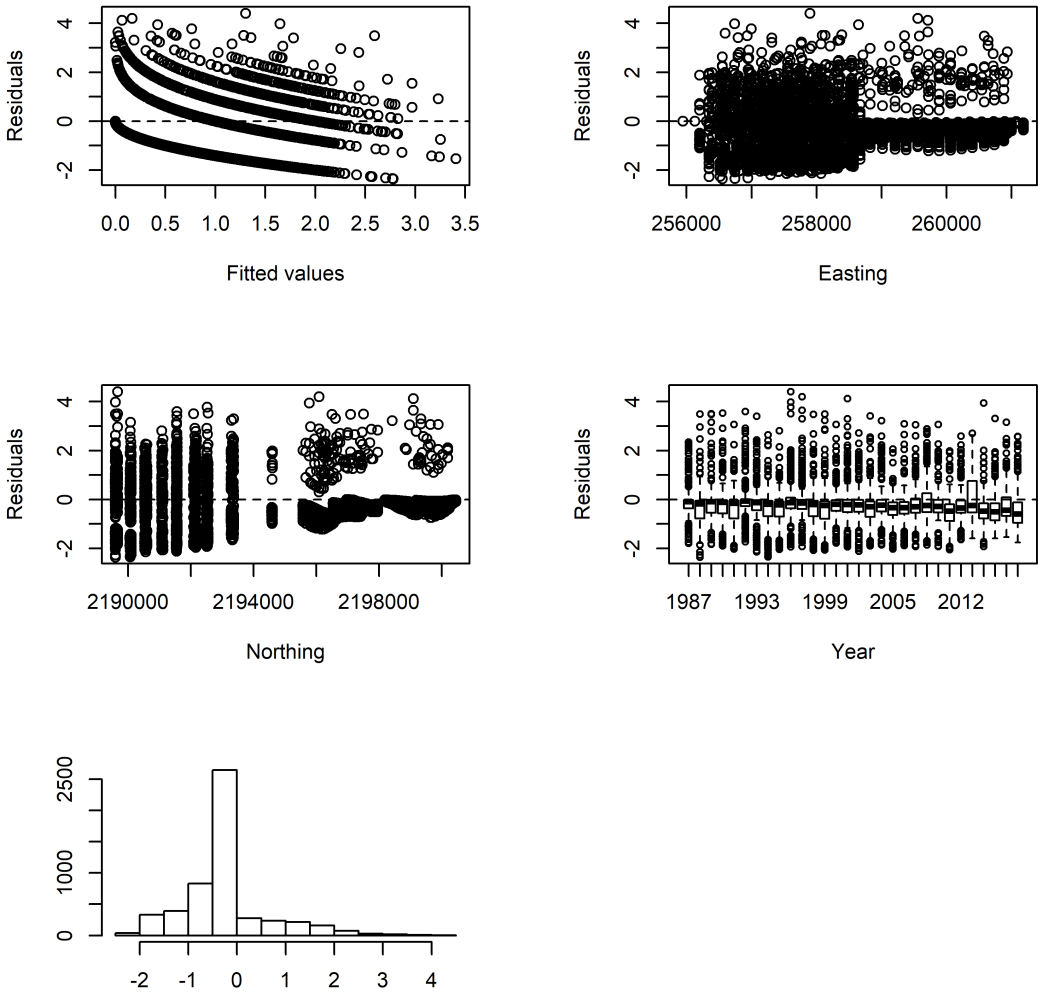

Figure 2.3: Diagnostic plots for spatio-temporal GAM with a Poisson distribution fitted to the 'ākepa count data. Residuals versus fitted values (top left panel), residuals versus easting (top right panel), residuals versus northing (middle left panel), residuals versus year (middle right panel), and histogram of residuals (bottom panel).

Table 2.1: Model selection statistics for the Poisson, negative binomial and Tweedie distributions. Presented are the smoother log-likelihood (logLik), effective degrees of freedom (EDF), Akaike's information criterion (AIC) and Δ AIC.

Model	logLik	EDF	AIC	Δ AIC
negative binomial	-3782.087	50.226	7664.627	0
Poisson	-3861.313	74.503	7871.632	207.005
Tweedie	-4301.308	50.214	8703.046	1038.419

predicted values fell outside the simulation along the entire quantile plot (Fig. 2.4).

For the negative binomial distribution the diagnostic plots were examined and revealed similar patterns as the Poisson distribution (Fig. 2.5). However, from the QQ-plot (Fig. 2.4) it was apparent that the negative binomial distribution, better modelled the residuals as there was less deviation from the straight line and the points stayed within the grey lines. The dispersion parameter for the negative binomial was 1.94 indicating the count data were over-dispersed relative to the Poisson.

Inspection of the diagnostic plots were examined and revealed that the residuals of the Tweedie distribution looked similar to those of the Poisson distribution, but that the Tweedie distribution did not perform as well as the negative binomial distribution. Again, this was particularly apparent in the QQ-plot (Figs. 2.4 and 2.6). The Tweedie dispersion parameter ϕ was 1.483 and the power parameter p was 1.1 for the full model.

In addition to model selection using residuals diagnostics, I also computed AIC with an additional penalty term to account for smoothing parameter issues (Wood 2017). The negative binomial had the lowest AIC value (Table 2.1). Given the residuals diagnostics and AIC statistics I chose the negative binomial distribution for the GAM.

The residual plots for the negative binomial distribution appeared reasonable with acceptable behaviour for the deviance residuals and error distribution for the spatio-temporal GAM (Figs. 2.4 and 2.5). In addition to the residuals diagnostics and summary statistics, violin plots allow for comparing the probability density of the residuals and identifying systematic departures from the distribution. Easting and Northing categories used in the violin plots can be compared to intervals in Chapter 1 Fig. 1.1. For the `Easting` variable the residuals were highly concentrated around the median with many outliers (Fig. 2.7). The distribution of the `Northing` residuals was mixed. In the southern portion of the study area the residuals were more evenly distributed than in the northern portion where the residuals were more concentrated around the median. Again, there were many outliers (Fig. 2.8). There was a concentration of the residuals around the median in the `Year` term and there were a large number of outliers (Fig. 2.9). The medians of the residuals were consistently below the zero line indicating the predicted values tended to be too high.

As described in the Methods, a model with maximum flexibility was fit to the residuals from the selected model to help uncover any remaining pattern. From this model, the EDF values were approximately zero and the basis complexity values were near 1.0 (Table 2.2) suggesting that there was little un-modelled residual auto-correlation. Unaccounted for residual pattern may be the result of not starting with sufficiently complex basis. As a final check I doubled the basis complexity of the full spatio-temporal model with a neg-

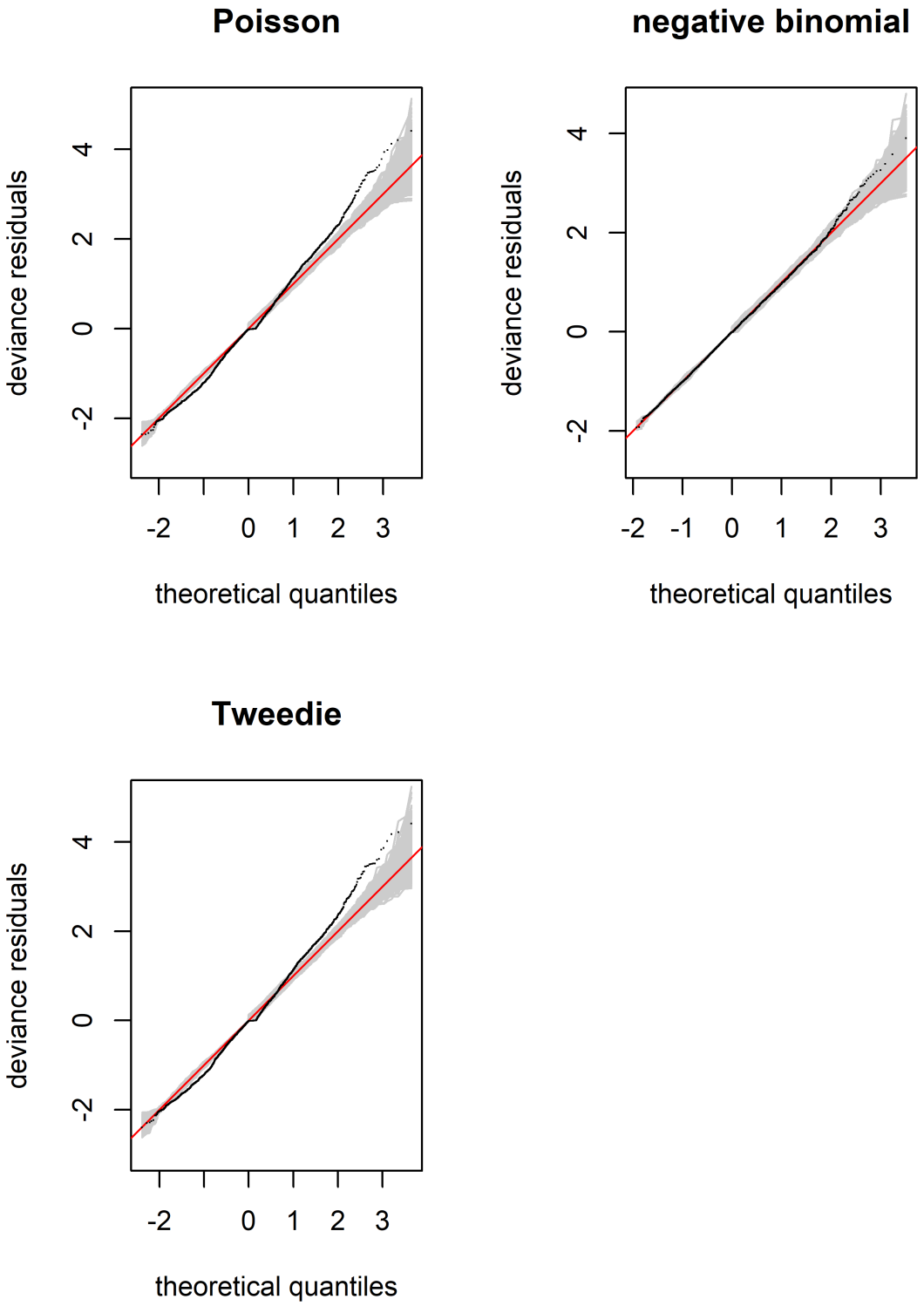

Figure 2.4: Sorted deviance residuals (black dots) for the spatio-temporal GAM versus simulated theoretical quantiles (grey lines; 1,000 replicates) fitted to the 'ākepa count data for the distributions Poisson, negative binomial and Tweedie.

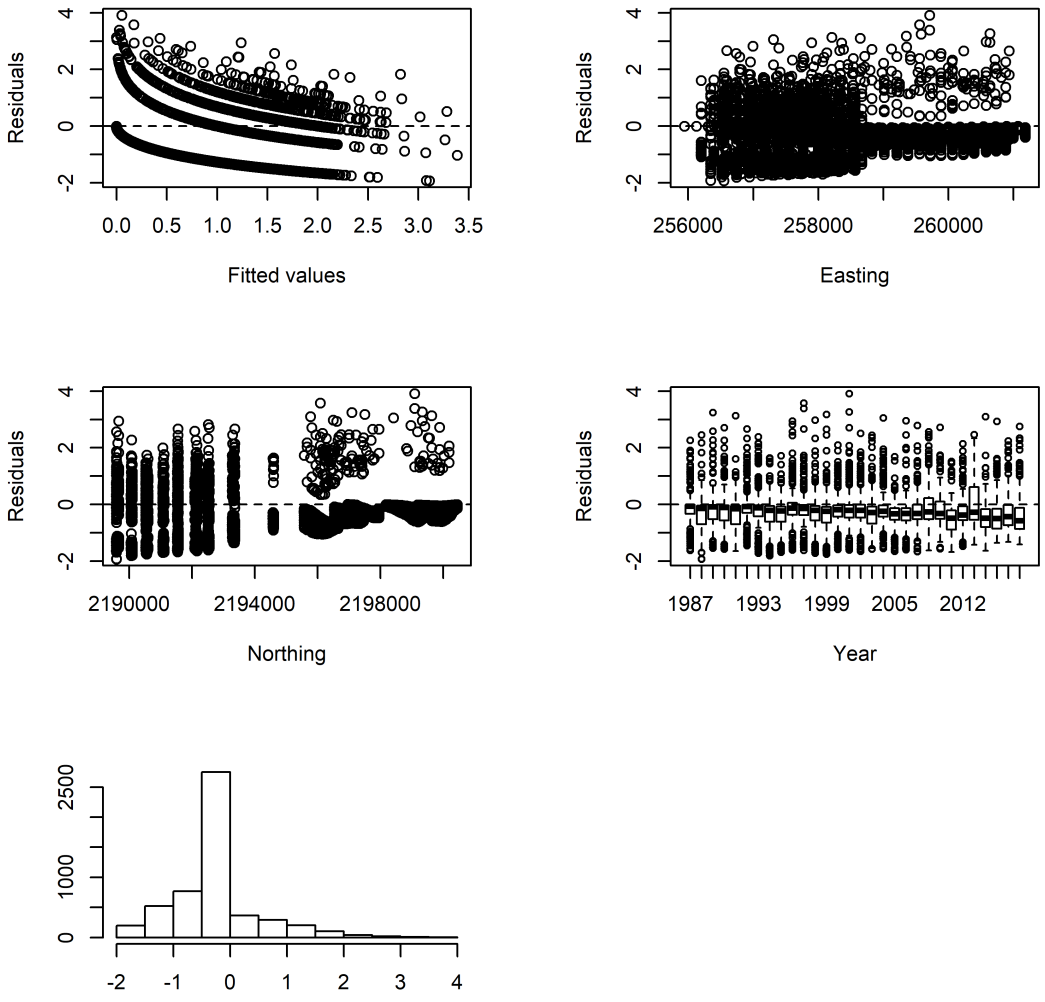

Figure 2.5: Diagnostic plots for spatio-temporal GAM with a negative binomial distribution fitted to the 'ākepa count data. Residuals versus fitted values (top left panel), residuals versus easting (top right panel), residuals versus northing (middle left panel), residuals versus year (middle right panel), and histogram of residuals (bottom left panel).

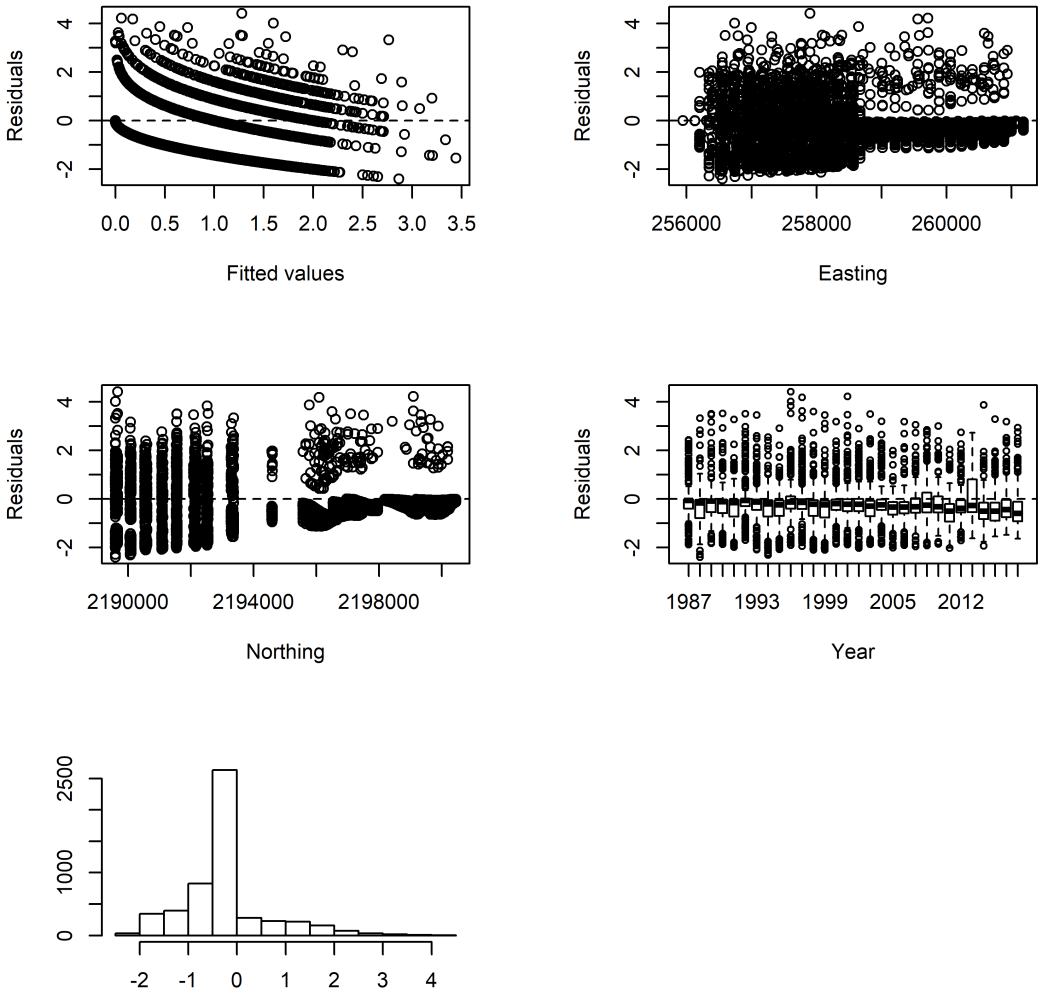

Figure 2.6: Diagnostic plots for spatio-temporal GAM with a Tweedie distribution fitted to the 'ākepa count data. Residuals versus fitted values (top left panel), residuals versus easting (top right panel), residuals versus northing (middle left panel), residuals versus year (middle right panel), and histogram of residuals (bottom left panel).

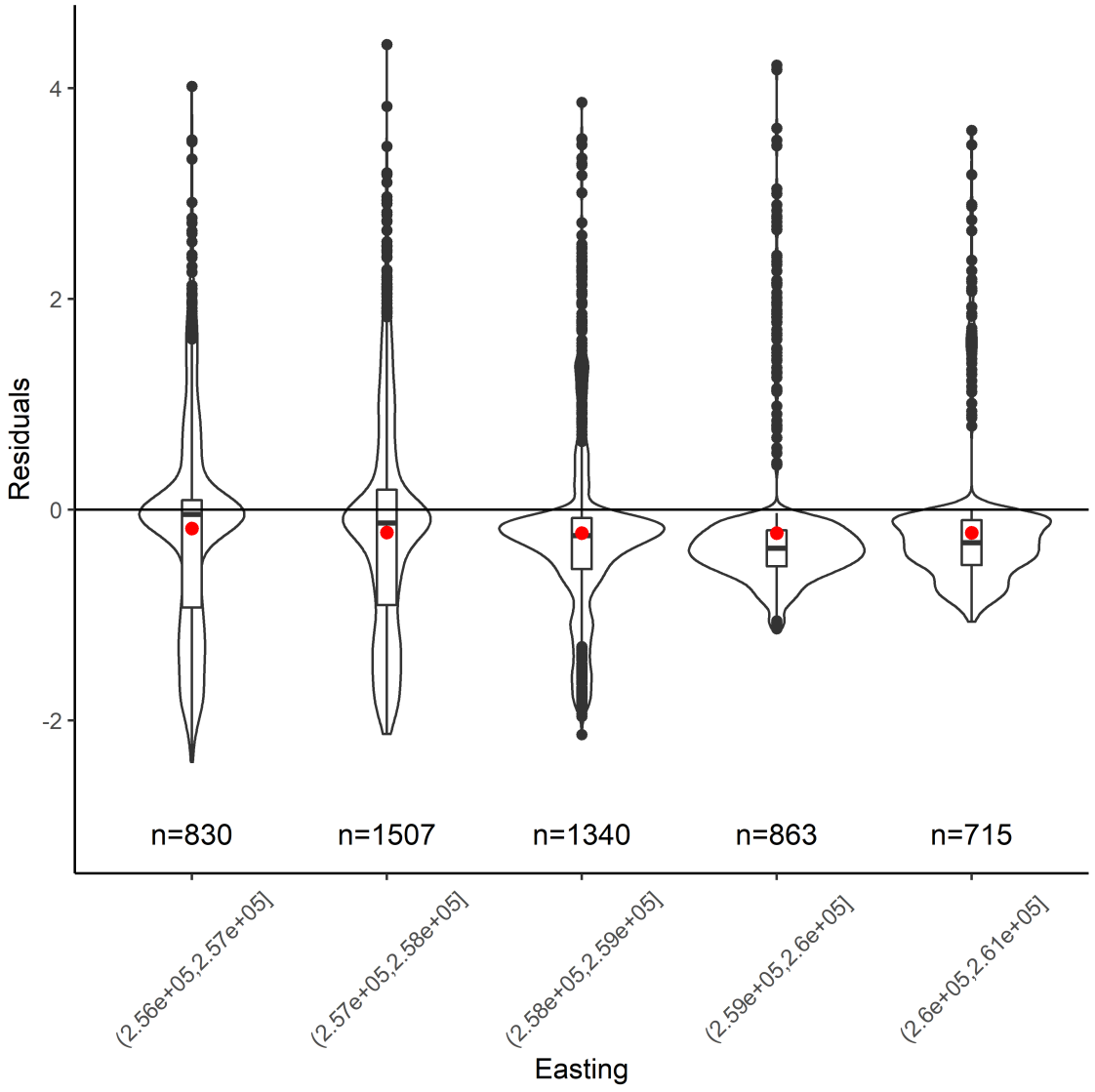

Figure 2.7: Violin plot of deviance residuals for the `Easting` term of the spatio-temporal GAM fitted to the ʻākepa count data. A violin plot is a combination of a box plot and density plot that shows the distribution shape of the data. The red dot is the median and the black bar the mean. The interquartile range is indicated by the box and the whiskers the upper and lower adjacent values. Black dots indicate outliers. The density plot portion reveals the distribution of the data showing probability, relative amplitude, of observations. Sample size is included for each category. The distribution of the `Easting` residuals were highly concentrated around the median with many outliers.

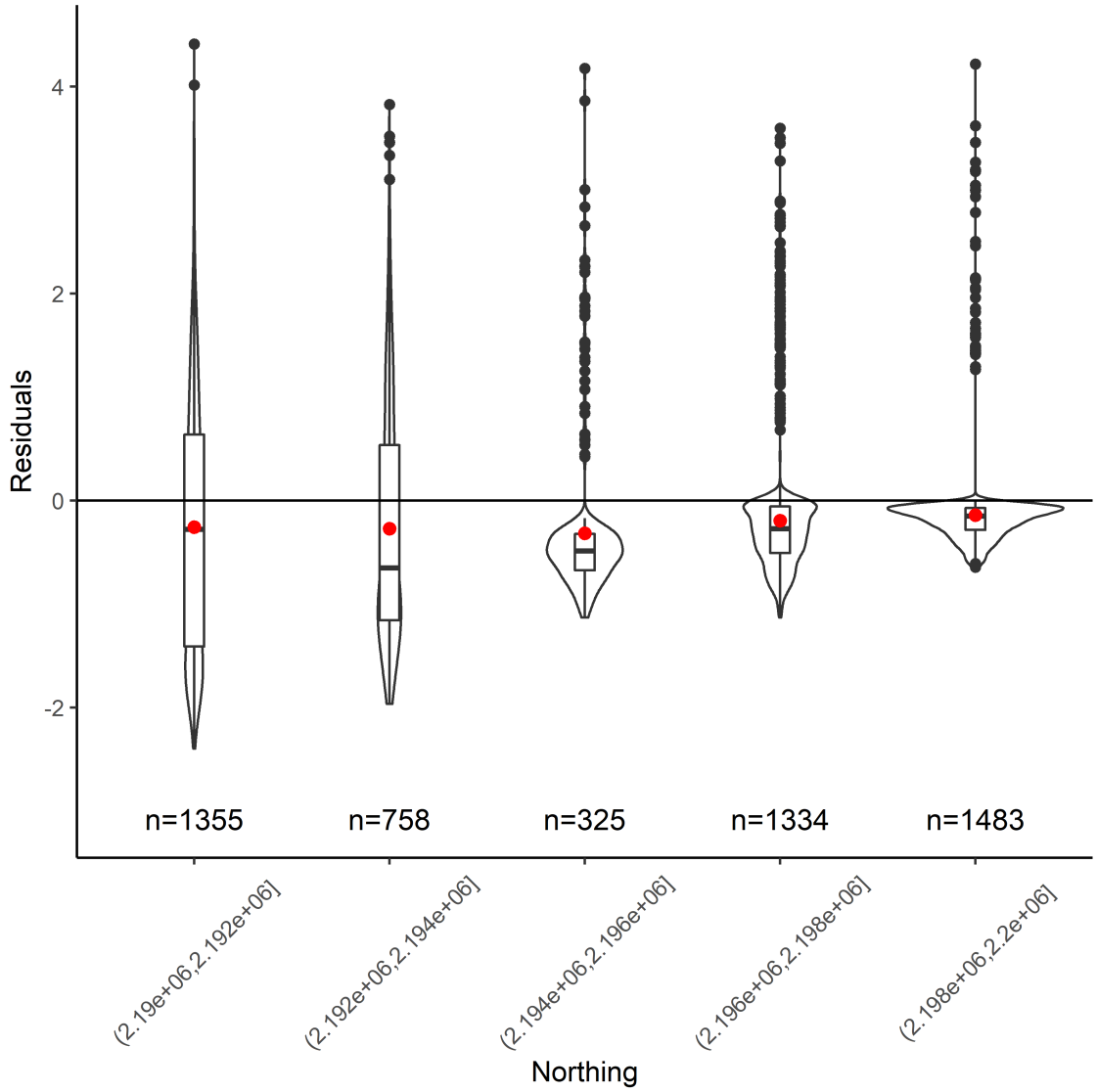

Figure 2.8: Violin plot of deviance residuals for the `Northing` term of the spatio-temporal GAM fitted to the 'ākepa count data. Sample size is included for each category. The distribution of the `Northing` residuals was mixed. In the southern portion of the study area the residuals were more evenly distributed than in the northern portion where the residuals were more concentrated around the median. Again, there are many outliers.

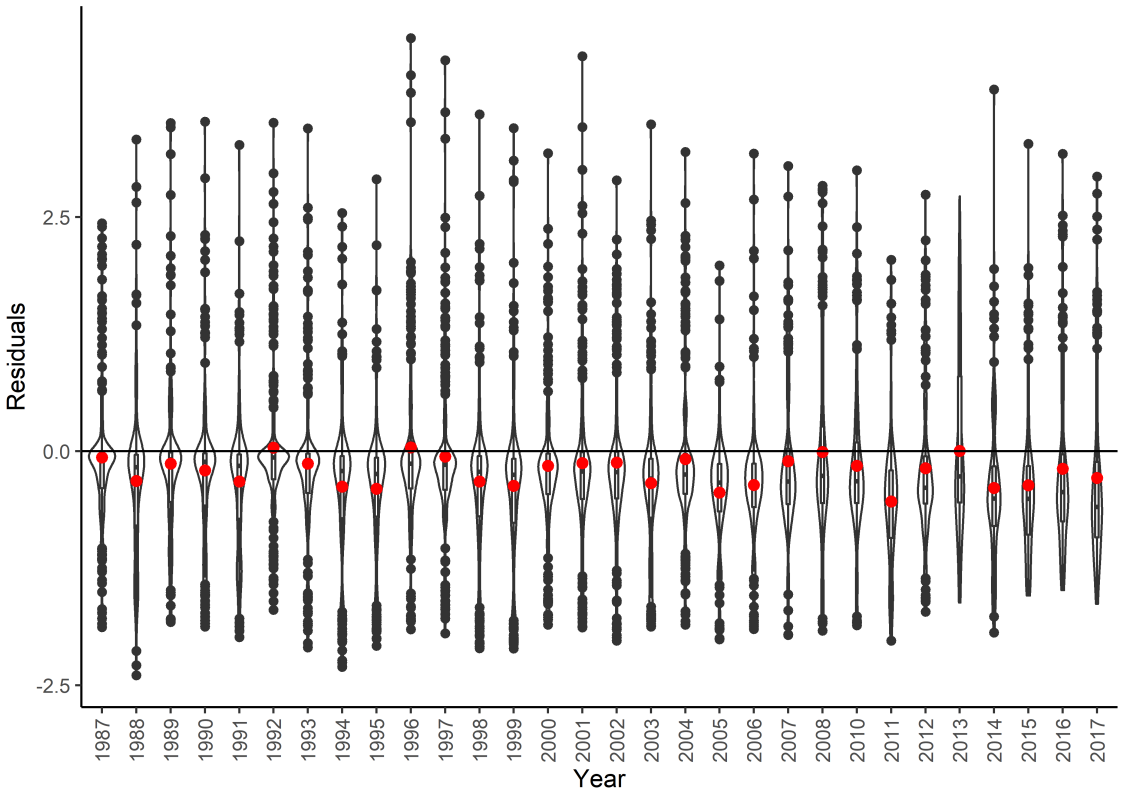

Figure 2.9: Violin plot of deviance residuals for the `Year` term of the detection probability and spatio-temporal GAM fitted to the 'ākepa count data. There was a concentration of the residuals around the median in the `Year` term and there were a large number of outliers. The medians of the residuals were consistently below the zero line indicating the predicted values tended to be too high.

Table 2.2: Effective degrees of freedom (EDF), reference degrees of freedom (rf) and basis complexity (k-index) for each term in the model fitted to the residuals.

Term	EDF	rf	k-index
`s(Easting)`	0.0004	9	0.98
`s(Northing)`	0.0004	9	0.99
`s(Year)`	0.0003	9	0.96
`ti(Easting, Northing)`	0.0009	16	0.97
`ti(Easting, Year)`	0.0006	16	1.02
`ti(Northing, Year)`	0.0005	16	0.84
`ti(Easting, Northing, Year)`	0.0002	88	0.86

ative binomial distribution. Residual plots were not much improved relative to the model with default basis factors and this procedure provides evidence against misspecification problems (plots not shown).

2.4.2 Fitted model

For the model fit to the data the estimated negative binomial dispersion parameter was 1.944 and the deviance explained was 52.7%. The estimated smooth function for the interaction of `Easting` and `Year` had shrunk to nearly zero, thus the influence of this term on the response was negligible (Table 2.3). The smooth functions were wiggly for the variables `Easting`, `Northing` and `Year` (Fig. 2.10). There was a clear pattern of lower densities in the east versus west side of Hakalau, as well there were lower densities in the north than in the south part of Hakalau, and there was a small general increase in densities over time. In addition, the interactions of `Easting` and `Northing`, `Northing` and `Year` (Fig. 2.10), and the three way interaction `Easting`, `Northing` and `Year` were nonlinear (Fig. 2.11). Densities in the `Easting` and `Northing` interaction ranged from 3 in the south-west corner to -3 at the west central lobe and north-east corner. The magnitude of densities for the `Easting` and `Year` interaction were very small ranging from -0.0014 in the upper left and right corners to 0.001 in the lower left and right corners and between the upper corners (Fig. 2.10, lower left panel). The magnitude change in densities was greater for the `Northing` and `Year` interaction ranging from -1.5 in the upper left and lower right corners to 1.5 in the opposite corners (Fig. 2.10, bottom right panel). The three way interaction `Easting`, `Northing` and `Year` prediction plots showed densities varied spatially and temporally (Fig. 2.11). At the beginning of the time series densities varied from -0.6 to 0.6 with highest contours in the north-east lobe and lowest contours in the central portion of Hakalau along the the west boundary (Fig. 2.11, bottom row). During the middle of the time series densities were more uniform across Hakalau with contours ranging from -0.2 to 0.2 or less (Fig. 2.11, middle row). By the end of the time series densities had again increased with contours ranging from -1.0 to 1.0, but between the beginning and end of the time series the location of the low and high contours had swapped sides of Hakalau (top row compared to bottom row; Fig. 2.11).

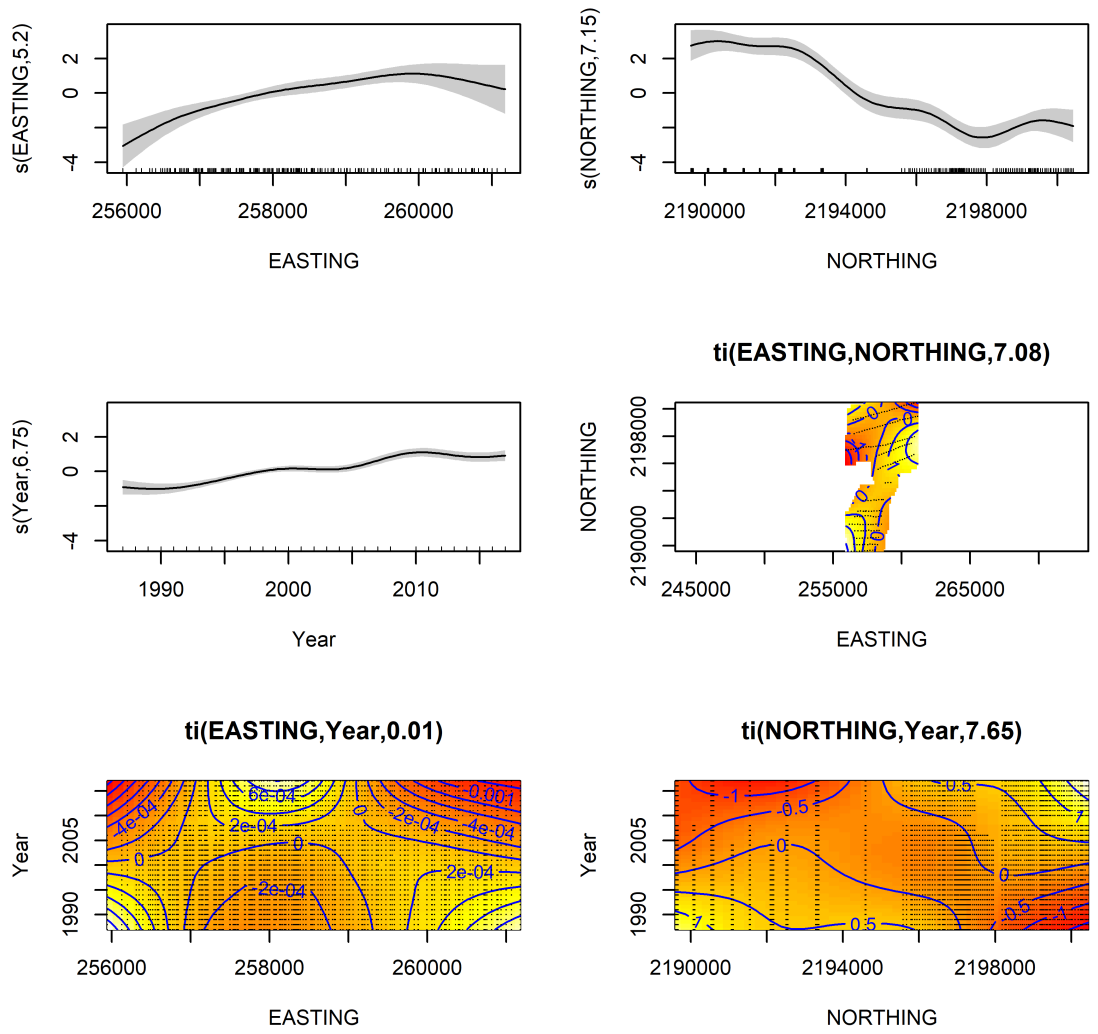

Figure 2.10: Estimated model terms for the spatio-temporal GAM fitted to the 'ākepa count data. The distribution of the data is visualized in the rug plot along the x-axis for the 1D `Easting`, `Northing` and `Year` plots, while the EDFs are presented on the y-axis labels. For the main effects the grey ribbon illustrates the error bounds of plus or minus one standard error from the estimates. The locations of the points are plotted as black dots on the 2D contour plots and the EDF is provided in the plot panel title. Contours in each 2D plot represent 1.0, 0.002 and 0.5 unit change (respectively) and are shown as blue lines. Estimates provided on the scale of the linear predictor.

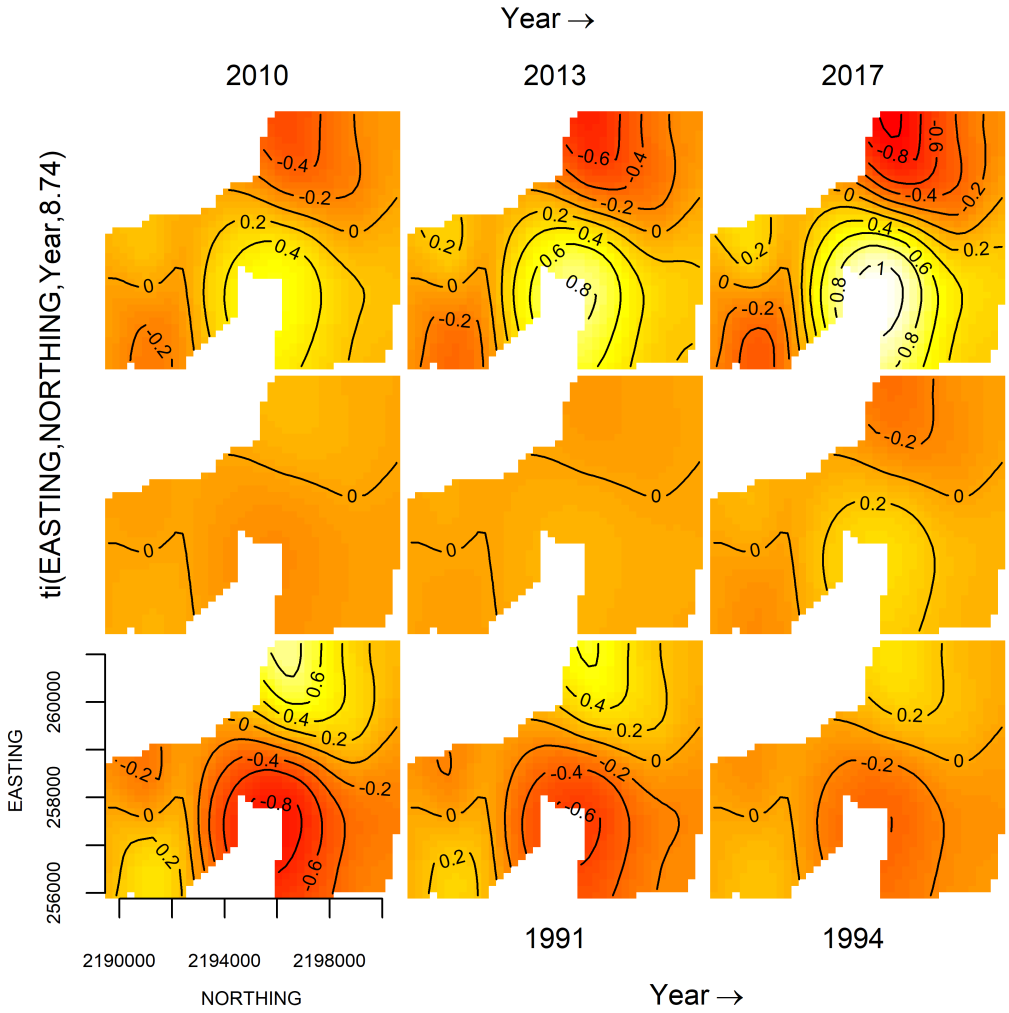

Figure 2.11: Estimated model terms for the 3-way smooths of the spatio-temporal GAM fitted to the 'ākepa count data. Maps shown for every three or four years between 1987 and 2017. Variability is minimal during the middle of the time series (middle row) and more variable early and late in the time series (bottom and top rows, respectively). The EDF is provided on the y-axis label and contours represent 0.2 unit change are shown as black lines.

Table 2.3: Effective degrees of freedom (EDF), reference degrees of freedom (rf) and basis complexity (k-index) for each term in the fitted spatio-temporal model.

Term	EDF	rf	k-index
`s(Easting)`	5.204	9	0.90
`s(Northing)`	7.145	9	0.89
`s(Year)`	6.755	9	0.91
`ti(Easting, Northing)`	7.084	16	0.89
`ti(Easting, Year)`	0.012	16	0.95
`ti(Northing, Year)`	7.653	16	0.76
`ti(Easting, Northing, Year)`	8.737	88	0.84

Table 2.4: Effective degrees of freedom (EDF) and basis complexity (k-index) for each smoother term in the fitted spatio-temporal model with `Habitat`.

Term	EDF	rf	k-index
`s(East)`	5.056	9	0.91
`s(North)`	7.101	9	0.91
`s(Year)`	6.680	9	0.89
`ti(East, North)`	6.507	16	0.89
`ti(East, Year)`	1.716	16	0.94
`ti(North, Year)`	3.513	16	0.75
`ti(East, North, Year)`	21.475	88	0.80

2.4.3 Spatial model including habitat

Results indicated that including `Habitat` minimally improved the spatio-temporal model. Residual plots (Fig. 2.12) appeared reasonable. The EDFs for the smoother terms were similar to those from the smoother-only model (compare Table 2.4 to Table 2.3). The deviance explained was 53%, providing only a small increase in modelling residual variance. Compared to the smoother-only model the AIC value for the smoother with habitat model was larger by >16 units. Adding the `Habitat` variable should change the AIC value by no more than 2 AIC units; however, the standard AIC formulation in `mgcv` is modified to account for the smoother EDF in the model. Adding another covariate changes the number of EDF parameters yielding an AIC value that can change by more than two AIC units (Hastie and Tibshiani 1990 pgs 157-158 and Wood 2017 pgs 301-302). Therefore, habitat was dropped and spatio-temporal inference was based on the smoother-only model.

2.4.4 Spatio-temporal patterns

Densities of Hawai'i 'ākepa vary both spatially and temporally (Fig. 2.13). Across the time series densities remained low in the northern portion of the refuge, but densities were much more dynamic in the central and southern parts of the refuge. Starting in 1987 an area of high density occurred in the south-west that diminished over several years before increasing and persisting into the mid-1990s. This high density area then appeared to diffuse into the central portion of the refuge through the early 2000s before a high density area reformed to the north-east of its original location, and by the late 2000s had reached densities of 6 birds ha^{-1}. The high density area subsequently diffused again to moderate numbers of birds by the end of the time series, 2-3 birds ha^{-1}.

Overshadowed by the dynamics in the southern half of Hakalau, subtle changes occurred throughout the north. Early in the time series the northern portion was roughly split between an area devoid of 'ākepa and an area with <0.25 birds ha^{-1}. This pattern persisted into the mid-1990s before 'ākepa started increasing and expanding so that by 2017 the area devoid of 'ākepa was restricted to a small patch in the north-west portion of Hakalau (Fig. 2.13).

Uncertainty in densities are shown in maps of coefficient of variation (Fig. 2.14). The per cell uncertainty in densities was large with CVs ranging from 0.09 to 2.02 per cell and varied spatially. Densities were most precise in the southern portion and most variable in

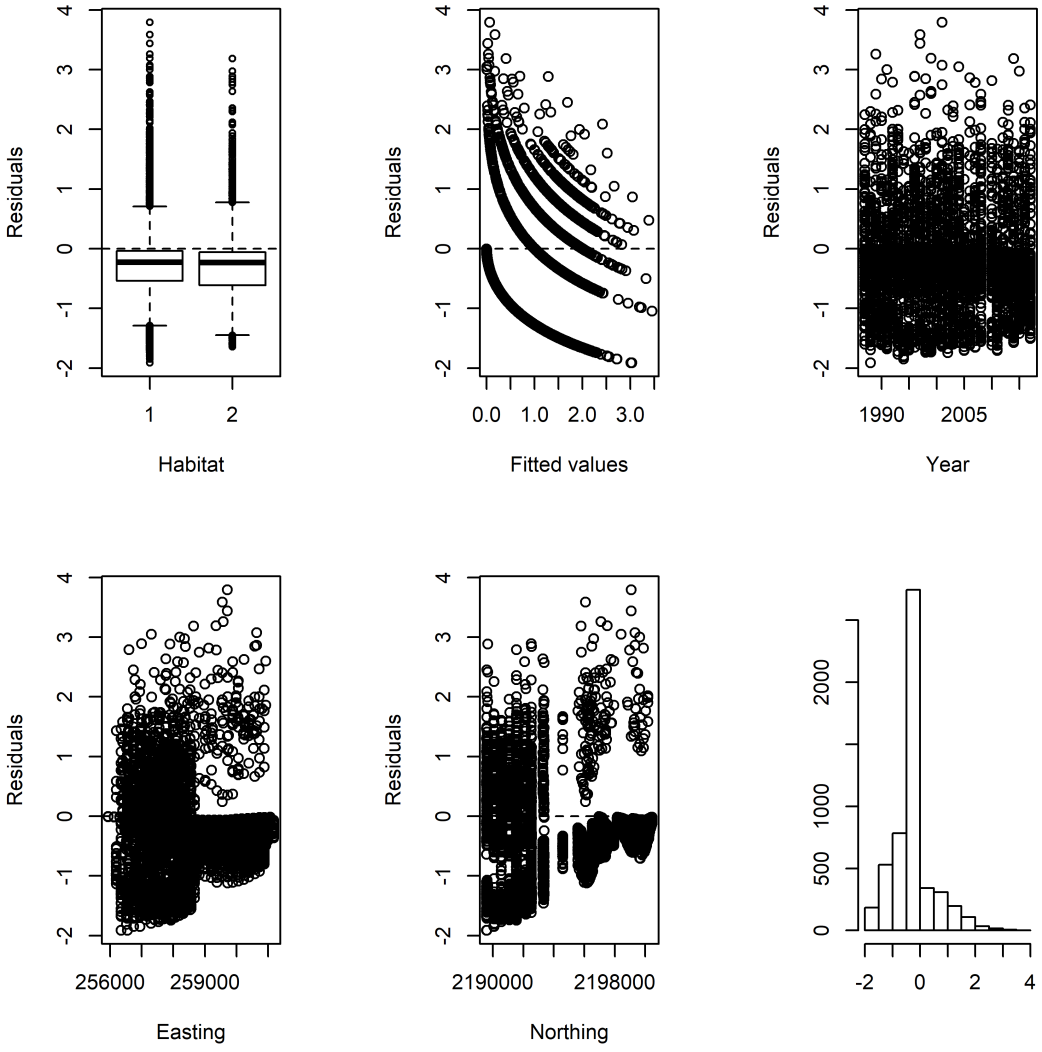

Figure 2.12: Diagnostic plots for spatio-temporal model that included categorical `Habitat` term fitted to the 'ākepa count data. Box plot of residuals versus habitat type (1 = wet and 2 = mesic; top left panel; the black bar is the mean while the interquartile range is indicated by the box, the whiskers are the upper and lower adjacent values and the black dots indicate outliers), residuals versus fitted values (top middle panel), residuals versus year (top right panel), residuals versus easting (bottom left panel), residuals versus northing (bottom middle panel), and histogram of residuals (bottom right panel).

the northwest portion of the study area which was consistent with the amount of effort that was put into those areas. These patterns persisted across the entire time series.

2.4.5 Temporal patterns

Initially estimated at 0.54 birds ha^{-1} the 'ākepa population increased between 1987 and the late 2000s to a maximum of 0.89 birds ha^{-1}, and subsequently declined to 0.84 birds ha^{-1} in 2017; note that these changes occurred within the confidence band (Fig. 2.15, top panel; Table 2.5). Trends in the two regions of the study area were substantially different. Trends in the north stratum were generally upward throughout the time series while trends in the south stratum oscillated (Fig. 2.15, bottom panels left and right, respectively). Average densities also differed between the two strata. Densities in the north stratum were more than an order of magnitude smaller than the densities observed in the south stratum (means of 0.16 birds ha^{-1} compared to 2.16 birds ha^{-1}, respectively; Tables 2.6 and 2.7). These patterns were reflected in the spatio-temporal maps (Fig. 2.13).

2.4.6 Uncertainty comparison between methods

I observed improvements in annual estimator precision for the model-based approaches, relative to the design-based approach of Chapter 1 (Fig. 2.15, Table 2.5). Although the pooled detection probability was very precise (pooled $\hat{p} = 0.489$, SE=0.006, %CV=1.20), the year-specific probabilities of detection were variable (see Chapter 1 Table A.1). The model-based estimate with delta method to combine variances gives on average a CI width that was 52.5% shorter than the CI width of the design-based method (SD=19.4%; Table 2.5). This pattern was more prominent in the north stratum where design-based CI widths were wider than in the south stratum. There was an average 90.5% reduction in the length of the CI widths (SD=6.4%; Table 2.6) in the north stratum, while the average CI width was 58.5% shorter in the south stratum (SD=16.0%; Table 2.7). The delta method violates the assumption that the detection probability is an independent parameter between the first- and second-stage models and the procedure produces confidence intervals that were too precise.

Using the approach of Bravington et al. (2018) avoids this assumption while simultaneously accounting for spatial and temporal correlation. I fitted a hazard-rate detection function with a covariate for each survey year to the distances in both Distance for Windows (Thomas et al. 2010) and the `ds` function of `Distance` for R (Miller et al. 2019). The two software packages use slightly different algorithms thus there were minor differences in the detection probabilities and variances (Fig. 2.16, Table 2.8). Although differences in the estimates exist, the advantage of using the `ds` generated parameters is that it integrates easily with `dsm`. The average CI width using the variance propagation method was 37.2% shorter than the design-based CI width (SD = 26.6%; Fig. 2.15, top panel; Table 2.5). This was a substantial improvement over estimates from design-based methods and was not reliant on the assumption of parameter independence. In the north stratum there was an average 83.3% reduction in the length of the CI widths (SD = 11.5%; Fig. 2.15, bottom left panel; Table 2.6). While in the south stratum the variance propagation method CI

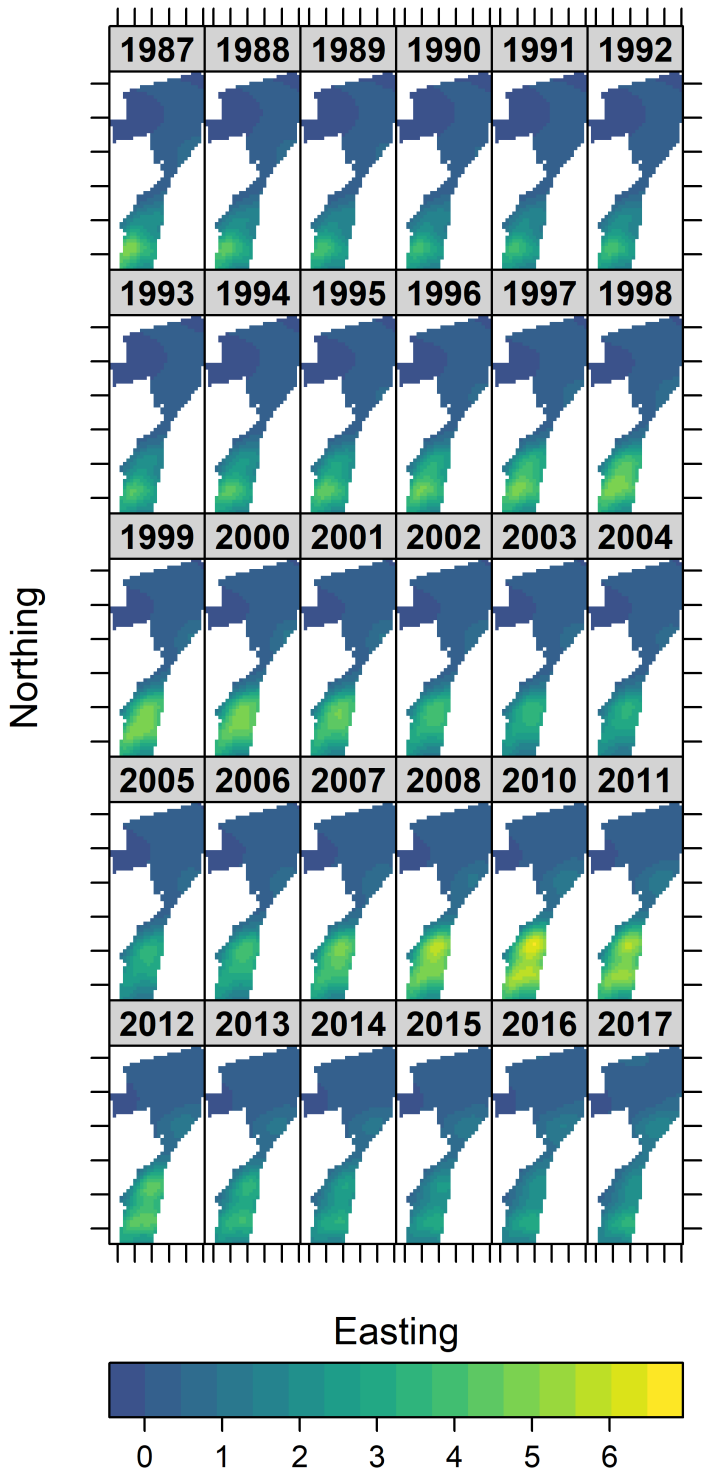

Figure 2.13: Predicted spatio-temporal surfaces of 'ākepa densities in Hakalau between 1987 and 2017. Densities range from 0 (violet) to 6 birds ha^{-1} (yellow) within the study area.

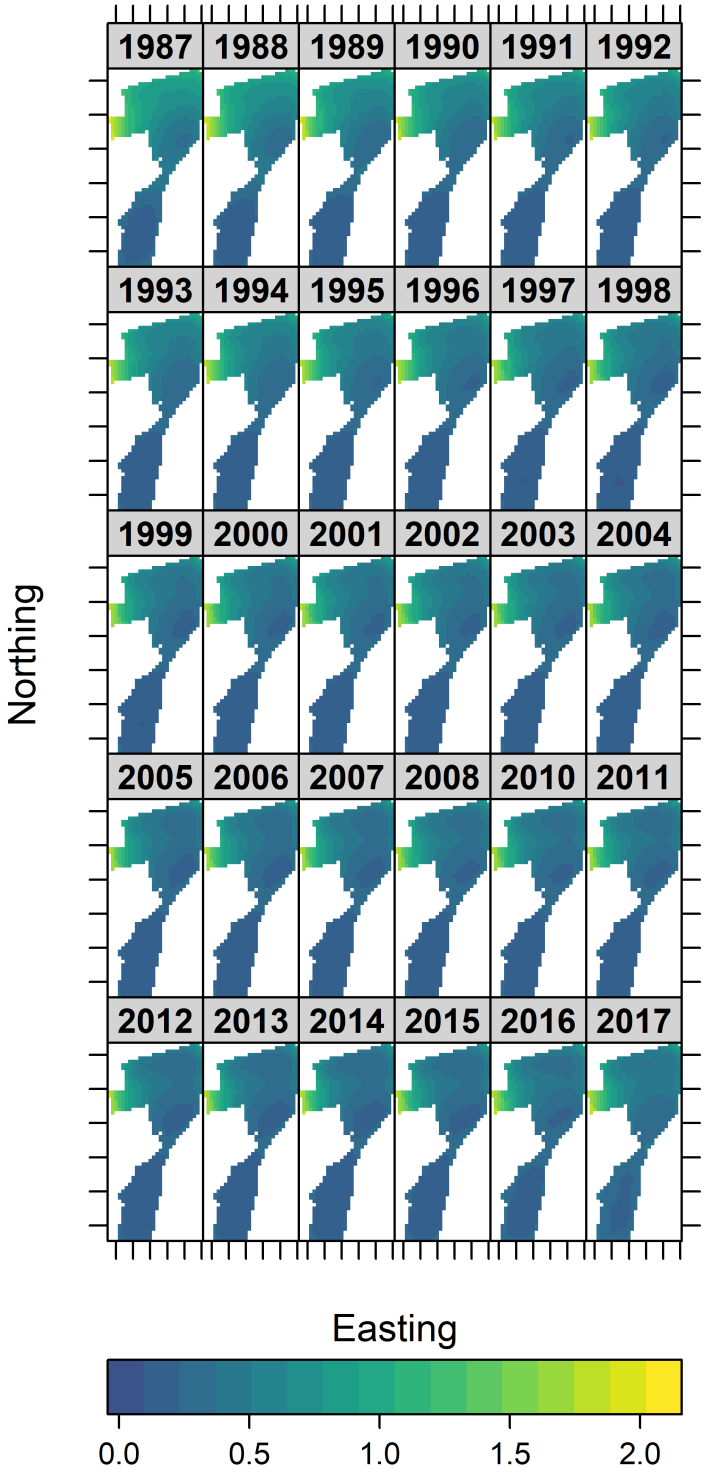

Figure 2.14: Predicted spatio-temporal maps of density (birds ha^{-1}) coefficient of variation.

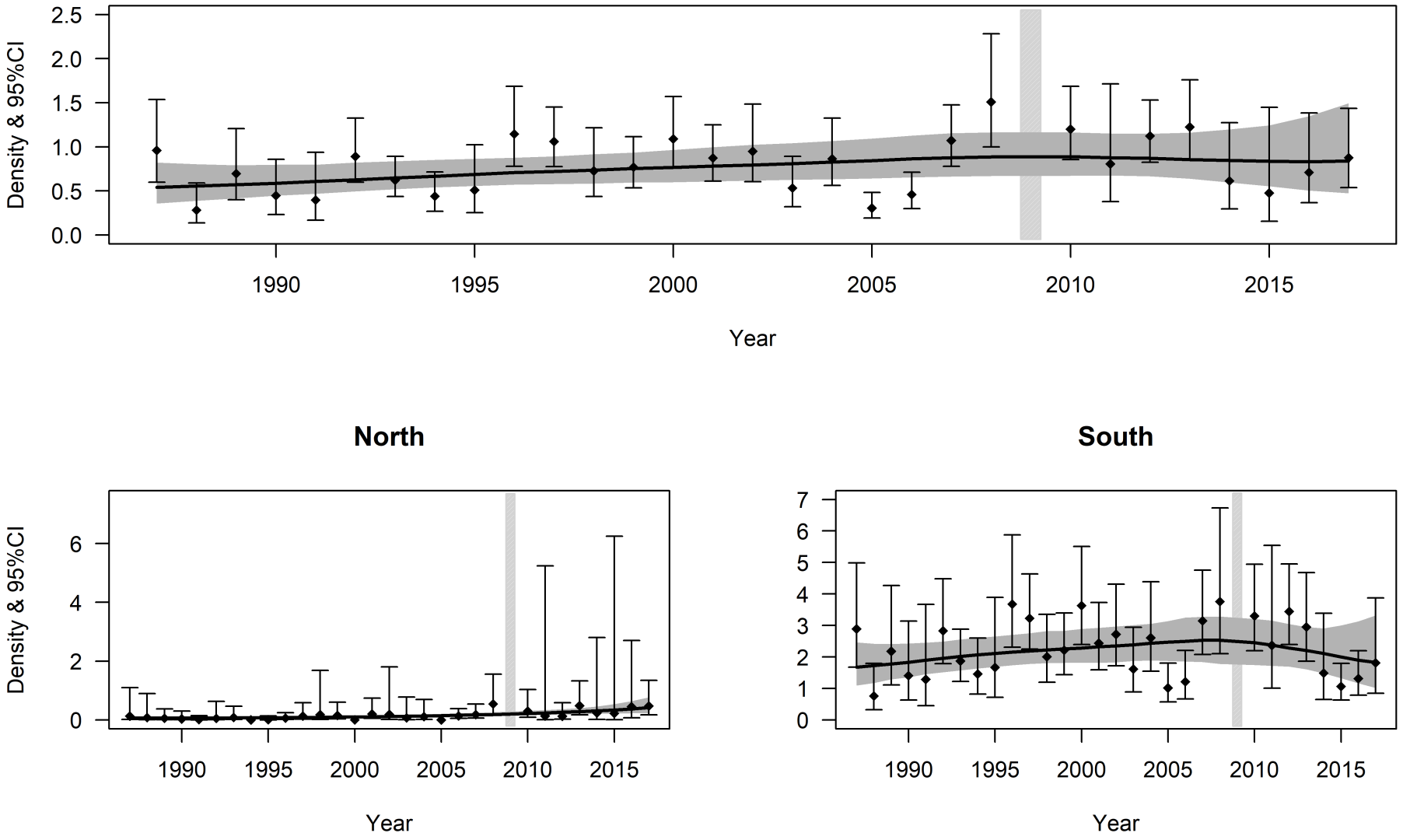

Figure 2.15: Predicted trends derived from the spatio-temporal GAM for the 'ākepa population across Hakalau (top panel), north (bottom left panel) and south (bottom right panel) strata of Hakalau. GAM generated density (birds ha^{-1}) estimates (black line) with detection probability variance propagated uncertainty (95%CI; grey ribbon). Density estimate with 95%CI from Distance for Windows (diamond and whisker bar). Surveys were not conducted in 2009 (vertical bar).

Table 2.5: Density (Est), width of confidence interval (CIW) and percent change in confidence interval width (%Chg) produced from design-based (DB), delta (DM) and variance propagation (VP) methods for the study area.

Year	Est_DB	CIW_DB	Est_DM	CIW_DM	%Chg_DM	Est_VP	CIW_VP	%Chg_VP
1987	0.959	0.937	0.871	0.453	-51.689	0.541	0.464	-50.505
1988	0.283	0.453	0.756	0.264	-41.687	0.556	0.415	-8.361
1989	0.696	0.807	0.673	0.286	-64.549	0.572	0.376	-53.378
1990	0.446	0.627	0.625	0.270	-56.896	0.587	0.350	-44.201
1991	0.396	0.769	0.611	0.250	-67.461	0.607	0.329	-57.189
1992	0.891	0.729	0.625	0.238	-67.321	0.625	0.325	-55.342
1993	0.622	0.455	0.662	0.198	-56.513	0.646	0.318	-30.089
1994	0.438	0.444	0.716	0.232	-47.718	0.666	0.311	-29.957
1995	0.509	0.769	0.781	0.252	-67.283	0.688	0.306	-60.190
1996	1.147	0.908	0.856	0.263	-71.011	0.707	0.307	-66.160
1997	1.061	0.676	0.931	0.324	-52.016	0.721	0.317	-53.136
1998	0.727	0.780	0.995	0.337	-56.788	0.737	0.333	-57.344
1999	0.770	0.580	1.025	0.316	-45.559	0.753	0.339	-41.676
2000	1.089	0.812	1.008	0.333	-58.928	0.766	0.366	-54.946
2001	0.874	0.638	0.948	0.303	-52.431	0.780	0.388	-39.075
2002	0.948	0.879	0.871	0.245	-72.138	0.794	0.404	-54.063
2003	0.534	0.572	0.811	0.270	-52.851	0.810	0.417	-27.112
2004	0.863	0.764	0.794	0.264	-65.470	0.828	0.434	-43.207
2005	0.305	0.291	0.836	0.320	9.842	0.844	0.451	54.939
2006	0.460	0.415	0.944	0.409	-1.383	0.863	0.474	14.219
2007	1.072	0.697	1.109	0.407	-41.644	0.877	0.490	-29.720
2008	1.509	1.282	1.292	0.500	-61.024	0.885	0.494	-61.478
2010	1.200	0.830	1.457	0.665	-19.905	0.889	0.491	-40.837
2011	0.806	1.335	1.355	0.589	-55.846	0.876	0.476	-64.358
2012	1.123	0.707	1.171	0.461	-34.827	0.870	0.483	-31.668
2013	1.225	0.905	0.986	0.380	-58.064	0.856	0.524	-42.143
2014	0.613	0.978	0.851	0.322	-67.046	0.845	0.600	-38.661
2015	0.476	1.293	0.778	0.355	-72.512	0.836	0.689	-46.692
2016	0.710	1.019	0.757	0.328	-67.775	0.831	0.843	-17.223
2017	0.878	0.900	0.767	0.401	-55.412	0.838	1.021	13.505

Table 2.6: Density (Est), width of confidence interval (CIW) and percent change in confidence interval width (%Chg) produced from design-based (DB), delta (DM) and variance propagation (VP) methods for the north stratum. Estimate not produced indicated with a —.

Year	Est_DB	CIW_DB	Est_DM	CIW_DM	%Chg_DM	Est_VP	CIW_VP	%Chg_VP
1987	0.131	1.087	0.047	0.056	-94.806	0.060	0.083	-92.353
1988	0.079	0.885	0.041	0.041	-95.342	0.061	0.074	-91.678
1989	0.059	0.368	0.036	0.034	-90.780	0.062	0.068	-81.602
1990	0.034	0.298	0.034	0.029	-90.309	0.063	0.061	-79.660
1991	0.014	0.148	0.033	0.026	-82.425	0.064	0.056	-62.253
1992	0.058	0.627	0.035	0.025	-95.967	0.066	0.053	-91.563
1993	0.086	0.452	0.037	0.025	-94.414	0.069	0.051	-88.705
1994	0	—	0.042	0.028	—	0.072	0.051	—
1995	0.012	0.136	0.047	0.031	-77.467	0.075	0.050	-63.127
1996	0.060	0.233	0.054	0.033	-85.758	0.079	0.051	-78.085
1997	0.131	0.555	0.061	0.038	-93.170	0.085	0.054	-90.228
1998	0.179	1.664	0.069	0.042	-97.503	0.090	0.058	-96.507
1999	0.153	0.564	0.075	0.044	-92.153	0.097	0.065	-88.467
2000	0	—	0.078	0.048	—	0.103	0.073	—
2001	0.204	0.680	0.078	0.048	-92.985	0.111	0.076	-88.769
2002	0.188	1.780	0.075	0.045	-97.497	0.119	0.082	-95.418
2003	0.070	0.775	0.074	0.045	-94.249	0.128	0.087	-88.794
2004	0.114	0.679	0.077	0.044	-93.469	0.137	0.094	-86.177
2005	0	—	0.086	0.050	—	0.148	0.101	—
2006	0.139	0.331	0.103	0.063	-81.055	0.159	0.110	-66.765
2007	0.182	0.482	0.130	0.074	-84.663	0.171	0.121	-74.932
2008	0.543	1.363	0.164	0.099	-92.772	0.186	0.131	-90.414
2010	0.300	0.951	0.226	0.148	-84.393	0.219	0.153	-83.944
2011	0.136	5.236	0.236	0.147	-97.196	0.240	0.168	-96.790
2012	0.127	0.562	0.231	0.131	-76.672	0.260	0.183	-67.489
2013	0.484	1.151	0.221	0.121	-89.470	0.285	0.207	-81.992
2014	0.238	2.778	0.218	0.121	-95.652	0.311	0.249	-91.025
2015	0.224	6.238	0.228	0.145	-97.672	0.341	0.319	-94.887
2016	0.452	2.629	0.251	0.166	-93.670	0.376	0.411	-84.366
2017	0.476	1.181	0.288	0.221	-81.276	0.420	0.539	-54.386

Table 2.7: Density (Est), width of confidence interval (CIW) and percent change in confidence interval width (%Chg) produced from design-based (DB), delta (DM) and variance propagation (VP) methods for the south stratum.

Year	Est_DB	CIW_DB	Est_DM	CIW_DM	%Chg_DM	Est_VP	CIW_VP	%Chg_VP
1987	2.891	3.313	2.601	1.332	-59.803	1.677	1.370	-58.647
1988	0.757	1.475	2.267	0.781	-47.003	1.723	1.246	-15.486
1989	2.181	3.151	2.022	0.850	-73.027	1.778	1.126	-64.265
1990	1.408	2.504	1.878	0.801	-68.008	1.833	1.077	-56.969
1991	1.286	3.218	1.831	0.743	-76.912	1.898	0.998	-68.983
1992	2.832	2.697	1.868	0.711	-73.643	1.955	0.977	-63.756
1993	1.873	1.658	1.973	0.590	-64.411	2.018	0.977	-41.079
1994	1.459	1.781	2.130	0.690	-61.269	2.067	0.980	-45.005
1995	1.668	3.171	2.327	0.755	-76.192	2.115	0.971	-69.381
1996	3.680	3.574	2.550	0.807	-77.409	2.156	0.963	-73.050
1997	3.227	2.385	2.775	1.001	-58.042	2.191	0.977	-59.040
1998	2.005	2.157	2.955	1.038	-51.886	2.225	1.018	-52.827
1999	2.210	1.958	3.033	0.970	-50.479	2.254	1.024	-47.715
2000	3.629	3.116	2.968	1.008	-67.660	2.281	1.069	-65.678
2001	2.436	2.140	2.778	0.900	-57.928	2.322	1.107	-48.259
2002	2.719	2.591	2.544	0.708	-72.695	2.355	1.137	-56.115
2003	1.615	2.055	2.360	0.773	-62.395	2.389	1.135	-44.748
2004	2.608	2.841	2.302	0.754	-73.477	2.440	1.169	-58.851
2005	1.016	1.234	2.412	0.910	-26.322	2.468	1.265	2.506
2006	1.210	1.537	2.707	1.155	-24.855	2.501	1.391	-9.537
2007	3.144	2.673	3.158	1.140	-57.345	2.529	1.439	-46.148
2008	3.759	4.628	3.653	1.415	-69.434	2.532	1.504	-67.514
2010	3.298	2.748	4.049	1.869	-31.994	2.458	1.461	-46.835
2011	2.367	4.532	3.717	1.638	-63.857	2.375	1.441	-68.215
2012	3.444	2.551	3.157	1.269	-50.264	2.287	1.346	-47.234
2013	2.953	2.813	2.600	1.025	-63.546	2.206	1.339	-52.400
2014	1.487	2.737	2.184	0.855	-68.775	2.111	1.431	-47.704
2015	1.063	1.164	1.932	0.922	-20.795	2.002	1.676	43.972
2016	1.313	1.411	1.808	0.859	-39.159	1.898	1.963	39.117
2017	1.814	3.026	1.754	1.019	-66.337	1.832	2.298	-24.069

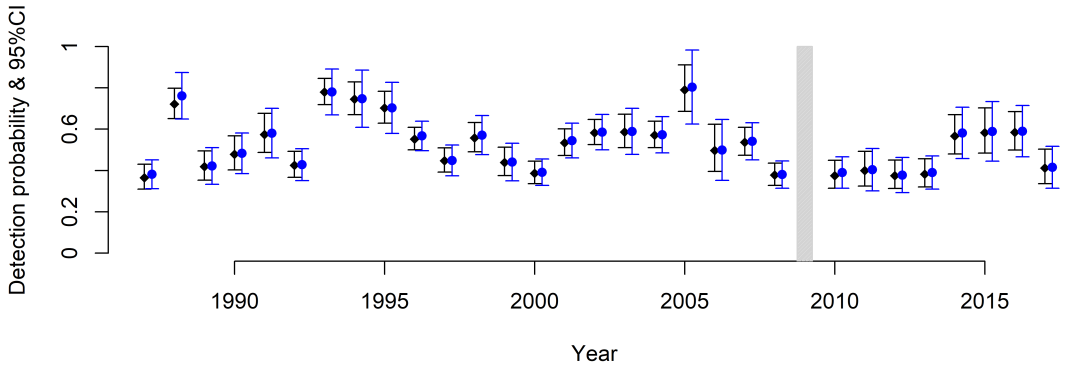

Figure 2.16: Annual detection probability and 95%CI estimates from the hazard-rate model without series expansion and with the covariate `Year` produced using Distance for Windows (black diamonds and whisker bars) and `ds` (blue diamonds and whisker bars). Surveys were not conducted in 2009 (vertical bar).

width was on average 43.8% shorter than the design-based method CI width (SD = 29.3%; Fig. 2.15, bottom right panel; Table 2.7). During all but three years the variance propagated methods produced narrower CI intervals (Fig. 2.17). All variance propagated CIs were narrower in the north stratum while all but two were narrower in the south stratum.

Table 2.8: Annual detection probability with SE estimates from the hazard-rate model without series expansion and with the covariate `Year` produced using `ds`. Estimates not produced indicated with a —.

Year	Estimate	SE
1987	0.381	0.036
1988	0.762	0.057
1989	0.422	0.045
1990	0.483	0.050
1991	0.581	0.061
1992	0.428	0.039
1993	0.780	0.057
1994	0.747	0.071
1995	0.703	0.063
1996	0.567	0.036
1997	0.449	0.038
1998	0.571	0.048
1999	0.440	0.046
2000	0.392	0.033
2001	0.545	0.043
2002	0.586	0.044
2003	0.589	0.057
2004	0.573	0.045
2005	0.804	0.092
2006	0.499	0.075
2007	0.541	0.046
2008	0.380	0.034
2009	—	—
2010	0.390	0.039
2011	0.404	0.052
2012	0.378	0.044
2013	0.390	0.041
2014	0.582	0.064
2015	0.589	0.074
2016	0.590	0.063
2017	0.415	0.052

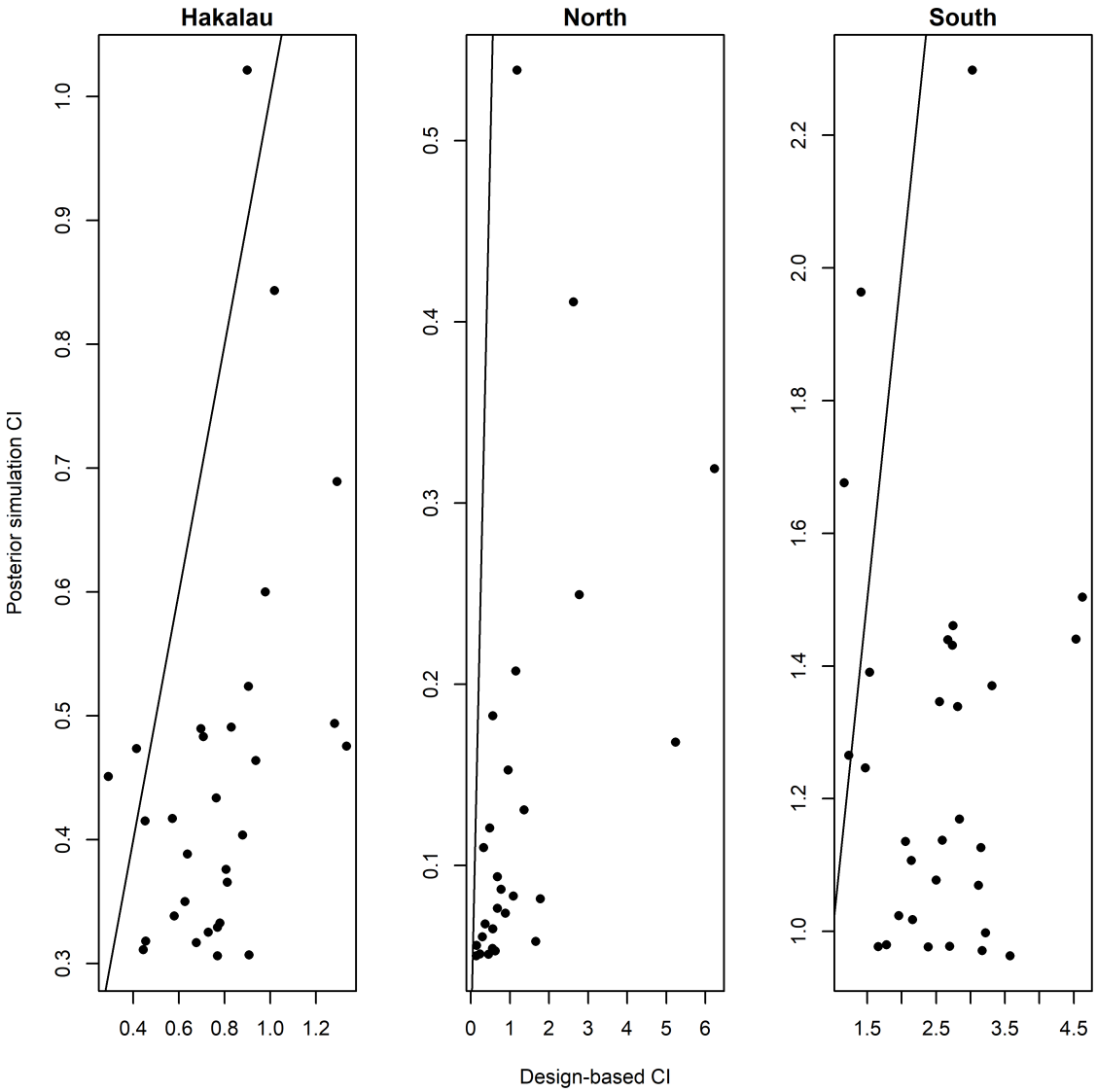

Figure 2.17: Comparison of uncertainty between confidence intervals (CIs) produced using model-based (density surface model) with variance propagation and design-based methods. The 1:1 lines are shown; points below the lines indicate uncertainty was improved with narrower intervals produced from the variance propagated method.

2.5 Discussion

2.5.1 Statistical methods

My analysis shows that precision in animal abundance estimates can be improved through the application of spatio-temporal modelling using GAMs and underscores the need to account for estimator uncertainty through variance propagation. I observed large variation in counts among different points, as well as between years, which is typical of Hawaiian forest bird monitoring (Camp et al. 2009), and counts elsewhere (Link and Sauer 1998). Accounting for the various sources of variation is critical to assess management and conservation goals. Established approaches to compute total variance include: (1) delta method assuming independence (Seber 1973); (2) bootstrap methods (Hedley and Buckland 2004); (3) fully Bayesian approaches (Niemi and Fernández 2010, Sigourney et al. 2018); and the approach here (4) using variance propagation methods (Bravington et al. 2018). The delta method assumption of independence is not appropriate here as the detection probabilities are not independent parameters between the first- and second-stage models. Under the sampling design in this study, bootstrap resampling would be of lines instead of points (Buckland et al. 2015). It is then unclear exactly how the different units (lines for the detection probability domain and blocks for the spatio-temporal domains) are resampled (Lahiri 2003). Bayesian methods such as Johnson et al. (2010), Niemi and Fernández (2010) and Sigourney et al. (2018) require writing custom code and checking priors and convergence, incurring a high computational cost. The variance propagation approach avoids the concerns of the above methods by accounting for possible interactions between detection and density models, non-independence between years and spatial correlation among points while still being computationally efficient.

Standard distance sampling, including the multiple covariate extension, is a hybrid of design- and model-based methods where inference comes from the design portion and detection probability from the model-based portion. Design-based methods are most appropriate if the primary goal of the surveys is to estimate population size (Buckland et al. 2015). The random placement of points in a study area allows for extrapolating densities at the points to the wider study area, providing inference about total abundance. When the goal of the survey is to map species distribution or compare whether densities on subregions differ model-based methods can be more appropriate. A model-based approach is particularly useful to assess the effectiveness of management actions under a control-treatment design, or to account for spatio-temporal pattern in the counts as I have done. The model-based methods produced finer-grained and more precise abundance estimates. Switching from design- to model-based methods requires a substitution of assumptions from a survey design, where it is assumed that sample locations are chosen using a random sampling scheme, to assumptions about the animal distribution, where it is assumed animal locations are a realisation of the spatial model. I assume that the design assumption is met, however I have no control of animal distribution. Thus, switching between the methods requires careful consideration of the survey goals, method-specific advantages and disadvantages, and available data. As long as the surveys are conducted following design-

based methods the data can be analysed using either design- or model-based methods as appropriate (Buckland et al. 2015).

Sampling at Hakalau is based on a stratified, systematic random sampling design. Therefore, the design-based analysis required that I stratify the study area by sampling intensity to produce unbiased density estimates using the design-based method. Standard distance sampling methods, even incorporating model-based analysis procedures, do not fully account for the spatial structure of the sampling design (Buckland et al. 2015). Spatial distance sampling models that integrate detection function modelling exploit the data more efficiently by avoiding the need to stratify the study area and can incorporate plot-level covariates that influence both bird detection probability and densities (Miller et al. 2013).

The covariate habitat I used classifies plant communities at the formation level of the U.S. National Vegetation Classification (Jennings et al. 2009, and http://usnvc.org). The formation level is defined by broad combinations of growth forms with moisture and temperature conditions, and is a classification level that is unlikely to change from management actions designed to enhance forest habitat. It is unlikely that 'ākepa and other Hawaiian forest birds are responding to habitat at the coarse formation level, which was reflected in my analyses where there was no strong evidence that habitat influenced 'ākepa densities. More likely, forest birds are responding to changes in crown cover and canopy height, floristic community composition, and understory components (Scott et al. 1986). Scott et al. (1986) found only limited response of native passerines to understory components; however, after the removal of ungulates from portions of the refuge (Maxfield 1998, Hess 2016) it appears that the forest birds may have positively responded to the recovering understory as the forest canopy has changed very little since the 1970s (Jacobi 2018, Hart et al. 2020). Point-level description of the understory vegetation is available only for surveys conducted in 2016 and 2017, which will be useful for future studies that wish to incorporate understory variables to describe its relationship with bird density and potentially increase the amount of variation explained by the model.

2.5.2 Biological findings

Estimating densities using smoothing methods eliminated biologically impossible changes in densities. While it is possible that a population can decrease by half or more from one year to the next, it is not possible for 'ākepa to double as they produce only one or two eggs per year yielding a 1.47 birth rate with hatch year survival ranging from 0.23 to 0.43 (Woodworth and Pratt 2009). The biologically realistic growth rate is thus between 0.97 and 1.12 indicating that the population could increase only slightly from year to year ($\lambda = 0.80 + 0.5\beta\phi$, where λ is the growth rate, mean adult survival is 0.80 (see Chapter 5), β is the birth rate and ϕ is juvenile survival probability; Newman et al. (2014)). Estimates produced through standard distance sampling analyses changed substantially (and unrealistically) between years, while annual density estimates from the spatio-temporal model are more biologically plausible (see Fig. 2.15) (though there is no constraint on survival or growth rate explicitly in the smoother model). More advanced demographic

modelling could be achieved by including the previous year estimate as an offset following Conn et al. (2015) and Swallow (2015), and/or through population dynamics modelling that combines bird abundance with priors on annual changes, which can be informed by demographic vital rates (Newman et al. 2014).

No survey was performed in 2009 and it is of interest to estimate density in that year. In the state-space modelling framework employed by Camp et al. (2016) estimated bird densities for the missing survey in 2009 using two draws from a random slope distribution. An uninformative prior was used within a Bayesian framework, which allowed for maximum change in the population and inflated the variance to allow for both substantial increasing and decreasing trajectories between the 2008 and 2010 density estimates. An alternative approach is to use posterior simulation from the DSM to estimate the 2009 'ākepa density. This approach would allow for both mapping the distribution of 'ākepa densities across the study area and predicting the annual density and variance estimates. The predicted uncertainty would be greater than estimates from adjacent years, but should be smaller than the estimate in Camp et al. (2016). This estimate would not include the detection probability uncertainty, so I did not generate a 2009 estimate via two-stage spatio-temporal modelling.

I used a simple spatial smoother that assumes the bird population is continuous across the refuge including proximate areas outside the study area. This assumption may be realistic to the north, east and south of the study area that juxtaposes contiguous 'ōhi'a dominated forest. The 'ākepa population, however, does not extend west into the pasture, especially early in the time series when grass dominated that habitat and prior to afforestation management. Not detected until 2011, 'ākepa moved into the afforested pasture once the trees had sufficient time to provide suitable habitat (Paxton et al. 2018). Understanding the spatial and temporal changes in the population is achieved by limiting inference of the spatio-temporal maps to the sampled area. From the initial Hawai'i Forest Bird Survey (HFBS), Scott et al. (1986) noted that 'ākepa are absent from about a fifth of the northern Hamakua study area. Juxtaposed is a relatively large area with very low densities of 1-10 birds/km^2, in which the northern portion of Hakalau occurs. At the start of the time series densities in the north region are comparable to HFBS densities. By the last survey, densities are nearly three times greater and the end-point credible intervals do not bracket the HFBS point estimate, despite relatively large CVs. Regardless of the increases, densities in the north region are still low at only 40 birds/km^2. Historically, 'ākepa could have been more numerous at the turn of the 19$^{\text{th}}$ century (Perkins 1903) and possibly remained abundant for several decades (Munro 1944). There is little evidence, however, that either naturalist surveyed in the northern portion of the study area, and instead they may have described the locally more abundant southern population where the density estimates are comparable to Scott et al. (1986) at 200+ birds/km^2.

2.5.3 Management implications

A main goal of spatio-temporal modelling was to unveil geographical and temporal patterns that can be used to identify population responses to management actions. Thus,

my modelling attempted to elucidate medium-term responses in population abundances to long-term management effects. My analyses show where the 'ākepa population has responded to management actions and changes in environmental conditions. Accounting for both spatial shifts and temporal changes in population abundance and distribution benefits conservation planning through improved management efficiency and reduced costs. Management actions can then be applied to priority areas where a species is most likely to respond or require further intervention. Since 1985, management in the open-forest stratum at Hakalau has consisted of fencing, removing and controlling non-native ungulates, and controlling invasive non-native plants (USFWS, U.S. Fish and Wildlife Service 2010). Removal of feral cattle (*Bos taurus*) was achieved promptly (Maxfield 1998) but control of pigs (*Sus scrofa*) has been more difficult (Hess et al. 2010, Hess 2016). After the release from grazing and trampling, vegetation in the study area has responded with evidence of early seral regeneration (Hess et al. 2010).

Controlling pigs has been more challenging due to their prolific reproductive rates, difficulties of locating and removing the last individuals, and egress into the study area from the surrounding reservoir populations (Hess 2016). Feral pigs were removed from management units in the south stratum by 2002 (Hess et al. 2006). Over this period 'ākepa increased by nearly one bird$^{-\text{ha}}$. Since 2008 though 'ākepa have decreased to densities that are similar to those at the start of the time series. These fluctuations occurred within the 95% credible interval of the posterior distribution, indicating that the south stratum 'ākepa population has fluctuated but that it has not increased or declined overall. The medium-term declining trajectory since 2008 coincided with a pig reinvasion that has yet to be eradicated. Continued abundance monitoring, focusing on 'ākepa densities along the eastern edge of the south stratum, will provide information of 'ākepa trends and track the trajectory to inform management and conservation planning. These data indicate that a response in 'ākepa densities lags pig eradication and habitat recovery by several years. Additional biological data, such as species' demographic data, may further improve decision making through prioritising management actions specific to improving species' productivity and mitigating threats. Detecting a response in demographic parameters, or derived demographic quantities of survival and reproduction, may be observed more quickly than detecting changes in just the abundance time series (Guillaumet et al. 2016).

It has been more difficult to remove pigs from the northern portion of the refuge. My results show that 'ākepa remained at low densities in this region for an extended period before increasing relatively rapidly. This increase occurred some time after numbers of pigs had been suppressed and there had been increases in native ferns and woody vegetation (Hess et al. 2010). By 2017, 'ākepa densities remained near zero in only the north-west portion of the north stratum. This area coincides with an infestation of banana poka vine (*Passiflora tarminiana*), a draping liana that can engulf the forest canopy layer. Loh and Tunison (1999) showed banana poka decreased by half after the removal of pigs in similarly managed rainforest habitat in Hawai'i Volcanoes National Park, Hawai'i Island. Refuge management includes controlling the vine and other invasive non-native plants. Eradicating this invasive vine on the refuge will benefit from removing it from adjacent reservoir

populations. Given increases in 'ākepa elsewhere in the north stratum it is reasonable to expect that 'ākepa will continue to increase with the removal of non-native ungulates and plants. This approach to identify and target priority areas assumes that there are positive responses between the level of management effort, spatial extent of the area managed and target species benefit, i.e., an immediate, proximate impact; assumptions I make influencing the changes observed in 'ākepa distribution and densities. Prioritised and efficient management will become more important as traditional approaches to conserving and managing species inadequately account for rapidly changing, uncertain environments and novel ecosystems (Hobbs et al. 2009).

My approach provides a framework for understanding changes in bird populations, it can also provide insight into anticipating management actions that may facilitate conservation. A limitation of Camp et al. (2016) analysis of 'ākepa abundance and trend is that they treated the entire study area as homogeneous, whereas I have shown that the distribution and density of 'ākepa are heterogeneous, varying over space and time. That is, my results provide unprecedented insights into the distribution of 'ākepa densities where my density surface maps illustrate the dynamics of the species throughout the study area, presumably in response to management. Extending the management that has improved habitat in the central portion of the open-forest stratum could benefit the adjacent population in the north region and where it extends east into lower elevations of the refuge (Camp et al. 2016). In addition, 'ākepa occur in five spatially disjunct sub-populations with the Hakalau sub-population being the largest (Judge et al. 2018). These sub-populations occur in comparable habitat, face similar threats, and hence the management at Hakalau may be beneficial. Management of these other sub-populations may benefit by coinciding with frequent monitoring and including spatio-temporal modelling similar to mine to maximize benefits from the management actions.

Adequate monitoring is required to meet regulatory requirements and determinations (USFWS, U.S. Fish and Wildlife Service 2006). My research emphasizes the importance of long-term monitoring data without which this analysis would not have been possible. Managers and policy makers have a wide range of often conflicting conservation objectives and priorities, and support for monitoring programs is regularly assigned low importance. The continued collection of ongoing, systematic data is essential to understanding population changes, particularly in the face of rapidly changing environments (Atkinson et al. 2014) and collapsing populations (Paxton et al. 2016). Without systematic data, evaluating population trends may not be possible and detection of end-point population change is difficult (Judge et al. 2019). Moreover, without systematic data it is not possible to understand the underlying processes, such as growth rates (Camp et al. 2016) or population dynamics (Guillaumet et al. 2016), that are driving population changes. Hawaiian forest bird monitoring programs would greatly benefit from ensured long-term support, including financial assistance; established institutional capacity; recruitment, training and retention of surveyors; and formalized cooperation between universities, NGOs and governments (Paxton et al. 2018).

Chapter 3

Point-process models to estimate abundance

3.1 Overview

An alternative approach to modelling a density surface with a GAM is to employ point process models. Andrew Seaton, fellow PGR student, University of St Andrews, School of Mathematics and Statistics, developed a one-stage model-based approach to model point-transect distance sampling (PTDS) data using point process (hereafter, point process approach). To demonstrate the point process approach, Seaton modelled the spatial distribution of 'ākepa to map and estimate their densities for a single survey from the 'ākepa time series. Bayesian inference was used to simultaneously estimate detection probability and spatial distribution, which naturally incorporates detection probability uncertainty into final variance estimates. A description of the methods and results to analyse PTDS using the point process approach have been assembled into a manuscript for peer-review and are referenced herein as Seaton et al. (In preparation)[1]. For comparative purposes I conducted a two-stage model-based analysis using TPRS to model the spatial distribution of birds accounting for spatial correlation (hereafter, DSM approach). I computed the combined detection probability and GAM uncertainties using the delta method assuming independence. In Section 3.2 I describe the principles of spatial point process modelling, present the point process approach framework, summarise the DSM approach, and describe how I compare estimates between the two approaches. I describe the data in Section 3.3 and the methods used for modelling each approach in Section 3.4. The results are presented in Section 3.5. I provide a discussion, specifically addressing model checking and the underlying smoothness of the data, in Section 3.6. Finally in Section 3.7 I present considerations when choosing between the two approaches.

[1]Paper co-authored by me as part of my thesis research.

3.2 Spatial modelling

In Chapter 2 I modelled the spatio-temporal densities of 'ākepa across a 31-year time series using two-stage model-based smoothing. Many studies, however, are a single snapshot of bird status or a series of snapshots infrequently collected that lack the temporal correlation of the 'ākepa time series. Standard distance sampling analyses can be applied to these data to estimate the detection function independently for each year, or have a common detection function across years, potentially with time-varying covariates, to estimate survey-specific densities. In these situations, and given adequate coverage of the study area, it is still useful to conduct analyses to account for spatial correlation to reduce the uncertainty in density estimates and produce density surface maps. Here I explore how two analytic approaches, point process and penalized spline-based smoothing handle uncertainty differently. It is important to note that I do not purport that one method is better than the other, instead the emphasis of this research focuses on why the uncertainties between the two models differ. I illustrate the similarities and differences between the two approaches as applied to the 2002 'ākepa PTDS data collected at Hakalau.

3.2.1 Point process approach

An alternative approach to modelling spatially referenced densities and spatial correlation with smoothers is to employ point process methods (Illian et al. 2008, Diggle 2014, Blangiardo and Cameletti 2015, Cressie and Wikle 2015). Based on point-referenced data an intensity function and extent of spatial correlation is estimated to estimate bird density. A classic point process modelling approach is to model the spatial correlation of bird detections where each bird seen is mapped and treated as a thinned point process where the detection process does the thinning (this is also referred to as a filtered point process; Cressie and Wikle (2015)). Within this framework, it is assumed that the true density is a point process and the observations a thinned version. Yuan et al. (2017) developed a full likelihood point process model for line-transect distance sampling data. Yuan et al. (2017) used Bayesian inference with integrated nested Laplace approximation (INLA), as opposed to Markov chain Monte Carlo, to simultaneously estimate the detection probability and spatial correlation to map an animal's spatial distribution and density.

In point process modelling the locations of all objects are known and mapped. When collecting Hawaiian forest bird PTDS data the location of the sampling point is recorded along with the horizontal distance to detected birds. The exact location of the birds therefore cannot be mapped. A thinning function is incorporated to overcome this limitation. Careful formulation of the thinning function allows for combining distance sampling methods with spatially explicit point process models. This can be achieved by selecting the half-normal function, or another member of the parametric family of functions common to distance sampling approaches where the numbers of detections decay with increasing distances. The thinning probability function then fulfils the requirements to model the detection and intensity functions for incomplete data, which Yuan et al. (2017) accomplished using a stochastic partial differential equation (SPDE; Lindgren et al. 2011). The

SPDE approach also avoids the need to aggregate detections at the point level.

Seaton et al. (In preparation) expanded on the approach Yuan et al. (2017) developed to model PTDS data. Similar to Yuan et al. (2017), Seaton et al. used the SPDE approach (Lindgren et al. 2011) that fits a Matérn-like model for spatial correlation. Based on simulations of the posterior predictive distribution, relevant parameter statistics can be estimated. I use the results from Seaton's modelling for comparative purposes with the DSM approach applied to the same dataset.

3.2.2 DSM approach

I provided a detailed description of the DSM approach using a two-stage model-based smoother method in Chapter 2. In the first stage I estimated the year-specific detection probability following conventional distance sampling procedures. In the second stage I modelled the spatial correlation of the counts of detections using penalized spline-basis smoothing with a GAM. I used the estimated detection probability as an offset in the second stage to model imperfect detection of counts, the response variable, to estimate densities. The detection function did not include covariates; therefore, I combine variance component estimates (detection probability and smooth terms) to calculate the sum of the variances using the delta method assuming independence.

3.2.3 Comparison between the two approaches

In order to compare the mean and variance between the point process and DSM approaches, I made the two modelling approaches as similar as possible by analysing a single survey and matching the model functionality of the two approaches. For each approach, the mean, median and uncertainty of the density were estimated using posterior simulation procedures of estimates fitted to a regular grid over the study area. I compared the overlap in 95% credible intervals (CrIs) of the point process approach with that of the 95% confidence interval (CIs) from the DSM. The posterior uncertainties were compared on a per cell basis.

3.3 Methods

3.3.1 Study species and survey

The analyses in this chapter are conducted on the Hawai'i 'ākepadata collected at Hakalau, described in Chapter 1. For purposes of this analysis, I selected a single survey from the 'ākepa time series based on broad sampling of the study area and sufficient numbers of detections. In 2002, 289 points were sampled using PTDS methods within the open- and closed-forest habitat (i.e., forest stratum; Chapter 1 Fig. 1.1). On 121 points, 276 'ākepa were detected (Fig. 3.1). The number of detections at points ranged from zero to 6 (Fig. 3.2). These data are used for both the point process and DSM approaches.

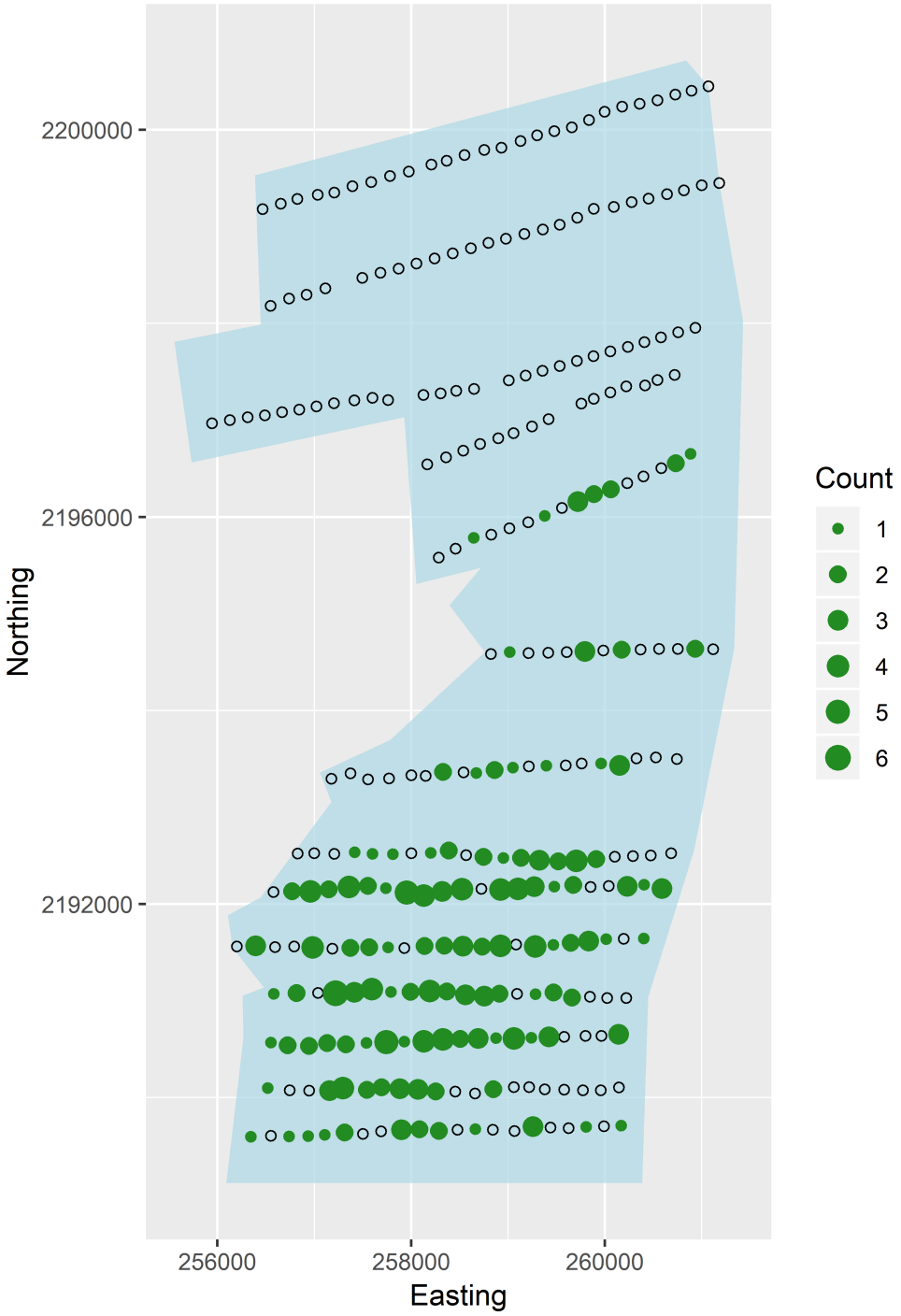

Figure 3.1: Sampling points and 'ākepa detections from the 2002 survey in Hakalau Forest National Wildlife Refuge, Hawai'i Island. Black circles are points without detections and green dots are points with detections (scaled by numbers of detections). The forest stratum includes open- and closed-forest strata points (light blue shaded polygon).

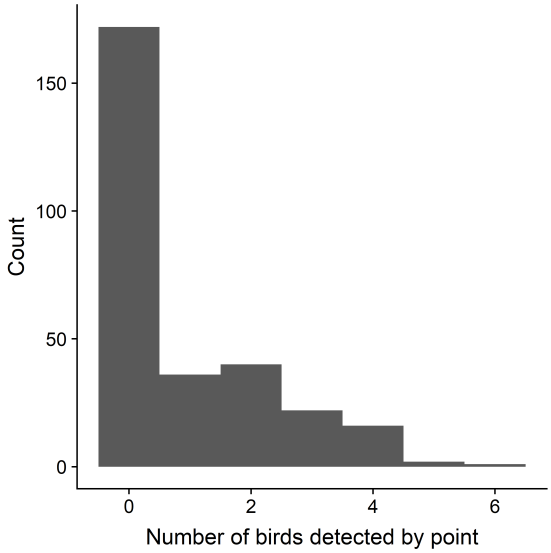

Figure 3.2: Counts of 'ākepa by point during the 2002 survey within the 58m truncation distance.

3.4 Modelling the 2002 'ākepa dataset

Here I describe the methods used to estimate and map densities of the 2002 'ākepa dataset using point process and DSM approaches.

3.4.1 Point process approach

The 2002 'ākepa counts were modelled with a one-stage Bayesian model to simultaneously estimate the detection probability and spatial distribution fitted using INLA to predict densities in `inlabru` (Bachl et al. 2019), an `R` package (R Core Team 2017). The forest stratum study area was defined as the domain with the PTDS points a random collection of points. Bird detections were taken from non-overlapping circles with centres at the PTDS points. The distribution of points was modelled using a thinned log-Gaussian Cox process where the detection function thins the process. The log-intensity of points was modelled using the SPDE approach of Lindgren et al. (2011) where the spatial correlation was defined by a Matérn covariance function. Details of the point process approach methods, including defining the model likelihood and priors, are provided in Yuan et al. (2017) and Seaton et al. (In preparation).

3.4.2 DSM approach

Stage one: Detection probability modelling

I estimated the 2002 'ākepa detection probability using conventional distance sampling procedures in the distance sampling package `Distance`, version 0.9.7 (Miller 2017), in program `R`. The half-normal detection function without series adjustments is the only model currently supported in `inlabru` to estimate point-transect detection probabilities. I estimated the detection probability for the 2002-specific dataset using the half-normal

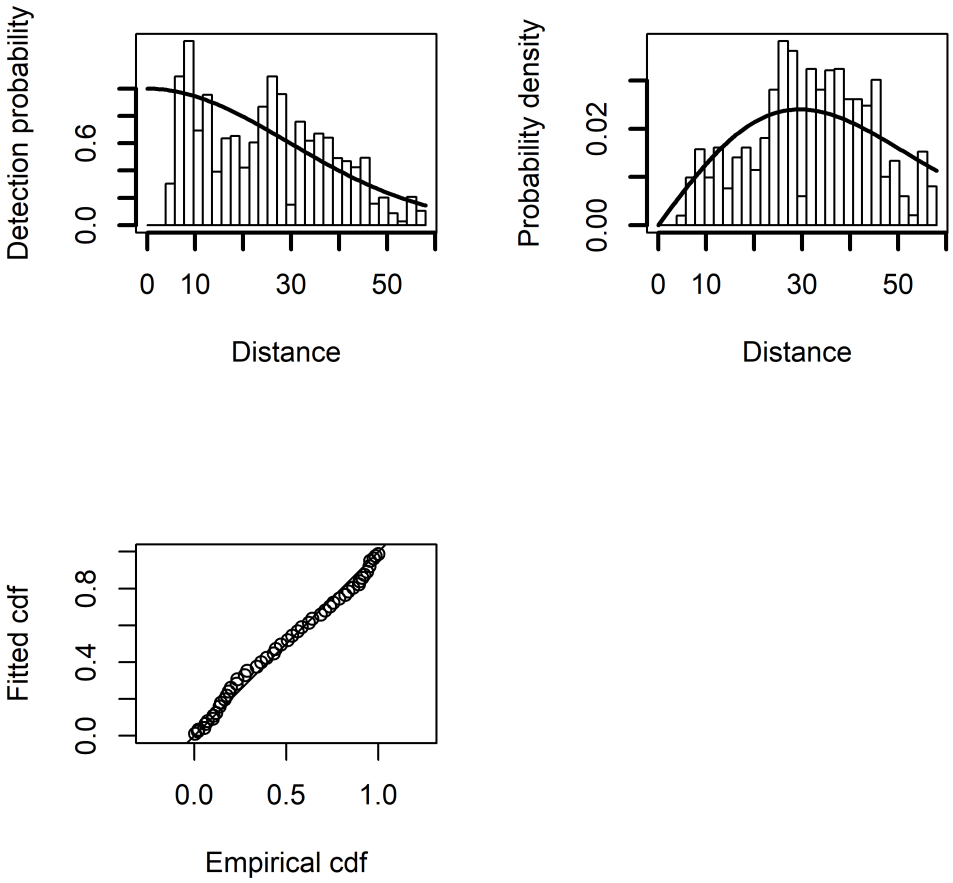

Figure 3.3: Detection function plots for the half normal detection function model selected to estimate the 2002 'ākepa detection probability. Plots represent the detection probability (top left panel), probability density (top right panel), and QQ plot (bottom panel). The points generally follow the the identity line, which provides evidence that the function adequately fits the data.

detection function with truncation at 58 m (the distance where the estimated detection probability was about 0.1). A total of 262 detections was modelled while 14 detections beyond 58 m were excluded. The unweighted Cramer-von Mises test was non-significant at the 5% level (test statistic = 0.428, $p = 0.061$) indicating that the detection function adequately fit the distance data (Fig. 3.3). The estimated detection probability was 0.443 (SE = 0.040) and the effective area surveyed per point was 4,681.8 m^2 or a searched area of 0.468 ha about each point. The effective area searched was estimated as $\hat{\nu} = \pi w^2 \hat{p}$ and was used as the offset in the second stage smoother model.

Stage two: Model-based density estimation

For the smoother modelling I dropped the temporal variable from the full time series analysis applied in Chapter 2 and fitted a smooth to just the spatial location variables `Easting` and `Northing`. The spatial, penalized spline-based smoother (TPRS) model has

Table 3.1: Model selection statistics for the Poisson, negative binomial and Tweedie distributions. Presented are the smoother log-likelihood (logLik), degrees of freedom (df), Akaike's information criterion (AIC) and Δ AIC.

Model	logLik	df	AIC	Δ AIC
Poisson	-277.735	13.938	583.346	0
negative binomial	-277.610	15.429	586.078	2.732
Tweedie	-293.081	16.406	618.974	35.628

the form

$$\begin{aligned}\log\{\mathbb{E}(n_k)\} =& f_1(\texttt{Easting}_k) + f_2(\texttt{Northing}_k) \\ &+ f_3(\texttt{Easting}_k, \texttt{Northing}_k) + \log(\hat{\nu})\end{aligned} \tag{3.1}$$

where n_k is the bird count at the k-th point, f_1 and f_2 are one-dimensional isotropic TPRS smooth functions [s()], f_3 is a two-dimensional interaction smooth function [ti()], $\hat{\nu}$ is the effective area searched and the offset is the log of $\hat{\nu}$. The model was built in `R` using the `mgcv` package (Wood 2016). REML was used to estimate model parameters and maximum basis size was set to allow flexible effects (Wood 2017). Coefficients were estimated using penalized likelihood maximisation. I evaluated the Poisson, negative binomial and Tweedie response distributions, each fit with a log-link function. For the Tweedie distribution I restricted the power parameter to $p = (1.1, 2)$ following recommendations provided in the `mgcv` package help pages. I conducted a linear search to bracket the power parameter between $(1.1, 2)$ and used a method of bisection to approximately identify the maximum.

Based on inspection of the residuals plots there were no clear distinctions or obvious problems with one or the other distributions (diagnostic figures are presented in Appendix C). The Tweedie distribution AIC was > 35 units larger than that of the Poisson distribution (Table 3.1). The Poisson and negative binomial distributions were within 2.8 AIC units. Besides visual inspection and evaluation of the standard residual and QQ plots, I assessed the residual errors for each of the individual parameters. Inspection of the diagnostic plots revealed that all three distributions handled residual errors adequately (Appendix C). Based on residuals diagnostics and AIC values I chose the Poisson distribution for making comparisons with the point process approach method.

The Poisson with log-link distribution had small effective degrees of freedom (EDF) relative to the reference degrees of freedom and with basis complexity (k-index) near one for each term (Table 3.2). Following model checking methods detailed in Chapter 2 the deviance residuals were fitted with a Gaussian distribution with an identity link. The effective area searched and offset, $\log(\nu)$, was removed for model checking. All other components of the model were retained. The model fitted to the deviance residuals revealed that no un-modelled structure in the residuals remained (Table 3.3), and that residual variance was removed in the model fitted at convergence (Table 3.4). This suggested that there were minimal un-modelled residual autocorrelation from the Poisson distribution model, and the deviance explained was 53.5%. The smooth function was convex for the `Easting` variable progressing from a density of 0.1 birds ha^{-1} at the west boundary to

Table 3.2: Effective degrees of freedom (EDF), reference degrees of freedom (rf) and basis complexity (k-index) for each term in the fitted Poisson distribution spatial model.

Term	EDF	rf	k-index
`s(Easting)`	3.227	9	0.89
`s(Northing)`	5.273	9	1.04
`ti(Easting,Northing)`	2.484	16	1.08

Table 3.3: Effective degrees of freedom (EDF), reference degrees of freedom (rf) and basis complexity (k-index) for each term in the model fitted to the deviance residuals.

Term	EDF	rf	k-index
`s(Easting)`	4.056e-05	2	0.93
`s(Northing)`	3.884e-04	2	1.09
`ti(Easting,Northing)`	5.672e-04	16	1.09

1.0 midway between the boundaries and declining to 0.6 at the east boundary (contour values of -2.0, 0 and -0.5, respectively; Fig. 3.4, top left panel). The `Northing` variable was moderately wiggly progressing from a density of 4.5 at the southern boundary to 0.002 at the northern boundary (contour values 1.5 to -6.5, respectively; Fig. 3.4, top right panel). The interaction was smooth with densities ranging from 0.05 to 20.1 (contour values -3 to 3, respectively; Fig. 3.4, bottom panel). For comparative purposes I also analysed these data with increased flexibility in the smoothing parameters. It is expected that increasing the flexibility in the smoothing parameters could make the estimates more similar to those of the point process approach that can produce a higher degree of spatial variation (i.e., a more wiggly surface). Methods and results are provided in Appendix C.

3.4.3 Density and abundance estimates

Following the procedures detailed in Chapter 2, I defined a spatial 200 x 200 m grid that coincided with the study area to which densities and standard errors were predicted from the fitted models. I drew 1,000 realisations from the posterior distribution. Mean, and 0.025, 0.5 and 0.975 quantiles were computed per cell from the model-specific prediction matrix realisations and summed to produce the total forest-stratum densities. The parameters of the posterior simulation maximum likelihood estimates are theoretically multivariate normally distributed (an approach also referred to as a parametric bootstrap), and are thus independent. As such, for each replicate the uncertainty from the detection probability was included with the spatial uncertainty using the delta method assuming independence.

Approach-specific abundance was calculated as the sum of the per realisation density

Table 3.4: Effective degrees of freedom (EDF), reference degrees of freedom (rf) and basis complexity (k-index) for each term in the model fitted at convergence.

Term	EDF	rf	k-index
`s(Easting)`	2.036e-05	2	0.93
`s(Northing)`	1.376e-05	2	1.08
`ti(Easting,Northing)`	1.376e-05	16	1.15

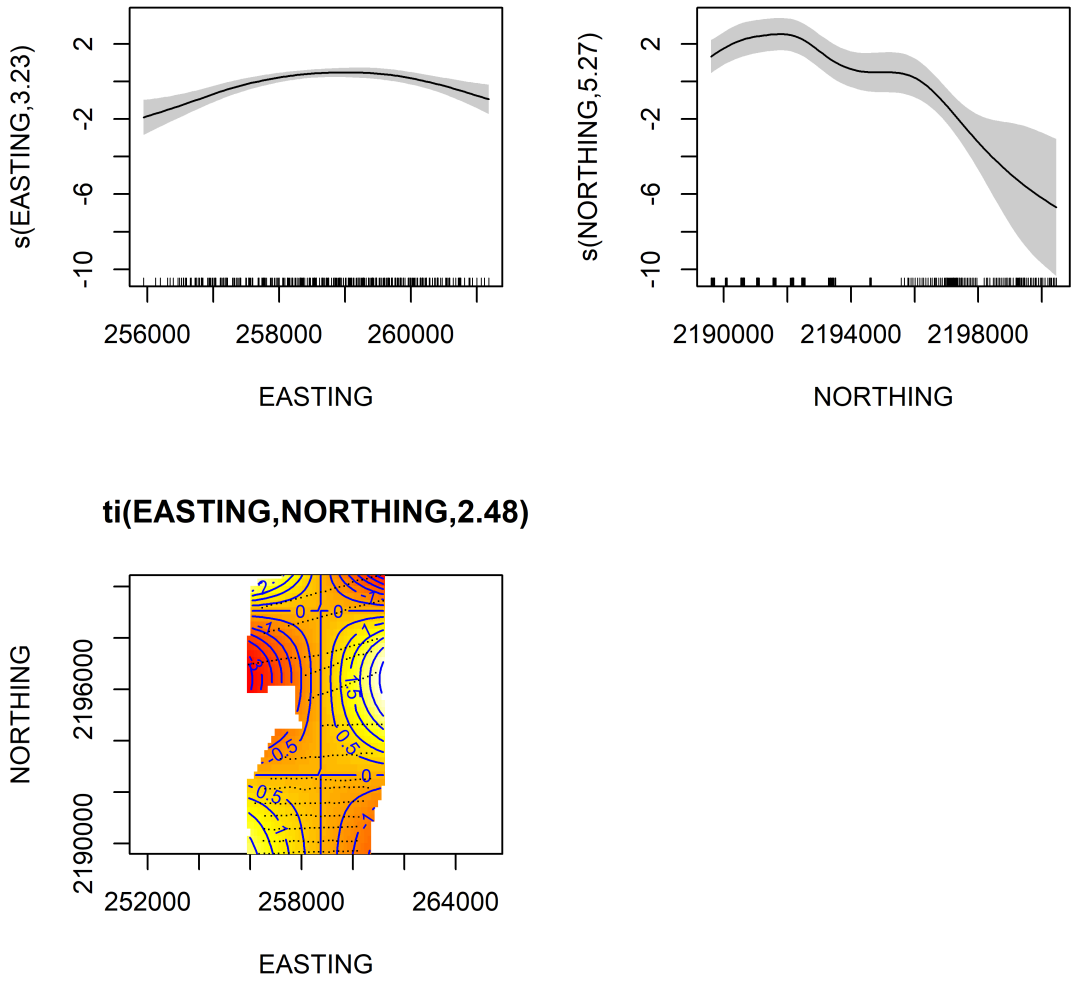

Figure 3.4: Estimated model terms for the spatial GAM fitted to the 2002 'ākepa count data. The distribution of the data is visualized in the rug plot along the x-axis for the 1D `Easting` and `Northing` plots, while the EDFs are presented on the y-axis labels. The ribbon illustrates the error bounds of plus or minus one standard error from the estimates. The locations of the points are plotted as black dots on the 2D contour plot and the EDF is provided in the plot panel title. Contours representing 0.5 unit change are shown as blue lines. Estimates provided on the scale of the linear predictor.

estimates times the area of the stratum times 4 ha per grid cell. The size of the forest stratum (4,602.7 ha) was computed using the `sp` (Pebesma et al. 2018) package in `R`. Variance of abundance was estimated analytically and 95%CIs were computed using quantile methods from the 1,000 realisations of the posterior simulation. For comparative purposes and following methods described in Chapter 1 Section 1.4.2 I combined the detection probability with counts using a design-based method to estimate densities (birds ha^{-1}). Abundance was estimated as density times the size of the forest stratum, and variance and 95%CI were calculated using analytic methods.

3.5 Results

Here, I present the results obtained from the point process and DSM approaches applied to the 2002 'ākepa dataset. Maps of predicted median, SE and 95% interval width estimates allow for visual comparison of both approaches. I also mapped per cell differences of the median and 95% interval widths to identify where the two approaches produce similar and different estimates. I interpreted these maps based on the extent to which the two approaches smooth the densities. I then compared the approach-specific 'ākepa abundance, SE and 95% interval width estimates for the forest stratum.

3.5.1 Mapping fitted estimates

Both the point process and DSM approaches produced visually near identical patterns for the 2002 'ākepa dataset (Figs. 3.5 and 3.6), while the DSM approach produced larger mean and median density estimates than the point process approach (Table 3.5). The density surface maps show a density hotspot in the southern portion of the study area that extended north-east to a second hotspot in the central portion. The entirety of the northern portion of the domain was a coldspot (Figs. 3.5 and 3.6) and reflected patterns in the count data (Fig. 3.1). The notable difference between the density surface maps was that the point process approach produced a higher degree of spatial variation (i.e., a more wiggly surface) than the DSM approach that was generally more smooth. Visually comparing the interval width maps (Figs. 3.5 and 3.6) revealed that locations of hot and cold spots were also similar.

There was good agreement in the spatial patterns of high and low uncertainties (SE; Fig. 3.7, left and middle panels), and the SE values generally overlapped between the two approaches (Fig. 3.7, right panel). For both approaches, uncertainty was small where density was low (in the northern portion of Hakalau). There was, however, more uncertainty at the hotspots reflecting that variance of the count increases with count. The wiggly versus smooth differences between the two approaches was also obvious in the SE plots (Fig. 3.7, left and middle panels).

3.5.2 Per cell differences

The difference in the per cell median densities were useful for identifying where the two approaches predicted similar and different densities. The per cell differences between the

Table 3.5: Detection probability $\hat{p}$, forest stratum density $\hat{d}$, abundance $\hat{N}$, SE, 95% interval limits (LCL = lower 95% interval limit and UCL = upper 95% interval limit), and coefficient of variance (CV%) estimates by modelling approach. Subscript indicates statistic.

Parameter	Point process	DSM
$\hat{p}_{\text{mean}}$	0.520	0.443
SE($\hat{p}$)	0.044	0.040
$\hat{d}_{\text{mean}}$	1.309	1.521
$\hat{d}_{\text{median}}$	0.832	0.984
SE($\hat{d}$)	0.147	0.185
LCL $\hat{d}$	1.040	1.181
UCL $\hat{d}$	1.311	1.903
$\hat{N}_{\text{mean}}$	6,034	7,010
$\hat{N}_{\text{median}}$	5,973	6,997
SE($\hat{N}$)	677	853
LCL $\hat{N}$	4,789	5,434
UCL $\hat{N}$	7,485	8,758
CV%	11.2	12.2

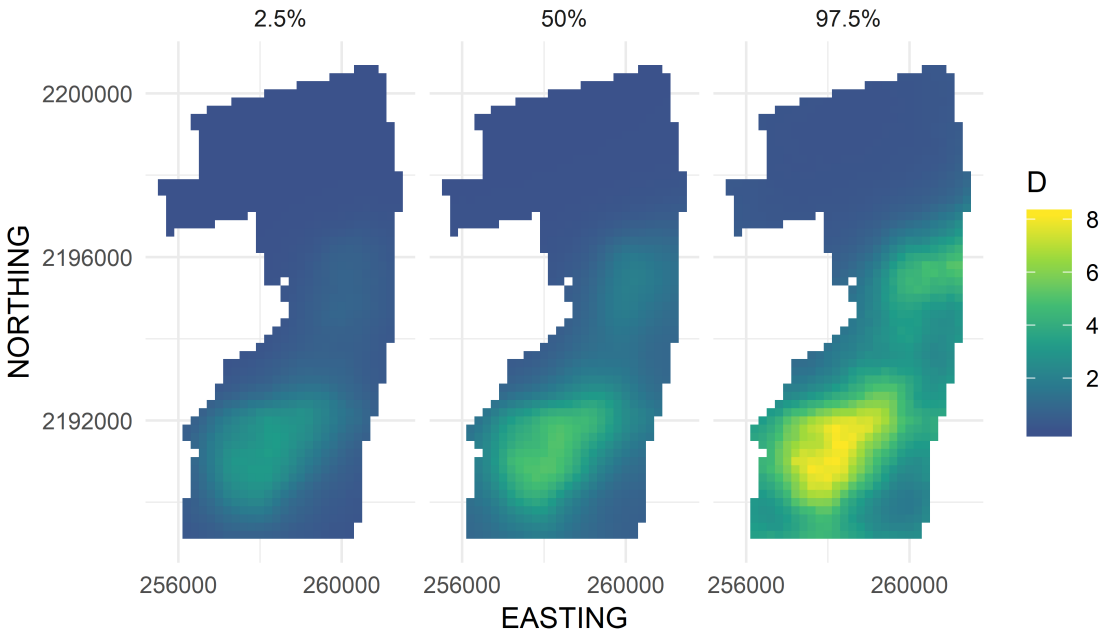

Figure 3.5: Median and 95%CrI density estimates from the point process approach.

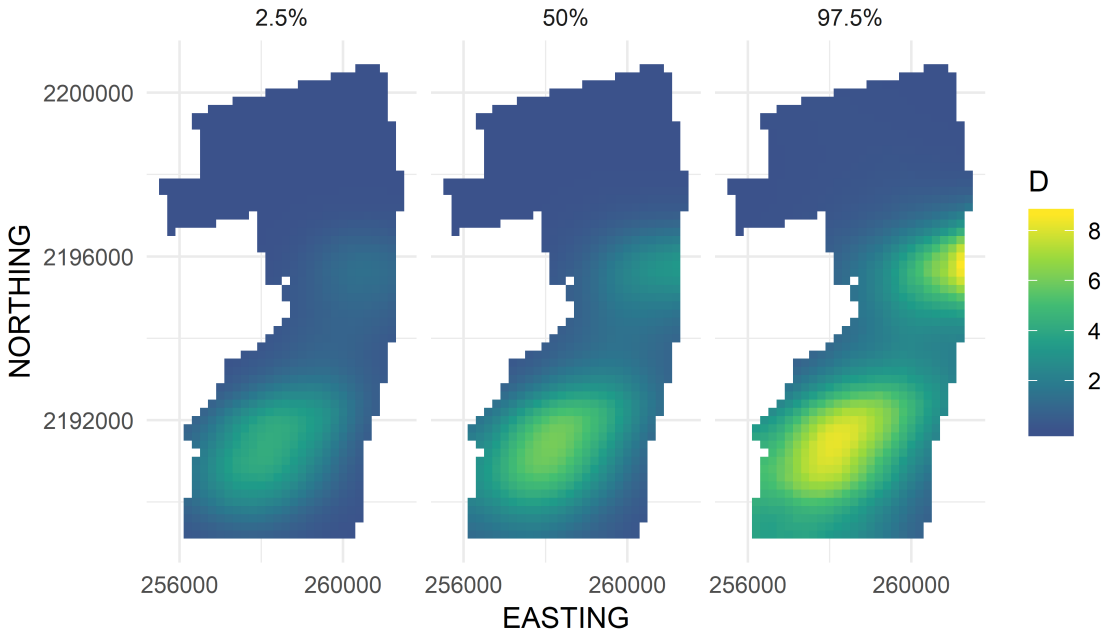

Figure 3.6: Median and 95%CI density estimates from the DSM approach.

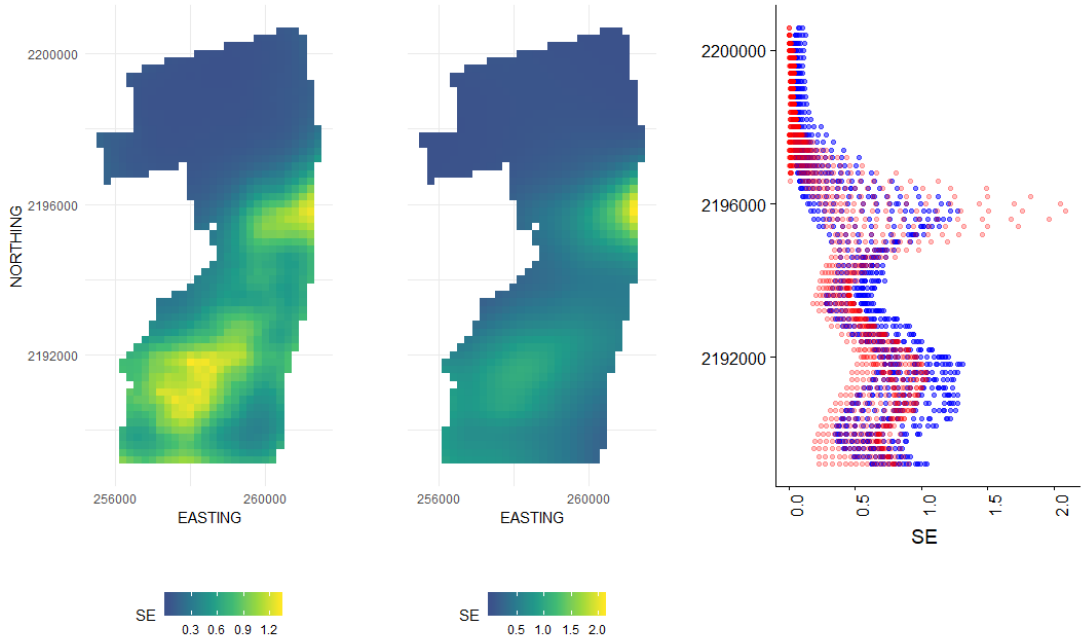

Figure 3.7: SE estimates from the (left panel) point process and (middle panel) DSM approaches. Scatterplot of the per cell SE estimates along the Northing axis (blue point process and red DSM approaches; right panel). Scales between the two approaches were not standardized.

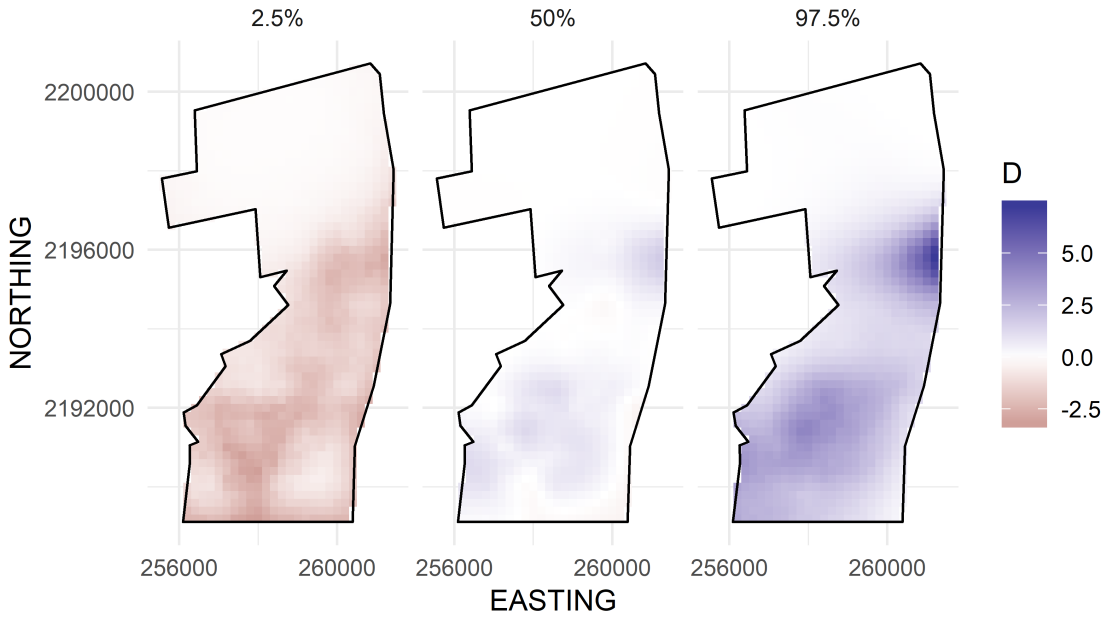

Figure 3.8: Difference in density median and 2.5% and 97.5% quantile estimates between the point process and DSM approaches. Per cell differences were calculated as the DSM estimate minus the point process estimate.

two approaches (DSM estimate - point process estimate) was small throughout most of the northern third of the study area, greatest along the east boundary in the middle of the study area and variable in the southern half of the study area (Fig. 3.8). Differences were relatively small where the average difference between the median estimates was 0.229 (SE = 0.358).

3.5.3 Abundance estimates

There was an almost 1,000 bird difference in abundance estimates between the two approaches (Table 3.5; Fig. 3.9). Mean abundances for both approaches were slightly larger than median abundances, indicating a small degree of skewness with heavier upper tails. The interval lengths of both approaches were relatively narrow, and the interval lengths bracketed the mean and median abundance estimates of each approach. The point process approach was slightly more precise with a CV of 11.2% than the DSM approach with a 12.2% CV. The design-based abundance point estimate was 8,920 birds (SE = 1,111; 95%CI 6,990–11,381). The 95%CI estimates from the design-based method bracketed the DSM point estimate but not the point estimate of the point process approach, and the interval lengths of all three approaches overlapped.

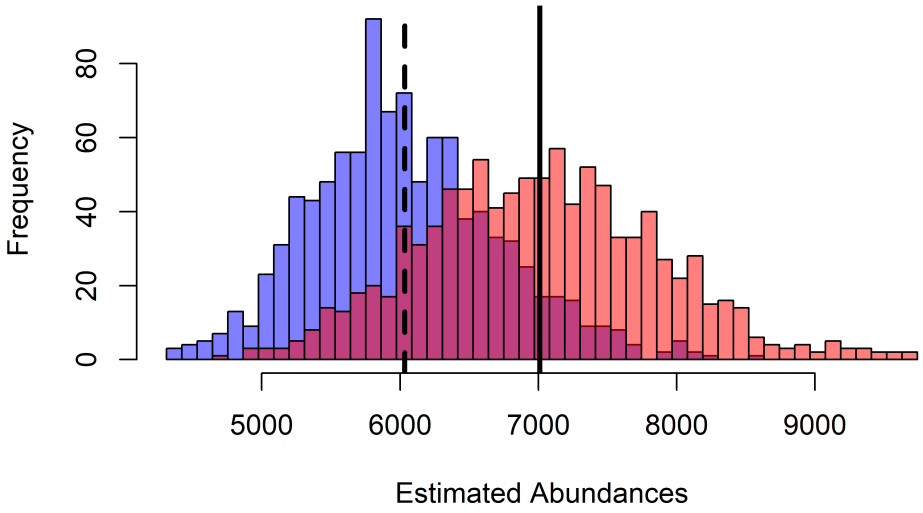

Figure 3.9: Histograms of the point process (blue) and DSM (red) approach posterior distribution of abundances. Overlap between the two distributions is indicated in purple. Vertical lines are the mean abundance for point process (dashed) and DSM (solid) distributions.

3.6 Discussion

I have presented results from estimating densities and abundances using point process and DSM approaches. Both approaches were applied to the 2002 'ākepa survey data from Hakalau. Seaton et al. (in preparation) fit a point process model with a thinned log-Gaussian Cox process where thinning was achieved by the detection function. The log-intensity of points was modelled using an SPDE with spatial correlation defined by the Matérn class in a Bayesian model fitted using INLA. I fit the DSM approach with a two-stage model-based analysis using TPRS in a GAM. The detection function was modelled in the first stage and the point counts were modelled in the second stage with an estimated offset to allow for imperfect detection. In general, both approaches produced similar density surfaces with coinciding hot and cold spots, densities and uncertainty. The point process approach produced a higher degree of spatial variation (i.e., a more wiggly surface) than the DSM approach that was generally more smooth.

No 'ākepa were detected in the northern third of the study area in 2002 and both modelling approaches predicted densities at or very near zero throughout the northern region. The main differences were that the point process approach estimated densities of approximately zero at the north-west boundary and low densities elsewhere, while the DSM approach estimated densities of approximately zero along the north-east corner and the peninsula on the western boundary. The point process approach produced marginally larger per cell estimates across the northern region. Within this region these patterns were also seen in the differences of the SEs where estimates were most different along the eastern

boundary and in the peninsula but otherwise were fairly consistent across the coldspot. In general, there was a tendency by the point process approach to produce slightly larger densities in areas without detections.

This tendency was reversed for the two hotspots where the DSM approach estimated larger densities. The hotspot at the east boundary in the middle of the study area radiated outward from the boundary in concentric contours between transects nine and 10 (see Fig. 3.1; Appendix C Figs. C.11 and C.12). Variability in the point process approach densities was greatest at the east boundary where survey effort was minimal, a similar pattern was seen in the point process approach (Fig. 3.7).

Both approaches had good spatial alignment of the hotspot in the southern part of the study area. Density contours roughly followed radiating ellipses along a south-west to north-east axis. The contours were generally less well defined for the point process approach relative to the DSM approach that predicted larger densities. In this area the greatest difference between the two approaches was in the SE estimates. The point process approach produced a patchwork of varying SEs whereas the SEs from the DSM approach were uniformly small across the entirety of the hotspot and with less cell-to-cell variability extending to the boundaries. Thus the point process approach produced a more wiggly surface, following the underlying assumption imposed by the Matérn field, while the DSM approach was generally more smooth that was induced by the underlying assumption of the TPRS.

3.6.1 Model checking

Sampling design

Spatial models assume that the relationship between the birds and spatial covariates is the same at sampled and un-sampled locations. This assumption allows for predictions based on this relationship using the observed data. As detailed in Chapter 1, the HFBS uses a spatially explicit randomized sampling design where survey points were established on transect lines following a systematic random design, thus helping to ensure this assumption is met.

Detection function

Both modelling approaches inherit the detection function modelling assumptions of distance sampling. This includes the assumption that the parametric function decays with increasing distance, in addition to the critical assumptions and additional requirements covered in Chapter 1 Section 1.4.1. As I noted in Chapter 1, it is likely that there are moderate violations to these assumptions. However, care is taken to ensure observers are aware of and sample so as to minimize the effects of model assumption violations (see details in Chapter 1 Section 1.4.1).

Point process approach

For the point process approach the sampling points are assumed to be non-overlapping discs with radius w, in this case the truncation distance. The counts from each point are then independent and Poisson distributed. The spatial arrangement of points and random component of the sampling design helps ensure this assumption is met. This assumption of non-overlapping points could be relaxed by including extra information such as the time of each sample; however, this is not required for this analysis.

Following from the spatial assumptions above, it is assumed that the location of birds are a point pattern that follows a log Gaussian Cox process with intensity process. That is, the observations are assumed to be conditionally independent, given the intensity function that describes the underlying dependence structure of the data. A measure of spatial dependence, called a K-function, was assessed to determine if the point process modelled captured the heterogeneity (Cressie and Wikle 2015). Estimation of the K-function is achieved by averaging pairs of events that are at distance h-apart or less from each other. Distances were selected to span the length of Hakalau and pairwise distance comparisons were generated from the fitted model using 100 thinned point patterns. The K-function indicated the model performed well, only showing potential clustering of counts between 1,000 and 2,500 m (Fig. 3.10; recreated from Seaton et al. (In preparation)). This results in over-predicting the strength of the clustering at these distances. The strength of clustering at these relatively large distances could be biased by an "edge effect" (Cressie and Wikle 2015, pg 212). All points in the study area are within 2,500 m of the boundary edge, and a majority are within 1,000 m of the boundary (Fig. 3.1). An additional source of this bias could come from the transect lines in the northern portion of Hakalau being about 1,000 m apart. Without control of this bias the point process approach may be applying long-distance smoothing of the counts which could yield biased estimates. Given the cell to cell heterogeneity in density and SE estimates this is not likely the case (see Figs. 3.5 and 3.7, and Appendix C Fig. C.11).

The specified point process approach assumes that the response variable is Poisson distributed. Bayesian analysis with INLA has a limited set of predictive measures of fit tests such as out-of-sample estimates that are appropriate for certain sub-cases of point processes (Rue et al. 2017); however, their application to inhomogeneous and thinned models used here is limited. The sensitivity to the response distribution choice assessment I conducted for the DSM approach supports that the response variable counts is approximately Poisson distributed.

DSM approach

The DSM approach allows for fitting residual errors through the GAM machinery following approaches suggested by Wood (2017) and detailed in Chapter 2. Response distribution selection was based on AIC, inspection of residual plots and sensitivity checking. There was little un-modelled residual autocorrelation from the Poisson distribution model, and the deviance explained was 53.5%. The percent of deviance explained is an effect size measure, and as such is context dependent. Marra et al. (2012) concluded that their

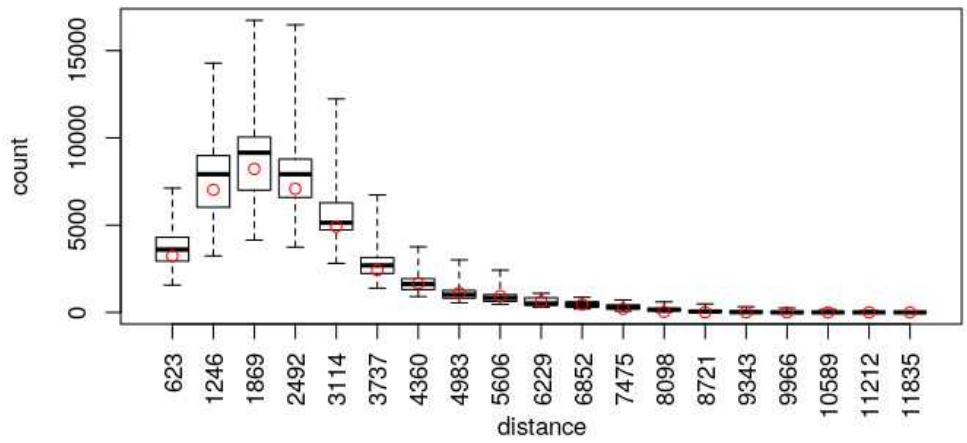

Figure 3.10: Boxplots of pairwise distances from 100 posterior samples. Bin widths indicated by tick marks. Observed pairwise distances between observations noted by red circles. Figure recreated from Seaton et al. (In preparation).

model, which explained 57% of the deviance, was adequate for spatial inference. Based on these model diagnostics, I chose the Poisson distribution with log-link for modelling the spatial patterns. This matched the distribution used in the point process approach, eliminating deriving conclusions from models with different distributions and allowing for more direct comparison of the underlying smoothness.

Underlying smoothness

An important assumption of spatial-analysis is that the response variable is a smooth function of the spatial parameters. That is, the underlying smoothness of the surface is such that neighbouring cells generally have similar values. The two approaches applied here enforce similarity among neighbours through penalties on the priors for the point process approach (Blangiardo and Cameletti 2015) and on coefficients for the DSM approach (Wood 2017). Assumptions on the prior variance of the coefficients also affects the smoothness of the point process approach. The two approaches thus vary in their ability to capture pattern in the data. The point process approach used a Matérn field that allows for short range dependence in the scale correlation that can account for greater heterogeneity in the underlying spatial patterns; i.e., the point process approach can fit a wiggly or smooth surface. Whereas the DSM approach assumes the data vary smoothly and the tension in the splines deforms to the data to fit a smooth surface.

Critical to understanding how the different approaches behave smoothly with this data is to understand the data itself, i.e., to understand the underlying smoothness/wiggleness of bird counts. Blangiardo and Cameletti (2015) recommend mapping the posterior means and associated uncertainty to provide useful information on how well the different approaches captured the non-smoothness of the data. The mapped posterior distributions

(Figs. 3.5 and 3.6, and Appendix C Figs. C.11 and C.12) and the per cell differences (Fig. 3.8) yielded significant insights into the data heterogeneity, particularly the hotspot in the southern portion of Hakala. In this hotspot the DSM approach provided a smoothed surface. In contrast, the point process approach was less smooth with adjacent cells varying considerably, reflecting the discontinuity of the counts. The end result was that the point process approach had lower uncertainty than the DSM approach, a feature of the point process approach to model the short-range dependency among counts to capture the non-smooth behaviour in the data.

3.7 Choosing between the two approaches

In this chapter I have focused on how the point process and DSM approaches are similar and different, and have avoided purporting that one approach is better than the other. I believe this is a more useful approach that will allow researchers to select one or the other analytic approach to model spatial processes based on the variability and underlying smoothness in the data. My overall objective is to produce a precise abundance estimate accounting for spatial variability in the 'ākepa data. As seen in Fig. 3.1 the 'ākepa counts vary in space with highest counts recorded in the southern portion of Hakalau while no birds were detected in the northern portion. Both modelling approaches produced visually similar hot and cold spots reflecting the count distribution (Figs. 3.5–3.7). In the southern hotspot, SEs from the point process approach were generally larger and much more variable than those estimated using the DSM approach. While in the central part of Hakalau the DSM approach SEs were larger than the point process approach estimates. The scatter of detections along transects nine and 10 was similar with one to three detections at a point or two interspersed between points with no detections. However, the distance between the transects increases to the east and predictions are made from increasingly distant survey points. On the western end of the transects the point process and DSM approach specific predictions were very similar but increasingly differed progressing eastward. With low numbers of detections and sparse survey effort the DSM approach appears to have suffered an "edge effect" (Miller et al. 2013) resulting in overestimated 'ākepa densities and large uncertainty estimates. As with all spatial models, smoother methods can produce questionable estimates if there are gaps over the range of covariate values or where predictions are made further away from the survey points (Miller et al. 2013). The large gap between transects nine and 10 adversely affected the DSM approach estimates with the greatest densities occurring at the eastern boundary. In contrast, the point process approach had the greatest densities well within the eastern boundary (between transects nine and 10, but slightly east of half the distance between the east-west boundaries).

A final consideration when choosing between the two approaches is the amount of statistical and computational skill necessary to apply the models. The point process approach requires an advanced level of statistical modelling and a thorough understanding of the procedures to ensure the models are reliable and results appropriately interpreted. For example, the point process approach requires the modeller to manually code the detection

function whether assuming the detection probability depends only on the horizontal distance or includes covariates which affect the detection probability. The theory underlying point process modelling is provided in Illian et al. (2008), Diggle (2014), Blangiardo and Cameletti (2015) and Cressie and Wikle (2015). Point process modelling using the software `inlabru` provides a statistical package for analyses (Bachl et al. 2019). The DSM approach provides more flexibility for non-statistically trained modellers to apply sophisticated and specialized software to model the detection function and evaluate if point- and individual-level covariates should be included. Well-established and documented software to model the detection probability is available in Distance for Windows and Distance for R with theory and examples provided in Buckland et al. (2015), and spatial modelling is available in the `mgcv` package with theory and examples provided in Wood (2017). Similar to `inlabru`, the `dsm` wrapper helps facilitate much of the detection probability and spatial modelling simplifying the analysis. This, however, does not minimize the need to understand flexible regression theory and its application. A limitation to the DSM approach is that more advanced modelling is required to incorporate the various sources of parameter uncertainty between model stages to estimate total uncertainty. The variance propagation methods I described in Chapter 2, including the delta method assuming independence used in this chapter, are applicable for propagating the detection probability uncertainty from the first-stage through to the second-stage.

Chapter 4

Controlling boundary behaviour

4.1 Overview

Here I apply a spatially-referenced soap-film smoother-based model to produce abundance estimates accounting for boundary effects. The thin plate regression spline (TPRS) basis-penalty smoother I applied in Chapters 2 and 3 can result in biased estimates and be biologically unrealistic because it is not constrained by the study area boundary (Wood 2006, pgs 223 & 368-370). In contrast, a soap-film smoother controls the boundary behaviour by using two separate but linked bases; one for the boundary and one for the domain film. In Section 4.2 I describe some conditions for which TPRS models may be biased and introduce soap-film smoother models that account for those conditions. Section 4.3 describes the data and boundary, methods to model abundance using `Distance` in `R`, spatial soap-film and TPRS smoother-based models, and methods to compare among the estimates. In Section 4.4 I present estimates derived from the three different modelling approaches and compare their estimates. Section 4.5 gives a discussion of the statistical methods, biological findings and management implications of applying soap-film smoothers to estimate population status.

4.2 Introduction

In Chapter 2 I modelled the spatio-temporal densities of 'ākepa across a 31-year time series using a two-stage model-based smoothing method. This method captured spatial and temporal correlation in bird densities, thus reducing estimates of uncertainty. In Chapter 3 I compared the uncertainty estimates accounting for spatial correlation between point process and DSM approaches for a single survey. In both of these chapters the penalized spline-based smoother predicted non-zero densities across the forest boundary into non-suitable habitat, a modelling artefact commonly termed "leakage." Leakage occurs when the smoother links data across a gap between separate parts of the study area and can result in over- or under-estimated densities. The leakage observed here was a result of the topological structure and contours extending across the relatively simple boundary (i.e., the pasture-forest boundary was not complicated or convoluted; Fig. 4.1).

Leakage is a concern in these analyses because no 'ākepa were detected in the pasture

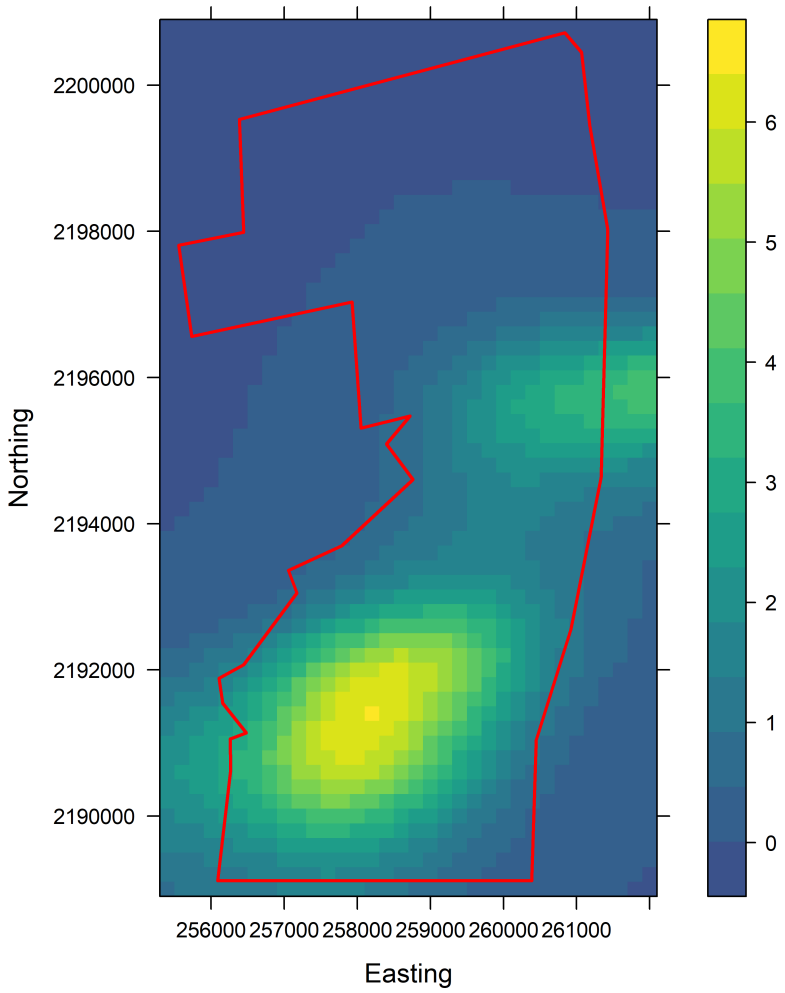

Figure 4.1: Density (birds ha^{-1}) estimates from the fitted GAM basis-penalty to the prediction surface that contains the forest stratum (red polygon). The predicted densities in the pasture stratum outside the forest stratum boundary were modelling artefacts, commonly termed "leakage."

stratum in 2002 (see Chapter 1 Fig. 1.1), and the afforestation in the pasture had not progressed to produce suitable 'ākepa habitat. While densities in the pasture stratum could easily be excluded by integrating over the forest strata (see the Bristol channel sole data example in Section 7.7.1 of Wood (2017)), the leakage draws into question the applicability of the model, impeding interpretation from the spatial analysis. That is, do 'ākepa occur at relatively high densities right to the pasture-forest boundary or do densities taper prior to declining rapidly to zero at the strata edge? This question can be addressed by modelling the surface of the boundary interior as well as estimating the boundary densities by applying a soap-film smooth (henceforth soap) to the data (Miller et al. 2013, Wood 2017). I modelled the 2002 'ākepa forest stratum data, re-selecting the detection function, soap smoother and residuals distribution models. I compare the soap smoother estimates to those of a TPRS smooth and conventional distance sampling analysis.

4.3 Methods

4.3.1 Study species and selected survey

The analyses in this chapter are conducted on the Hawai'i 'ākepa data collected at Hakalau, see Chapter 1 for detailed description. For this analysis I selected a single survey from the 'ākepa time series based on broad sampling of the study area and sufficient numbers of detections. In 2002, 289 points were sampled using PTDS methods within the forest stratum where 276 'ākepa were detected at 121 points (see Chapter 3 Fig. 3.1).

4.3.2 Study area

Managers and policy makers require population estimates applied to representative political or management boundaries. Here, I expanded the forest stratum study area used in Chapter 3 to include the surveyed portions of the open- and closed-forest strata as well as extending the extrapolation area to coincide with plausible management units. The western edge of the boundary was set to the coordinates of the pasture-forest boundary, while the north, east and south boundaries were squared off (hereafter, referred to as the "soap boundary") using the function `locator` (Becker et al. 1988) (Fig. 4.2). In addition to defining the soap boundary, soap-film smoothing also required *a piori* defining the number and location of knots to be spread throughout the bounded domain. I defined a set of knots on a regular grid with locations every 730m east and 670m north across the study area; this ensured that all knots occurred either inside or outside the soap boundary to choose those within the soap boundary domain (Fig. 4.2).

4.3.3 Design-based density estimation

For comparative purposes I estimated the 'ākepa abundance using conventional distance sampling methods (Buckland et al. 2015). Using the R package `Distance` (hereafter, DistR) (Miller 2017) I evaluated if a half-normal or hazard-rate key detection function

Figure 4.2: Plot of forest stratum study area (red polygon) with points and knots located within the soap boundary (blue polygon). The open circles are sampling points. Knots within the boundary are orange circles.

without adjustment terms or covariates better fit the 2002 forest stratum data. Data were truncated at a distance w where the estimated detection probability (using a preliminary detection function model) was about 0.1. Model selection for the best approximating detection function followed AIC methods (Burnham and Anderson 2002) and model fit was evaluated with a Cramér-von Mises test (Buckland et al. 2015). I then combined the estimated detection probability with counts using a design-based method to estimate densities following the methods described in Chapter 1 Section 1.4.2. Density was estimated as birds ha^{-1} and abundance was estimated as density times the area of the soap boundary (5,671.8 ha). Variance and 95%CI were calculated using analytic methods.

4.3.4 Model-based density estimation

Soap-film smoother model

Previous analysis revealed that leakage occurred with the TPRS model (Fig. 4.1). To control leakage Miller et al. (2013) suggest using a soap-film smooth (Wood et al. 2008) to fit the surface instead of a TPRS smoother (Wood et al. 2008, Marra et al. 2012, Wood 2017). The soap smoother consists of two component smooths, one delineated by a domain Ω and one modelling the values on the polygon bounding the domain (i.e., the soap boundary). The former basis function smooths within the surface of the domain while the latter smoother conforms to the boundary conditions. Densities in Ω are derived from a smooth of the data. Density values on the boundary can either be fixed or estimated. When birds occur in proximity to the boundary and the boundary density is fixed to be zero, the domain smooth will distort as it is forced to decrease to meet the boundary condition. When birds occur at the boundary, the boundary smooth can be used to estimate densities. A cyclic spline smoother is employed along the boundary. The cyclic spline smooth matches the spline "end points," ensuring that the value of the first and last knots are equal. Thus, in the cases where boundary densities are estimated the boundary condition is enforced while allowing smooth departures into the interior of the domain: the interior smooth is dependent on the data (Wood 2017, pg 223-227).

To meet soap smoother model requirements, I modified the spatial smoother model from Chapter 3. The model was built in `R` (R Core Team 2017) using the `mgcv` package (Wood 2016). I specified the basis in two parts to ensure adequate complexity for both the boundary and interior smoother components. The soap model has the form

$$\begin{aligned}\log\{\mathbb{E}(n_k)\} =& f_1(\texttt{Easting}_k, \texttt{Northing}_k) \\ &+ f_2(\texttt{Easting}_k, \texttt{Northing}_k) + \log(\hat{\nu})\end{aligned} \tag{4.1}$$

where n_k is the bird count at the k-th point, f_1 is the boundary smooth `bs="sf"` that was estimated and defined with a maximum basis size of 20. Although the maximum number of basis dimension is arbitrary, it is sufficiently large to permit enough degrees of freedom to represent the underlying smooth reasonable well (see Chapter 2). f_2 is the interior smooth that was fit with `bs="sw"` and with up to 108 basis dimensions which is equal to the number of knots within the boundary. $\hat{\nu}$ is the effective area searched and the

offset is the log of $\hat{\nu}$. Covariates were not included when modelling the detection function; therefore, the effective area searched was constant across all points. The soap model was fitted with a negative binomial response distribution with a log link (see Appendix D for response distribution modelling, evaluation and selection). REML method was used to estimate smoothing parameters and density estimates were predicted from the fitted model to generate a density surface model of densities and standard errors. Model assumptions were checked using methods detailed in Chapter 2.

TPRS smooth model

I fitted a spatial, penalized spline-based smoother following the same spatial TPRS smoother modelling procedures used in Chapter 3. The model was built in `R` using the `mgcv` package. The TPRS model has the form

$$\begin{aligned}\log\{\mathbb{E}(n_k)\} =& f_1(\texttt{Easting}_k) + f_2(\texttt{Northing}_k) \\ &+ f_3(\texttt{Easting}_k, \texttt{Northing}_k) + \log(\hat{\nu})\end{aligned} \tag{4.2}$$

where n_k is the bird count at the k-th point, f_1 and f_2 are one-dimensional isotropic TPRS smooth functions, f_3 is a two-dimensional interaction smooth function generated via tensor products, $\hat{\nu}$ is the effective area searched and the offset is the log of $\hat{\nu}$. The basis was set to match the maximum complexity of the soap smoother (above), with 14 basis dimensions each for the one-dimensional basis terms and a combined set of 11 by 11 bases for the interaction term, that when smoothed yielded a total of 126 knots (1 degree of freedom per term is allotted for the identifiability constraints, 4 in total; Wood (2016) help pages). REML methods were used for estimating smoothing parameters. A negative binomial response distribution with a log link was used to model the response distribution (see Appendix D for response distribution modelling, evaluation and selection). Density surface model and corresponding standard errors were generated from the fitted model.

4.3.5 Comparison among estimates

Estimated coefficients cannot be directly compared between most spline models. To assess how the TPRS and soap smoothers predicted density and uncertainty estimates I mapped the distribution of 'ākepa densities across the soap boundary on a grid with cells 200 x 200 m. I also evaluated the model predictions at even distances along the boundary.

Following methods detailed in Chapter 2, estimates of abundance and 95% confidence intervals (CI) were independently computed from the posterior distribution of the TPRS and soap fitted models (Wood 2017). A total of 10,000 replicate parameter value sets were drawn from the posterior distribution of the model coefficients, $\hat{\boldsymbol{\beta}}$, based on a random multivariate normal distribution with a vector of covariates conditional on the data and the posterior variance-covariance matrix for $\hat{\boldsymbol{\beta}}$. I refitted the linear predictor matrix to the replicate sets and estimated abundance as the mean of the replicate sets, SE as the standard deviation of the replicates and 95%CIs were computed from the 2.5th and 97.5th quantiles. The detection function uncertainty was not propagated with the uncer-

tainty from either model-based approach as the detection probability does not contain any spatial variability (modelled without covariates since there were no detection covariates). For plotting purposes I used the `boxplot` function to identify outliers as estimates that exceeded the boxplot extreme upper whisker value (the third quartile plus 1.5 times the interquartile range). There were 685 outliers in the posterior distribution of the TPRS (range = 11,308 to 430,771) and 224 outliers in the soap smoothers (range = 5,547 to 14,369) that were removed for plotting purposes. Outliers were included when computing summary statistics. Similar to the comparisons of CI widths between models in Chapter 2, I computed the change in uncertainty as the percentage change in CI widths (CIW) between soap and TPRS, and soap and DistR abundance estimates.

4.4 Results

4.4.1 Design-based density estimation

Using a preliminary detection function model, truncation was set at 58m. The AIC for the hazard-rate detection function model was 11 units smaller than that of the half-normal model (Table 4.1). The Cramér-von Mises test was non-significant at the $\alpha = 0.05$ level indicating that the detection function did not statistically differ from the distance histogram. Inspection of diagnostic plots indicated that the model adequately fit the data (Appendix D Fig. D.6). The shoulder of the detection probability extends out to 30 m before decaying rapidly. The estimated detection probability of a bird that was within 58m of a point was 0.631 (SE = 0.035) and the effective area surveyed per point was 6,668.6 m^2.

4.4.2 Soap-film smoother

The soap smoother with 3.0 of 18 boundary degrees of freedom and 14.4 of 108 interior degrees of freedom (Table 4.2) explained 54.6% of the variance in the data. The negative binomial dispersion parameter was 10.55 indicating that the counts were over-dispersed. As expected, the contours of the interior smooth paralleled the soap boundary particularly along the pasture-forest boundary where densities were 1.0 (coefficient zero; Fig. 4.3, left panel).

The main advantage of using the soap smooth is that there was no leakage across the pasture-forest boundary (Fig. 4.4, top left panel). 'Ākepa densities occurred at relatively high densities of about 1.25 birds ha^{-1} right to the pasture-forest boundary in the

Table 4.1: Detection function model selection statistics and parameter estimates. Key function without adjustment terms ranked by AIC. Presented are the model unweighted Cramér-von Mises (C-vM) statistic and p-value, and the estimated detection probability with SE.

Key function	Δ AIC	C-vM	p-value	$\hat{P}_a$	se($\hat{P}_a$)
Hazard-rate	0	0.042	0.920	0.631	0.035
Half-normal	11.094	0.428	0.061	0.443	0.040

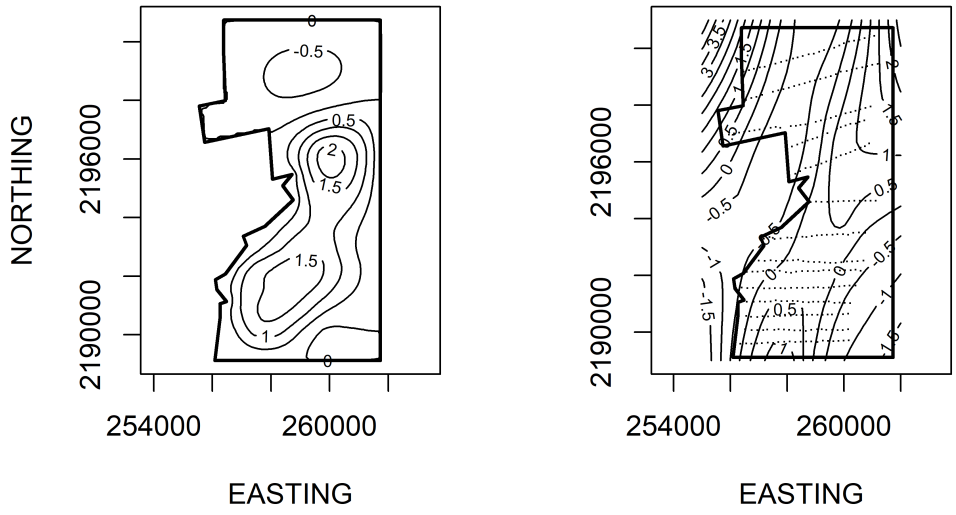

Figure 4.3: Comparison of smoothing using a soap-film (interior smooth; left panel) and thin plate regression spline (right panel) based GAMs. The soap boundary is outlined by the polygon (bold line) while the contours (thin lines) show the estimates of the smooth on the linear predictor scale. The dots in the right panel are the sampling points. Predictions were made over a larger area with the `too.far` argument to illustrate that the TPRS model suffers from leakage along the west boundary.

Table 4.2: Effective degrees of freedom (EDF), reference degrees of freedom (rf), and basis complexity (k-index) for each term in the soap-film smooth spatial model.

Term	EDF	rf	k-index
`ti(Easting, Northing)`	2.978	18	1.01
`ti(Easting, Northing)`	14.448	108	1.01

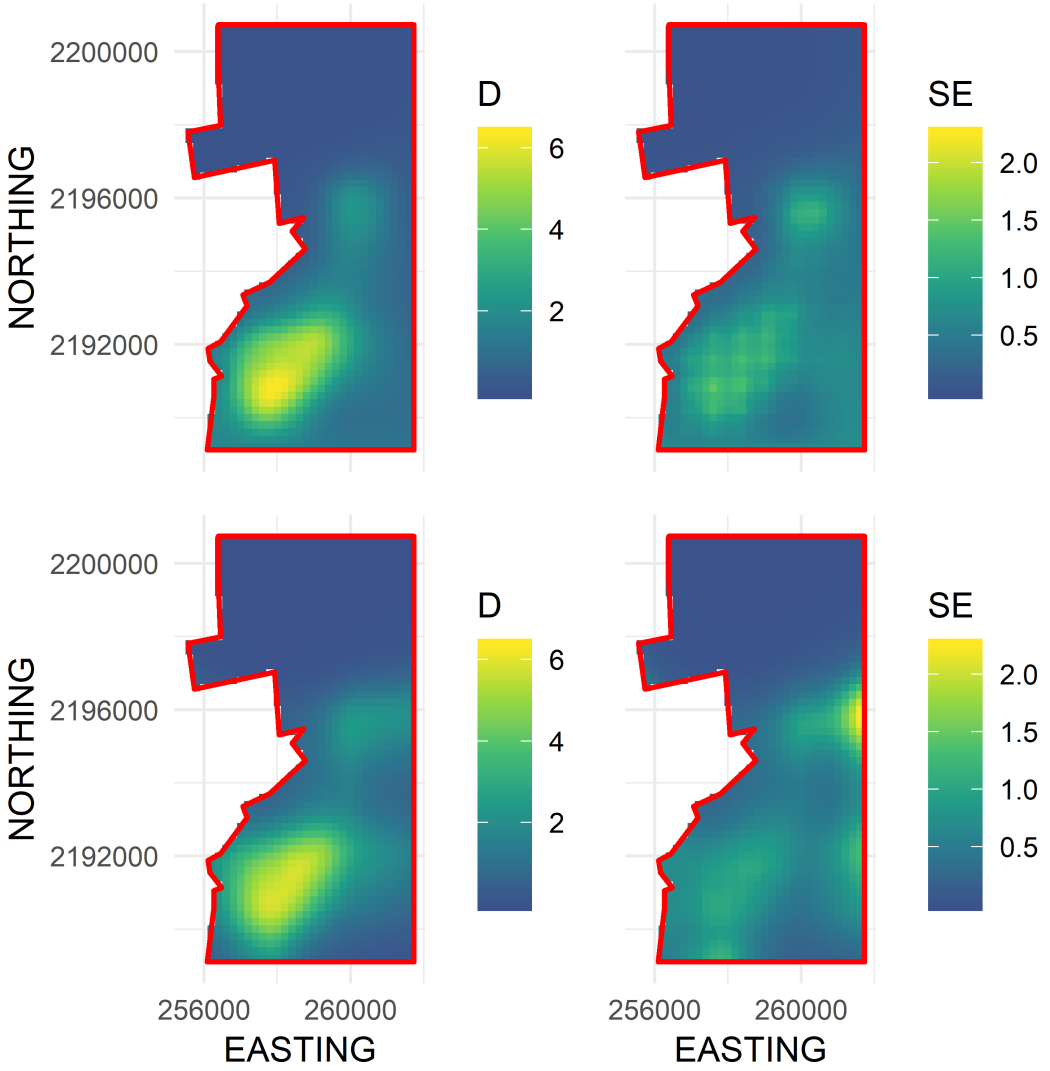

Figure 4.4: Predicted density surface map of 'ākepa densities (birds ha^{-1}; left column) and SE (right column) for the 2002 dataset using a soap-film (top row) and TPRS (bottom row) based smooths. Fitted values projected to the soap-film boundary (red polygon).

south-west, but decreased to near zero along the north-west boundary (Fig. 4.5). Density estimates along the north, east and south boundaries varied. The density surface maps showed an 'ākepa density hotspot in the southern portion of the domain that extended north-east to a second hotspot in the central portion of the domain (Fig. 4.4, top left panel). Densities throughout the north portion of the domain were zero or near zero. The uncertainty estimates portrayed the same pattern with large SEs predicted in the southern portion that extended north-east to the central portion of the domain (Fig. 4.4, top right panel). SEs in the north portion of the domain were near zero while SEs were moderate adjacent to the south boundary and throughout a swath along the south-east boundary.

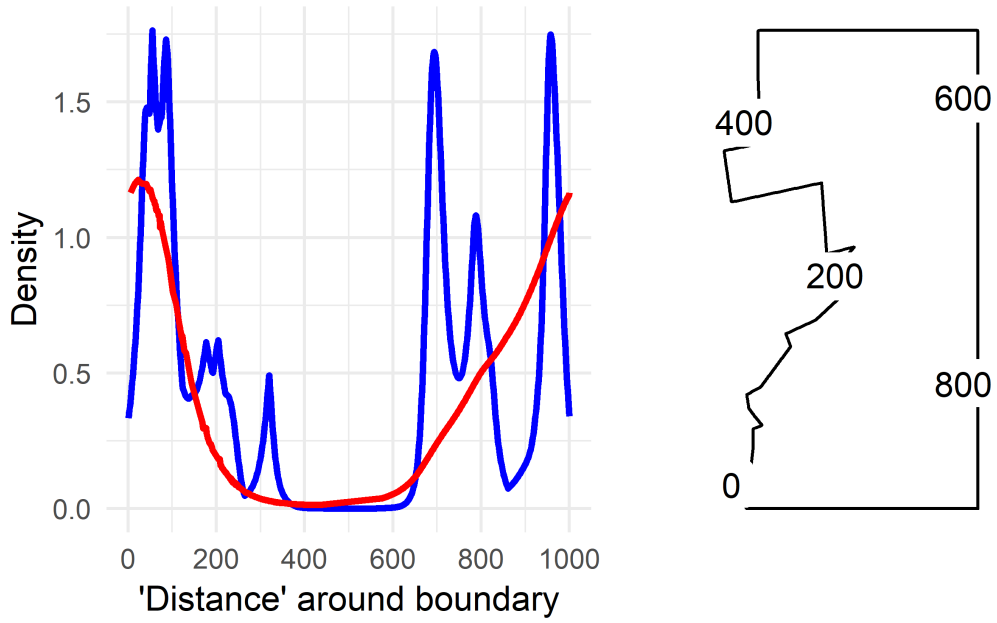

Figure 4.5: Predicted 'ākepa densities along the boundary (left panel) for the 2002 dataset using the soap-film (red) and TPRS (blue) smoother. Location of "distance" around the soap-film boundary (point 0 and 1000 are at the same location; right panel).

Table 4.3: Effective degrees of freedom (EDF), reference degrees of freedom (rf), and basis complexity (k-index) for each term in the TPRS smooth spatial model.

Term	EDF	rf	k-index
`s(Easting)`	3.655e-05	13	0.86
`s(Northing)`	5.870	13	1.01
`ti(Easting, Northing)`	8.097	100	1.02

4.4.3 TPRS smoother

The TPRS smoother had an estimated negative binomial dispersion parameter of 12.217 and explained 54.5% of the deviance. The EDF on `Easting` was approximately zero, non-significant and the smooth function was linear (Table 4.3; Appendix D Fig. D.5, top left panel). The EDF on `Northing` was greater than zero, significant and the function was wiggly (Table 4.3; Appendix D Fig. D.5, top right panel). There was a clear pattern of lower densities in the north than in the south part of Hakalau. The interactions of `Easting` and `Northing` were also greater than zero, significant and the function was nonlinear (Table 4.3; Appendix D Fig. D.5, bottom panel).

There were two density hotspots and three SE hotspots in the density surface maps predicted from the TPRS model (Fig. 4.4, bottom left and right panels respectively). The hotspot in the south portion had a maximum contour of 2.7 with slightly larger estimates at the south boundary (Fig. 4.3, right panel). In this area the contour coefficients decreased to 0.4 along both the west and east boundaries. The opposite pattern was fitted in the north half of the study area. Minimum values were centrally located between the maximum values of greater than 7.4 at both the west and east boundaries. The contours of the TPRS

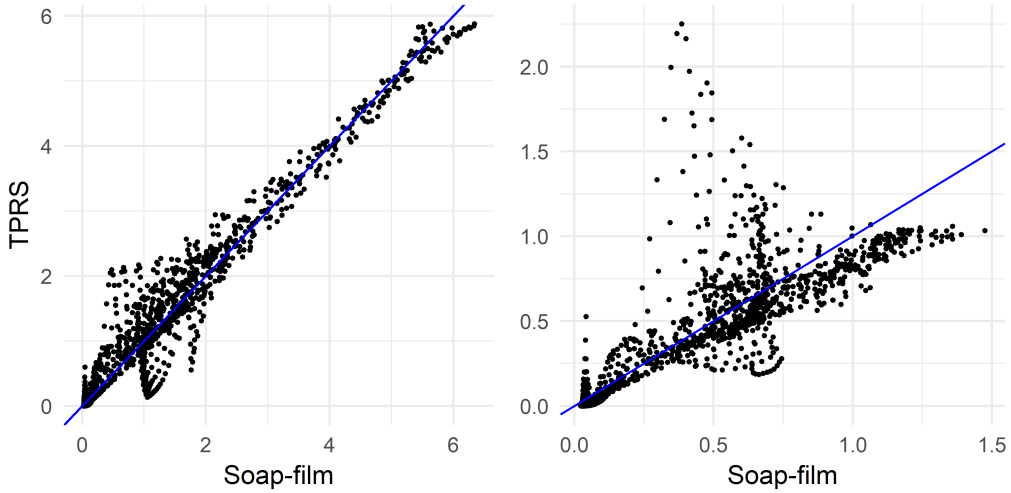

Figure 4.6: Scatterplot of the pointwise soap-film and TPRS smoother predicted density (birds ha^{-1}; left panel) estimates, and SE estimates (right panel). Dots are the grid pointwise estimates. The identity line (blue) passing through the origin with unit slope is added as a visual aid.

model continued beyond the soap boundary, which resulted in very convoluted densities along the boundary (Fig. 4.5).

Comparison of smooths predictions

Both smoothers had visually similar cold and hotspots in the domain with similar predicted densities and SEs (Fig. 4.4). Both smoothers predicted zero or near zero densities in the northern part of the domain. The extent of the coldspot was much larger for the soap smooth than for the TPRS smooth extending from the central hotspot to the north boundary, while the TPRS smooth predicted approximately zero densities to about half the area of that predicted by the soap smooth. The large hotspot in the southern part of the study area was similar in shape and extent between the two smoothers. The local hotspot in the central part of the study area was more symmetrical for the soap smooth than for the TPRS smooth which was more triangularly-shaped. For the TPRS, both hotspots extended to the boundary. In contrast, both soap smooth hotspots occurred interior to the boundary, even though the parametrization allowed for fitted values to persist right to and including the boundary. There was very little scatter in the predicted-predicted density plot for cells with higher densities while the scatter was greater for cells with low densities (Fig. 4.6, left panel). The plotted densities followed the identity line indicating the soap densities were similar to those predicted by the TPRS smooth.

Greater differences between the two smoothers were observed in the fitted SE than the fitted density estimates (Fig. 4.4). The TPRS had three SE hotspots while the soap had two hotspots. These differences may be due to lack of coverage by the data or differences in knot number and placement (although this latter point is not likely as the EDF were small compared to the maximum degrees of freedom). For the TPRS, the SE global maximum occurred in the central part of the domain adjacent to the boundary. The equivalent soap

SE hotspot was more centrally located between the east and west boundaries and the SE estimates were smaller. The soap smooth global maximum was in the southern part of the domain and the hotspot portrayed a patchwork of varying SEs while the TPRS SEs were relatively uniform across the entirety of the hotspot with less cell-to-cell variability. There was greater scatter between the predicted soap and TPRS smooth SE estimates than in their predicted densities estimates (Fig. 4.6, right panel). There was little scatter for higher predicted SE estimates while the scatter was large for low to moderate SE estimates. The plotted SE estimates followed but lie below the identity line indicating that soap SE were slightly larger than the TPRS estimates.

The soap-film basis argument controlling the boundary smooth eliminated the extreme rough densities of the TPRS smooth (Fig. 4.5). On the boundary the largest densities predicted by the soap smooth occurred in the south-west corner of Hakalau (labelled zero in Fig. 4.5). Densities declined smoothly to near zero by and along the northern boundary (occurring between 300 and 600 in Fig. 4.5) and then increased progressively along the eastern boundary until again reaching maximum densities of nearly 1.25 birds ha^{-1} at the south-west corner. Predicted densities from the TPRS smooth were more rough with peaks at points 80, near 700 and at 950 along the boundary (Fig. 4.5). There were minor peaks at about points 200, 300 and 800. Each of these peaks occurred where contours intersected the boundary (compare Figs. 4.3, right panel, and 4.5). In between each peak the TPRS smooth predicted small to very small densities before increasing rapidly to the next peak. Similar to the soap smooth, the TPRS smooth predicted near zero densities along the northern boundary, between points 400 and 600. The peak at 300 suggests leakage by the TPRS smooth where the nearest birds were detected more than 2 km distant (see Chapter 3 Fig. 3.1).

Abundance estimates

Sampling from the posterior distribution showed that both the TPRS and soap smooths produced many very large abundance estimates (greater than 12,000 birds; Appendix D Figs. D.7 and D.8). These outliers strongly skewed the abundance estimates of the TPRS smoother and resulted in very large SE estimates (Table 4.4; Fig. 4.7). The median abundances of the two approaches differed by more than 500 birds, and the confidence interval widths differed by nearly 6,500 birds. Estimates of the 2002 'ākepa abundance using conventional distance sampling analyses were more similar to estimates produced by the soap smooth (Table 4.4). The 95%CIs of each approach bracketed the mean abundance estimates of the other approaches. The soap CIW was 208.3% shorter than the TPRS CIW, but was 0.8% longer than the DistR CIW.

Table 4.4: Abundance, standard error, coefficient of variation, and 95% confidence limits (LCL = lower 95%CI limit and UCL = upper 95%CI limit) estimates for the TPRS and soap smooth models, and conventional distance sampling methods fitted to the 2002 'ākepa for the soap boundary. Outliers in the TPRS and soap smooth posterior distributions were included in these estimates.

Estimator	Abundance	SE	CV	LCL	UCL
TPRS	8,274	10,919.60	1.162	6,796	16,392
soap	7,734	794.10	0.102	6,518	9,630
DistR	7,713	782.55	0.101	6,323	9,410

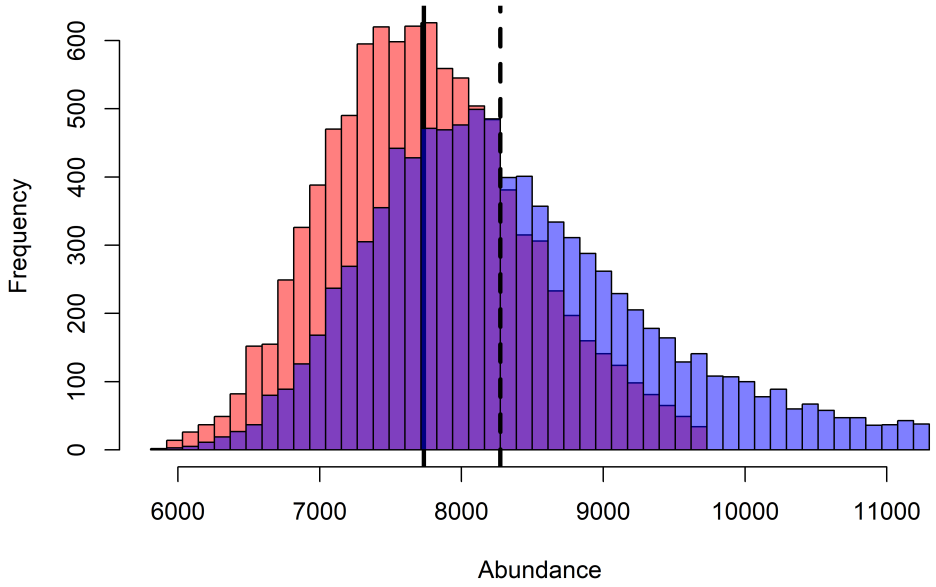

Figure 4.7: Histograms of the soap-film (red) and TPRS (blue) smoother posterior distributions. Overlap between the two distributions is substantial (purple). Vertical lines are the median abundance for soap-film (solid) and TPRS (dashed) distributions. Outliers have been removed for plotting.

4.5 Discussion

4.5.1 Statistical methods

I used a soap-film smoother for modelling spatial densities of 'ākepa from PTDS count data. The two dimensional soap-film smoother is comprised of two separate but linked bases; one for the boundary and one for the film itself. In this case the soap basis arguments provide a good approach for estimating the boundary and interior surface splines. If the value of the response at the boundary is known everywhere then the boundary can be fixed at that value without needing a spline to model the boundary values. Alternatively the boundary effect can be estimated using the boundary spline if the response at the boundary is unknown or if the suitability of the habitat varies along the boundary. This can result in varying densities along the boundary. As seen in the 'ākepa densities, estimating the

boundary is more realistic since it is not certain that the boundary value will be zero.

This latter approach of estimating densities along the boundary allowed me to answer the question posed in the Introduction to this chapter: do 'ākepa occur at relatively high densities right to the pasture-forest boundary? Densities at the boundary varied along the pasture-forest boundary as well as across the domain (see Figs. 4.4 and 4.5). As seen in Fig. 4.5, the predicted values on the boundary were smallest in the north-west corner and increased along the western boundary toward the south-west corner. Thus, in the southern portion of Hakalau 'ākepa occur at relatively high densities right to the edge of the pasture-forest boundary while in the northern portion 'ākepa densities were near zero inside the domain and on the boundary, as well as outside the domain in the pasture stratum.

The soap smooth model estimating the boundary reflects that 'ākepa densities may extend beyond the soap boundary. This is a "soft" boundary that poses no real physical barrier in the 'ākepa distribution. Along the eastern and southern boundaries the coefficient indicates that the population extends beyond the boundary into the adjacent forest habitat.

Fixing the boundary to zero instead of estimating it would force the smooth of the interior surface to decrease to zero at the boundary. This "hard" boundary approach may be appropriate for island populations where birds are restricted to suitable habitat that is located within an inhospitable matrix. Examples of this include bird populations on Pacific islands such as Aguiguan in the Mariana Islands (Amidon et al. 2014), Tau in American Samoa (Judge et al. 2013) and Nihoa in the Hawaiian Islands (Gorresen et al. 2016) where suitable forest bird habitat occurs across these islands and extends right to the coastal non-forest habitat or high-tide water line.

Ideally, the 'ākepa population at Hakalau requires a blend of fixing a portion of the boundary while estimating the boundary density elsewhere would be optimal. In this scenario the boundary would be fixed at zero on the north-west end of the study area along the pasture-forest boundary, while being estimated on the north, east, south and south-west boundaries. Densities in the north-west end of the domain were zero along the boundary and for some distance into the interior (Fig. 4.4). Thus fixing the boundary basis argument in this area to zero would not require contortions of the interior basis argument to meet boundary requirements. This could free up knots to be used in modelling the interior and could better estimate uncertainty by ascribing zero where densities are known. Conceptually this is possible, but to my knowledge it has not been implemented in `mgcv` or other software.

I specified the boundary and interior basis arguments for the soap-film smooth separately. An alternative formulation is to use the `bs="so"` argument. This construct is a wrapper for the boundary and interior smooths. While the `bs="so"` construct is easier to use, it does not allow for checking that sufficiently large k-basis factors have been selected for each components to account for residual errors.

Alternative methods that respect complex boundaries include finite element L-splines (Ramsay 2002), geodesic low rank thin plate spline methods (Wang and Ranalli 2007),

and complex region spatial smoother (CReSS; Scott-Hayward et al. 2014). Each method has several advantages and disadvantages, and comparisons conducted by Scott-Hayward et al. (2014) indicate that the CReSS and soap-film methods perform better than the other methods. They suggested that the main limitation of the soap-film smoother is that it can be difficult to construct in software.

4.5.2 Biological findings

The hotspot in the southern part of the domain coincides with the locally abundant density estimates identified by Scott et al. (1986) at 200+ birds/km^2. Similarly to the Scott et al. (1986) predictions, my results indicate that 'ākepa densities decrease outside the hotspot. 'Ākepa extend outside the domain on three sides of the soap boundary but are restricted to forest habitats above 1,500m elevation. On the north and east sides of the domain this is within several hundred meters of the boundaries. The 'ākepa distribution to the south of Hakalau continues along the 1,500m elevation contour before terminating several kilometres south of the study area (Judge et al. 2018). Although the extent of the survey is limited, the soap smoother based density estimates appear to be a good approximation of the 'ākepa distribution and abundance in the region (Scott et al. 1986, Lepson and Freed 1997).

Abundances of between 6,300 to 9,700 'ākepa in the extended forest stratum boundary seems realistic for the 2002 survey in this high density 'ākepa population (Gorresen et al. 2009, Camp et al. 2010, 2016). Simulation studies of design-based distance sampling have shown that method to be unbiased when the critical assumptions are met or possess low bias when assumptions fail (Buckland et al. 2001, 2015). This is not necessarily the case with model-based approaches and model mis-specification can lead to bias. The standard procedure in this case is to check the residual structure of the selected model. The residual plots were qualitatively similar and the desired refitted model EDF was approximately zero for each term with basis complexity (k-index) near one for the selected model. While I am not able to assess bias in either the TPRS or soap estimates, it is insightful to compare these model estimates to those produced using the design-based approach assuming that the latter approach is unbiased. In this case it appears that the soap smoother is also unbiased while the TPRS smooth may be positively biased. The 95%CIs among the three estimators overlapped the mean abundances, where the DistR and soap CIs just include the TPRS point estimate (by 17 and 237 birds, respectively; Table 4.4). The CV of abundance was very small at about 10% for the DistR and soap models while the CV of abundance was 116.2% for the TPRS model. This is not surprising as the TPRS smooth does not constrain the boundary condition resulting in a much larger CV and much wider CI than that of the DistR and soap models.

Along the southern portion of the pasture-forest boundary 'ākepa occur in relatively large densities (see Fig. 4.5). The combination of suitable habitat and high densities provides the potential for 'ākepa to colonize the pasture-stratum naturally. It was not until 2011 that 'ākepa had been detected in the afforested pasture (Paxton et al. 2018). Surveys subsequent to 2012 indicate that 'ākepa continue to use the kao in the pasture

stratum (Steve Kendall, U.S. Fish and Wildlife Service, Big Island Complex Wildlife Biologist, personal communication, 21 January 2020). As afforestation of the pasture stratum progresses 'ākepa appear poised to colonize this restored forest.

4.5.3 Management implications

Extending the extrapolation area to coincide with plausible management units, i.e. making predictions outside the range of the data, should be made with caution. This appears to pertain more to the TPRS than the soap smooth. Relative to the DistR and soap abundances, the TPRS abundance may be positively biased with large SEs. In Chapter 3 I showed that with low numbers of detections and sparse survey effort the TPRS smooth appeared to have suffered from edge effect (Miller et al. 2013). The TPRS smooth applied in this chapter also suffered edge effect in the central part of the domain adjacent to the boundary. Thus adding to the overestimated abundances and large uncertainty estimates. These limitations did not appear to have as large an affect in the spatio-temporal smooth of Chapter 2, likely due to borrowing information through space and time. These limitations were also not seen in the soap smooth estimates applied here; however, further investigation could confirm that the soap-film smooth is unbiased, precise and widely applicable with forest bird survey data.

Chapter 5

Population dynamics modelling

5.1 Overview

Understanding the patterns of population status change through space and time does not address why densities are changing. In this chapter I explore what may be driving population dynamics. I employ state-space models (SSMs), a class of models that are comprised of a state model and a measurement model. The state model describes the change of the state parameter, the true population size, from the previous time, N_{t-1}, to the current time, N_t, and reflects the stochastic sub-processes driving population change. The measurement model describes the relationship between the observations, i.e., annual abundance estimate corrected for detection probability $\hat{N}_t$, and the state parameter N_t. I apply SSMs to abundance time-series data to make inferences about the underlying rates of change. SSMs can be expanded to incorporate demographic data, or derived demographic quantities, to make inferences about states and vital rate parameters. This allows for the formulation of integrated population dynamic models (PDMs; Zipkin et al. 2019). 'Ākepa demographic quantities of survival and reproduction were incorporated as within-year sub-processes to produce multi-stage SSMs to describe population dynamics and trends (Newman et al. 2014). I used PDMs in a Bayesian framework, which allows for including information on the vital rates in the form of prior distributions derived from the literature, propagating uncertainty, estimating missing values and sharing information among population processes (Plard et al. 2019). This approach ensures that the predicted abundances more closely follow population trajectories that are biologically realistic. I compared the percentage change in abundance confidence interval widths from Distance for Windows (from Chapter 1) with the credible interval widths from the SSMs to discern improvements in estimator precision.

In Section 5.2 I introduce SSMs and how they can be expanded on to explicitly incorporate demographic parameters in PDMs. I describe the 'ākepa abundance survey, provide an overview of Hawaiian forest bird demography and detail the 'ākepa-specific demographic data and the formulation of the SSM and PDMs in Section 5.3. The results are presented in Section 5.4. I discuss in Section 5.5 the statistical methods, biological findings and management implications of applying PDMs to estimate population dynamics, status and trends.

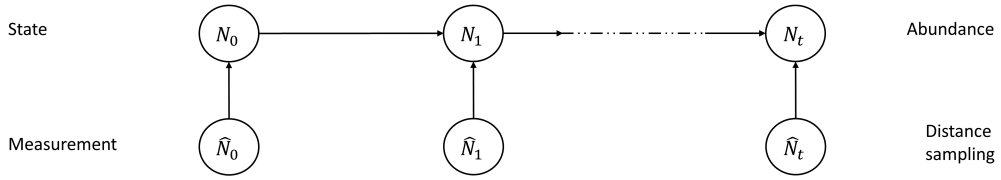

Figure 5.1: Diagram of a state space model. The true abundance is a hidden or latent process called the state process. The measurements, abundance estimates generated using distance sampling methods, are independent given the state. A conditional probability density function is used to model the change in the state over time.

5.2 Introduction

Up to this point in my thesis I have applied generalized additive models (GAMs) and results from a point process model to estimate 'ākepa densities. These are empirical modelling approaches that do not incorporate biological processes that govern population changes (Besbeas et al. 2002, Buckland et al. 2004, Schaub and Abadi 2011, Newman et al. 2014, Zipkin et al. 2019). Long-term abundance monitoring provides information on population change as abundances fluctuate in response to changes in underlying demographics of survival and recruitment. Incorporating population dynamics in abundance time series can be achieved with SSMs. SSMs differentiate between state process variation and measurement error. Process variation is the naturally occurring variation in abundances due to changing demographic and environmental conditions. Measurement error results from changing sampling conditions, availability of birds to be sampled and stochastic measurement error. By partitioning the error into its component parts of process variation and measurement error more precise abundance estimates can be produced. In their simplest form, SSMs are a joint distribution of states and measurements, two discrete time processes, that are run in parallel. The unobserved states are modelled in a state model, while the measurements of the state, along with measurement errors, are modelled in a measurement model. The measurement model describes the relationship between the unobserved states, i.e., true annual abundances, and the observed data, i.e., estimated annual abundances. The state model is also called a process model and the measurement model is synonymous with an observation model. Figure 5.1 shows this relationship graphically.

In this framework a SSM has a measurement model for $\hat{\mathbf{N}} = (\hat{N}_1, \hat{N}_2, \ldots, \hat{N}_T)$ estimated abundances for the years $t = (1, \ldots, T)$ in a time series of length T, usually collected on a regular time interval. The estimated abundance $\hat{N}_t$ is conditional on the current state N_t. The state model of the true abundances $\mathbf{N} = (N_0, N_1, \ldots, N_T)$, with N_0 the abundance of the initial state, is modelled such that N_t is conditional on the previous state N_{t-1}. The state model is thus treated as an autocorrelated process. In this framework the SSM is a first-order Markov process modelling the temporal autocorrelation of abundances. An SSM that assumes stochastic exponential growth or decline in time has

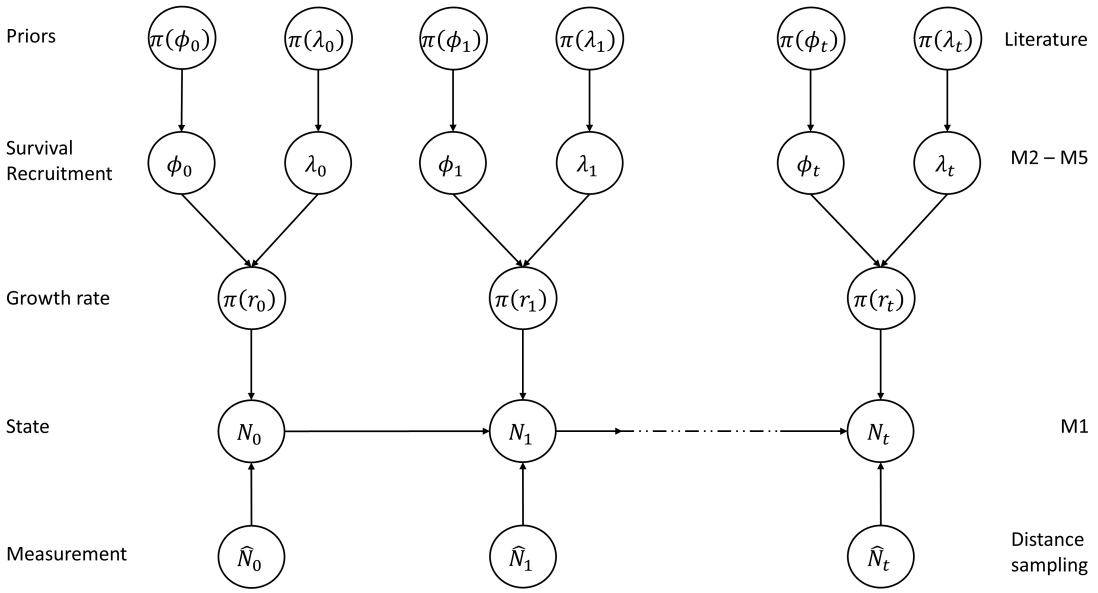

Figure 5.2: Flow chart of the states and parameters used in the SSMs and PDMs. The data and Models M1-M5 are shown on the right column.

the form

$$\text{state eqn} \qquad N_t = pN_{t-1} + \eta_t \qquad \eta_t \sim \text{normal}(0, \sigma_\eta^2), \tag{5.1a}$$

$$\text{measurement eqn} \qquad \hat{N}_t = N_t + \epsilon_t \qquad \epsilon_t \sim \text{normal}(0, \sigma_\epsilon^2) \tag{5.1b}$$

where $t \geq 1$, the population rate of change is $0 \leq p \leq \infty$, the state variance is $\sigma_\eta \geq 0$ and the measurement variance is $\sigma_\epsilon \geq 0$. Distributions other than normal may be substituted for the errors. The state model is initiated with the abundance N_0 at the initial time point. The true number of birds is a discrete non-negative value that I assume is a continuous random variable. These models are often reparameterized and conveniently approximated with a log-normal distribution.

SSMs are modular in that parameters describing different demographic processes can be layered onto the state equation (Fig. 5.2). In the simple SSM, population rates of change describing changes in 'ākepa abundance can be estimated. Rates of change are indices of the population mean fitness, where abundances change in response to the demographic mechanisms of survival, recruitment and movement (Koons et al. 2016, Ross et al. 2018). Building upon the simple SSM, demographic parameters can be included to construct a multi-stage, sequentially-fitted PDM (Newman et al. 2014) of the abundance time series and population dynamics (Fig. 5.2).

Bayesian inference has been used in ecology for many decades (e.g., Casella 1985, Ver Hoef 1996) with early applications of PDMs predominantly applied in fisheries (e.g., Meyer and Millar 1999). Within terrestrial ecosystems Borchers et al. (2002) proposed using SSMs to estimate state processes for open populations. Buckland et al. (2004, 2015, 2016) and Thomas et al. (2005) expanded on that framework to provide a general approach

for modelling demographic processes with survey data to estimate population dynamics and abundance trends. PDMs provide a unified and flexible modelling framework to combine multiple data types including conflicting or spatially and temporally piecemeal data on abundance and demographic parameters to simultaneously estimate population trajectories and demographic processes driving population change (Besbeas et al. 2002, Buckland et al. 2004, Schaub and Abadi 2011, Abadi et al. 2010, Newman et al. 2014, Plard et al. 2019, Saunders et al. 2019). Although the SSM framework has been developed relatively recently, it has been applied widely (see, e.g., Nadeem et al. 2016, Rushing et al. 2016, 2017, Ahrestani et al. 2017, Chandler et al. 2018, Ross et al. 2018, Hostetter et al. 2019, Roy et al. 2019, Margalida et al. 2020, Saracco and Rubenstein 2020). Newman et al. (2014) details the theory, presents well developed examples and covers the background of SSMs. Moreover, a Bayesian approach allows for incorporating annual variation in demographic rates characterized by the variation in the state model, and parameter estimates with their uncertainty quantified from the posterior distribution (Buckland et al. 2004, 2015, Riecke et al. 2019, Zipkin et al. 2019).

SSMs can have parameter estimability issues (see Auger-Méthé et al. 2016, and references therein). One approach to overcome this is to incorporate additional information in the SSM, such as estimates of measurement error, survival, reproduction or other demographic traits (Besbeas et al. 2003). Knape et al. (2013) showed there was little information lost in fitting SSMs using derived MLE-based estimates for parameters with their variances instead of modelling the raw data. This substantially simplifies the SSM and specialized, sophisticated software can be used for the analysis of distance sampling and mark-recapture data (Besbeas et al. 2002). Uncertainty in the annual 'ākepa abundances is measurement error and can be estimated using distance sampling methods (Buckland et al. 2016; described in Chapter 1). An advantage of this approach is that abundances are estimated accounting for the detection probability and the detection probability variance is included in the total abundance estimate variance, which is σ^2_ϵ in Eqn. 5.1. Including estimates of measurement error then eliminates the strong correlation between it and the process error when simultaneously solving the measurement and state equations.

In the SSM framework the combination of the state and measurement models can be mathematically described as

$$\begin{aligned} \text{Prior pdf} &: \pi(\boldsymbol{\theta}) \\ \text{Initial state pdf} &: g_0(N_0|\sigma^2_{N_0}) \\ \text{State at time } t \text{ pdf} &: g_t(N_t|N_{t-1}, \boldsymbol{\theta}) \\ \text{Measurement at time } t \text{ pdf} &: f_t(\hat{N}_t|N_t, \mathbf{z}, \hat{\sigma}^2_\epsilon), \end{aligned} \tag{5.2}$$

corresponding to the time series with $t = 1, \ldots, T$. The point estimate $\hat{N}_t$ is estimated using conditional likelihood methods of distance sampling with measurement error ($\hat{\sigma}^2_\epsilon$; Chapter 1 Sections 1.4.2 and 1.4.4). Specific to distance sampling methods, the vector of covariates corresponding with the measurement model are the covariates $\mathbf{z}$ from Chapter 1 Section 1.4.4. The state process is modelled as a conditional pdf g_t that describes

the change from time N_{t-1} to N_t. The vector of parameters corresponding to the state model are $\boldsymbol{\theta}$, and includes the stochastic sub-processes driving population change. The initial conditions on the state N_0 needs to be specified or estimated to inform N_1, and is included as a conditional pdf g_0 in the SSM. The building block approach allows for adding a conditional pdf π layer that explicitly models variability $\boldsymbol{\theta}$ in survival and recruitment. SSMs are flexible and the parameter pdf π can be written to be conditional on previous states (e.g., explicitly modelling density dependence in the demographic parameters).

In Bayesian inference the parameters $\boldsymbol{\theta}$ are considered random variables that are specified with a prior distribution, $\pi(\boldsymbol{\theta})$. Bayesian inference is based on the likelihood and parameter prior distributions, thus the posterior distribution is a conditional probability distribution. In this form the likelihood for the SSM can be written as

$$\begin{aligned} \mathscr{L}(\boldsymbol{\theta}|\hat{\mathbf{N}}_{1:T}) &\equiv \prod_{t=1}^{T} f_{1:T}(\hat{\mathbf{N}}_{1:T}|\boldsymbol{\theta}) \\ &= \int g_0(N_0|\boldsymbol{\theta}) \prod_{t=1}^{T} g_t(N_t|N_{t-1},\boldsymbol{\theta}) f_t(\hat{N}_t|N_t) d\mathbf{N}_{0:T}, \end{aligned} \tag{5.3}$$

integrating out the states in the joint distribution of states and measurements.

For additional flexibility and realism, state parameters can be allowed to vary over time, for which I use the notation $\boldsymbol{\theta}_t$. This can be modelled using a hierarchical Bayes framework, where the priors on the $\boldsymbol{\theta}_t$s depend on random variables $\boldsymbol{\Gamma}$, which in turn have a hyperprior $\pi(\boldsymbol{\Gamma})$. This hierarchical form of the SSM is then formulated as

$$\begin{aligned} \text{Hyperprior pdf} &: \pi(\boldsymbol{\Gamma}) \\ \text{Prior pdf} &: h(\boldsymbol{\theta}_t|\boldsymbol{\Gamma}) \\ \text{Initial state pdf} &: g_0(N_0|\sigma^2_{N_0}) \\ \text{State at time } t \text{ pdf} &: g_t(N_t|N_{t-1},\boldsymbol{\theta}_t) \\ \text{Measurement at time } t \text{ pdf} &: f_t(\hat{N}_t|N_t,\mathbf{z},\hat{\sigma}^2_\epsilon). \end{aligned} \tag{5.4}$$

For example, I may wish to specify that survival ϕ varies by year with prior distribution $h(\phi_t|\boldsymbol{\Gamma})$ where $\boldsymbol{\Gamma}$ contains parameters for the mean and variance of annual survival, and these are given prior distributions specified by $\pi(\boldsymbol{\Gamma})$.

In this chapter, I fit a series of models of increasing biological complexity. I start by analysing the 31-year 'ākepa abundance time series with Model M1 a model where true population size follows a random walk on the log scale. Vague priors are given on process variance and I incorporate the abundance variance estimates from distance sampling as the measurement error variance. This first model is presented as a simple case for expository reasons and I identify limitations of parameter estimability or identifiability. Bayesian inference allows for incorporating external information or beliefs in the form of informative parameters. This allows for quantifying our beliefs about the values of parameters. I develop PDM Models M2-M5 by adding stochastic demographic sub-processes of survival and reproduction driving population change. Modelling the underlying demographic dynamics provides information on the vital rates that drive population change

and improve abundance estimator certainty. These models incorporate biological realism to evaluate trends as abundances change in response to the demographic mechanisms of survival and recruitment, and how they may vary temporally. The complexity of the models increases progressively by incorporating additional information collected to better understand drivers of the 'ākepa population at Hakalau. I evaluate model performance by comparing the percentage change in abundance CI width from Distance for Windows (Chapter 1) with the credible interval widths from the SSMs.

5.3 Methods

5.3.1 Study species and survey

The analyses in this chapter are conducted on the 31-year Hawai'i 'ākepa point-transect distance sampling (PTDS) time series data collected at Hakalau in the open-forest stratum (Chapter 1 Fig. 1.1). In Chapter 1 I described the design-based methods I used to fit a detection function, evaluate covariates and estimate 'ākepa densities and their variances for each of the 1987 to 2017 surveys. Abundances and their SE were then calculated as density and SE estimates multiplied by the size of the 3,061 ha study area (Chapter 1 Fig. 1.7).

5.3.2 Demographic data

Here I summarize the life history traits, particularly those of 'ākepa, relevant to making decisions about the SSM structure and parameter priors. Priors can be set either as vague (also called diffuse) if no knowledge of the system exists, or can incorporate relevant biological knowledge from previous studies or expert opinion to partially inform the priors. Models formulated with biologically informed priors give increased biological realism that is lacking in models using uninformed or arbitrarily specified priors (Newman et al. 2014, pg 86; Schaub and Fletcher 2015). Woodworth and Pratt (2009) provide a thorough review of Hawaiian forest bird demography. Life history traits of tropical birds are thought to be adaptations that result from life history trade-offs in response to tropical environmental conditions relative to temperate conditions. Tropical birds typically exhibit slow life histories (Roff 2002) where individuals are long-lived producing small clutches of 1-2 eggs with extended incubation, nestling, and post-fledging dependent periods. Adult birds have relatively high annual survival rates, while there are high rates of nest loss resulting in low reproduction as well as low juvenile survival.

Hawaiian honeycreepers are, in general, sedentary and highly site philopatric. During the breeding season honeycreepers defend only the immediate nest site, not the all-purpose breeding and foraging territories typical of temperate species. Females build the nest and incubate alone while the male feeds the nesting female, defends the nest site, and both sexes care for young. Honeycreepers are socially monogamous for a breeding season. After the breeding season, 'ākepa join in mixed-species flocks. It is during this time that I expect mixing of the population and any movement within the study area to occur. The PTDS surveys are conducted during the breeding season when birds are most detectable and

before nestlings have fledged; therefore, population size is an estimate of the adult bird class that presumably is breeding and after winter mortality has occurred.

I compiled vital rates from the 'ākepa literature instead of estimating demographic parameters from raw data (summarized in Table 5.1). The demographic data are derived from a handful of studies conducted over a 40 year time period. Data were collected roughly during three time periods: (1) the 1970s and 1980s; (2) 1990s; and (3) 2010s. Between 1976 and 1982 Ralph and Fancy (1994) mist netted 'ākepa at a site in Keauhou Ranch, about 30 km south of Hakalau (Fig. 1.1). The Keauhou Ranch site is similar to that in Pua 'Ākala but had a discontinuous canopy and a relatively more dense understory, although it also had a long history of cattle grazing. Annual survival rate was calculated for adults only, pooling across sexes. Freed (1988) mist netted on Mauna Loa, about 60 km southwest of Hakalau, in 1985 and 1987, and computed a minimum annual adult survival rate assuming constant survival over the two-year period. Habitat in this area is similar to that in Pua 'Ākala. The more recent studies are all from Hakalau. Lepson and Freed (1995) surveyed 'ākepa in the Pua 'Ākala study site between 1987 and 1993, and estimated adult survival for both males and females. Between 1994 and 1999 USGS mist netted for birds in the Nauhi study site. There were relatively low numbers of 'ākepa captures but sufficient to make estimates for data pooled across sexes (Guillaumet et al. 2016). In addition to estimating adult survival, Guillaumet et al. (2016) used integrated population models to estimate recruitment and population change from a model that assumes constant survival and recruitment over the 5-yr study.

Following the Bird Banding Laboratory, U.S. Geological Survey, age classes are a_0 for a juvenile bird banded after the breeding season and before 1 January, a_1 for a juvenile bird known to have hatched the calendar year before banding and includes birds that have graduated from a_0 on 1 January, and a_{1+} for an adult bird, presumed sexually mature, known to have graduated from a_1 on 1 January. It is difficult to distinguish between a_0 and a_1 age classes and the breeding period occurs over a large time span (Lepson and Freed 1997); therefore, I model just two age classes with a combined juvenile a_0 and a_1 class and a separate adult class a_{1+}. The age at first breeding is generally age 2, although some females breed successfully at age 1. Some males are not sexually mature their first year after hatching and delay breeding until their second year after hatching; at which time they have full breeding plumage. I assume that all adult aged birds breed, which may overestimate reproduction yet should not affect survival estimates. I assume that any juvenile birds that survive to the next breeding season have transitioned to the breeding adult age class a_{1+}. Little is known of the non-breeding adult age class (Lepson and Freed 1997, Woodworth and Pratt 2009), and is not included in these analyses.

Survival is the expected number of birds that survive the year given the number alive during the last breeding season. Adult survival ranges from 0.70 to 0.83, while juvenile survival is much lower at 0.42 (range 0.31 to 0.80; Table 5.1). Lepson and Freed (1995) showed that male survival was slightly higher than that of females, but not significantly different. Therefore, I assumed that adult survival is the same by sex and constant over time. Juvenile survival includes surviving hatching, nestling and fledging stages

with age incrementation occurring with the next breeding season. Medeiros and Freed (2009) found that fledging mass strongly affects juvenile survival with larger fledglings having approximately equal survival as adult birds while smaller fledglings have lower survival. They provided estimates with standard errors for the high-mass juvenile and adult birds, but not the low-mass and average-mass juveniles. I extracted the survival rate estimates for the low-mass and average-mass juveniles using the on-line graph reading tool (http://www.graphreader.com/). Uncertainty estimates for these rates are not available. Most juvenile survival rates reported in Lepson and Freed (1997) and Woodworth and Pratt (2009) had survival rates similar to the low and average mass fledglings.

Recruitment represents the offspring that transition to the adult age class. Determining direct measures of 'ākepa recruitment into the population is difficult requiring finding 'ākepa cavity nests, and follow the numbers of eggs that hatch and survival of nestling birds through to fledgling. Even when breeding 'ākepa are located, most cavity nests are located high in the tall stature trees which limits the ability to see inside most nests. Clutch size is 1-2 eggs per year per female with the maximum number of young fledged per year per female is 2. Annual reproductive success varies widely. Based on data from Nauhi collected during the 1990s, Guillaumet et al. (2016) estimated recruitment to be 0.35 (SE = 0.19) while Lepson and Freed (1995) followed 53 nests in Pua 'Ākala between 1987 and 1993 and computed a 0.79 annual nest success rate. Cummins et al. (2014) conducted nest searches in Pua 'Ākala and Pedro study sites at Hakalau in 2013 and 2014 and found five 'ākepa nests. One of two survived in 2013 and one of three in 2014, giving an overall success rate of 0.40 (Table 5.1).

Population dynamics models commonly use only the number of females in a population and track the numbers of daughters born from one female annually or throughout her life. Lepson and Freed (1995) computed the sex ratio in Pua 'Ākala between 1987 and 1993 at 1.14:1 male to female ratio, while Hart (2001) estimated the ratio in both Pua 'Ākala and Pedro study sites between 1994 and 1996 at a 1.14:1 and 1.21:1 male to female ratio, respectively (these ratios are based on the numbers presented in Figure 6 of Hart (2001) and differ from what he presented in his text; Table 5.1). In many of the demographic studies cited herein, however, a distinction between males and females was not made. It is not possible to consistently identify between sexes during the PTDS surveys. I assume that the sex ratio is sufficiently close to parity to use a PDM that does not distinguish between sexes and offspring can be either male or female.

Inference from demographic research is typically limited to mist-netting locations, i.e., site-restricted. Spatially limited inference was observed in the analyses of Chapter 2; PDMs offer a means for evaluating the landscape-scale demography-density relationship synoptically, rather than site by site. To make the local-scaled demographic studies relevant to the larger-scaled abundance surveys I used the individual study estimates, where more one was available, as the basis of a meta-analysis (i.e., coupling the microscale in the macroscale). The lower bounds for each parameter were set to non-negative values while the upper bounds were limited by rational biological arguments.

For convenience, I set the modelling annual cycle to coincide with the start of the

breeding season and match the schedule for monitoring Hawaiian forest bird abundances. Annual changes in 'ākepa abundances thus reflect an annual process that runs from one breeding season to the next and all biological sub-processes, such as survival, transition from juvenile age class to adult age class, birth and movement, occur within the annual cycle. Over the course of a year the sub-processes are assumed to be temporally sequential; i.e., adult mortality takes place followed by maturation and age-class transition, and then births occur restarting the cycle. The 'ākepa breeding season is relatively long lasting from March through June with the bulk occurring in April and May, and young care extends from April to September (Lepson and Freed 1997). Thus treating the sub-processes as discrete with sequentially non-overlapping time intervals results in the parameters being approximations. I do not address bird movement here but in Chapter 6 I identify how immigration and emigration movement could be included in SSMs.

Table 5.1: Demographic estimates of Hawai'i 'ākepa from published literature. Estimates (Est.), standard errors (SE) and sample sizes (no.) are provided. Parameters are juvenile ϕ_1 survival, adult ϕ_{1+} survival, population rate of change r, recruitment λ, sex ratio 'c', and apparent nest success n_s. Subscripts for estimates specifically calculated for female 'f' and male 'm' birds, and juveniles of low-mass 'l', average-mass 'a', and high-mass 'h'. Years in which data were collected is provided in the text.

Area/Year	Par	Est.	SE	no.	Source
Keauhou Ranch	ϕ_{1+}	0.70	0.27	61	Ralph and Fancy (1994)
Kau FR	ϕ_{1+}	0.77	–	5	Freed (1988)
Pua 'Ākala	ϕ_1	0.42	0.10	57	Lepson and Freed (1995)
	$\phi_{1+,f}$	0.80	0.04	46	
	$\phi_{1+,m}$	0.83	0.04	36	
Pua 'Ākala	$\phi_{1,l}$	0.36	–	18	Medeiros and Freed (2009)
	$\phi_{1,a}$	0.31	–	29	
	$\phi_{1,h}$	0.80	0.10	19	
	ϕ_{1+}	0.78	0.04	–	
Nauhi	ϕ_{1+}	0.817	0.112	19	Guillaumet et al. (2016)
	r	1.172	0.167	19	
	λ	0.354	0.190	19	
Pua 'Ākala	n_s	0.79	–	53	Lepson and Freed (1995)
2013	n_s	0.50	–	2	Cummins et al. (2014)
2014	n_s	0.33	–	3	
Total	n_s	0.40	–	5	
Pua 'Ākala	c	1.14:1	–	–	Lepson and Freed (1995)
Pua 'Ākala	c	1.14:1	–	107	Hart (2001)
Pedro	c	1.21:1	–	42	

5.3.3 State space models

I fit a SSM of 'ākepa abundances with the measurement and state models of Eqn. 5.2 with measurement error from the Distance for Windows; Model M1. I then incorporated vital rate sub-processes to form PDMs (Models M2-M5). The connected likelihood approach described here, see also Eqn. 5.3, assumes that the distribution of the data can

be appropriately modelled, suitable priors can be specified and that the SSM partitions variation between state and measurement processes correctly. The structure of the data, parameters and models are shown in Fig. 5.2.

Model M1: Time-varying rate of population change

Model M1 is a state space model where the trend in abundance follows a linear function of the log of abundance. In this model, annual growth rate is the parameter describing population change on the log scale, where growth rate is the proportional change in population size from one time period to the next and reflects change in annual recruitment and annual adult survival. The state process of the model that transitions from one year to the next is formulated as

$$\log\left(N_{t+1}\right) = \log\left(N_t\right) + r_t,$$

where N_t is the population size in year t, and $\exp\left(r_t\right)$ is the annual growth rate. Log annual growth rate is a random variable with a normally distributed prior with mean $\bar{r}$ and state process error σ^2_η, i.e.,

$$r_t \sim \text{normal}\left(\bar{r}, \sigma^2_\eta\right),$$

while the trend model assumes that the measurement process abundance estimates $\log\left(\hat{N}_t\right)$ follow a normal distribution with measurement error $\sigma^2_{\epsilon_t}$,

$$\log\left(\hat{N}_t\right) \sim \text{normal}\left(\log\left(N_t\right), \sigma^2_{\epsilon_t}\right).$$

Knape et al. (2013) showed that inference from simple linear SSMs can be limited when simultaneously estimating process and measurement variances as they are confounded. I overcame this confounding problem (also called an identifiability issue) by setting the measurement variance to be the variance of the logged density estimates from Chapter 1 where $\sigma^2_{\epsilon_t} = \widehat{\text{var}}\left(\log\left(\hat{N}_t\right)\right)$. The log transformed variance is calculated as $\log\left(1 + \frac{\widehat{\text{var}}\left(\hat{N}_t\right)}{\hat{N}^2_t}\right)$ (Buckland et al. 2001). This assumes the estimates are temporally independent. Inspection of the correlation and partial correlation plots indicated that none of the lags exceeded the significance bounds (average correlation between pairs of successive years = 0.004; maximum correlation = $|0.256|$). The Ljung-Box test statistic was 9.35 with 14 degrees of freedom and the p-value was 0.81 indicating there is little evidence of non-zero autocorrelation in the abundances, supporting the independence assumption. This correlation may be underestimated because bootstrap estimates sampled lines within years but not across years (see Chapter 2), and would benefit from further investigation.

The mean growth rate prior for the annual growth rate was specified as $\bar{r} \sim \text{normal}(0, 10)$. This is equivalent to a stable population with reasonably high variation that extends broadly over the plausible range of population change. The prior for the variance of the state process is $\sigma_\eta \sim \text{uniform}(0, 10)$. This SSM requires that the initial value be estimated or defined. I used the 1977 Hawaii Forest Bird Survey (HFBS) abundance point estimate to

define N_0. Camp et al. (2010) estimated the 1977 density at 0.445, times 3,061 ha yields an abundance of 1,362 'ākepa. This estimate is for a slightly larger open forest stratum, but for modelling purposes is a reasonable approximation of the initial population size. To be consistent with the other models I set the normal prior on N_0 with low precision ($\sigma^2_{N_0} = 1000$). The initial population size is formulated as $\log(N_0) \sim \text{normal}\left(\log\left(\hat{N}_0\right), 1000\right)$.

Model M2: Constant recruitment and survival

Research at Hakalau has simultaneously provided separate information about population abundances and individual-level demographic processes. SSMs can be expanded into PDMs that incorporate these different sources of information (Newman et al. 2014). Building on Model M1 I incorporated a Poisson process for recruitment λ and a binomial process for adult survival ϕ. This model has the expectation

$$\mathbb{E}(N_{t+1}) = (\lambda_t + \phi_t) N_t. \tag{5.5}$$

Guillaumet et al. (2016) is the only demographic study to have estimated recruitment (λ = 0.354, SE = 0.190), which was used for setting the prior. There were five adult 'ākepa survival estimates (Table 5.1) that have point and variance estimates. Following methods described in Lee et al. (2016), I used a meta-analysis approach to synthesize the survival estimates using an inverse-variance-weighted average method to produce weighted mean adult survival estimate 0.803 with SE 0.022. Using conjugate priors for both parameters, prior distributions suggested from these literature-based parameters are mean recruitment $\bar{\lambda} \sim \text{gamma}(3.471, 9.806)$ and weighted adult mean survival $\bar{\phi} \sim \text{beta}(261.335, 51.439)$ (calculations for computing priors from the parameters for each distribution are presented in Appendix E).

Setting biologically realistic priors is critical for this model to have reasonable results. The priors on recruitment and adult survival seemed realistic, except that the 'ākepa clutch size is 1-2 eggs per year per female with a maximum number of young fledged per year per female of 2. The prior for the annual recruitment, right truncated at twice the annual population size, is a Poisson distribution with rate $\bar{\lambda} N_t$ and truncated at $2\hat{N}_t$, designated as $\text{RTPoisson}\left(\bar{\lambda} N_t, 2\hat{N}_t\right)$. Truncating recruitment in this way ensures that annual reproduction cannot more than double the population size and satisfies the maximum number of eggs laid and young fledged per female.

I adapted Model M1 replacing random effect of growth rate with random effects of recruitment and adult survival. Then the number of birds recruited each year t is R_t and

the number of adults surviving each year t is S_t. Model M2 with priors is

$$\begin{aligned}
\bar{\lambda} &\sim \text{gamma}(3.471, 9.806) \\
\bar{\phi} &\sim \text{beta}(261.335, 51.439) \\
\log(N_0) &\sim \text{normal}\left(\log\left(\hat{N}_0\right), 1000\right) \\
R_t &\sim \text{RTPoisson}\left(\bar{\lambda} N_t, 2\hat{N}_t\right) \\
S_t &\sim \text{binomial}\left(N_t, \bar{\phi}\right) \\
\log(N_{t+1}) &= R_t + S_t \\
\log\left(\hat{N}_t\right) &\sim \text{normal}\left(\log(N_t), \widehat{\text{var}}\left(\log\left(\hat{N}_t\right)\right)\right).
\end{aligned}$$

Model M3: Time-varying recruitment, constant survival

Model M2 allows for only demographic stochasticity; i.e., random variation in realized recruitment and survival given constant underlying annual values. Because of the relatively large population size the amount of demographic stochasticity was small and Model M2 produced near constant rates of population change (see Results). Model M2 misses biological details as the constant average recruitment and survival model does not fit the observed time series very well. That is, Model M2 misses runs of positive and negative trajectories in the abundances. In general, there are three options to incorporate additional variation in the parameters to better capture fluctuations in the abundances: random variation in the recruitment and/or survival parameters. Studies over three decades conducted within and outside Hakalau consistently show that adult survival is relatively constant and high (Table 5.1), which is typical for tropical passerines (Woodworth and Pratt 2009). Modelling random variation in adult survival, therefore, may not be biologically realistic or especially useful to capture population dynamics. Medeiros and Freed (2009) observed that the survival rates for low- and average-mass juvenile 'ākepa were <0.4, which Cox et al. (2014) identified as a minimum threshold level that results in population declines even for populations with high adult survival. Overall, 'ākepa hatch-year survival that includes nestling and fledglings of both sexes surviving their first year was 0.42 (Lepson and Freed 1997), or just above Cox et al.'s minimum threshold level. Thus, it is likely that even minor amounts of environmental stochasticity will affect juvenile survival, and thus recruitment, more than adult survival will influence population change (Newton 1998, Sæther and Bakke 2000, Boyce et al. 2006).

I adapted Model M2 by replacing $\bar{\lambda}$ in the state process with an annually varying

recruitment, λ_t. Model M3 with priors is

$$\begin{aligned}
\lambda_t &\sim \text{gamma}(3.471, 9.806) \\
\bar{\phi} &\sim \text{beta}(261.335, 51.439) \\
\log(N_0) &\sim \text{normal}\left(\log\left(\hat{N}_0\right), 1000\right) \\
R_t &\sim \text{RTPoisson}\left(\lambda_t N_t, 2\hat{N}_t\right) \\
S_t &\sim \text{binomial}\left(N_t, \bar{\phi}\right) \\
\log(N_{t+1}) &= R_t + S_t \\
\log\left(\hat{N}_t\right) &\sim \text{normal}\left(\log(N_t), \widehat{\text{var}}\left(\log\left(\hat{N}_t\right)\right)\right).
\end{aligned}$$

Model M4: Time-varying recruitment via random effect, constant survival

Model M4 allows for substantial variability in recruitment over time, by specifying recruitment as a random effect. This allows for plausible biological or environmental influences that vary in an uncorrelated way over time. Recruitment is modelled as being normally distributed, with mean set to the mean recruitment $\bar{\lambda}$ and a variance assumed known. Preliminary analyses of variances equal to 0.0025, 0.01, 0.04 and 0.25 were evaluated (not shown) and the value 0.01 was chosen as it produced a flexible curve that generally followed changes in abundances. Model M4 with priors is

$$\begin{aligned}
\bar{\lambda} &\sim \text{gamma}(3.471, 9.806) \\
\lambda_t &\sim \text{normal}(\bar{\lambda}, 0.01) \\
\bar{\phi} &\sim \text{beta}(261.335, 51.439) \\
\log(N_0) &\sim \text{normal}\left(\log\left(\hat{N}_0\right), 1000\right) \\
R_t &\sim \text{RTPoisson}\left(\lambda_t N_t, 2\hat{N}_t\right) \\
S_t &\sim \text{binomial}\left(N_t, \bar{\phi}\right) \\
\log(N_{t+1}) &= R_t + S_t \\
\log\left(\hat{N}_t\right) &\sim \text{normal}\left(\log(N_t), \widehat{\text{var}}\left(\log\left(\hat{N}_t\right)\right)\right).
\end{aligned}$$

Model M5: Time-varying recruitment with random walk, constant survival

It is possible that recruitment varies more smoothly over time in response to periods of good years where large numbers of birds are recruited into the population followed by periods of poor years with little recruitment. This is conveniently represented by modelling recruitment as a temporal random walk. A random walk model is appropriate when the environmental conditions that are driving recruitment change or vary slowly over time. Relevant examples at Hakalau include removal of ungulates leading to habitat restoration that has subsequently declined due to feral pig (*Sus scrofa*) incursion (see Chapter 2 Section 2.5) and climate variability due to the Pacific decadal oscillation particularly as it affects rainfall (Chu and Chen 2005). The random walk is formulated by making recruitment on year t a normal distribution with mean equal to recruitment in the pre-

vious year $t-1$ and the same between-year variance as Model M4 (variance 0.01). The parameterization is such that annual recruitment is centred around a mean value $\bar{\lambda}$, as with Model M4. Model M5 with priors is

$$
\begin{aligned}
\bar{\lambda} &\sim \text{gamma}(3.471, 9.806) \\
\bar{\phi} &\sim \text{beta}(261.335, 51.439) \\
H_t &\sim \text{normal}(\bar{\lambda}, 0.01) \\
D_t &= J_t - \bar{J} \\
J_t &= J_{t-1} + H_t, t > 1; J_0 = 0 \\
\lambda_t &= \bar{\lambda} + D_t \\
\log(N_0) &\sim \text{normal}\left(\log\left(\hat{N}_0\right), 1000\right) \\
R_t &\sim \text{RTPoisson}\left(\lambda_t N_t, 2\hat{N}_t\right) \\
S_t &\sim \text{binomial}\left(N_t, \bar{\phi}\right) \\
\log(N_{t+1}) &= R_t + S_t \\
\log\left(\hat{N}_t\right) &\sim \text{normal}\left(\log(N_t), \widehat{\text{var}}\left(\log\left(\hat{N}_t\right)\right)\right),
\end{aligned}
$$

where $\bar{J} = 1/T \sum_{i=1}^{T} J_i$.

5.3.4 Parameter estimation

Monte Carlo sampling procedures with Markov chain Monte Carlo (MCMC) were used to generate posterior distributions. MCMC modelling was implemented in `JAGS` software (Plummer 2017) using the `jagsUI` wrapper (Kellner 2019) for the `rjags` package (Plummer 2018) in `R` (R Core Team 2017). The `jagsUI` package allows for parallel processing making use of multiple CPU cores and substantially reduced computation time. To ensure chains converge to the posterior distribution I used a burn-in of 10,000 samples, a further 1,000,000 samples were used for inference from six parallel chains. Each chain was down-sampled to 10,000 using a thinning interval of 100. Initial values for each chain were randomly selected from distributions based on the literature, which approximately samples from different regions of the parameter spaces (Hogg and Foreman-Mackey 2018). I computed summary statistics of abundance, growth rate, adult survival and recruitment parameters from the posterior distributions. Each parameter was calculated as the mean of the 60,000 posterior samples while 95% credible intervals (95 %CrIs) were calculated as the 0.025 and 0.975 quantiles of the posterior distribution of each model.

MCMC checking

MCMC checking was assessed using visual inspection of trace plots, computing Gelman-Rubin convergence diagnostics ($\hat{R}$), computing the degree to which the prior informs the posterior distribution (prior posterior overlap; PPO), and computing mean and minimum Monte Carlo effective sample size (ESS) for all model parameters (Gelman et al. 2013). For each model parameter an $\hat{R} < 1.1$ indicates model convergence. Following guidance

from Gimenez et al. (2009) a small degree of PPO is desired, $< 35\%$, indicating that the parameters are identifiable and the data influenced the results. The desired mean ESS values are several thousand to tens of thousands and minimum ESS values are several hundred, which are large enough to report values that are accurate to three significant figures. For each model an assessment of the trace plots, $\hat{R}$, PPO, and ESS are presented in Appendix E.

5.4 Results

5.4.1 Model M1: Time-varying rate of population change

Model M1 closely followed the year-to-year fluctuations observed in the Distance for Windows abundances and generally had narrow 95%CrIs (Fig. 5.3). The estimated annual rates of change r fluctuated around 0 with a mean growth rate $\bar{r} = 0.002$ over the time series (SE = 0.063; Fig. 5.4). Credible interval widths were on average 20.6% narrower than the length of the design-based confidence interval widths (SE = 13.7%).

5.4.2 Model M2: Constant recruitment and survival

Model M2 showed a strong posterior correlation between the ϕ and λ parameters (correlation = -0.965; Fig. 5.5). A limitation of the parameterization of Model M2 is that the year-to-year realized levels of survival and recruitment can only vary by the constraints of the binomial and Poisson distributions, not very much in practice. As a result, Model M2 produced an almost constant growth rate over time (mean growth rate 1.016; Fig. 5.6). Model M2 analyses were not further considered because of identifiability issues and the estimates did not capture the trajectories in the time series.

5.4.3 Model M3: Time-varying recruitment, constant survival

Model M3 produced a relatively flexible curve of 'ākepa abundances that captures three prominent trajectories: relatively flat from 1987 to 1994, and declining from 1997 to 2005 and 2009 to 2017 (Fig. 5.7). Large increases in the population occurred in 1995 and 1996 and again in 2006, 2007 and 2008. Mean recruitment $\bar{\lambda}$ was 0.264 (SE=0.110) and annual λ_t estimates varied widely (Fig. 5.8). The largest increase occurred in 2007, which was the only year that the recruitment point estimate λ_t was near 1 and the 95%CrI did not bracket the mean. Although this value is relatively large, it retained biological realism given the species maximum population change (less than doubling). Recruitment point estimates λ_t exceeded 0.4 in 1995, 2006 and 2007. Mean adult survival $\bar{\phi}$ over the 31-year time series was 0.764 (SE=0.018). There was little correlation between the ϕ and λ parameters (correlation=0.004; Appendix E Fig. E.4). Uncertainty in the Model M3 abundance estimates was substantially smaller than that estimated using design-based methods with an average 43.5% reduction in the length of the interval widths (SD=14.7%).

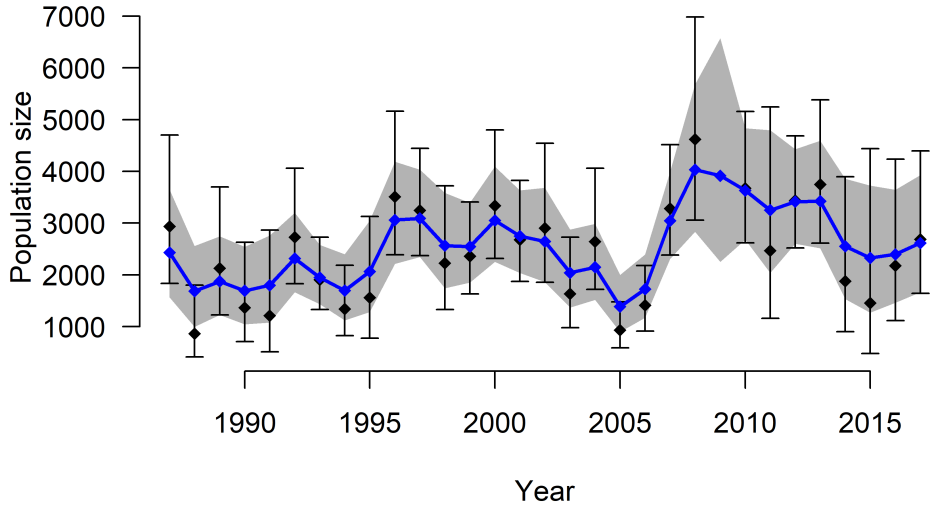

Figure 5.3: ʻĀkepa abundance estimates (blue line) from Model M1 with measurement variation assumed known (from the Distance for Windows analysis) and vague priors on process variation for the 31-year time series (95%CrI; grey ribbon). Abundance estimate with 95%CI from Distance for Windows (diamond and whisker bar).

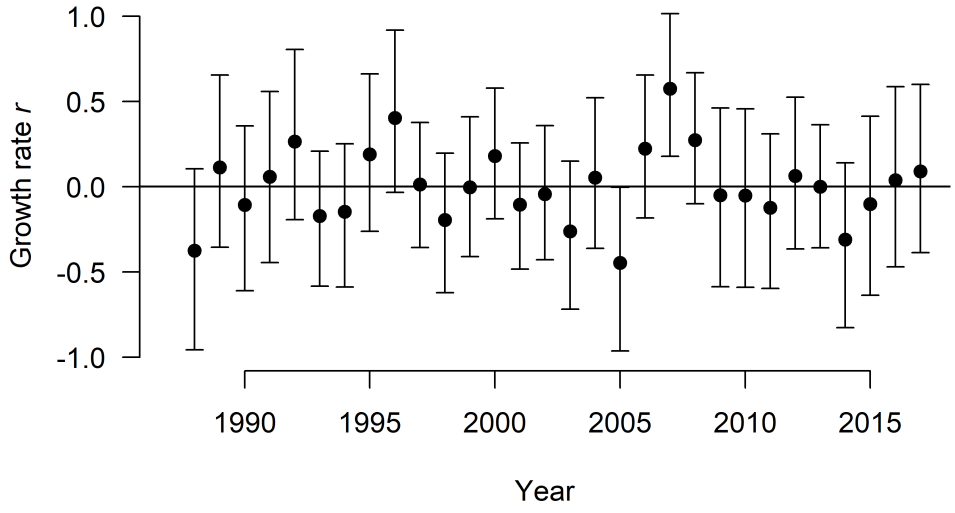

Figure 5.4: Growth rate r estimates generated from Model M1 with measurement variation assumed known (from the Distance for Windows analysis) and vague priors on process variance. Dots represent the point estimates and whisker bars are 95%CrIs. Black horizontal line is the mean growth rate $\bar{r}$ over the time series (0.002).

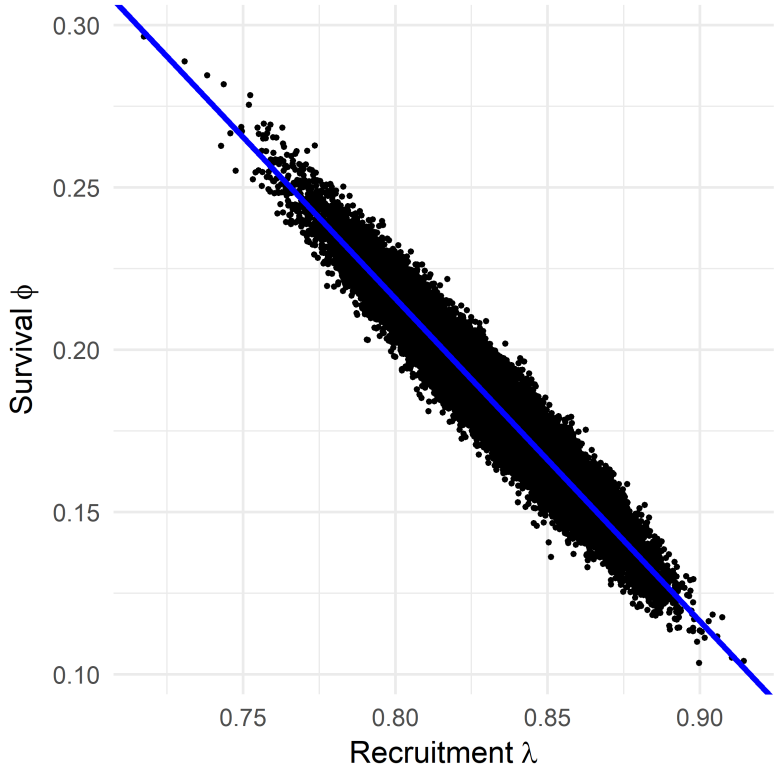

Figure 5.5: Correlation of survival ϕ and recruitment λ are confounded from Model M2 (correlation = -0.965). The blue line is the fitted linear regression.

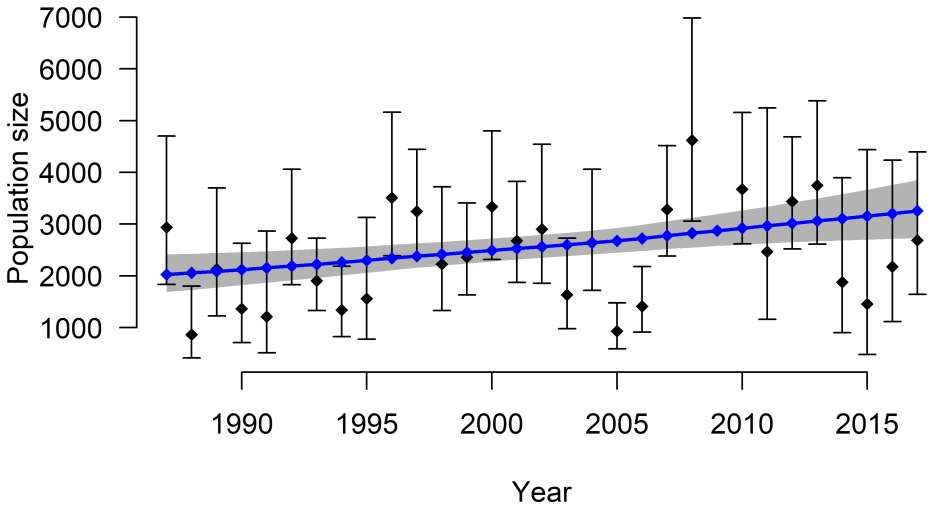

Figure 5.6: 'Ākepa abundance estimates (blue line; 95%CrI grey ribbon) from Model M2 with constant mean annual adult survival and recruitment (beta and Poisson variation, respectively). Abundance estimate with 95%CI from Distance for Windows (diamond and whisker bar).

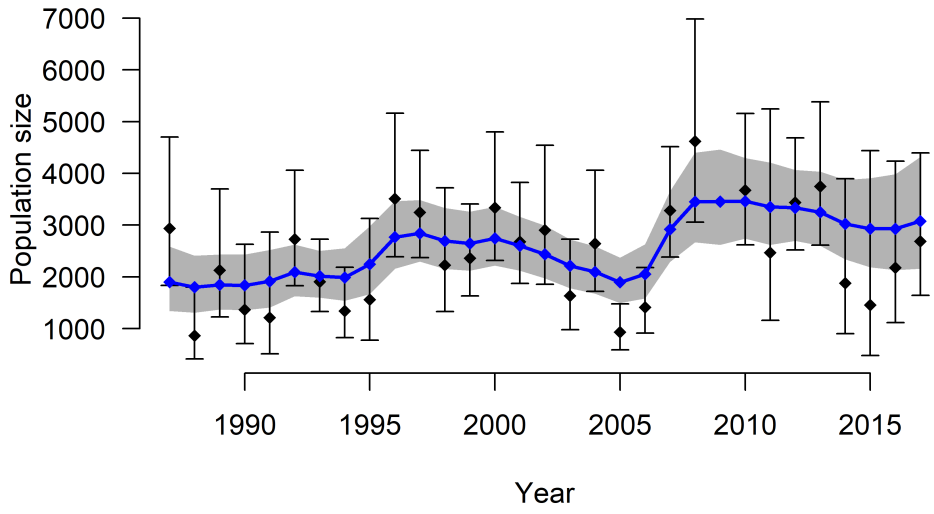

Figure 5.7: Predicted abundances (blue line) and 95%CrI (grey ribbon) estimates from Model M3 with time-varying recruitment λ_t and adult survival ϕ. Abundance estimate with 95%CI from Distance for Windows (diamond and whisker bar).

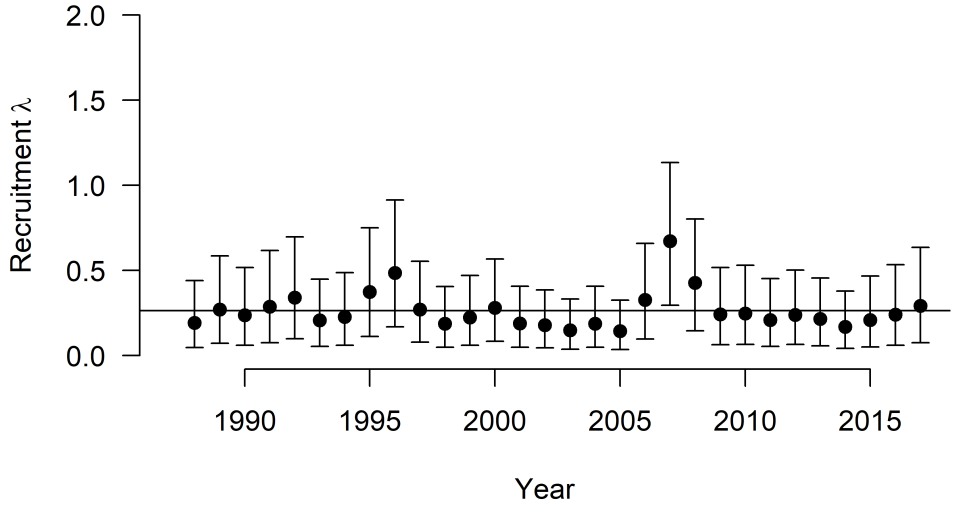

Figure 5.8: Recruitment λ estimates generated from Model M3. Dots represent the point estimates and whisker bars are 95%CrIs. Black horizontal line is the mean recruitment $\bar{\lambda}_t$ over the time series.

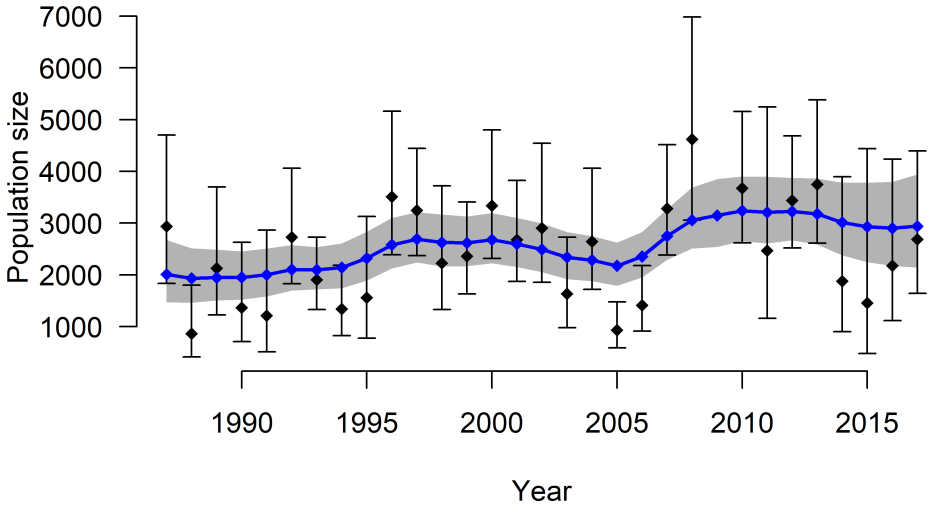

Figure 5.9: Predicted abundances (blue line) and 95%CrI (grey ribbon) estimates from Model M4 with independent time-varying recruitment and adult survival. Abundance estimate with 95%CI from Distance for Windows (diamond and whisker bar).

5.4.4 Model M4: Random effect on recruitment, constant survival

Model M4 produced a considerably smoother curve to the 'ākepa abundances that generally captured the same trajectories described in Model M3 above (Fig. 5.9). Increases in the population occurred in 1996 and between 2005 and 2010. Mean recruitment $\bar{\lambda}_t$ was 0.197 (SE=0.027), and all annual recruitment 95%CrIs bracketed the mean (Fig. 5.10). Mean adult survival $\bar{\phi}_t$ over the 31-year time series was 0.822 (SE=0.020). ϕ and λ were moderately correlated (-0.687; Appendix E Fig. E.6). Uncertainty in the Model M4 abundance estimates was substantially smaller than that estimated using design-based methods with an average 51.2% reduction in the length of the interval widths (SD=13.9%).

5.4.5 Model M5: Random walk on recruitment, constant survival

Model M5 produced smooth increases between 1990 to 1997 and from 2005 to 2010 with declines between 1998 to 2004 and since 2010 (Fig. 5.11). Mean recruitment $\bar{\lambda}_t$ was 0.192 (SE=0.021), and all annual recruitment 95%CrIs bracketed the mean except in 2007 and 2008 (Fig. 5.12). Mean adult survival $\bar{\phi}_t$ over the 31-year time series was 0.821 (SE=0.020). Correlation of ϕ and λ were high (correlation = -0.908; Appendix E Fig. E.8). Uncertainty in the Model M5 abundance estimates was substantially smaller than that estimated using design-based methods with an average 48.4% reduction in the length of the interval widths (SD=14.2%).

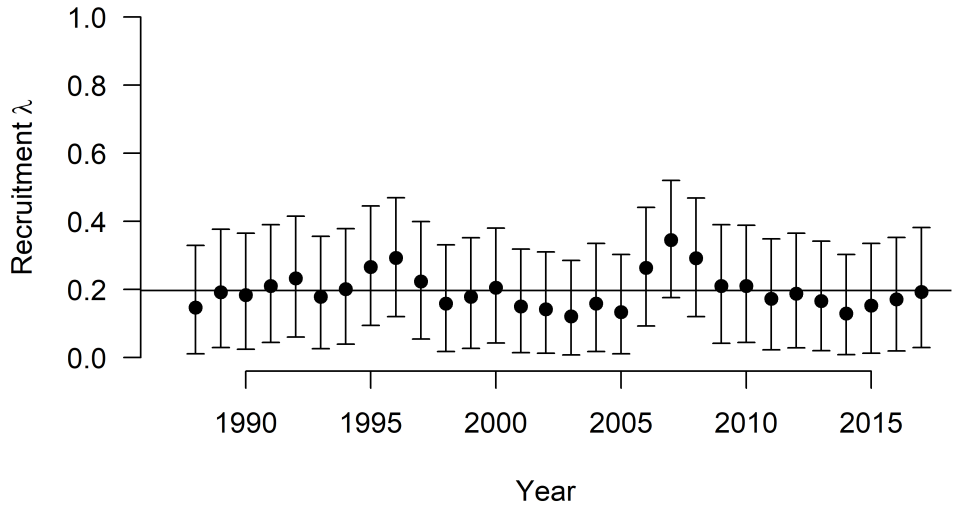

Figure 5.10: Recruitment λ estimates generated from Model M4. Dots represent the point estimates and whisker bars are 95%CrIs. Black horizontal line is the mean recruitment $\bar{\lambda}_t$ over the time series.

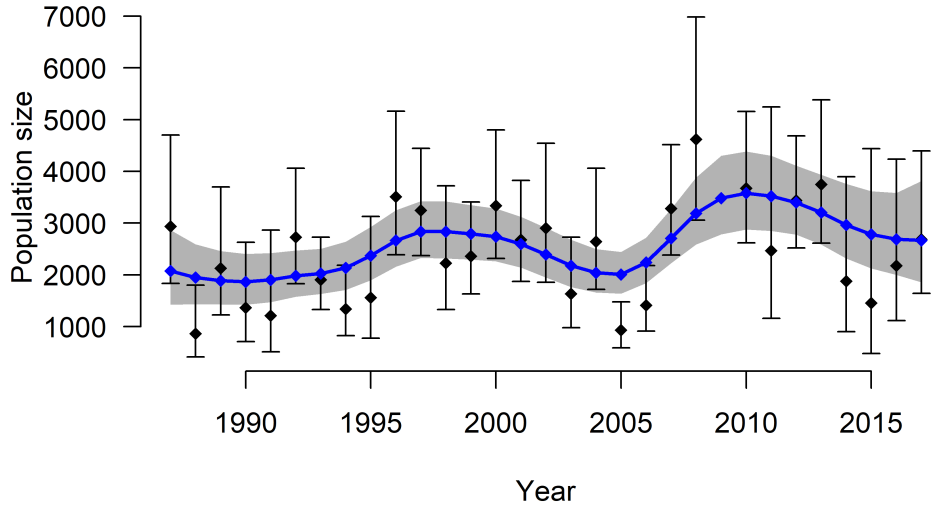

Figure 5.11: Predicted abundances (blue line) and 95%CrI (grey ribbon) estimates from Model M5 with time-varying recruitment with random walk and adult survival. Abundance estimate with 95%CI from Distance for Windows (diamond and whisker bar).

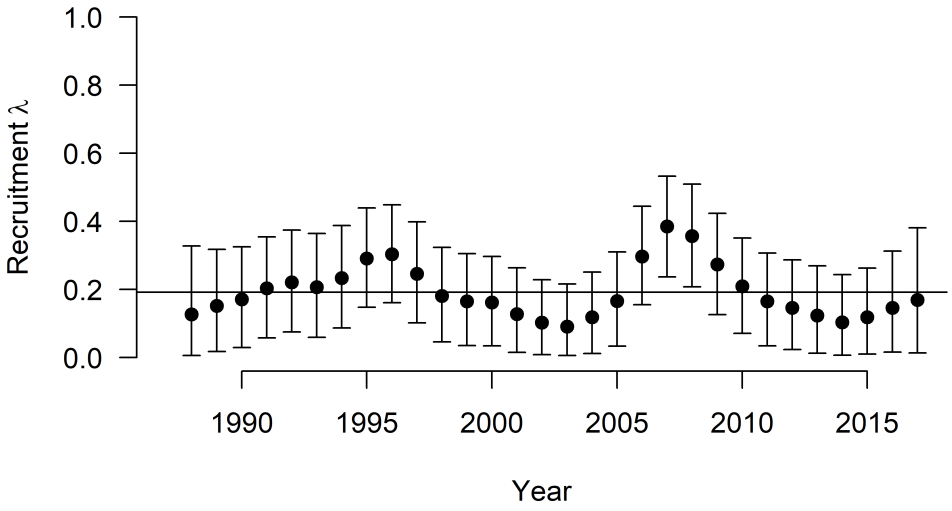

Figure 5.12: Recruitment λ estimates generated from Model M5. Dots represent the point estimates and whisker bars are 95%CrIs. Black horizontal line is the mean recruitment $\bar{\lambda}_t$ over the time series.

5.5 Discussion

Statistical methods

In this chapter, I used multi-stage fitting procedures to fit PDMs as SSMs that combine population- and individual-level information. SSMs provide a unifying framework to develop PDMs with Bayesian inference which coherently combines sources of uncertainty from data collected at different spatial and temporal scales. The data, abundances from monitoring surveys and vital rates from demographic studies, were analyzed separately using specialized distance sampling and mark-recapture software, respectively. I initiated the models as a SSM of the time series abundance estimates that included estimates of observation error and progressively added model complexity to include demographic subprocesses, thus, incorporating biological processes governing population changes. Changes in abundances are a result of losses from and gains to the population. PDMs reduce the magnitude change between abundance estimates by only allowing biologically realistic rates of change.

Biological relevance modelled as latent variables or random effects in SSMs provides greater understanding of population processes. This is an advantage over the smoother-based modelling and DSM methods from Chapter 2 that did not explicitly constrain demographic vital rates. Modelled as a net effect of demographic processes, these SSMs provide insight into mean and annual rates of change (Model M1; Camp et al. 2016). The overall long-term population trends (Urquhart and Kincaid 1999) can be assessed with consistent recruitment and survival models (Model M2). These models, however, can miss important trajectories and may not be biologically realistic over long time series (Thomas

et al. 2004). PDMs model the biological processes governing how the population changes over time (Newman et al. 2014). Incorporating demographic sub-processes of recruitment and survival specifically controls the magnitude of the rates of change. The general sub-processes recruitment and survival are analytically intractable; i.e., λ and ϕ are strongly correlated. Allowing λ to vary temporally ($\lambda_t \sim \text{gamma}\,(3.741, 9.806)$; Model M3) or vary as a stochastic distribution ($\lambda_t \sim \text{normal}\left(\bar{\lambda}, \sigma^2_\lambda\right)$ where the prior on $\bar{\lambda}$ is a gamma distribution; Model M4) decouples the parameters reducing their correlation. In these two models, all parameters were estimatable and the data were sufficiently influential to move the posteriors away from the priors. In Model M5, λ and ϕ are again strongly correlated; however, this was purposeful through the temporal regressive random walk formulation.

Modelling limitations

As a special case of SSMs with Bayesian inference, PDMs have many advantages including a unifying framework, combining data from multiple sources, accounting for correlations and coherently combining variances (Newman et al. 2014). PDMs are also useful when the raw data for the sub-processes are not available. My approach of using derived quantities through informed priors in a multi-stage fitting procedure avoids the computationally intensive costs of integrated population models (King et al. 2009). A key assumption of the state process is that the abundance and demographic data are independent of each other. This assumption was likely violated as some individuals in the demographic studies may also have been included in the abundance survey data. Abadi et al. (2010) showed that these violations negligibly effect parameter estimate accuracy, while simulations by Besbeas et al. (2009) revealed that estimator precision may be reduced when the data are not completely independent. The data independence assumption is convenient, seems to work well in many contexts, and this violation is minor as only a few individuals occurred in both datasets. There is a mismatch in paradigms when using the abundance estimates as input to a Bayesian model, although this mismatch does not necessarily invalidate inference (Abadi et al. 2010, Newman et al. 2014, Schaub and Fletcher 2015, Plard et al. 2019).

There is only one recruitment estimate (Guillaumet et al. 2016), which was estimated as a latent variable of an IPM. Although this recruitment estimate is biologically realistic for a rapidly increasing population, a sustained 17% or more per year increase is unrealistic for an established population. Therefore, the estimate is likely limited to the mist netting location at Nauhi and not applicable to the greater open-forest stratum. This limited inference is further supported by the small to moderate overlap of the marginal prior to posterior distributions which indicates that the data were sufficient to move the posterior away from the prior and the results are based on the data, not the prior (Appendix E Figs. E.2, E.3, E.5 and E.7).

I used the inverse variance-weighted average method as a meta-analysis of the five ϕ estimates (see Table 5.1) to set the survival prior. This method assumes that all studies in the meta-analysis share the same true parameter mean with variance equal to the error in the observations (Lee et al. 2016). Estimates from studies with lower precision are

given less weight than more precise estimates. This is a reasonable assumption given our understanding of 'ākepa survival from multiple sub-populations over several decades.

A normal distributed prior was assigned for annual recruitment λ_t in Model M4. In theory this distribution can produce inadmissible negative values for recruitment, a positive bounded parameter. An alternative would be a lognormal, for example, but I found the normal distribution worked well in practice because the left-tail was entirely non-negative, given the small variance used. It gave a symmetrical distribution of positive values around the mean on the natural scale (Appendix E Fig. E.7).

Cummins et al. (2014) showed that high precipitation and cooler temperatures affected nest success. Long-term climatic data are not available at Hakalau so I did not directly include covariates to demonstrate relationships between environmental stressors, such as extreme weather conditions, and demographic parameters influence on population changes. Conclusions associated with climatic events are therefore correlative.

Biological findings

The 'ākepa population at Hakalau has experienced three prominent trajectories over the 31-year time series. These trajectories reveal a pattern of recovery followed by a slow decline to about one-half the peak abundance. The recoveries coincided with large increases in recruitment but not adult survival, discussed below. Although abundances have fluctuated markedly, the population has increased by more than 900 birds between the time series end point estimates (95%CrI limits overlapped; Model M4). This positive trend was captured in all of the models, particularly Model M2 which was formulated to describe the long-term, overall directional trend (Urquhart and Kincaid 1999), and corroborates earlier analyses by Camp et al. (2010, 2014, 2016) that the 'ākepa population is stable to slightly increasing in the open forest stratum at Hakalau.

In general, my annual open-forest stratum abundance estimates from 1987 to 2012 were 1,000 to 2,000 birds fewer than those estimated by Camp et al. (2016). To avoid extrapolating too far from the points, I used a smaller study area than that used in Camp et al. (2016); therefore, the abundances estimated are necessarily smaller. Besides the 300 ha smaller study area, I estimated lower densities throughout the overlapping time period (Appendix A Table A.3; Fig. 1.7 compared to Figure 3 in Camp et al. 2016). Despite the smaller densities, the population at Hakalau remains the most abundant 'ākepa subpopulation on Hawai'i Island (Judge et al. 2018) and of utmost conservation concern.

A common benefit of SSMs is that partitioning estimator uncertainty into its component parts of state and measurement errors produces more precise abundance estimates (Schaub and Abadi 2011, Newman et al. 2014, Plard et al. 2019). The model formulated in Camp et al. (2016) failed to improve estimator certainty due to identifiability issues. These issues were overcome by incorporating demographic vital rates as random effects, which resulted in about a 50% reduction in average abundance credible interval widths compared to confidence interval widths from standard Distance for Windows (Chapter 1). The more precise estimates facilitates detecting impacts of management actions and making conservation and regulatory decisions.

The 'ākepa abundance time series data contains additional information about relative temporal changes in population size – rates of change. Population change estimates can be directly estimated as a latent variable in the SSM (i.e., $\bar{r}$ and r_t in Model M1), also called the per capita rate of growth δ_t of a population by Sibly and Hone (2002). A growth rate of zero indicates a static population (commonly referred to as a stable population in ecological literature). The mean 'ākepa growth rate was 0.002 (estimated from Model M1) indicating a roughly stable population over the time series that fluctuated around zero (Fig. 5.4). The geometric mean growth rate can be computed as $1 + \prod (r_t)^{1/T-1}$. The geometric mean growth rate for a stable population will be very near one and was computed at 1.02 from Model M4. Camp et al. (2016) computed an equivalent estimate of 1.01 for the 'ākepa population in the open-forest stratum for the period 1987 to 2012.

Rates of change can be biased by spatial heterogeneity in densities, spatio-temporal correlation and study area scale (Sibly and Hone 2002). Bias from the first two sources is reduced when logging the abundance quotients as is done when computing r_t (Steen and Haydon 2000). Spatial and temporal scales can strongly influence growth rate bias. Small study areas, e.g., typical in demographic studies, are affected by location-specific rates of change. This affect can be amplified if the data are collected during a rapidly changing trend. The estimated growth rate of Guillaumet et al. (2016) is 1.172 and is likely positively biased as 'ākepa were increasing rapidly in the middle of Hakalau during the 1990s (see Fig. 2.13). Similarly, the study area size and sampling time period could also influence population rates of change estimated in the Pua 'Ākala and Pedro study sites. Similarly, drawing conclusions of average vital rates from across the open forest stratum can obscure important details such as the regional increase in densities in the northern portion of the refuge and the dynamic density pattern in the southern portion. Besides site-restricted inference, another explanation could be a violation of the assumption that there was no immigration or emigration during their study. Guillaumet et al. (2016) showed that there was transience in 'ākepa in the Nauhi study area. It is likely that the demographic studies of Lepson and Freed (1995) and Medeiros and Freed (2009) were also from an open population leading to the incorrect generalization Freed and Cann (2010) reached.

Population dynamics are driven by recruitment and survival, assuming a closed system. I assumed that recruitment has greater influence on population changes than survival. This contradicts Sæther and Bakke (2000) who concluded that adult survival rate is the predominant driver of change in growth in long-lived avian species. However, 'ākepa adult survival rates are similar over decades and among the three large sub-populations in Keauhou Ranch (Ralph and Fancy 1994), Kau FR (Freed 1988), and in Hakalau (Lepson and Freed 1995, Medeiros and Freed 2009, Guillaumet et al. 2016). A slow life history pattern sacrifices current reproduction in favour of future reproduction, which necessitates species be long-lived with high adult survival (Dobson 2012). This lifestyle approach is typical of Hawaiian forest birds, and specific to 'ākepa (Woodworth and Pratt 2009)

I observed varying, declining recruitment with periodic recovery, which resulted in high amplitude fluctuations in population size. In most years recruitment was very low

($\leq$ 0.35), with a large number of birds recruited in occasional good years. Cummins et al. (2014) found that rainy weather, particularly high amounts of precipitation and cooler temperatures associated with storm system events, lead to dramatic differences in nest success and productivity. Rainfall can affect reproduction directly (e.g. onset of egg laying and thermoregulation) or indirectly (e.g. reduced foraging opportunities and prey availability). Climate data for Hakalau are only available from October 2009 through the end of the time series (Ostertag et al. 2015), after the large recruitment events that occurred in 1995, 1996 and 2006 through 2008 resulted in population increases and the trajectories switching direction (declining switching to increasing; Figs. 5.9 and 5.10). For this to occur, it is likely that there were no or few storm events during the breeding and post-breeding seasons prior to the recovery pulses.

Given the periodic pulses to the 'ākepa population highlights the need for long-term monitoring. Studies spanning shorter intervals of three, five, or even 10 (e.g., the period from 1996 through 2005) years could easily miss critical pulses that recover the 'ākepa population. Similarly, studies that sample less frequently, such as every other or every fifth year, are likely to miss dynamic patterns observed in this study and for other Hawaiian forest bird populations such as the palila (*Loxioides bailleui*; Johnson et al. 2006, Genz et al. 2018) and additional species monitored at Hakalau (Camp et al. 2009, 2016). Shorter term studies could, therefore, yield uninformative or misleading results, while longer time series are needed to estimate abundance trajectories and vital rates that occur over short time intervals.

Management implications

Abundance monitoring is a cornerstone of conservation and management where population states are used for policy, regulation and action assessment. Long-term abundance monitoring is useful for evaluating trends (this study; Knape et al. 2013, Camp et al. 2016), estimating latent vital rate parameters (this study; Guillaumet et al. 2016, Schmidt and Robison 2020), reducing parameter variances (this study; Besbeas et al. 2002, Schaub and Abadi 2011), making predictions about future patterns such as identifying indicators of impending population collapse (Rozek et al. 2017, Plard et al. 2019), and are essential for evidence-based management (Lindenmayer and Likens 2010, Lindenmayer et al. 2012). To provide population level inference, these analyses require large-scale annual monitoring collected frequently and over long periods to discern biologically meaningful patterns and evaluate the effectiveness of management actions.

Over the 31-year time series the 'ākepa population has fluctuated slightly and it appears that abundances are stable to slightly increasing (Chapter 2; Model M4; Camp et al. 2016, Rozek et al. 2017). However, I identified data deficiencies in our understanding of 'ākepa demography – nest success and juvenile survival. Inference into population changes could be improved by getting reliable estimates of nest success and juvenile survival including survival of hatchlings, nestlings and fledglings. Of particular interest is the interaction between weather events such as heavy rainfall, high wind and cold temperatures with low nest success and low juvenile survival. Combining those sub-processes with climate data in

PDMs could lead to improved understanding of demographic and environmental drivers of population changes. Obtaining sufficient demographic trait information to establish informed priors for those sub-processes may require substantial increases in current costs. At Hakalau, 'ākepa nests are located high in the canopy, typically in cavities and inaccessible for banding nestlings. It is difficult to identifying distinct and consistent juvenile classes (e.g. hatch year, second-year) and juvenile capture rates are very low (Woodworth and Pratt 2009). Until such data are available it may be possible to parameterize and set priors assuming fairly heterogeneous survival rates and possibly an index of age based on capture dates if banding is continuous throughout the year. Moreover, limited conservation resources may be better allocated to support continued abundance monitoring, demographic studies and habitat restoration at Hakalau while bolstering monitoring and research to better understand trends and drivers in the other 'ākepa sub-populations. Integrating sub-population information in an overall species conservation program with analyses using PDMs could lead to improved study design and inference without substantial increases in costs.

Chapter 6

Conclusions

6.1 Summary

I conclude with a summary of my thesis and identify possible future research. Much of species management and conservation starts with and requires estimating abundances that are sufficiently precise for evaluating population trends. The main aims of my thesis were to precisely estimate population sizes by (1) accounting for correlation in spatial (single annual survey) and spatio-temporal (time series of surveys) dependencies in counts, and (2) by combining abundance and demographic data on population vital rates. I demonstrated that penalized spline-based smoothing, point process, soap-film smoothing and population dynamics modelling procedures reduced the variance in density estimates in both single year and time series data compared to conventional distance sampling estimators. The density surface model (DSM) and point process approaches also provided maps of how 'ākepa densities were distributed and have changed over time in Hakalau. 'Ākepa are not uniformly distributed and the density surface maps are an effective tool to identify priority areas where the species is most likely to respond or require further intervention, thus benefiting conservation planning through improved management efficiency and reduced costs.

The long-term trend for 'ākepa is stable to slightly increasing. Population dynamics models (PDMs) can be used to identify biological processes governing population changes. Understanding which demographic traits may be driving population change further benefits species conservation and management. Short-term trajectories reveal a pattern of recovery followed by a slow decline before recovering again. These recoveries coincided with large increases in recruitment, which appears to be a limiting trait restricting the 'ākepa population growth.

The combined DSM and PDM analyses provides critical information for identifying population responses to environmental conditions and management actions. This information provides managers and regulators with the metrics needed to justify costly efforts to restore habitats, increase population abundances and curtail species declines.

6.2 Potential future research

Here I identify some key issues that I anticipate may be the focus of future research.

6.2.1 Sampling design & data collection

Long-term monitoring with consistent and frequent surveys is an essential component of evidence-based management. A review of Hawaiian forest bird survey protocols would ensure that operating procedures including consistency and frequency of surveys, data collected, and analyses are adequate to address monitoring objectives. Consistent and frequent surveys over the long-term time series facilitated DSM and PDM analyses herein. Applying standard generalized additive models (GAMs) allows for predicting the missing 2009 survey abundances; however, predicting missing estimates is not possible using the DSM approach without making a strong assumption that an average detection probability represents annual detectability. Annual detection probabilities varied widely (Appendix A Table A.1); evidence of a plausible assumption violation. State space models (SSMs) overcome this limitation and the 2009 abundance was predicted relatively precisely (Chapter 5, Model M4: 11 %CV). Uncertainty will increase if additional surveys are missed, eventually resulting in low power to detect population change (Brinck et al. 2012). This effect will be greater in monitoring programs that sample less frequently than annually, such as the National Park Service Pacific Island Landbird Monitoring Program of the Pacific Island Network Inventory and Monitoring Program and the State of Hawaii Division of Forestry and Wildlife (Camp et al. 2009, 2011). A review of Hawaiian forest bird monitoring protocols could include evaluating that the data and analyses provide the information needed to address monitoring and conservation objectives, priorities and questions.

Inference may be biased and imprecise when predictions are made from increasingly distant survey points; i.e. sparse survey effort (see Chapters 3 and 4; Miller et al. 2013). The spatio-temporal modelling in Chapter 2 was unlikely affected by sparse survey effort because of the restricted sampling frame. Annual surveys are conducted at Hakalau from a systematic sampling design, while elsewhere in Hawai'i forest bird surveys are conducted less frequently from sampling designs that are generally sparse and less systematic (Camp et al. 2009). Establishing additional points could mitigate issues resulting from sparse survey effort. This could be particularly important for range restricted species such as the critically endangered palila (*Loxioides bailleui*), kiwikiu (Maui parrotbill; *Pseudonestor xanthophrys*), 'akiapōlā'au (*Hemignathus munroi*) and 'ākohekohe (*Palmeria dolei*). One possible direction to selecting the intensity and location of points, retaining and building on the current Hawaiian randomised survey design, is to apply optimal experimental design procedures applicable for GAMs (Ryan et al. 2016). Another option is the balanced acceptance sampling ideas of Foster et al. (2017) and van Dam-Bates et al. (2018). An alternative direction is to switch to a model-based design incorporating spatial location and other covariates, such as habitat and environmental factors, following guidance by Peel et al. (2013). Switching from random- to model-based designs requires assumptions about the species distribution and spatial covariates that are a realisation of spatial models.

Therefore, switching to a model-based design requires careful consideration of the survey goals, method-specific advantages and disadvantages, and how the data will be analysed.

6.2.2 Habitat and environmental covariates

Analysis incorporating the general, coarse-level wet and mesic montane forest vegetation was uninformative when modelling 'ākepa spatio-temporal patterns in Chapter 2. Since 2016, a more detailed fine-scaled habitat description of forest structure and composition has been collected at Hakalau that includes tree crown cover, tree height, tree species composition, understory type and ground cover. It could be informative to remodel a concurrent subset of the time series to determine if this more detailed habitat description is an explanatory variable of 'ākepa densities. Jacobi (2018) produced a Hakalau vegetation map with the fine-scaled habitat descriptions that could allow for extrapolating and mapping bird densities to the entirety of Hakalau. If fine-scaled habitat is informative, then predicting 'ākepa densities more broadly to un-sampled areas across the species range and along elevation gradient is possible, although caution is required given the thin plate regression spline (TPRS) results in Chapter 4.

The periodic pulses to the 'ākepa population may be in response to a lack of normal annual storm system events such as heavy rainfall, high wind and cold temperatures that typically result in low nest success (Cummins et al. 2014) and presumably low juvenile survival. Acquiring and including climate data in the PDMs could shed light on interaction between weather events and recovery pulses. Climate change is expected to increase the intensity and frequency of extreme storm system events on Hawai'i Island (Chen and Chu 2014), although there is uncertainty about the magnitude of change in these factors. Forecasts about climate-driven events could shed light on 'ākepa persistence (Møller et al. 2010) and its ability to adapt to climate change (Fortini et al. 2015).

6.2.3 Underlying smoothness assumption

Point process and DSM approaches were applied to predict and map 'ākepa densities in Chapter 3. Both approaches make assumptions about the underlying smoothness of the data. My analysis showed that the approaches produced different smoothing resulting with a more heterogeneous surface from the point process and a more uniformly smooth surface from the DSM. This pattern was most noticeable in the hotspot in the southern portion of Hakalau (see Figs. 3.5 and 3.6). In this area differences in detections among points were relatively substantial with counts at adjacent points ranging from 0 to 6 birds (see Fig. 3.1) and is common of Hawaiian forest bird counts (Camp et al. 2016, Genz et al. 2018). The underlying model smoothness assumption should be carefully considered to ensure that insights into a species' spatial ecology approximates the reality of how the birds use space.

6.2.4 Controlling boundary behaviour

In Chapter 4 I modelled the survey data using a soap-film smoother with a formulation interpolating the boundary density instead of a fixed boundary density. How the data behaves at the boundary is based on the study design and species biology. Ignoring study design issues, the hardness or permeability of the boundary depends on the suitability of the habitat on each side of the boundary. For 'ākepa at Hakalau the boundary is permeable on the north, east and south boundaries. In 2002, no 'ākepa occupied the pasture stratum and the western, pasture-forest boundary was semi-permeable. Since 2002 a few individuals have been detected in the pasture stratum, within a few hundred meters of the forest edge (Paxton et al. 2018). Thus, the more prudent modelling approach is to use the two linked smooths to estimate the boundary density as it can always estimate an effect that is zero or near zero.

Applying the soap-film smooth analyses elsewhere in Oceania could be modelled with a fixed boundary value formulated using the single element basis smooth (*a priori* specification of the boundary density, e.g., zero). Suitable forest bird habitat intersects with the coastline and unsuitable beach or ocean habitat. On these islands coastlines are narrow with cliffs plunging to the ocean and most beaches are only a few meters wide. In this situation a single element basis may be more appropriate with the boundary density defined at zero. This approach is applicable to other island populations such as the critically endangered Nihoa millerbird (*Acrocephalus familiaris kingi*) and Nihoa finch (*Telespiza ultima*) on Nihoa in the Hawaiian archipelago.

6.2.5 Modelling additional sub-processes in the PDM

In Chapter 5 I incorporated the sub-processes adult survival and recruitment with abundances to determine population trends. There are additional sub-processes driving population change that could be modelled similarly. Birth rates and juvenile survival are not separated in the current model; however, they could be individually parameterized. There is limited information on the birth sub-process as only a handful of 'ākepa nests have been followed through nestlings fledging (Cummins et al. 2014); however, this may be sufficient to inform priors and avoid non-identifiability issues. As additional information is gathered, it may be possible to parameterize birth rate probabilities based on female age with possible age-based classes of one-year-old and older females giving birth. Heterogeneity on when individuals first breed, whether their first or second year after fledging, could be captured with a first-year breeder class and an experienced breeder class instead of the age-based classes.

Juvenile survival includes surviving hatching, nestling and fledging stages, as well as surviving post-fledging through the next year, with age incrementation occurring with the next breeding season. Medeiros and Freed (2009) showed body size influences juvenile survival. It is likely that juvenile size is affected by both the population abundance through density dependence as well as winter rainfall and possibly temperatures and storm events. Climate and weather data at Hakalau are available but incomplete for the entire time series. Both juvenile survival and climate data could be incorporated in a model following

the formulation of the independent time-varying recruitment (Model M4) and time-varying recruitment with random walk (Model M5) models.

For my modelling I assumed the sex ratio was at parity despite that Hart (2001) found sex ratios at Pua 'Ākala and Pedro sites at a 1.14:1 and 1.21:1 male to female ratio, respectively, and Lepson and Freed (1995) estimated a 1.14:1 male to female ratio at the Pua 'Ākala site. Adult male-biased sex ratios is common in birds, is more severe in threatened species and the extinction risk is greatest in heavily skewed populations (adult sex ratio $>$ 1.66:1; Donald 2007). Sex-specific adult survival could be added to the PDMs as a prior based on the observed proportions. Sex-specific survival may be an important early warning factor to track as an indication of increased extinction risk (Rozek et al. 2017). Assigning sex to fledglings based on the observed proportion of females could also be included as a prior in the PDMs if fledgling survival differs by sex as well as weight (Medeiros and Freed 2009).

At what age 'ākepa recruit into the breeding population is poorly understood. I assumed that all adult aged birds breed and that any juvenile birds that survive to the next breeding season have transitioned to the breeding adult age class. Some males are not sexually mature their first year after hatching and delay breeding until they have full breeding plumage their second year after hatching (Lepson and Freed 1997, Woodworth and Pratt 2009). Parameterizing a breeding age sub-process could capture this dynamic, and may help explain why the species persists despite the observed skewed sex ratio.

A final sub-process not considered here is the potential for immigration and emigration; the movement or dispersal of birds among areas. Movement in 'ākepa is limited (Reding et al. 2010), but what movement there is likely occurs outside the breeding season and differs between age and sex classes. Almost two-thirds of juvenile 'ākepa either left the Keauhou Ranch study area or died after being captured (Ralph and Fancy 1994). The authors note that 'ākepa show strong philopatry, particularly adult males. In an example provided by Ralph and Fancy (1994), a male bird remained in the study area for one year after the female disappeared and probably longer but the study ended. In addition, the authors observed one or more unpaired males remained within paired birds' home ranges instead of dispersing. A fully parametrised movement model would include age and sex classes. However, data for 'ākepa is relatively sparse so an initial model could consider a class undifferentiated movement model.

Guillaumet et al. (2016) showed that there was temporary migration in the 'ākepa population in Hakalau at Nauhi (see Fig. 1.1). 'Ākepa numbers in the south portion of Hakalau were increasing in the late 1980s through the 1990s (Fig. 2.15), which may have influenced abundance trends at Nauhi. This could be indicative of a within-recovery-unit sub-process partially driving population trends (Allison and McLuckie 2018) or possibly a source-sink scenario (Plard et al. 2019). Newman et al. (2014) provides a parameterization for a PDM movement sub-process model with movement among colonies. In the case of 'ākepa at Hakalau, populations in the north and south parts of the study area could be treated equivalent to colonies. In a metapopulation framework, this model could be expanded to model movement among the five 'ākepa sub-populations on Hawai'i Island.

In this model region density, site fidelity and distance between sub-populations could affect the probability of movement and be parameterized accordingly (Millon et al. 2019). Information from ongoing demographic and radio telemetry studies at Hakalau could shed light on movement sub-processes, which could be made spatially explicit following formulation by Nadeem et al. (2016) to determine if within-recovery-unit or source-sink status are population drivers.

6.3 Concluding remarks

The analytic methods applied herein are useful broadly for Hawaiian forest bird management and conservation, and these analyses can be applied to other taxa to aid in global efforts to arrest declines in populations and the loss of biodiversity. The DSM analyses could be used to improve estimator certainty and provide insights into density patterns for endangered forest bird species on Layson, Nihoa, Kaua'i, Maui and Hawai'i, as well as the common species throughout Hawai'i, while PDMs could identify drivers of population change. These analyses however will not be useful for species that persist in numbers too low to reliably model including species that are presumed extinct (Gorresen et al. 2009) and presumably the 'akikiki (*Oreomystis bairdi*) that has recently declined dramatically to very low numbers (Paxton et al. 2016). These analytic methods can be applied to bird species in American Samoa, Guam, the Commonwealth of the Northern Mariana Islands, other island populations in Oceania and more broadly to continental populations. The DSM and PDM methods can be applied to other taxa that are routinely monitored where information to estimate species detection probabilities, counts and demographic vital rates are collected.

Appendix A

Appendix for Chapter 1

This appendix includes the hazard-rate detection function plot with individual `Year` covariates (Appendix A Fig. A.1), tables of the annual detection probabilities (Appendix A Table A.1), encounter rates (Appendix A Table A.2), 95% confidence intervals produced using analytic and bootstrap methods (Appendix A Fig. A.2), and density estimates for both, south and north regions from point-transect distance sampling surveys on Hakalau Forest National Wildlife Refuge, Hawai'i, between 1987 and 2017 (Appendix A Tables A.3–A.5).

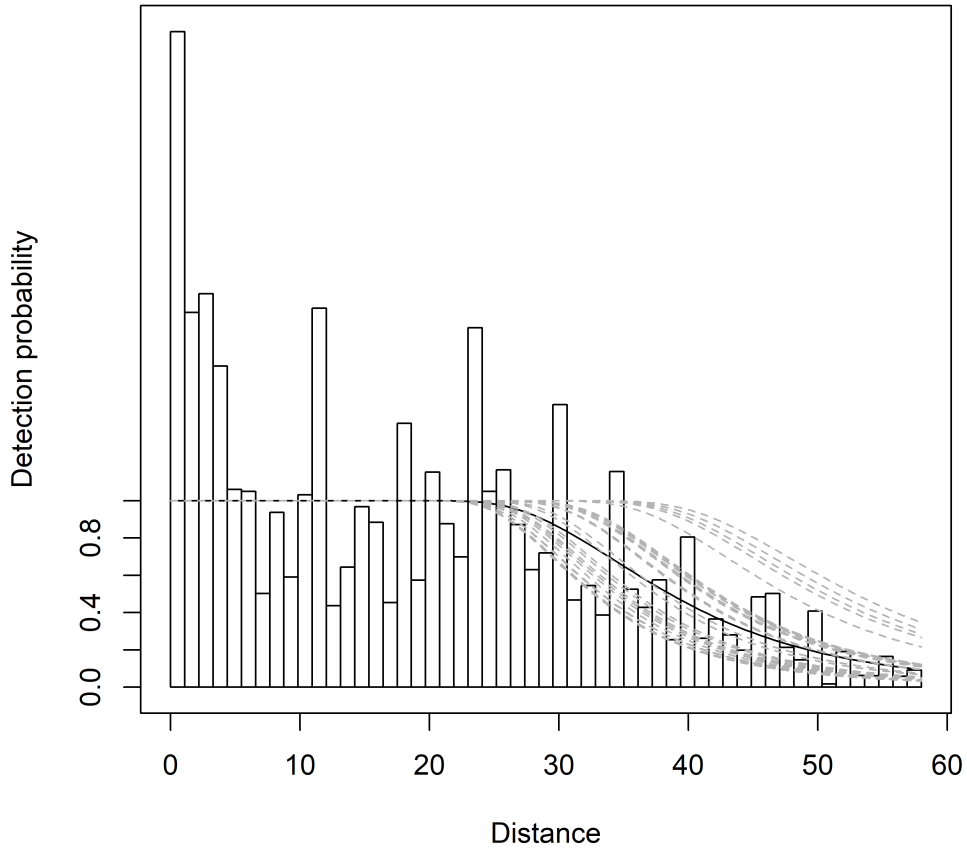

Appendix A Figure A.1: Average detection probability (dark solid line) for the hazard-rate model without series expansion and with `Year` as a covariate plotted on the data histogram. Each `Year` covariate is shown by a grey dashed line. There was a clear pattern in the decay phase where several detection probabilities were cluster below, slightly above and well above the average detection probability.

Appendix A Table A.1: Annual detection probability with SE estimates from the hazard-rate model without series expansion and with the covariate `Year` produced using Distance for Windows. Survey not sampled indicated with a —.

Year	Detection Probability	SE
1987	0.365	0.030
1988	0.721	0.037
1989	0.418	0.036
1990	0.478	0.041
1991	0.574	0.047
1992	0.425	0.032
1993	0.780	0.032
1994	0.746	0.040
1995	0.702	0.039
1996	0.551	0.028
1997	0.447	0.029
1998	0.557	0.036
1999	0.439	0.035
2000	0.386	0.027
2001	0.533	0.033
2002	0.583	0.031
2003	0.586	0.041
2004	0.571	0.032
2005	0.790	0.056
2006	0.496	0.056
2007	0.537	0.034
2008	0.378	0.027
2009	—	—
2010	0.375	0.034
2011	0.400	0.042
2012	0.375	0.034
2013	0.382	0.034
2014	0.567	0.047
2015	0.583	0.054
2016	0.585	0.047
2017	0.411	0.042

Appendix A Table A.2: Annual encounter rate with SE estimates from the hazard-rate model without series expansion and with the covariate `Year` produced using Distance for Windows. Survey not sampled indicated with a —.

Year	Encounter Rate	SE
1987	0.472	0.202
1988	0.371	0.149
1989	0.414	0.202
1990	0.330	0.171
1991	0.330	0.229
1992	0.538	0.215
1993	0.686	0.257
1994	0.474	0.220
1995	0.513	0.303
1996	0.919	0.377
1997	0.668	0.235
1998	0.558	0.207
1999	0.472	0.168
2000	0.621	0.242
2001	0.648	0.217
2002	0.779	0.276
2003	0.442	0.187
2004	0.692	0.271
2005	0.271	0.142
2006	0.253	0.109
2007	0.789	0.295
2008	0.795	0.272
2009	—	—
2010	0.574	0.220
2011	0.410	0.211
2012	0.503	0.239
2013	0.568	0.199
2014	0.400	0.190
2015	0.345	0.138
2016	0.482	0.134
2017	0.424	0.155

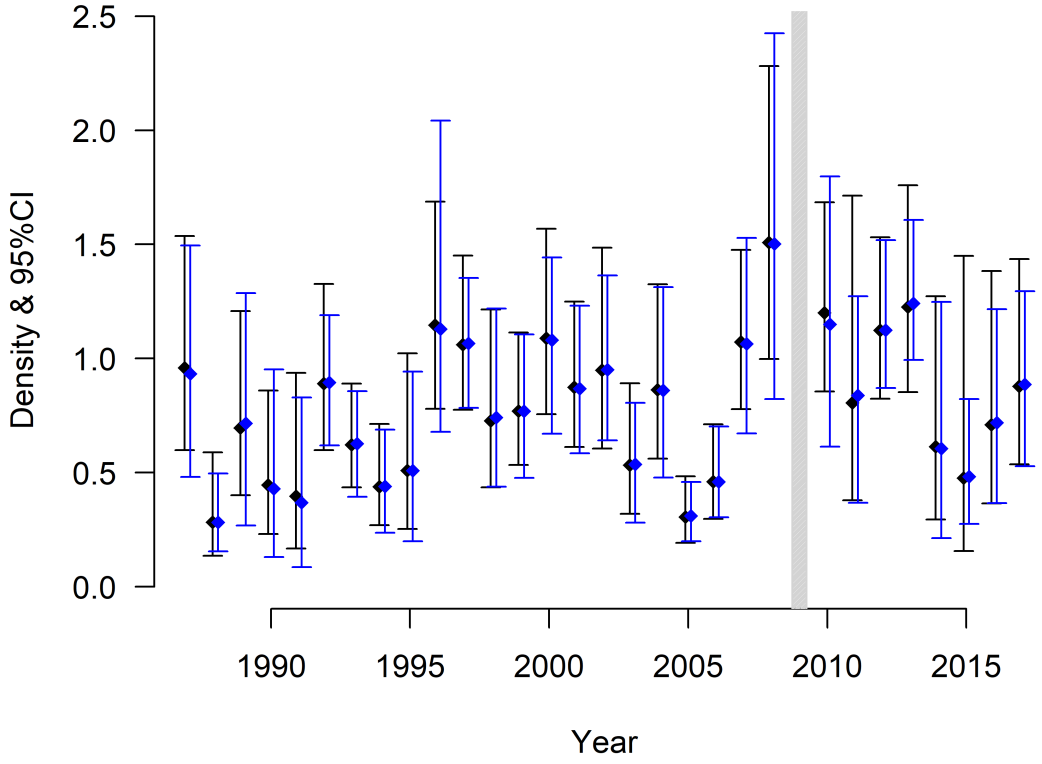

Appendix A Figure A.2: Annual density and 95%CI estimates from the hazard-rate model without series expansion and with the covariate `Year` produced using Distance for Windows using analytic (black diamonds and whisker bars) and bootstrap (blue diamonds and whisker bars) methods. Surveys were not conducted in 2009 (vertical bar).

Appendix A Table A.3: Density estimates for both regions from point-transect distance sampling surveys on Hakalau Forest National Wildlife Refuge, Hawai'i, between 1987 and 2017. The design-based estimates include density (Est_DB), standard error (SE_DB), coefficient of variation (CV_DB), lower 95% confidence limit (LCL_DB), upper 95% confidence limit (UCL_DB), and width of the confidence interval (CIW_DB). Estimates not produced indicated with a —.

Year	Est_DB	SE_DB	CV_DB	LCL_DB	UCL_DB	CIW_DB
1987	0.959	0.234	0.244	0.599	1.536	0.937
1988	0.283	0.110	0.388	0.136	0.589	0.453
1989	0.696	0.200	0.287	0.401	1.207	0.807
1990	0.446	0.153	0.344	0.232	0.859	0.627
1991	0.396	0.183	0.461	0.168	0.937	0.769
1992	0.891	0.183	0.205	0.598	1.326	0.729
1993	0.622	0.115	0.184	0.435	0.890	0.455
1994	0.438	0.111	0.253	0.269	0.713	0.444
1995	0.509	0.187	0.368	0.253	1.023	0.769
1996	1.147	0.228	0.199	0.779	1.687	0.908
1997	1.061	0.171	0.161	0.775	1.451	0.676
1998	0.727	0.194	0.267	0.435	1.215	0.780
1999	0.770	0.146	0.190	0.533	1.113	0.580
2000	1.089	0.204	0.188	0.757	1.569	0.812
2001	0.874	0.161	0.184	0.612	1.249	0.638
2002	0.948	0.220	0.232	0.606	1.485	0.879
2003	0.534	0.142	0.267	0.319	0.892	0.572
2004	0.863	0.191	0.222	0.562	1.326	0.764
2005	0.305	0.073	0.238	0.193	0.484	0.291
2006	0.460	0.104	0.226	0.297	0.712	0.415
2007	1.072	0.176	0.164	0.779	1.475	0.697
2008	1.509	0.322	0.213	0.998	2.280	1.282
2009	—	—	—	—	—	—
2010	1.200	0.209	0.174	0.855	1.685	0.830
2011	0.806	0.322	0.400	0.379	1.714	1.335
2012	1.123	0.179	0.159	0.824	1.531	0.707
2013	1.225	0.228	0.186	0.853	1.759	0.905
2014	0.613	0.237	0.386	0.295	1.273	0.978
2015	0.476	0.294	0.617	0.156	1.449	1.293
2016	0.710	0.249	0.350	0.365	1.384	1.019
2017	0.878	0.224	0.255	0.536	1.436	0.900

Appendix A Table A.4: Density estimates for the north region from point-transect distance sampling surveys on Hakalau Forest National Wildlife Refuge, Hawai'i, between 1987 and 2017. The design-based estimates include density (Est_DB), standard error (SE_DB), coefficient of variation (CV_DB), lower 95% confidence limit (LCL_DB), upper 95% confidence limit (UCL_DB), and width of the confidence interval (CIW_DB). Estimate not produced indicated with a —.

Year	Est_DB	SE_DB	CV_DB	LCL_DB	UCL_DB	CIW_DB
1987	0.131	0.140	1.069	0.015	1.103	1.087
1988	0.079	0.097	1.225	0.007	0.892	0.885
1989	0.058	0.055	0.938	0.009	0.377	0.368
1990	0.034	0.039	1.157	0.004	0.302	0.298
1991	0.014	0.014	0.991	0.001	0.149	0.148
1992	0.058	0.074	1.286	0.005	0.632	0.627
1993	0.086	0.066	0.763	0.016	0.467	0.452
1994	0.000	—	—	—	—	—
1995	0.012	0.015	1.320	0.001	0.137	0.136
1996	0.060	0.040	0.677	0.014	0.248	0.233
1997	0.131	0.092	0.700	0.029	0.584	0.555
1998	0.179	0.196	1.096	0.019	1.683	1.664
1999	0.153	0.097	0.636	0.039	0.602	0.564
2000	0.000	—	—	—	—	—
2001	0.204	0.116	0.570	0.057	0.736	0.680
2002	0.188	0.208	1.102	0.020	1.800	1.780
2003	0.070	0.087	1.250	0.006	0.782	0.775
2004	0.114	0.097	0.845	0.019	0.698	0.679
2005	0.000	—	—	—	—	—
2006	0.139	0.065	0.471	0.050	0.381	0.331
2007	0.182	0.087	0.478	0.061	0.543	0.482
2008	0.543	0.242	0.446	0.190	1.553	1.363
2009	—	—	—	—	—	—
2010	0.300	0.164	0.548	0.087	1.038	0.951
2011	0.136	0.305	2.242	0.004	5.240	5.236
2012	0.127	0.090	0.710	0.028	0.589	0.562
2013	0.484	0.209	0.433	0.176	1.328	1.151
2014	0.238	0.268	1.123	0.020	2.799	2.779
2015	0.224	0.408	1.821	0.008	6.246	6.238
2016	0.452	0.334	0.740	0.075	2.704	2.629
2017	0.476	0.210	0.442	0.168	1.349	1.181

Appendix A Table A.5: Density estimates for the south region from point-transect distance sampling surveys on Hakalau Forest National Wildlife Refuge, Hawai'i, between 1987 and 2017. The design-based estimates include density (Est_DB), standard error (SE_DB), coefficient of variation (CV_DB), lower 95% confidence limit (LCL_DB), upper 95% confidence limit (UCL_DB), and width of the confidence interval (CIW_DB). Estimate not produced indicated with a —.

Year	Est_DB	SE_DB	CV_DB	LCL_DB	UCL_DB	CIW_DB
1987	2.891	0.709	0.245	1.675	4.989	3.313
1988	0.757	0.288	0.380	0.319	1.794	1.475
1989	2.181	0.653	0.299	1.115	4.266	3.151
1990	1.408	0.503	0.357	0.632	3.136	2.504
1991	1.286	0.608	0.472	0.451	3.669	3.218
1992	2.832	0.585	0.206	1.788	4.485	2.697
1993	1.873	0.350	0.187	1.219	2.877	1.658
1994	1.459	0.368	0.252	0.819	2.600	1.781
1995	1.668	0.622	0.373	0.716	3.887	3.171
1996	3.680	0.754	0.205	2.304	5.878	3.574
1997	3.227	0.528	0.164	2.248	4.633	2.385
1998	2.005	0.457	0.228	1.198	3.355	2.157
1999	2.210	0.432	0.196	1.438	3.396	1.958
2000	3.629	0.681	0.188	2.391	5.507	3.116
2001	2.436	0.462	0.190	1.591	3.731	2.140
2002	2.719	0.550	0.202	1.716	4.308	2.591
2003	1.615	0.428	0.265	0.887	2.942	2.055
2004	2.608	0.597	0.229	1.549	4.390	2.841
2005	1.016	0.242	0.238	0.572	1.806	1.234
2006	1.210	0.310	0.257	0.665	2.202	1.537
2007	3.144	0.551	0.175	2.080	4.753	2.673
2008	3.759	0.916	0.244	2.100	6.729	4.628
2009	—	—	—	—	—	—
2010	3.298	0.584	0.177	2.199	4.947	2.748
2011	2.367	0.804	0.340	1.011	5.543	4.532
2012	3.444	0.557	0.162	2.397	4.948	2.551
2013	2.953	0.584	0.198	1.864	4.677	2.813
2014	1.487	0.482	0.324	0.652	3.389	2.737
2015	1.063	0.236	0.222	0.630	1.794	1.164
2016	1.313	0.284	0.216	0.785	2.196	1.411
2017	1.814	0.565	0.311	0.849	3.875	3.026

Appendix B

Appendix for Chapter 2

R code to compute variance estimates through posterior simulation.

```
# Define grid over the study area for each year in the time
# series with grid size adjusted offset (4, 1-ha plots per
# 200x200m grid)
pred.SpTm <- expand.grid(Year=unique(PointDataHI$Year),
                         East=seq(from=255400, to=261200,
                                  by=200),
                         North=seq(from=2189000, to=2200800,
                                   by=200),
                         off.set=4)

# Restrict predictions to within study area defined by polys.map
pred.SpTmInfer <- pred.SpTm[with(pred.SpTm, inSide(polys.map,
                                                   East, North)),]

# Predict density estimates to grid
pred.SpTmInfer[, "fit"] <- predict(dsmPredModel,
                                   pred.SpTmInfer,
                                   type="response")

# coerce the structure of Year in newdata to match to
# structure of the data used in fitted model
pred.SpTmInfer$Year <- as.integer(pred.SpTmInfer$Year)

# Propagate the detection probability uncertainty
dsm.SpTm.varprop <- dsm.var.prop(dsmPredModel,
                                 pred.data=pred.SpTmInfer,
                                 off.set=1,
                                 seglen.varname="Effort",
                                 type.pred="response")
```

```
# Predict the propagated non-linear and detection probability
# uncertainty
ts.year <- unique(PointDataHI$Year) # years in time series

n.rep <- 999 # number of replicate draws

pred.SpTmInfer.b <- pred.SpTmInfer[,c(1:4)] # added post run

# add extra column for additional parameters in the refitted model
pred.SpTmInfer.b[["XX"]] <- matrix(0, nrow(pred.SpTmInfer.b),
                                   length(dsm.SpTm$ddf$par))

pred.SpTmInfer.b$Year <- as.integer(pred.SpTmInfer.b$Year)

pred.SpTmInfer.b[, "fit"] <- predict(dsm.SpTm.varprop$model,
                                     pred.SpTmInfer.b,
                                     type="response")

# form the matrix X_p above
Lp.b <- predict(dsm.SpTm.varprop$model,
                newdata=pred.SpTmInfer.b, type="lpmatrix")}

# create storage for the results
PredVar.b <- matrix(NA, nrow=30, ncol=n.rep)

# loop over the number of replicates
for (i in 1:n.rep){
  # generate new betas
  br.b.u <- rmvn(n=1, coef(dsm.SpTm.varprop$model),
                         vcov(dsm.SpTm.varprop$model,
                              unconditional=TRUE))

  # calculate the predicted values
  ex <- 40000*exp(Lp.b %*% matrix(br.b.u, ncol=1))

  # calculate the estimates per year
  for (j in 1:30){
     PredVar.b[j,i] <- sum(ex[pred.SpTmInfer$Year ==
                           ts.year[j],])/3061
     }
}
```

```
# Extract quantiles and variances
PredVar.b.out <- apply(PredVar.b, 1, quantile,
                       probs = c(0.025, 0.5, 0.975))

# print variance for each year
for (i in 1:nrow(PredVar.b)){
     print(var(as.vector(as.matrix(PredVar.b[i,]))))
}
```

Spatial position of points sampled per year. Roughly every other transect was dropped starting in 2005 in the southern half of the study area (Appendix B Fig. B.1).

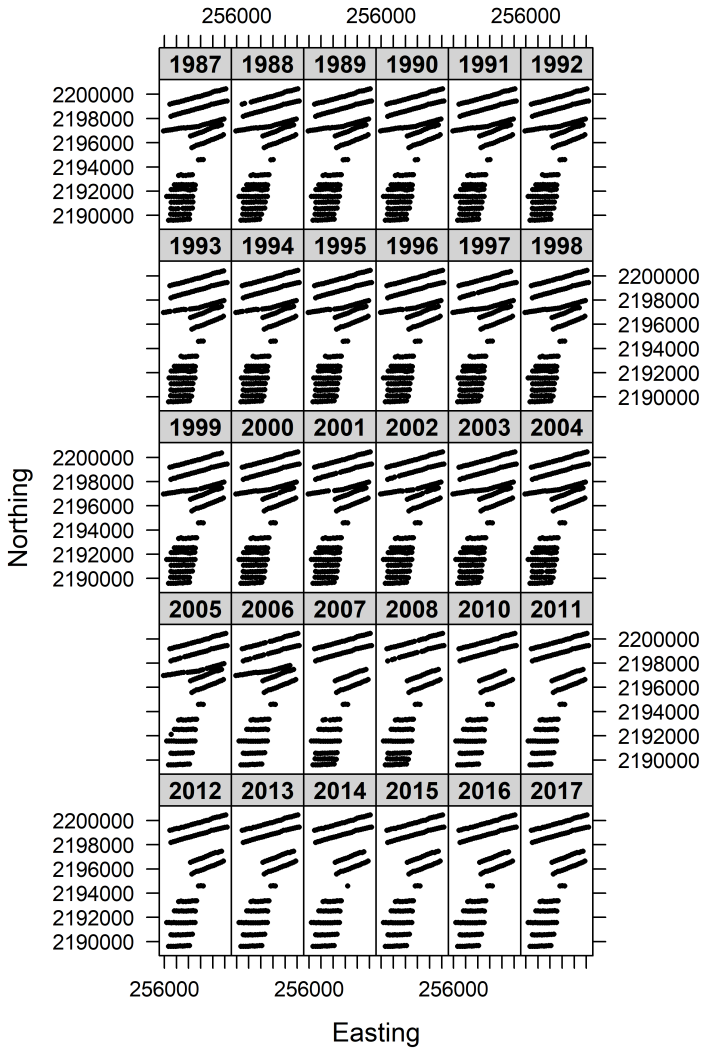

Appendix B Figure B.1: Spatial position of each point sampled by year.

Appendix C

Appendix for Chapter 3

Diagnostic plots of Poisson, Tweedie and negative binomial distributions fitted to the 2002 'ākepa data. Inspection of residual diagnostic plots revealed that there were no obvious residual problems with one or the other distributions (Appendix C Figs. C.1–C.9).

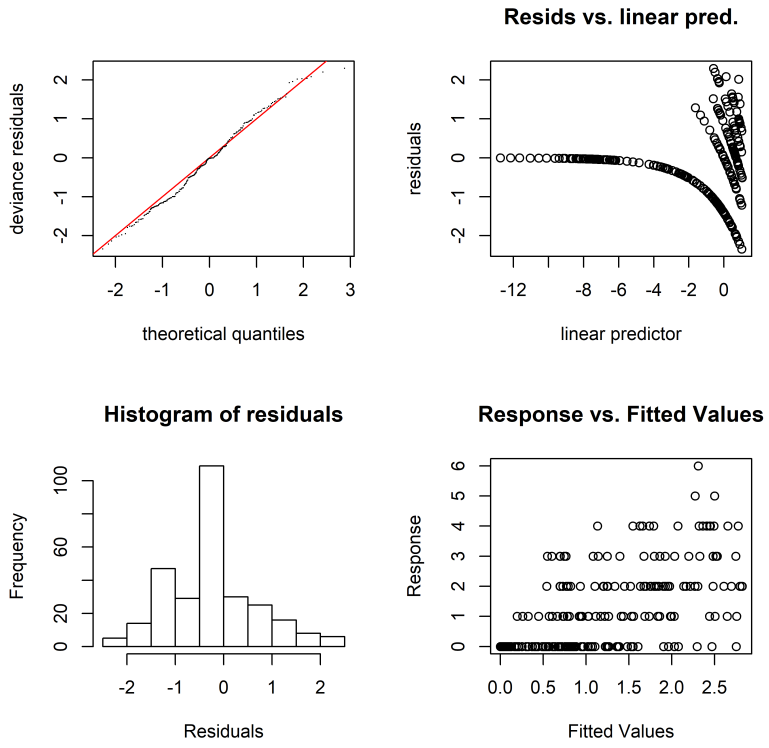

Appendix C Figure C.1: Diagnostic plots for spatial GAM with a Poisson distribution fitted to the 'ākepa count data for the 2002 survey. Deviance residuals versus theoretical quantiles (top left panel), residuals versus fitted values (top right panel), histogram of residuals (bottom left panel), and response versus fitted values (bottom right panel). The plots show acceptable behaviour for the deviance residuals and error distribution.

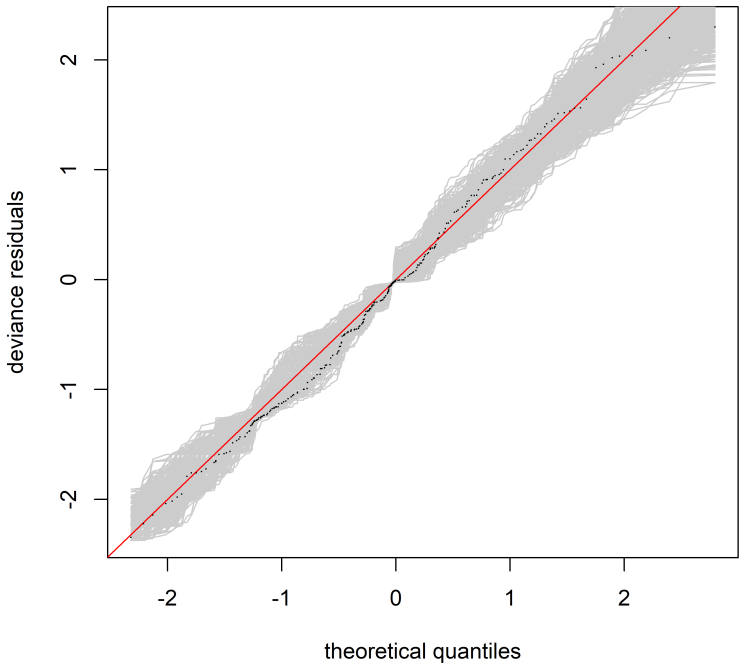

Appendix C Figure C.2: Sorted deviance residuals (black dots) for the spatial GAM versus simulated theoretical quantiles (grey lines; 1,000 replicates) fitted to the 2002 'ākepa count data for the Poisson distribution. The points seem to fall about the straight line, which provide evidence the numbers came from the theoretical distribution.

The degree of flexibility in the smoother of the DSM is controlled by the smoothing penalty. Removing the penalty would increase the model flexibility and could make the DSM estimates more similar to those of the point process approach that can produce a higher degree of spatial variation (i.e., a more wiggly surface). There are two arguments in `mgcv` that allow for the manual manipulation of the influence of the penalty: `sp` and `fx`. I formulated two models that separately used arguments setting the smoothing parameter `sp` to zero or fixing the degrees of freedom in the regression spline `fx` to true. The models are

$$\begin{aligned}\log\{\mathbb{E}(n_k)\} =& s(\texttt{Easting}_k, \texttt{Northing}_k, k = 20, bs = \text{"}tp\text{"}) \\ &+ \log(\hat{\nu}).\end{aligned}$$

For the 2002 dataset, both arguments require a term setting the basis complexity and a term defining the basis which was set to "tp" for an isotropic, penalized thin plate regression spline smooth. with the argument `sp=0` added to the `gam()` function, while `fx=TRUE` was added to the smooth term. A maximum basis complexity of 20 was selected by decreasing from 30 till the models converged. Both models produced the same smooth as evidenced by matching coefficient, EDF and fitted predicted values (not presented). Both models predicted biologically realistic densities with similar spatial locations of hot/cold spots, but variances were large resulting in biologically unrealistic abundance estimates.

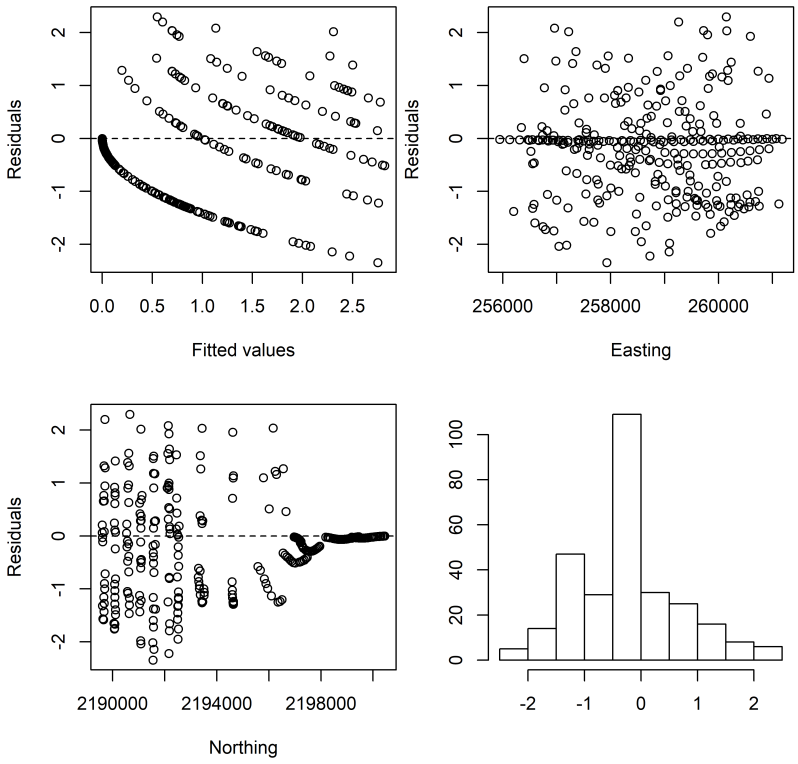

Appendix C Figure C.3: Diagnostic plots of individual parameters for spatial GAM with a Poisson distribution fitted to the 'ākepa count data for the 2002 survey. Residuals versus fitted values (top left panel), residuals versus easting (top right panel), residuals versus northing (bottom left panel), and histogram of residuals (bottom right panel). The plots show acceptable behaviour for the deviance residuals and error distribution.

Abundances were estimated using posterior simulation procedures (1,000 repetitions) of estimates fitted to a regular grid over the study area as described in Chapters 2 and 3. A density plot for abundances $< 10{,}000$ revealed a peak at slightly greater than 2,000 birds (Appendix C Fig. C.10). However, skew in the abundance estimates was 31.5 with a maximum abundance estimate of 1.268212e+75 birds which is biologically unrealistic. Forcing `mgcv` to fit maximally flexible smooths is contradictory to the penalized smoothing framework, and, as seen here, can yield biologically unrealistic estimates.

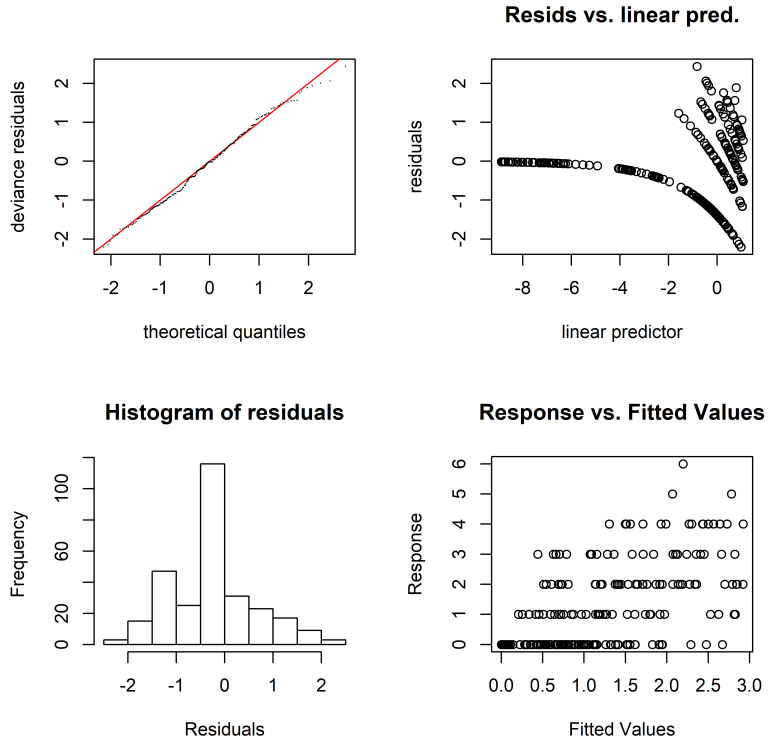

Appendix C Figure C.4: Diagnostic plots for spatial GAM with a negative binomial distribution fitted to the 'ākepa count data for the 2002 survey. Deviance residuals versus theoretical quantiles (top left panel), residuals versus fitted values (top right panel), histogram of residuals (bottom left panel), and response versus fitted values (bottom right panel). The plots show acceptable behaviour for the deviance residuals and error distribution.

Density surface maps of fitted means and SEs for both the one- and two-stage approaches for the 2002 'ākepa dataset (Appendix C Figs. C.11 and C.12).

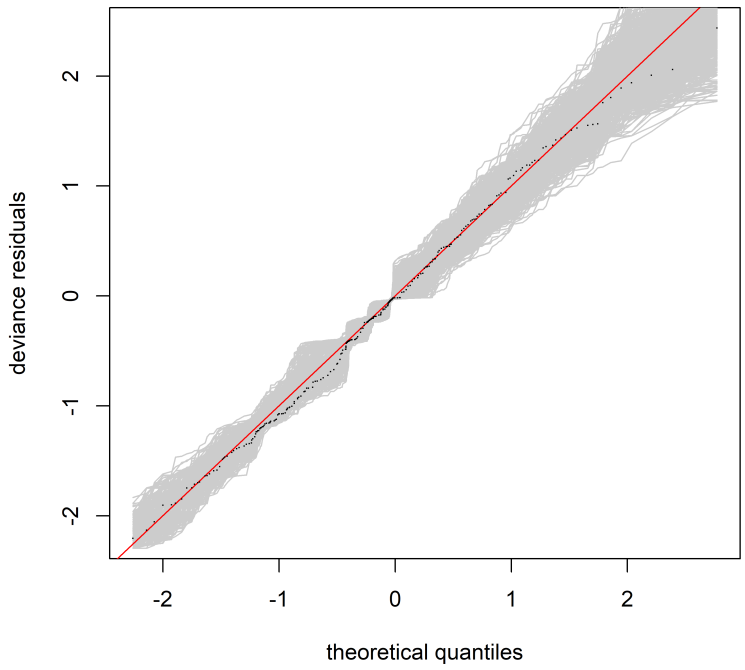

Appendix C Figure C.5: Sorted deviance residuals (black dots) for the spatial GAM versus simulated theoretical quantiles (grey lines; 1,000 replicates) fitted to the 2002 'ākepa count data for the negative binomial distribution. The points seem to fall about the straight line, which provide evidence the numbers came from the theoretical distribution.

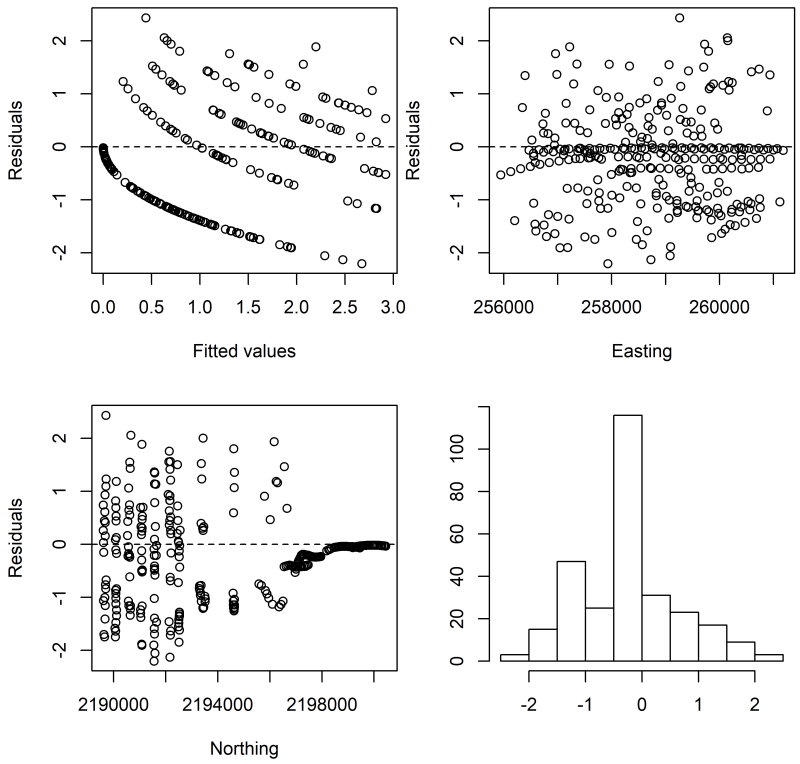

Appendix C Figure C.6: Diagnostic plots of individual parameters for spatial GAM with a negative binomial distribution fitted to the 'ākepa count data for the 2002 survey. Residuals versus fitted values (top left panel), residuals versus easting (top right panel), residuals versus northing (bottom left panel), and histogram of residuals (bottom right panel). The plots show acceptable behaviour for the deviance residuals and error distribution.

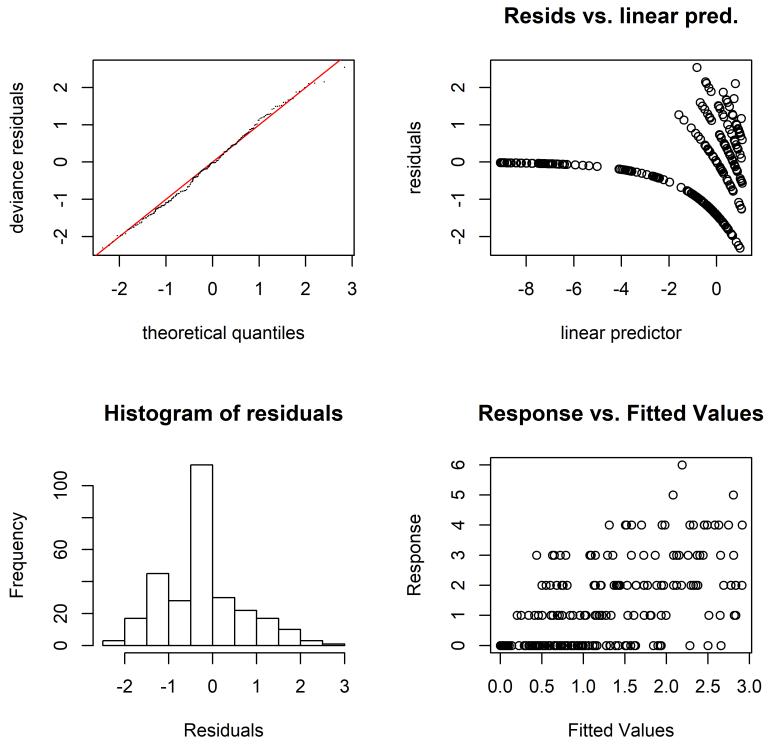

Appendix C Figure C.7: Diagnostic plots for spatial GAM with a Tweedie distribution fitted to the 'ākepa count data for the 2002 survey. Deviance residuals versus theoretical quantiles (top left panel), residuals versus fitted values (top right panel), histogram of residuals (bottom left panel), and response versus fitted values (bottom right panel). The plots show acceptable behaviour for the deviance residuals and error distribution.

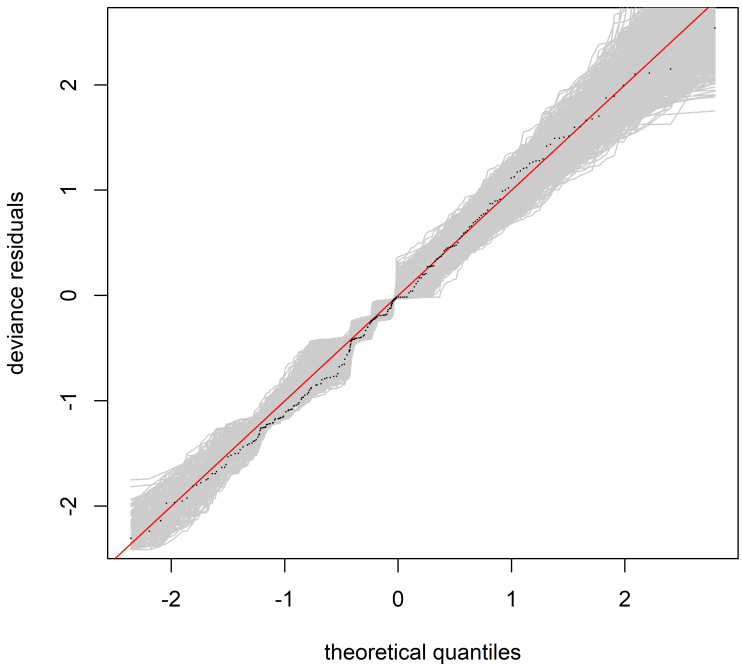

Appendix C Figure C.8: Sorted deviance residuals (black dots) for the spatial GAM versus simulated theoretical quantiles (grey lines; 1,000 replicates) fitted to the 2002 'ākepa count data for the Tweedie distribution. The points seem to fall about the straight line, which provide evidence the numbers came from the theoretical distribution.

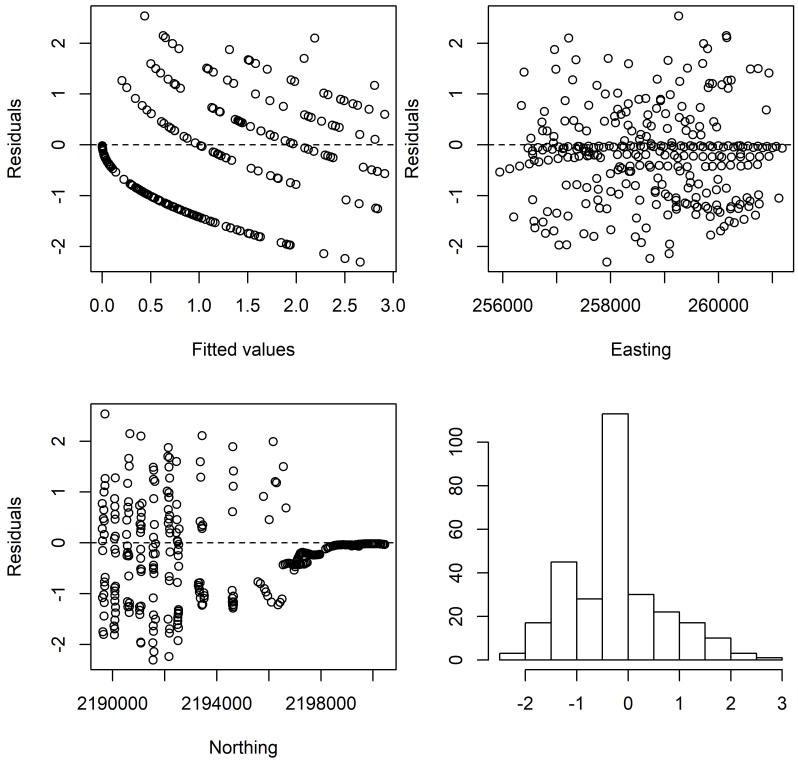

Appendix C Figure C.9: Diagnostic plots of individual parameters for spatial GAM with a Tweedie distribution fitted to the 'ākepa count data for the 2002 survey. Residuals versus fitted values (top left panel), residuals versus easting (top right panel), residuals versus northing (bottom left panel), and histogram of residuals (bottom right panel). The plots show acceptable behaviour for the deviance residuals and error distribution.

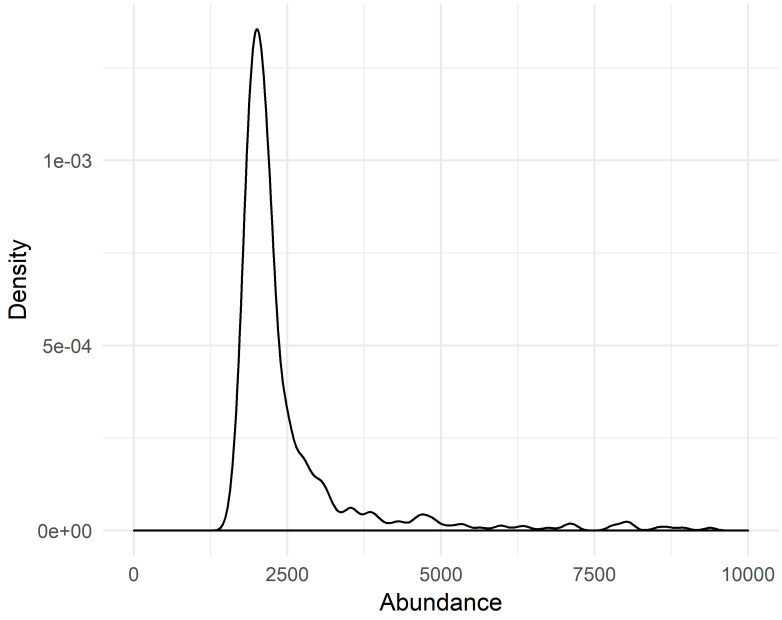

Appendix C Figure C.10: Density plot of estimated abundances < 10,000 individuals from smooth model formulated with a Poisson distribution and maximum flexibility fitted to the 'ākepa count data for the 2002 survey.

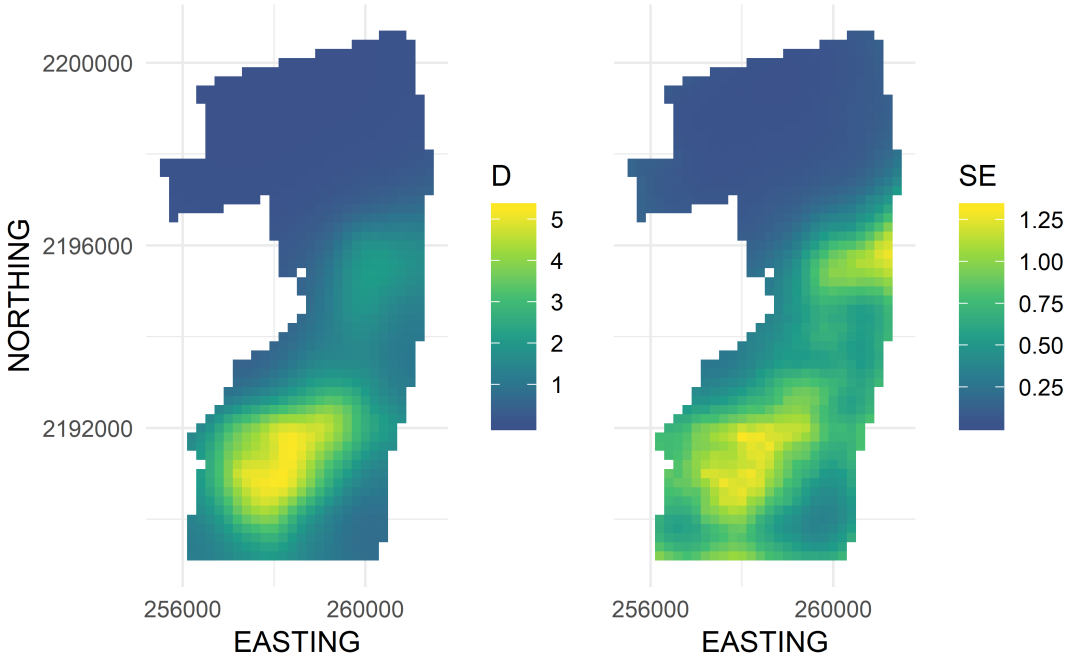

Appendix C Figure C.11: Mean and SE estimates from the point process approach.

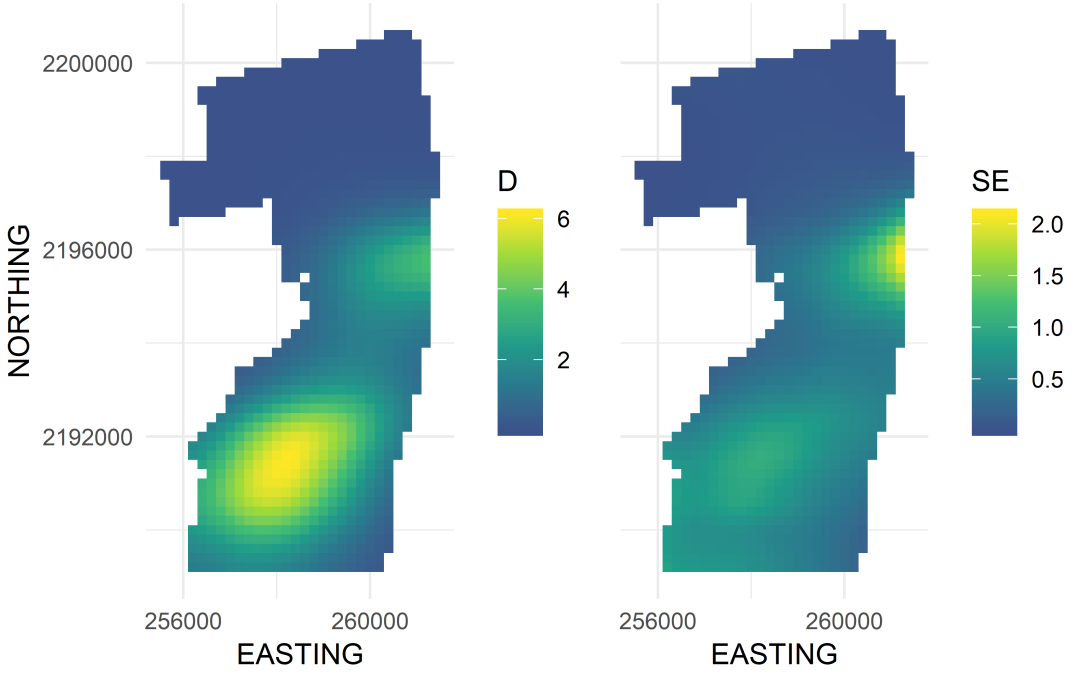

Appendix C Figure C.12: Mean and SE estimates from the DSM approach.

Appendix D

Appendix for Chapter 4

In a preliminary analysis I selected among Poisson, negative binomial and Tweedie distributions to model the response distribution using methods detailed in Chapter 2. These analyses were performed on the TPRS smooth and the selected distribution applied to both the soap and TPRS smooths. I again restricted the Tweedie distribution power parameter to $p = (1.1, 2)$ following recommendations provided in the `mgcv` package help pages and used a method of bisection to approximately identify the likelihood maximum. Sensitivity to the response distribution choice and model assumptions were checked using methods detailed in Chapter 2.

I chose the negative binomial distribution with log-link for modelling the 2002 'ākepa spatial patterns. This model provided a reasonably good fit to the residuals (Appendix D Figs. D.1 and D.2). The AIC value for the negative-binomial distributed, TPRS model was about 2 AIC units larger than the Poisson distributed model (Appendix D Table D.1). Thus, AIC alone could not be used to select between these two models (Burnham and Anderson 2002). AIC statistics clearly eliminated the Tweedie distribution (Appendix D Table D.1). QQ-plots showed the negative binomial distribution did a better job of following the identity line from the smallest through middle values than the other two models (Appendix D Fig. D.1). All three models deviated at the largest values. Therefore, I based my model selection on the QQ-plots.

Diagnostic plots for the negative binomial distribution fitted with the TPRS model formulation to the 2002 'ākepa data (Appendix D Figs. D.1 and D.2). The QQ-plot is very close to the straight line suggesting that the distribution is reasonable (Appendix D Fig. D.2, top left panel), the residuals versus linear predictor values appears to be reasonable, although strong banding patterns are obvious (Appendix D Fig. D.2, top right panel), the

Appendix D Table D.1: Model selection statistics for the Poisson, negative binomial and Tweedie distributions. Presented are the smoother log-likelihood (logLik), effective degrees of freedom (EDF), Akaike's information criterion (AIC), and Δ AIC.

Model	logLik	EDF	AIC	Δ AIC
Poisson	-275.961	20.754	593.432	0
negative binomial	-276.677	21.107	595.569	2.137
Tweedie	-293.101	20.920	628.043	34.611

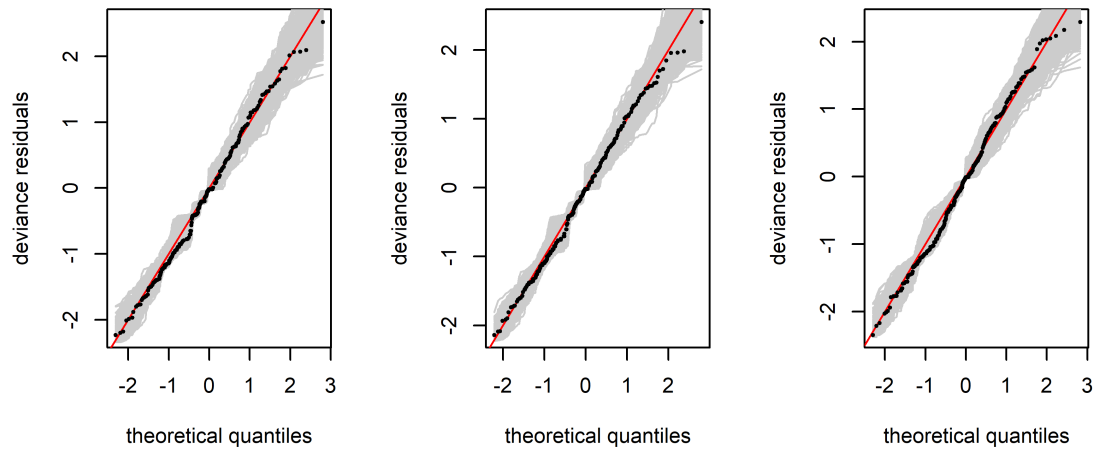

Appendix D Figure D.1: QQ plots of sorted deviance residuals (black dots) for the spatial GAM against theoretical quantiles (grey lines; 1,000 replicates) fitted with the Poisson (left panel), negative binomial (middle panel) and Tweedie (right panel) distributions to the 2002 'ākepa count data from the TPRS model.

histogram of residuals approximates normality with a spike at zero (Appendix D Fig. D.2, bottom left panel), and the diagonal pattern in the response versus fitted values reveals that the assumption of constant variance is questionable, again with a strong banding pattern (Appendix D Fig. D.2, bottom right panel). Points from the sorted deviance residuals seem to fall about the straight line and well within the simulated theoretical quantiles band of grey lines, which provides evidence the numbers came for the theoretical distribution (Appendix D Fig. D.1).

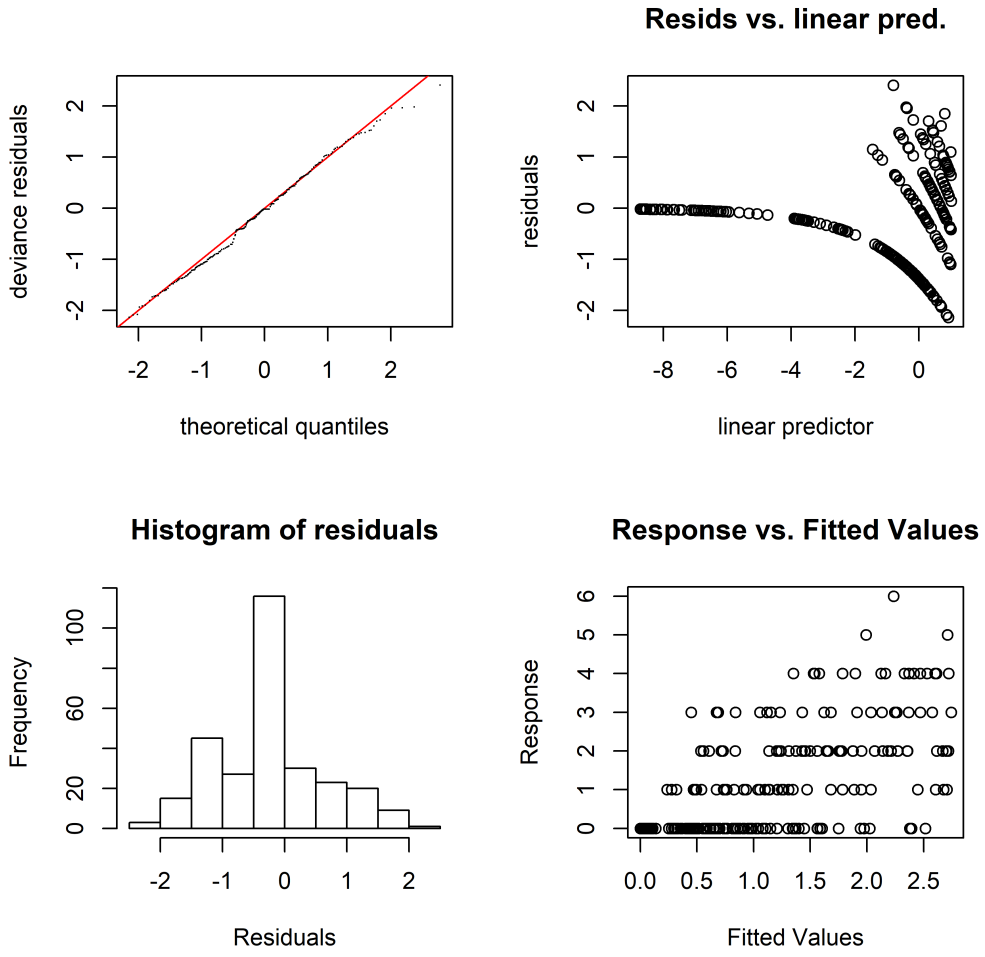

Appendix D Figure D.2: Diagnostic plots of individual parameters for spatial GAM with a negative binomial distribution fitted with the TPRS model formulation to the 'ākepa count data for the 2002 survey. Diagnostic are QQ-plot (top left panel), residuals versus linear predictor (top right panel), histogram of residuals (bottom left panel), and response versus fitted values (bottom right panel).

The EDF values were approximately zero for the TPRS model fit to the residuals (Appendix D Table D.2) and suggests that there was little un-modelled residual auto-correlation.

Diagnostic plots for the negative binomial distribution fitted with soap-film model formulation to the 2002 'ākepa data. Inspection of residual diagnostic plots appeared reasonable with acceptable behaviour for the deviance residuals and error distribution (Appendix D Figs. D.3 and D.4). The diagnostics of the soap-film residuals are very similar to those of the TPRS model where the QQ-plot is very close to the straight line suggesting that the distribution is reasonable (Appendix D Fig. D.3, top left panel), the residuals versus linear predictor values appears to be reasonable with a strong banding pattern (Appendix D Fig. D.3, top right panel), the histogram of residuals approximates normality with a spike at zero (Appendix D Fig. D.3, bottom left panel), and the diagonal pattern in the response versus fitted values draws into question the assumption of constant

Appendix D Table D.2: Effective degrees of freedom (EDF) and basis complexity (k-index) for each term in the model fitted to the residuals.

Term	EDF	k-index
`s(Easting)`	2.61e-05	0.92
`s(Northing)`	1.48e-05	1.07
`ti(Easting, Northing)`	4.01e-04	1.16

variance (Appendix D Fig. D.3, bottom right panel). Points from the sorted deviance residuals seem to fall about the straight line and well within the simulated theoretical quantiles band of grey lines, which provides evidence the numbers came for the theoretical distribution (Appendix D Fig. D.4). Effect plots for the TPRS model terms are shown in Appendix D Fig. D.5, while a description of the effects is presented in the text.

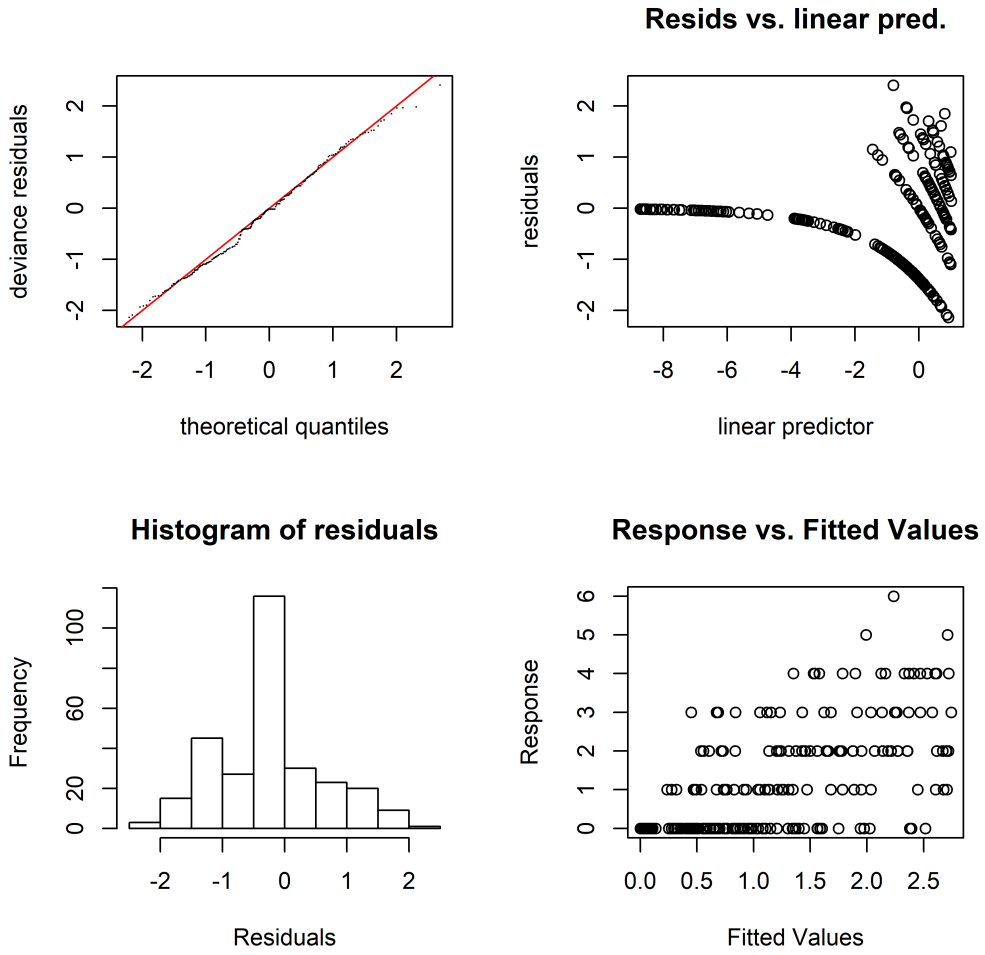

Appendix D Figure D.3: Diagnostic plots of individual parameters for spatial GAM with a negative binomial distribution fitted with soap-film model formulation to the ʻākepa count data for the 2002 survey. Diagnostic are QQ-plot (top left panel), residuals versus linear predictor (top right panel), histogram of residuals (bottom left panel), and response versus fitted values (bottom right panel).

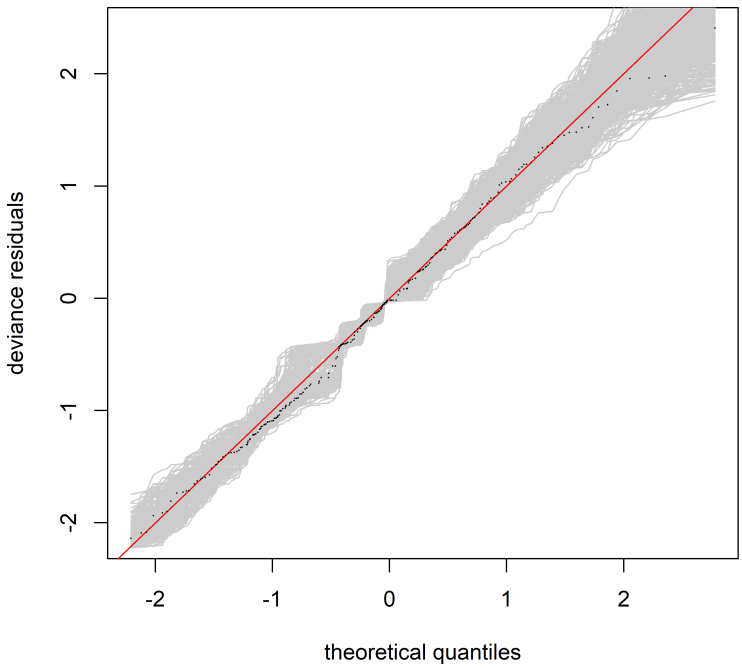

Appendix D Figure D.4: Sorted deviance residuals (black line) for the spatial GAM against theoretical quantiles (grey lines; 1,000 replicates) fitted to the 2002 'ākepa count data for the negative binomial distribution with the soap-film model formulation.

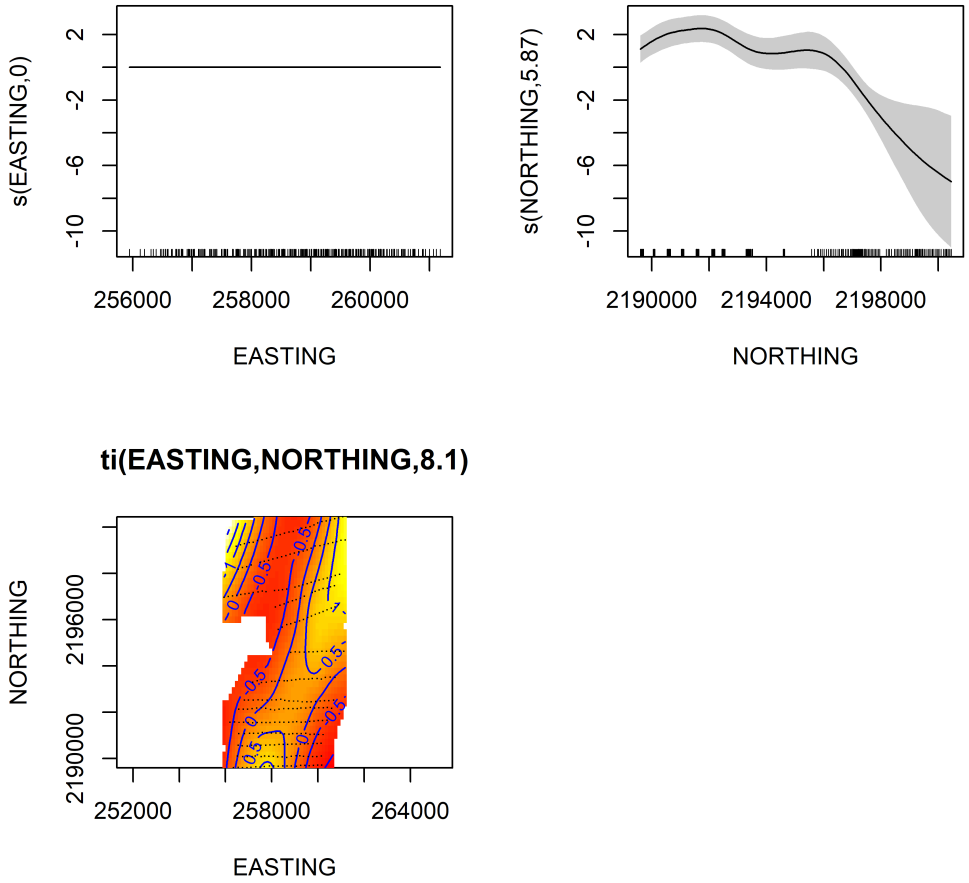

Appendix D Figure D.5: Estimated model terms for the spatial TPRS fitted to the ʻākepa count data. The distribution of the data is visualized in the rug plot along the x-axis for the 1D `Easting` and `Northing` plots, while the EDFs are presented on the y-axis labels. The grey ribbon illustrates the error bounds of plus or minus one standard error from the estimates. The locations of the points are plotted as black dots on the 2D contour plots and the EDF is provided in the plot panel title. Contours represent 0.5 unit change and are shown as blue lines. Estimates provided on the scale of the link function.

Hazard-rate detection function diagnostic plots indicated that the model adequately fit the data (Appendix D Fig. D.6).

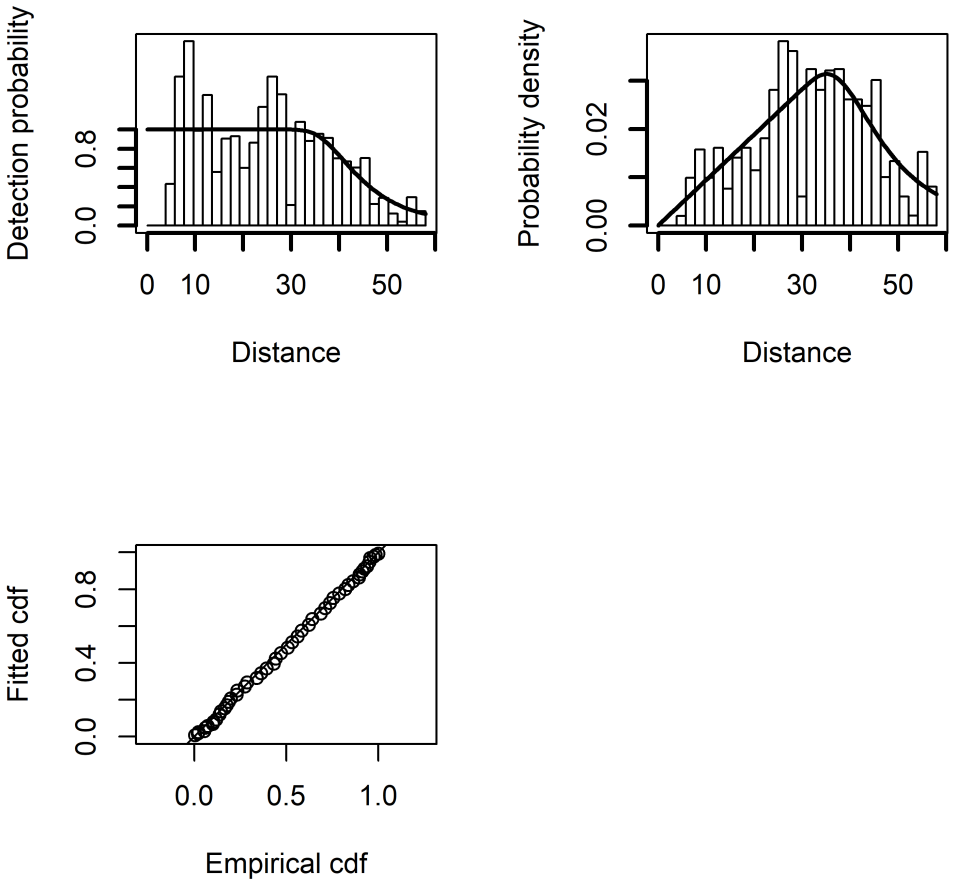

Appendix D Figure D.6: Detection function plots for the hazard-rate model without series expansion or covariates fitted to the 2002 'ākepa detections in the forest stratum. Plots represent the average detection probability (left top panel), probability density (right top panel) and QQ-plot (bottom panel). There is moderate deviation in the histogram in the probability plots and the points seem to fall about the straight line of the QQ-plot, which provides evidence the function adequately fits the data.

Histograms and boxplots of posterior distributions of 'ākepa abundances from the two smoothers (Appendix D Figs. D.7 and D.8).

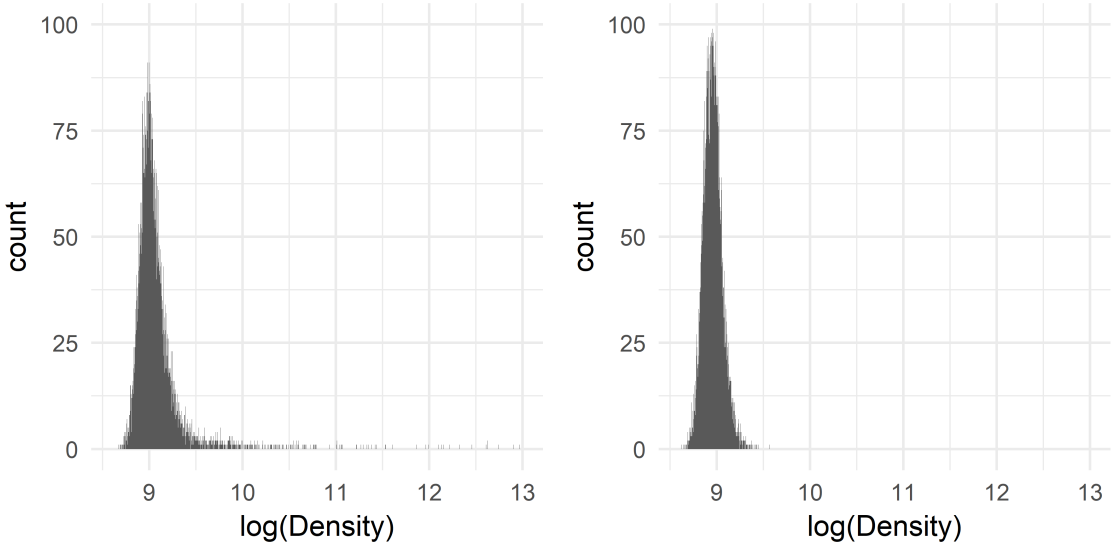

Appendix D Figure D.7: Histogram of log-abundances from the TPRS (left panel) and soap-film (right panel) posterior distributions. Maximum log-abundance from the TPRS smoother was 12.97, while the maximum log-abundance was 9.57 for the soap-film smoother.

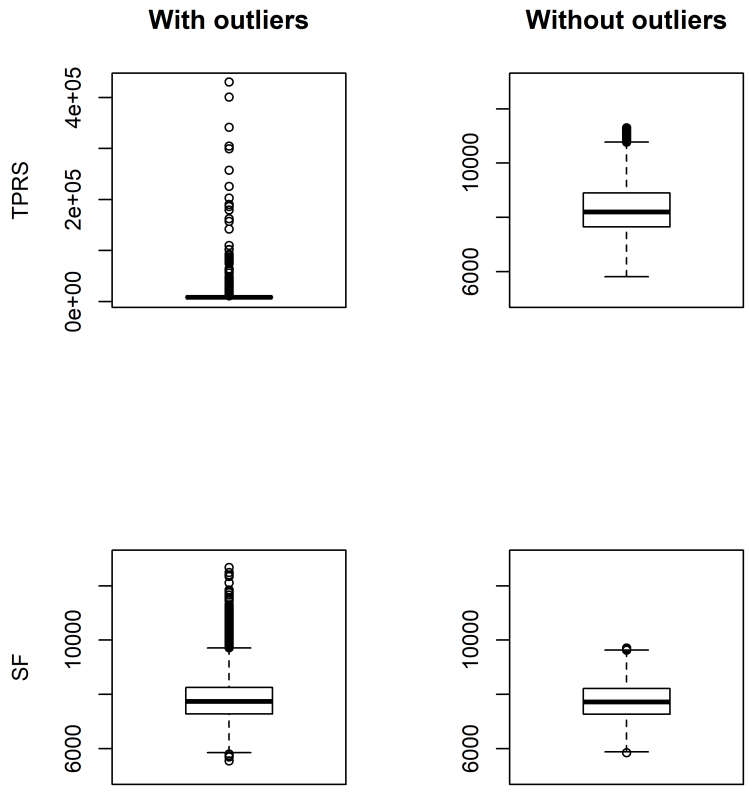

Appendix D Figure D.8: Boxplots of TPRS (top row) and soap-film (bottom row) posterior distributions of 'ākepa abundances. The TPRS distribution is highly skewed while the soap-film distribution was moderately skewed (left column); therefore, outliers were removed using the `boxplot` function (right column).

Appendix E

Appendix for Chapter 5

Computing prior values from literature-based parameters

The gamma(α, β) prior is the conjugate of the Poisson distribution parameter and the beta(α, β) distribution is the conjugate prior for binomial sampling. The prior of the survival model comes from literature with a distribution of $\phi_{1+} \sim \text{Beta}(\alpha, \beta)$. The Beta distribution parameters α and β can be algebraically calculated from the mean and variance estimates where $\mu = \frac{\alpha}{\alpha+\beta}$ and $\sigma^2 = \frac{\alpha\beta}{(\alpha+\beta)^2(\alpha+\beta+1)}$. Then starting with the mean and solving for β

$$\begin{aligned} \mu &= \frac{\alpha}{\alpha+\beta} \\ \mu(\alpha+\beta) &= \alpha \\ \mu\alpha + \mu\beta &= \alpha \\ \beta &= \frac{\alpha - \mu\alpha}{\mu} \\ &= \frac{\alpha(1-\mu)}{\mu}. \end{aligned}$$

Substituting β into the variance equation and solving for α is

$$\begin{aligned}
\sigma^2 &= \frac{\alpha\beta}{(\alpha+\beta)^2(\alpha+\beta+1)} \\
\sigma^2 &= \frac{\alpha\frac{\alpha(1-\mu)}{\mu}}{\left(\alpha+\frac{\alpha(1-\mu)}{\mu}\right)^2\left(\alpha+\frac{\alpha(1-\mu)}{\mu}+1\right)} \\
\sigma^2 &= \frac{\frac{\alpha(1-\mu)}{\mu}}{\left(\alpha+2\frac{\alpha(1-\mu)}{\mu}+\frac{1-\mu}{\mu}\frac{\alpha(1-\mu)}{\mu}\right)\left(\alpha+\frac{\alpha(1-\mu)}{\mu}+1\right)} \\
\sigma^2 &= \frac{\frac{1-\mu}{\mu}}{\left(1+2(\frac{1-\mu}{\mu})+(\frac{1-\mu}{\mu})^2\right)\left(\alpha+\frac{\alpha(1-\mu)}{\mu}+1\right)} \\
\sigma^2\frac{1}{\mu^2}\left(\alpha+\frac{\alpha(1-\mu)}{\mu}+1\right) &= \frac{1-\mu}{\mu} \\
\sigma^2\frac{1}{\mu}\left(\alpha+\frac{\alpha(1-\mu)}{\mu}+1\right) &= 1-\mu \\
\sigma^2\frac{1}{\mu}\frac{\alpha}{\mu}+\sigma^2\frac{1}{\mu} &= 1-\mu \\
\frac{\alpha}{\mu} &= \frac{1-\mu-\sigma\frac{1}{\mu}}{\sigma^2\frac{1}{\mu}} \\
\alpha &= \mu\left(\frac{\mu(1-\mu)}{\sigma^2}-1\right), \text{ and} \\
\beta &= (1-\mu)\left(\frac{\mu(1-\mu)}{\sigma^2}-1\right).
\end{aligned}$$

Using the adult survival estimates from Table 5.1 that have point estimates and variances produces inverse-variance-weighted mean = 0.803 and SE = 0.022, from which I compute $\alpha = 261.335$ and $\beta = 51.439$ for the beta distribution.

Similarly, the gamma distribution shape, α, and rate, β, parameters can be calculated algebraically from the mean and variance estimates where $\mu = \frac{\alpha}{\beta}$ and $\sigma^2 = \frac{\alpha}{\beta^2}$. Solving β in terms of μ and substituting into the variance gives

$$\begin{aligned}
\beta &= \frac{\alpha}{\mu} \\
\sigma^2 &= \frac{\alpha}{\left(\frac{\alpha}{\mu}\right)^2} \\
&= \frac{\alpha\mu^2}{\alpha^2} \\
&= \frac{\mu^2}{\alpha} \\
\alpha &= \frac{\mu^2}{\sigma^2}, \text{ and} \\
\beta &= \frac{\mu}{\sigma^2}
\end{aligned}$$

Using the recruitment mean and variance estimates shown in Table 5.1 from Guillaumet et al. (2016) I compute $\alpha = 3.471$ and $\beta = 9.806$.

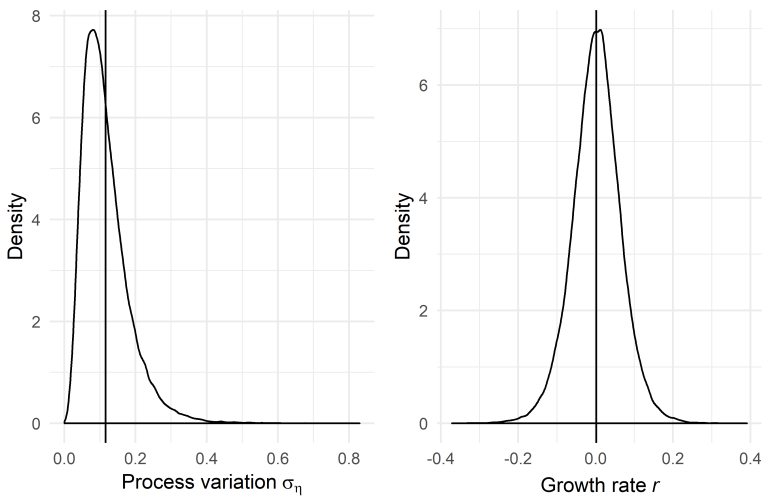

Appendix E Figure E.1: Model M1 posterior distributions for process variation σ_η and mean rates of change $\bar{r}$. Black curve is the posterior density and black vertical line the posterior mean. Priors were process variation $\sigma_\eta \sim \text{uniform}(0, 10)$ and mean growth rate $\bar{r} \sim \text{normal}(0, 10)$, respectively (not plotted).

MCMC checking and model diagnostics

For each model trace plots indicated good mixing after burn-in, convergence was achieved with $\hat{R} < 1.1$, ESS values were relatively large, and the percent overlap of prior and posterior distributions varied.

Model M1

Inspection of the trace plots indicated good mixing after burn-in and convergence was achieved ($\hat{R} < 1.001$). The data were sufficient to move the posterior from the prior for both the process variation σ_η and mean growth rate $\bar{r}$ (Appendix E Fig. E.1). The posterior overlap of the process error prior was 2.9%, while the the posterior overlap of the mean growth rate prior was 5.1%. The average ESS was 51,110 with a minimum ESS of 25,674.

Model M2

Inspection of the trace plots indicated good mixing after burn-in and convergence was achieved ($\hat{R} < 1.002$). However, the data were insufficient to move the posterior from the prior for mean adult survival $\bar{\phi}$ (overlap 95.6%) and moderately sufficient to move the posterior for mean recruitment $\bar{\lambda}$ (overlap 18.0%; Appendix E Fig. E.2). Mean ESS was 9,888 with a minimum ESS of 2,588.

Model M3

Visual inspection of of the trace plots from Model M3 indicated that there was good mixing after burn-in and convergence was achieved ($\hat{R} < 1.002$). The data were sufficient to move the posterior from the prior for mean adult survival $\bar{\phi}$ (overlap 4.7%) and moderately

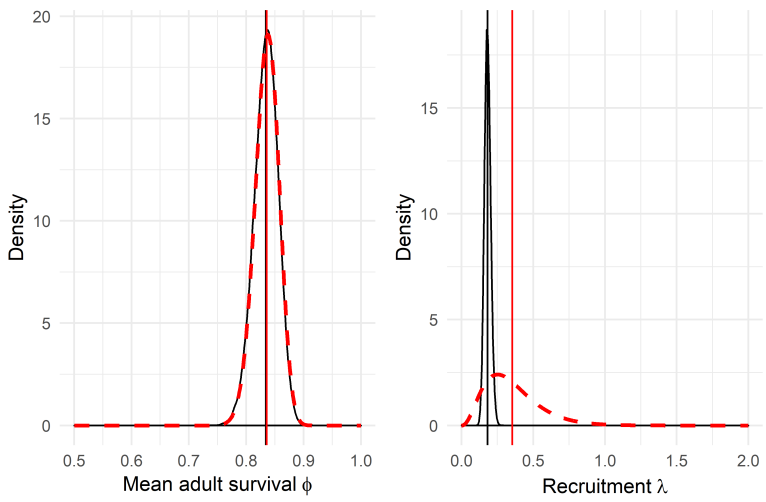

Appendix E Figure E.2: Model M2 posterior distributions for mean adult survival $\bar{\phi}$ and recruitment $\bar{\lambda}$. Black curve is the posterior density and black vertical line the posterior mean. Red dashed curve is the prior density and the vertical red line the prior mean.

sufficient to move the posterior for mean recruitment $\bar{\lambda}$ (overlap 53.3%; Appendix E Fig. E.3). Mean ESS was 12,087 with a minimum ESS of 2,929. Correlation between between the ϕ and λ parameters is shown in Appendix E Fig. E.4.

Model M4

Inspection of the trace plots indicated good mixing after burn-in and convergence was achieved ($\hat{R} < 1.002$). The data were moderately sufficient to move the posterior from the prior for mean adult survival $\bar{\phi}$ (overlap 56.7%) and sufficient to move the posterior from the mean recruitment prior $\bar{\lambda}$ (overlap 22.5%; Appendix E Fig. E.5). Mean ESS was 15,107 with a minimum ESS of 3,213. Correlation between between the ϕ and λ parameters is shown in Appendix E Fig. E.6.

Model M5

Inspection of the trace plots indicated good mixing after burn-in and convergence was achieved ($\hat{R} < 1.006$). The data were moderately sufficient to move the posterior from the prior for mean adult survival $\bar{\phi}$ (overlap 56.6%) and from the mean recruitment $\bar{\lambda}$ (overlap 19.0%; Appendix E Fig. E.7). Mean ESS was 5,129 with a minimum ESS of 720. Correlation between between the ϕ and λ parameters is shown in Appendix E Fig. E.8.

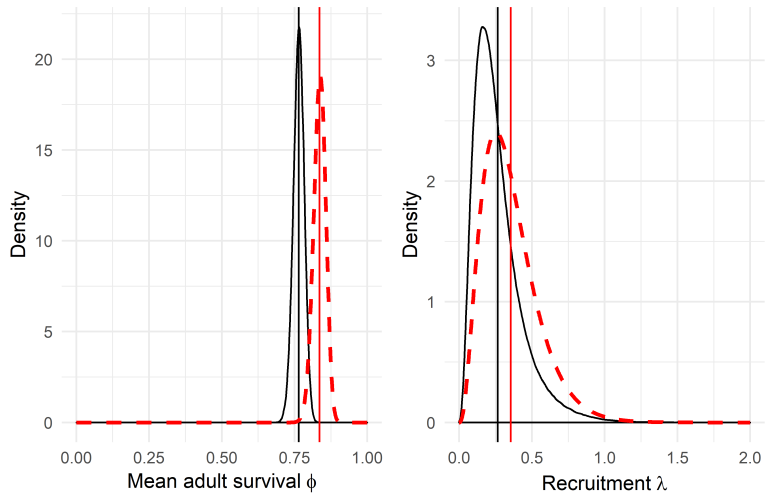

Appendix E Figure E.3: Model M3 posterior distributions for mean adult survival $\bar{\phi}$ and recruitment $\bar{\lambda}$. Black curve is the posterior density and black vertical line the posterior mean. Red dashed curve is the prior density and the vertical red line the prior mean.

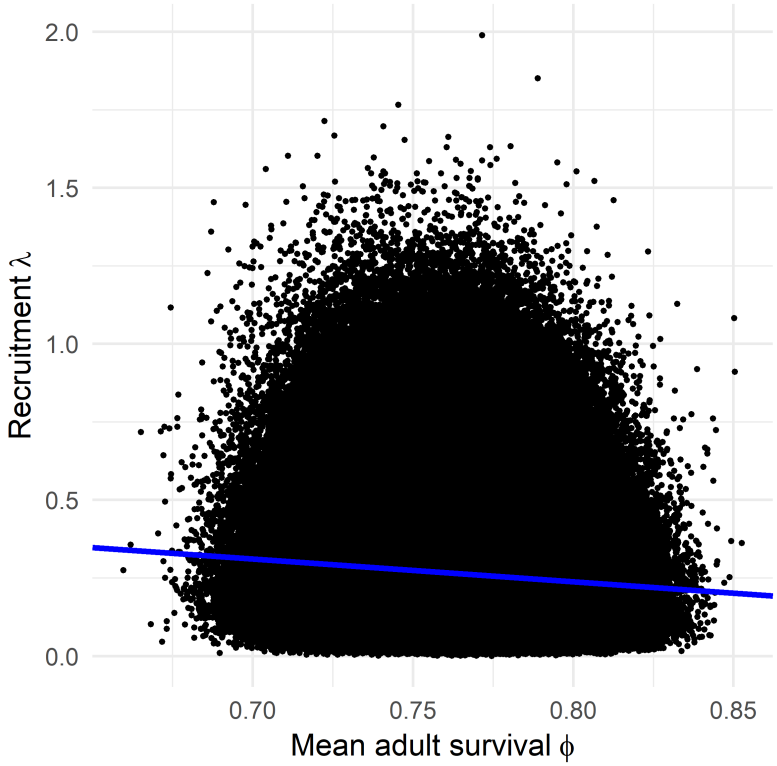

Appendix E Figure E.4: Correlation of survival $\bar{\phi}$ and recruitment $\bar{\lambda}$ are not confounded in Model M3 (correlation = 0.004). The blue line is the fitted linear regression.

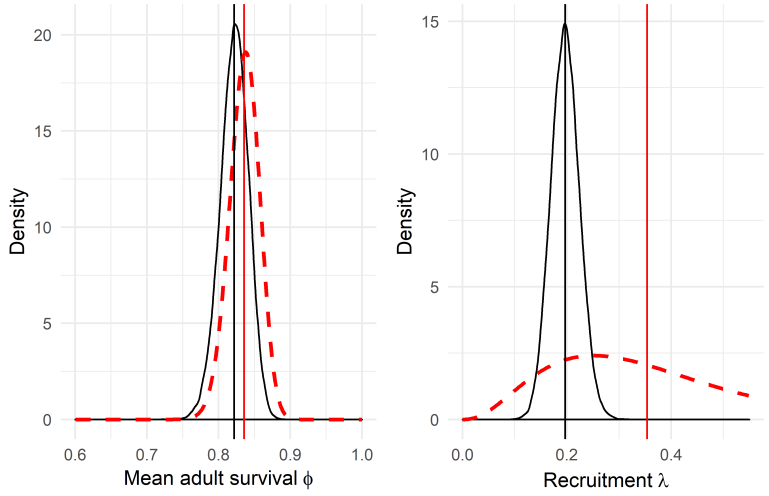

Appendix E Figure E.5: Model M4 posterior distributions for mean adult survival $\bar{\phi}$ and recruitment $\bar{\lambda}$. Black curve is the posterior density and black vertical line the posterior mean. Red dashed curve is the prior density and the vertical red line the prior mean.

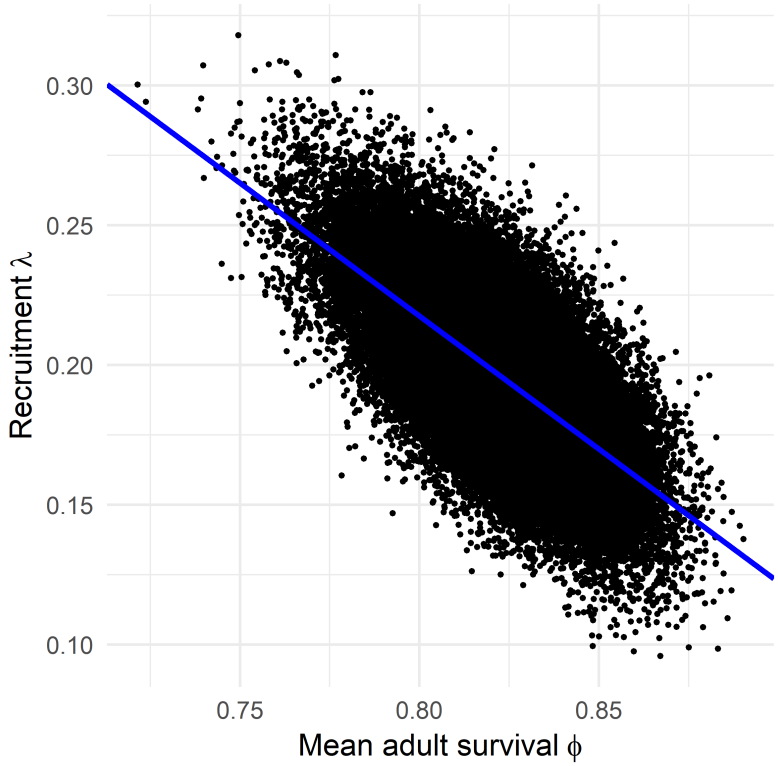

Appendix E Figure E.6: Correlation of survival $\bar{\phi}$ and recruitment $\bar{\lambda}$ are moderately confounded in Model M4 (correlation = -0.687). The blue line is the fitted linear regression.

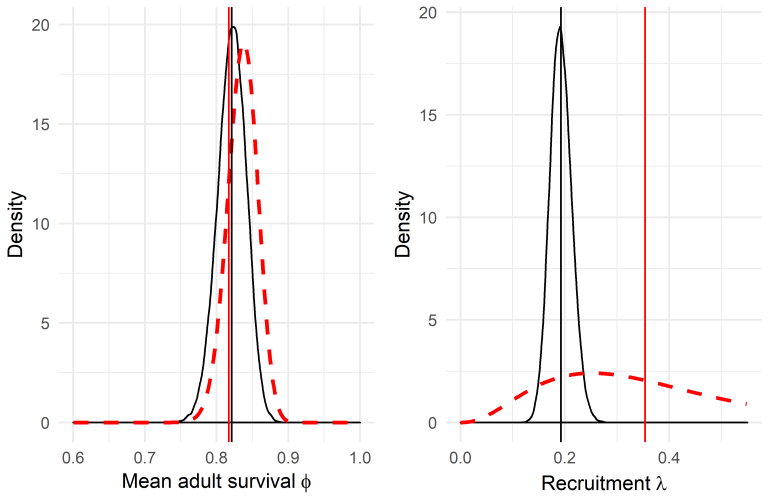

Appendix E Figure E.7: Model M5 posterior distributions for mean adult survival $\bar{\phi}$ and recruitment $\bar{\lambda}$. Black curve is the posterior density and black vertical line the posterior mean. Red dashed curve is the prior density and the vertical red line the prior mean.

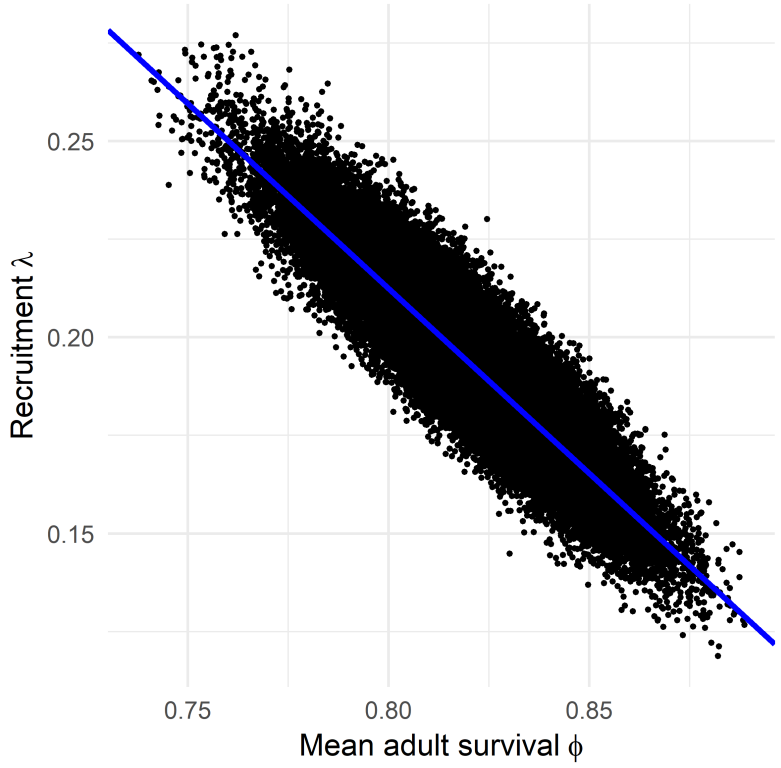

Appendix E Figure E.8: Correlation of survival $\bar{\phi}$ and recruitment $\bar{\lambda}$ is high in Model M5 (correlation = -0.908). The blue line is the fitted linear regression.

Bibliography

Abadi, F., O. Gimenez, R. Arlettaz, and M. Schaub (2010). An assessment of integrated population models: Bias, accuracy, and violation of the assumption of independence. *Ecology 91*(1), 7–14.

Ahrestani, F. S., J. F. Saracco, J. R. Sauer, K. L. Pardieck, and J. A. Royle (2017). An integrated population model for bird monitoring in North America. *Ecological Applications 27*(3), 916–924.

Allison, L. J. and A. M. McLuckie (2018). Population trends in Mojave desert tortoises (*Gopherus agassizii*). *Herpetological Conservation and Biology 13*(2), 433–452.

Amidon, F., R. J. Camp, A. P. Marshall, T. K. Pratt, L. Williams, P. Radley, and J. B. Cruz (2014). Terrestrial bird population trends on Aguiguan (Goat Island), Mariana Islands. *Bird Conservation International 24*(4), 505–517.

Anderson, D. R. (2001). The need to get the basics right in wildlife field studies. *Wildlife Society Bulletin 29*(4), 1294–1297.

Atkinson, C., K. Woods, R. J. Dusek, L. Sileo, and W. Iko (1995). Wildlife disease and conservation in Hawaii: Pathogenicity of avian malaria (*Plasmodium relictum*) in experimentally infected Iiwi (*Vestiaria coccinea*). *Parasitology 111*(S1), S59–S69.

Atkinson, C. T., R. B. Utzurrum, D. A. Lapointe, R. J. Camp, L. H. Crampton, J. T. Foster, and T. W. Giambelluca (2014). Changing climate and the altitudinal range of avian malaria in the Hawaiian Islands–an ongoing conservation crisis on the island of Kauaí. *Global Change Biology 20*(8), 2426–2436.

Auger-Méthé, M., C. Field, C. M. Albertsen, A. E. Derocher, M. A. Lewis, I. D. Jonsen, and J. M. Flemming (2016). State-space models' dirty little secrets: Even simple linear Gaussian models can have estimation problems. *Scientific reports 6*(1), 1–10.

Bachl, F. E., F. Lindgren, D. L. Borchers, and J. B. Illian (2019). inlabru: An R package for Bayesian spatial modelling from ecological survey data. *Methods in Ecology and Evolution 10*(6), 760–766.

Banko, W. E. and P. C. Banko (2009). Historic decline and extinction. In T. K. Pratt, C. T. Atkinson, P. C. Banko, J. D. Jacobi, and B. L. Woodworth (Eds.), *Conservation Biology of Hawaiian Forest Birds: Implications for Island Avifauna*, Chapter 2, pp. 25–58. New Haven, CT, USA: Yale University Press.

Becker, R. A., J. M. Chambers, and A. R. Wilks (1988). *The New S Language*. Wadsworth & Brooks/Cole.

Besbeas, P., R. S. Borysiewicz, and B. J. Morgan (2009). Completing the ecological jigsaw. In D. L. Thomson, E. G. Cooch, and M. J. Conroy (Eds.), *Modeling Demographic Processes in Marked Populations*, pp. 513–539. New York, NY, USA: Springer.

Besbeas, P., S. N. Freeman, B. J. Morgan, and E. A. Catchpole (2002). Integrating mark–recapture–recovery and census data to estimate animal abundance and demographic parameters. *Biometrics 58*(3), 540–547.

Besbeas, P., J.-D. Lebreton, and B. J. Morgan (2003). The efficient integration of abundance and demographic data. *Journal of the Royal Statistical Society: Series C (Applied Statistics) 52*(1), 95–102.

Best, L. (1981). Seasonal changes in detection of individual bird species. *Studies in Avian Biology 6*, 252–261.

BirdLife International (2016). *Loxops coccineus*. The IUCN Red List of Threatened Species 2016:e.T103823991A94685811. http://dx.doi.org/10.2305/IUCN.UK.2016-3.RLTS.T103823991A94685811.en.

Blangiardo, M. and M. Cameletti (2015). *Spatial and Spatio-Temporal Bayesian Models with R-INLA*. New York, NY, USA: John Wiley & Sons.

Borchers, D. L., S. T. Buckland, W. Stephens, W. Zucchini, et al. (2002). *Estimating Animal Abundance: Closed Populations*, Volume 13. New York, NY, USA: Springer Science & Business Media.

Boyce, M. S., C. V. Haridas, C. T. Lee, N. S. D. W. Group, et al. (2006). Demography in an increasingly variable world. *Trends in Ecology & Evolution 21*(3), 141–148.

Bravington, M. V., D. L. Miller, and S. L. Hedley (2018). Reliable variance propagation for spatial density surface models. *arXiv preprint arXiv:1807.07996*.

Brinck, K. W., R. J. Camp, P. M. Gorresen, D. L. Leonard, H. L. Mounce, K. J. Iknayan, and E. H. Paxton (2012). 2011 kiwikiu (Maui parrotbill) and Maui 'alauahio abundance estimates and the effect of sampling effort on power to detect a trend. Technical Report HCSU-035, University of Hawai'i at Hilo, Hawai'i Cooperative Studies and Unit.

Buckland, S., K. Newman, L. Thomas, and N. Koesters (2004). State-space models for the dynamics of wild animal populations. *Ecological Modelling 171*(1-2), 157–175.

Buckland, S. T. (2006). Point-transect surveys for songbirds: Robust methodologies. *The Auk 123*(2), 345–357.

Buckland, S. T., D. R. Anderson, K. P. Burnham, J. L. Laake, D. L. Borchers, and L. Thomas (2001). *Introduction to Distance Sampling: Estimating Abundance of Biological Populations*. Oxford, UK: Oxford University Press.

Buckland, S. T., D. R. Anderson, K. P. Burnham, J. L. Laake, D. L. Borchers, and L. Thomas (2004). *Advanced Distance Sampling*. Oxford, UK: Oxford University Press.

Buckland, S. T., C. S. Oedekoven, and D. L. Borchers (2016). Model-based distance sampling. *Journal of Agricultural, Biological, and Environmental Statistics 21*(1), 58–75.

Buckland, S. T., E. A. Rexstad, T. A. Marques, and C. S. Oedekoven (2015). *Distance Sampling: Methods and Applications*. London, UK: Springer.

Burnham, K. P. and D. R. Anderson (2002). *Model Selection and Multimodel Inference: A Practical Information-Theoretic Approach, 2nd ed.* New York, NY, USA: Springer-Verlag.

Camp, R. J. (2007). Measurement errors in Hawaiian forest bird surveys and their effect on density estimation. Technical Report HCSU-005, Hawai'i Cooperative Studies Unit, University of Hawai'i at Hilo.

Camp, R. J. (2019). Hakalau Forest National Wildlife Refuge Hawaii Akepa point-transect surveys, 1987-2017: U.S. Geological Survey data release. http://doi.org/10.5066/P98IO297.

Camp, R. J. (2020). Hakalau Forest National Wildlife Refuge, Hawaii Akepa point-transect survey, 2002: U.S. Geological Survey data release. https://doi.org/10.5066/P9Q9UXMZ.

Camp, R. J., K. W. Brinck, P. M. Gorresen, and E. H. Paxton (2016). Evaluating abundance and trends in a Hawaiian avian community using state-space analysis. *Bird Conservation International 26*(2), 225–242.

Camp, R. J. and A. S. Genz (2017). Hawai'i forest bird monitoring database: Database dictionary. Technical Report HCSU-039, Hawai'i Cooperative Studies Unit, University of Hawai'i at Hilo.

Camp, R. J., P. M. Gorresen, T. K. Pratt, and B. L. Woodworth (2009). Population trends of native Hawaiian forest birds, 1976-2008. Technical Report HCSU-012, Hawai'i Cooperative Studies Unit, University of Hawai'i at Hilo.

Camp, R. J., D. L. Miller, L. Thomas, S. T. Buckland, and S. J. Kendall (2020). Using density surface models to estimate spatio-temporal changes in population densities and trend. *Ecography 43*(7), 1079–1089.

Camp, R. J., T. K. Pratt, C. Bailey, and D. Hu (2011). Landbirds vital sign monitoring protocol-Pacific Island Network. Technical report, Natural Resources Report NPS/PACN/NRR—2011/402.

Camp, R. J., T. K. Pratt, P. M. Gorresen, J. J. Jeffrey, and B. L. Woodworth (2010). Population trends of forest birds at Hakalau Forest National Wildlife Refuge, Hawai'i. *The Condor 112*(2), 196–212.

Camp, R. J., T. K. Pratt, P. M. Gorresen, B. L. Woodworth, and J. J. Jeffrey (2014). Hawaiian forest bird trends: Using log-linear models to assess long-term trends is supported by model diagnostics and assumptions (reply to Freed and Cann 2013). *The Condor 116*(1), 97–101.

Camp, R. J., M. H. Reynolds, P. M. Gorresen, T. K. Pratt, and B. L. Woodworth (2009). Monitoring Hawaiian forest birds. In T. K. Pratt, C. T. Atkinson, P. C. Banko, J. D. Jacobi, and B. L. Woodworth (Eds.), *Conservation Biology of Hawaiian Forest Birds: Implications for Island Avifauna*, Chapter 4, pp. 83–107. New Haven, CT, USA: Yale University Press.

Carlin, B. P. and A. E. Gelfand (1990). Approaches for empirical Bayes confidence intervals. *Journal of the American Statistical Association 85*(409), 105–114.

Casella, G. (1985). An introduction to empirical Bayes data analysis. *The American Statistician 39*(2), 83–87.

Chandler, R. B., K. Engebretsen, M. J. Cherry, E. P. Garrison, and K. V. Miller (2018). Estimating recruitment from capture–recapture data by modelling spatio-temporal variation in birth and age-specific survival rates. *Methods in Ecology and Evolution 9*(10), 2115–2130.

Chen, Y. R. and P.-S. Chu (2014). Trends in precipitation extremes and return levels in the Hawaiian Islands under a changing climate. *International Journal of Climatology 34*(15), 3913–3925.

Chesser, R. T., R. C. Banks, C. Cicero, J. L. Dunn, A. W. Kratter, I. J. Lovette, P. C. Rasmussen, J. V. Remsen Jr, D. F. Stotz, B. M. Winger, and K. Winker (2018). Checklist of North American Birds (online). Website http://checklist.aou.org/taxa; Accessed 3 December 2018. American Ornithological Society.

Chu, P.-S. and H. Chen (2005). Interannual and interdecadal rainfall variations in the Hawaiian Islands. *Journal of Climate 18*(22), 4796–4813.

Conn, P. B., D. S. Johnson, J. M. V. Hoef, M. B. Hooten, J. M. London, and P. L. Boveng (2015). Using spatiotemporal statistical models to estimate animal abundance and infer ecological dynamics from survey counts. *Ecological Monographs 85*(2), 235–252.

Cox, W. A., F. R. Thompson III, A. S. Cox, and J. Faaborg (2014). Post-fledging survival in passerine birds and the value of post-fledging studies to conservation. *The Journal of Wildlife Management 78*(2), 183–193.

Cressie, N. and C. K. Wikle (2015). *Statistics for Spatio-Temporal Data*. New York, NY, USA: John Wiley & Sons.

Cummins, G., S. Kendall, and E. Paxton (2014). Productivity of forest birds at Hakalau Forest NWR. Technical Report HCSU-056, Hawai'i Cooperative Studies Unit, University of Hawai'i at Hilo.

Diefenbach, D. R., D. W. Brauning, and J. A. Mattice (2003). Variability in grassland bird counts related to observer differences and species detection rates. *The Auk 120*(4), 1168–1179.

Diggle, P. J. (2014). *Statistical Analysis of Spatial and Spatio-Temporal Point Patterns*. Boca Raton, FL, USA: Chapman and Hall/CRC.

Dobson, F. S. (2012). Lifestyles and phylogeny explain bird life histories. *Proceedings of the National Academy of Sciences 109*(27), 10747–10748.

Donald, P. F. (2007). Adult sex ratios in wild bird populations. *Ibis 149*(4), 671–692.

Fewster, R. M., S. T. Buckland, K. P. Burnham, D. L. Borchers, P. E. Jupp, J. L. Laake, and L. Thomas (2009). Estimating the encounter rate variance in distance sampling. *Biometrics 65*(1), 225–236.

Fewster, R. M., S. T. Buckland, G. M. Siriwardena, S. R. Baillie, and J. D. Wilson (2000). Analysis of population trends for farmland birds using generalized additive models. *Ecology 81*(7), 1970–1984.

Fortini, L. B., A. E. Vorsino, F. A. Amidon, E. H. Paxton, and J. D. Jacobi (2015). Large-scale range collapse of Hawaiian forest birds under climate change and the need 21st century conservation options. *PloS One 10*(10), e0140389.

Foster, S. D. and M. V. Bravington (2012). A Poisson–Gamma model for analysis of ecological non-negative continuous data. *Environmental and Ecological Statistics 20*(4), 533–552.

Foster, S. D., G. R. Hosack, E. Lawrence, R. Przeslawski, P. Hedge, M. J. Caley, N. S. Barrett, A. Williams, J. Li, T. Lynch, et al. (2017). Spatially balanced designs that incorporate legacy sites. *Methods in Ecology and Evolution 8*(11), 1433–1442.

Freed, L. A. (1988). Demographic and behavioral observations of the Hawai‘i ‘Akepa on Mauna Loa. *Elepaio 48*(5), 37–39.

Freed, L. A. and R. L. Cann (2009). Negative effects of an introduced bird species on growth and survival in a native bird community. *Current Biology 19*(20), 1736–1740.

Freed, L. A. and R. L. Cann (2010). Misleading trend analysis and decline of Hawaiian forest birds. *The Condor 112*(2), 213–221.

Freed, L. A., R. L. Cann, and G. R. Bodner (2008). Incipient extinction of a major population of the Hawaii akepa owing to introduced species. *Evolutionary Ecology Research 10*(7), 931–965.

Gelman, A., J. B. Carlin, H. S. Stern, D. B. Dunson, A. Vehtari, and D. B. Rubin (2013). *Bayesian Data Analysis*. Boca Raton, FL, USA: CRC Press.

Genz, A. S., K. W. Brinck, R. J. Camp, and P. C. Banko (2018). 2017-2018 palila abundance estimates and trend. Technical Report HCSU-086, Hawai'i Cooperative Studies Unit, University of Hawai'i at Hilo.

Gibbs, J. P. (2000). Monitoring populations. In M. C. Pearl (Ed.), *Research Techniques in Animal Ecology*, Chapter 7, pp. 213–252. New York, NY, USA: Columbia University Press.

Gill, F. and D. Donsker (2019). IOC World bird list (v 9.1). Website http://www.worldbirdnames.org; Accessed 1 November 2019. International Ornithological Congress.

Gimenez, O., B. J. Morgan, and S. P. Brooks (2009). Weak identifiability in models for mark-recapture-recovery data. In *Modeling Demographic Processes in Marked Populations*, pp. 1055–1067. New York, NY, USA: Springer.

Glennie, R., S. T. Buckland, R. Langrock, T. Gerrodette, L. Ballance, S. Chivers, M. Scott, and W. Perrin (2020). Incorporating animal movement into distance sampling. *Journal of the American Statistical Association*. In press.

Gorresen, P. M., K. W. Brinck, R. J. Camp, C. Farmer, S. M. Plentovich, and P. C. Banko (2016). State-space modeling of population sizes and trends in Nihoa Finch and Millerbird. *The Condor: Ornithological Applications 118*(3), 542–557.

Gorresen, P. M., R. J. Camp, M. H. Reynolds, B. L. Woodworth, and T. K. Pratt (2009). Status and trends of native Hawaiian songbirds. In T. K. Pratt, C. T. Atkinson, P. C. Banko, J. D. Jacobi, and B. L. Woodworth (Eds.), *Conservation Biology of Hawaiian Forest Birds: Implications for Island Avifauna*, Chapter 5, pp. 108–136. New Haven, CT, USA: Yale University Press.

Guillaumet, A., B. L. Woodworth, R. J. Camp, and E. H. Paxton (2016). Comparative demographics of a Hawaiian forest bird community. *Journal of Avian Biology 47*(2), 185–196.

Hart, P. (2001). Demographic comparisons between high and low density populations of Hawaii Akepa. *Studies in Avian Biology 22*, 185–193.

Hart, P. J., T. Ibanez, S. Uehana, and J. Pang-Ching (2020). Forest regeneration following ungulate removal in a montane Hawaiian wet forest. *Restoration Ecology*. In press.

Hastie, T. and R. Tibshirani (1986). Generalized additive models (with discussion). *Statistical Science 1*(3), 297–310.

Hastie, T. J. and R. J. Tibshiani (1990). *Generalized Additive Models*. Chapman and Hall/CRC.

Hedley, S. L. (2000). *Modelling heterogeneity in cetacean surveys*. Ph. D. thesis, University of St Andrews.

Hedley, S. L. and S. T. Buckland (2004). Spatial models for line transect sampling. *Journal of Agricultural, Biological, and Environmental Statistics 9*(2), 181.

Hess, S. C. (2016). A tour de force by Hawaii's invasive mammals: Establishment, takeover, and ecosystem restoration through eradication. *Mammal Study 41*(2), 47–60.

Hess, S. C., J. J. Jeffrey, D. L. Ball, and L. Babich (2006). Efficacy of feral pig removals at Hakalau Forest National Wildlife Refuge, Hawaii. *Transactions of the Western Section of the Wildlife Society 42*, 53–67.

Hess, S. C., J. J. Jeffrey, L. W. Pratt, and D. L. Ball (2010). Effects of ungulate management on vegetation at Hakalau Forest National Wildlife Refuge, Hawaii Island. *Pacific Conservation Biology 16*(2), 144–150.

Hobbs, R. J., E. Higgs, and J. A. Harris (2009). Novel ecosystems: Implications for conservation and restoration. *Trends in ecology & evolution 24*(11), 599–605.

Hogg, D. W. and D. Foreman-Mackey (2018). Data analysis recipes: Using Markov Chain Monte Carlo. *The Astrophysical Journal Supplement Series 236*(1), 1–18.

Högmander, H. (1991). A random field approach to transect counts of wildlife populations. *Biometrical Journal 33*(8), 1013–1023.

Hostetter, N. J., B. Gardner, T. S. Sillett, K. H. Pollock, and T. R. Simons (2019). An integrated model decomposing the components of detection probability and abundance in unmarked populations. *Ecosphere 10*(3), e02586.

Hutto, R. L. (2016). Should scientists be required to use a model-based solution to adjust for possible distance-based detectability bias? *Ecological Applications 26*(5), 1287–1294.

Illian, J., A. Penttinen, H. Stoyan, and D. Stoyan (2008). *Statistical Analysis and Modelling of Spatial Point Patterns*, Volume 70. Chichester, UK: John Wiley & Sons.

IUCN (2018). The IUCN Red List of Threatened Species, version 2018-2. Website http://www.iucnredlist.org; Accessed 3 December 2018. International Union for Conservation of Nature.

Jacobi, J. D. (2018). Vegetation map for the Hakalau Forest Unit of the Big Island National Wildlife Refuge Complex on the Island of Hawai'i. Technical Report HCSU-084, Hawai'i Cooperative Studies Unit, University of Hawai'i at Hilo.

Jennings, M. D., D. Faber-Langendoen, O. L. Loucks, R. K. Peet, and D. Roberts (2009). Standards for associations and alliances of the US National Vegetation Classification. *Ecological Monographs 79*(2), 173–199.

Johnson, D. S., J. L. Laake, and J. M. Ver Hoef (2010). A model-based approach for making ecological inference from distance sampling data. *Biometrics 66*(1), 310–318.

Johnson, L., R. J. Camp, K. W. Brinck, and P. C. Banko (2006). Long-term population monitoring: Lessons learned from an endangered passerine in Hawai'i. *Wildlife Society Bulletin 34*(4), 1055–1063.

Judge, S. W., R. J. Camp, P. J. Hart, and S. T. Kichman (2018). Population estimates of the Endangered Hawai'i 'Ākepa (*Loxops coccineus*) in different habitats on windward Mauna Loa. *Journal of Field Ornithology 89*(1), 11–21.

Judge, S. W., R. J. Camp, V. Vaivai, and P. J. Hart (2013). Pacific Island landbird monitoring annual report, National Park of American Samoa, Ta ʻu and Tutuila units, 2011. Technical Report Natural Resource Technical Report NPS/PACN/NRTR—2013/666, National Park Service, Fort Collins, CO.

Judge, S. W., R. J. Camp, C. C. Warren, L. K. Berthold, H. L. Mounce, P. J. Hart, and R. J. Monello (2019). Pacific Island landbird monitoring annual report, Haleakalā National Park and East Maui Island, 2017. Technical Report Natural Resouces Report NPS/PACN/NRR—2019/1949, National Park Service, Fort Collins, CO.

Juvik, S. P. and J. O. Juvik (1998). *Atlas of Hawai'i, Third Edition*. Honolulu, HI, USA: University of Hawai'i Press.

Kellner, K. (2019). A wrapper around 'rjags' to streamline 'jags' analyses. https://CRAN.R-project.org/package=jagsUI. R package version 2.14.0.

King, R., B. Morgan, O. Gimenez, and S. Brooks (2009). *Bayesian Analysis for Population Ecology*. Boca Raton, FL, USA: Chapman and Hall/CRC.

Knape, J. (2016). Decomposing trends in Swedish bird populations using generalized additive mixed models. *Journal of Applied Ecology 53*(6), 1852–1861.

Knape, J., P. Besbeas, and P. de Valpine (2013). Using uncertainty estimates in analyses of population time series. *Ecology 94*(9), 2097–2107.

Koons, D. N., D. T. Iles, M. Schaub, and H. Caswell (2016). A life-history perspective on the demographic drivers of structured population dynamics in changing environments. *Ecology Letters 19*(9), 1023–1031.

Lahiri, S. N. (2003). *Resampling Methods for Dependent Data*. New York, NY, USA: Springer Science & Business Media.

Lee, C. H., S. Cook, J. S. Lee, and B. Han (2016). Comparison of two meta-analysis methods: Inverse-variance-weighted average and weighted sum of z-scores. *Genomics & informatics 14*(4), 173.

Lepson, J. and L. Freed (1997). Akepa (*Loxops coccineus*). In A. Pool and F. Gill (Eds.), *The Birds of North America*, Number 294, pp. 1–23. Philadelphia, PA, USA: The Academy of Natural Sciences.

Lepson, J. K. and L. A. Freed (1995). Variation in male plumage and behavior of the Hawaii Akepa. *The Auk 112*(2), 402–414.

Lindenmayer, D. B. and G. E. Likens (2010). The science and application of ecological monitoring. *Biological conservation 143*(6), 1317–1328.

Lindenmayer, D. B., G. E. Likens, A. Andersen, D. Bowman, C. M. Bull, E. Burns, C. R. Dickman, A. A. Hoffmann, D. A. Keith, M. J. Liddell, A. J. Lowe, D. J. Metcalfe, S. R. Phinn, J. Russell-Smoth, N. Thurgate, and G. M. Wardle (2012). Value of long-term ecological studies. *Austral Ecology 37*(7), 745–757.

Lindgren, F., H. Rue, and J. Lindström (2011). An explicit link between Gaussian fields and Gaussian Markov random fields: The stochastic partial differential equation approach. *Journal of the Royal Statistical Society: Series B (Statistical Methodology) 73*(4), 423–498.

Link, W. A. and J. R. Sauer (1998). Estimating population change from count data: Application to the North American Breeding Bird Survey. *Ecological Applications 8*(2), 258–268.

Loh, R. K. and J. T. Tunison (1999). Vegetation recovery following pig removal in Olaa-Koa Rainforest Unit, Hawai'i Volcanoes National Park. Technical Report 123, University of Hawai'i, Cooperative National Park Resources Studies Unit, Honolulu.

Margalida, A., J. Jiménez, J. M. Martínez, J. A. Sesé, D. García-Ferré, A. Llamas, M. Razin, M. Colomer, and B. Arroyo (2020). An assessment of population size and demographic drivers of the Bearded Vulture using integrated population models. *Ecological Monographs 90*(3), e01414.

Marques, F. and S. T. Buckland (2004). Covariate models for the detection function. In S. Buckland, D. Anderson, K. Burnham, J. Laake, D. Borchers, and L. Thomas (Eds.), *Advanced Distance Sampling*, Chapter 3, pp. 31–47. Oxford, UK: Oxford University Press.

Marques, T. A., L. Thomas, M. Kéry, S. T. Buckland, D. L. Borchers, E. Rexstad, R. M. Fewster, D. I. MacKenzie, J. A. Royle, G. Guillera-Arroita, C. M. Handel, D. C. Pavlacky, and R. J. Camp (2017). Model-based approaches to deal with detectability: A comment on Hutto (2016). *Ecological Applications 27*(5), 1694–1698.

Marques, T. A. L. O. (2007). *Incorporating measurement error and density gradients in distance sampling surveys*. Ph. D. thesis, University of St Andrews.

Marra, G., D. L. Miller, and L. Zanin (2012). Modelling the spatiotemporal distribution of the incidence of resident foreign population. *Statistica Neerlandica 66*(2), 133–160.

Marra, G. and S. N. Wood (2011). Practical variable selection for generalized additive models. *Computational Statistics & Data Analysis 55*(7), 2372–2387.

Maxfield, B. (1998). Hakalau Forest National Wildlife Refuge. *Endangered Species Bulletin 23*(6), 26–27.

Medeiros, M. C. and L. A. Freed (2009). A fledgling-mass threshold greatly affects juvenile survival in the Hawaii Akepa (*Loxops coccineus coccineus*). *The Auk 126*(2), 319–325.

Meyer, R. and R. B. Millar (1999). Bayesian stock assessment using a state–space implementation of the delay difference model. *Canadian Journal of Fisheries and Aquatic Sciences 56*(1), 37–52.

Miller, D. L. (2017). *Distance sampling detection function and abundance estimation*. University of St Andrews. R package version 0.9.7.

Miller, D. L., M. L. Burt, E. A. Rexstad, and L. Thomas (2013). Spatial models for distance sampling data: Recent developments and future directions. *Methods in Ecology and Evolution 4*(11), 1001–1010.

Miller, D. L., E. Rexstad, L. Burt, M. V. Bravington, and S. Hedley (2018). *dsm: Density Surface Modelling of Distance Sampling Data*. University of St Andrews. R package version 2.2.16.

Miller, D. L., E. Rexstad, L. Thomas, L. Marshall, and J. Laake (2019). Distance Sampling in R. *Journal of Statistical Software, Articles 89*(1), 1–28.

Millon, A., X. Lambin, S. Devillard, and M. Schaub (2019). Quantifying the contribution of immigration to population dynamics: A review of methods, evidence and perspectives in birds and mammals. *Biological Reviews 94*(6), 2049–2067.

Møller, A. P., W. Fiedler, and P. Berthold (2010). *Effects of Climate Change on Birds*. Oxford, UK: Oxford University Press.

Munro, G. C. (1944). *Birds of Hawaii*. Ruthland, VT, USA: Tuttle.

Nadeem, K., J. E. Moore, Y. Zhang, and H. Chipman (2016). Integrating population dynamics models and distance sampling data: A spatial hierarchical state-space approach. *Ecology 97*(7), 1735–1745.

Newman, K., S. Buckland, B. Morgan, R. King, D. Borchers, D. Cole, P. Besbeas, O. Gimenez, and L. Thomas (2014). *Modelling Population Dynamics*. New York, NY, USA: Springer.

Newton, I. (1998). *Population Limitation in Birds*. New York, NY, USA: Academic press.

Niemi, A. and C. Fernández (2010). Bayesian spatial point process modeling of line transect data. *Journal of Agricultural, Biological, and Environmental Statistics 15*(3), 327–345.

Norvell, R. E., F. P. Howe, and J. R. Parrish (2003). A seven-year comparison of relative-abundance and distance-sampling methods. *The Auk 120*(4), 1013–1028.

Ostertag, R., S. Cordell, T. Giambelluca, C. Giardina, C. Litton, M. Nullet, and L. Sack (2015). Climatological data summaries: Hakalau Unit of the Hakalau Forest National

Wildlife Refuge Complex. Retrieved from Hawaii Permanent Plot Network on July 24, 2020.

Paxton, E. H., R. J. Camp, P. M. Gorresen, L. H. Crampton, D. L. Leonard, and E. A. VanderWerf (2016). Collapsing avian community on a Hawaiian island. *Science Advances 2*(9), e1600029.

Paxton, E. H., M. Laut, J. P. Vetter, and S. J. Kendall (2018). Research and management priorities for Hawaiian forest birds. *The Condor 120*(3), 557–565.

Paxton, E. H., S. G. Yelenik, T. E. Borneman, E. T. Rose, R. J. Camp, and S. J. Kendall (2018). Rapid colonization of a Hawaiian restoration forest by a diverse avian community. *Restoration Ecology 26*(1), 165–173.

Pebesma, E., R. Bivand, B. Rowlingson, V. Gomez-Rubio, R. Hijmans, M. Sumner, D. MacQueen, J. Lemon, J. O'Brien, and J. O'Rourke (2018). *Classes and Methods for Spatial Data*. Universität Münster. R package version 1.3-1.

Peel, D., M. Bravington, N. Kelly, S. N. Wood, and I. Knuckey (2013). A model-based approach to designing a fishery-independent survey. *Journal of Agricultural, Biological, and Environmental Statistics 18*(1), 1–21.

Perkins, R. C. L. (1903). Vertebrata. In D. Sharp (Ed.), *Fauna Hawaiiensis*, pp. 365–466. Cambridge, UK: Cambridge University Press.

Plard, F., R. Fay, M. Kéry, A. Cohas, and M. Schaub (2019). Integrated population models: Powerful methods to embed individual processes in population dynamics models. *Ecology 100*(6), e02715.

Plard, F., D. Turek, M. U. Grüebler, and M. Schaub (2019). Ipm 2: Toward better understanding and forecasting of population dynamics. *Ecological Monographs 89*(3), e01364.

Plummer, M. (2017). *JAGS Version 4.3.0 User Manual*. Lyon, France: International Agency for Research on Cancer.

Plummer, M. (2018). rjags: Bayesian Graphical Models using MCMC. https://CRAN.R-project.org/package=rjags. R package version 4-8.

Pratt, H. D. (1994). Avifaunal change in the Hawaiian Islands, 1893–1993. *Studies in Avian Biology 15*, 103–118.

Pratt, T. K. (2009). Origins and evolution. In T. K. Pratt, C. T. Atkinson, P. C. Banko, J. D. Jacobi, and B. L. Woodworth (Eds.), *Conservation Biology of Hawaiian Forest Birds: Implications for Island Avifauna*, Chapter 1, pp. 3–24. New Haven, CT, USA: Yale University Press.

R Core Team (2017). *R: a Language and Environment for Statistical Computing. Version 3.4.1*. Vienna, Austria: R Foundation for Statistical Computing.

Ralph, C. J. and S. G. Fancy (1994). Demography and movements of the endangered Akepa and Hawaii Creeper. *The Wilson Bulletin 106*(4), 615–628.

Ramsay, T. (2002). Spline smoothing over difficult regions. *Journal of the Royal Statistical Society: Series B (Statistical Methodology) 64*(2), 307–319.

Reding, D. M., L. A. Freed, R. L. Cann, and R. C. Fleischer (2010). Spatial and temporal patterns of genetic diversity in an endangered Hawaiian honeycreeper, the Hawaii Akepa (*Loxops coccineus coccineus*). *Conservation Genetics 11*(1), 225–240.

Riecke, T. V., P. J. Williams, T. L. Behnke, D. Gibson, A. G. Leach, B. S. Sedinger, P. A. Street, and J. S. Sedinger (2019). Integrated population models: Model assumptions and inference. *Methods in Ecology and Evolution 10*(7), 1072–1082.

Roff, D. A. (2002). *Life History Evolution*. Sunderland, MA, USA: Sinauer Associates.

Ross, B. E., D. A. Haukos, C. A. Hagen, and J. Pitman (2018). Combining multiple sources of data to inform conservation of lesser prairie-chicken populations. *The Auk: Ornithological Advances 135*(2), 228–239.

Roy, C., N. Michel, C. Handel, S. Van Wilgenburg, J. Burkhalter, K. Gurney, D. Messmer, K. Princé, C. Rushing, J. Saracco, et al. (2019). Monitoring boreal avian populations: How can we estimate trends and trajectories from noisy data? *Avian Conservation and Ecology 14*(2), 8.

Rozek, J. C., R. J. Camp, and J. M. Reed (2017). No evidence of critical slowing down in two endangered Hawaiian honeycreepers. *PloS One 12*(11), e0187518.

Rue, H., A. Riebler, S. H. Sørbye, J. B. Illian, D. P. Simpson, and F. K. Lindgren (2017). Bayesian computing with INLA: A review. *Annual Review of Statistics and Its Application 4*, 395–421.

Rushing, C. S., J. A. Hostetler, T. S. Sillett, P. P. Marra, J. A. Rotenberg, and T. B. Ryder (2017). Spatial and temporal drivers of avian population dynamics across the annual cycle. *Ecology 98*(11), 2837–2850.

Rushing, C. S., T. B. Ryder, A. L. Scarpignato, J. F. Saracco, and P. P. Marra (2016). Using demographic attributes from long-term monitoring data to delineate natural population structure. *Journal of Applied Ecology 53*(2), 491–500.

Ryan, E. G., C. C. Drovandi, J. M. McGree, and A. N. Pettitt (2016). A review of modern computational algorithms for Bayesian optimal design. *International Statistical Review 84*(1), 128–154.

Sæther, B.-E. and Ø. Bakke (2000). Avian life history variation and contribution of demographic traits to the population growth rate. *Ecology 81*(3), 642–653.

Saracco, J. F. and M. Rubenstein (2020). Integrating broad-scale data to assess demographic and climatic contributions to population change in a declining songbird. *Ecology and Evolution 10*(4), 1804–1816.

Saunders, S. P., M. T. Farr, A. D. Wright, C. A. Bahlai, J. W. Ribeiro Jr, S. Rossman, A. L. Sussman, T. W. Arnold, and E. F. Zipkin (2019). Disentangling data discrepancies with integrated population models. *Ecology 100*(6), e02714.

Schaub, M. and F. Abadi (2011). Integrated population models: A novel analysis framework for deeper insights into population dynamics. *Journal of Ornithology 152*(1), 227–237.

Schaub, M. and D. Fletcher (2015). Estimating immigration using a Bayesian integrated population model: Choice of parametrization and priors. *Environmental and Ecological Statistics 22*(3), 535–549.

Schmidt, J. H. and H. L. Robison (2020). Using distance sampling-based integrated population models to identify key demographic parameters. *The Journal of Wildlife Management 84*(2), 372–381.

Scott, J. M., S. Mountainspring, F. L. Ramsey, and C. B. Kepler (1986). Forest bird communities of the Hawaiian Islands: Their dynamics, ecology, and conservation. *Studies in Avian Biology, No. 9*, 1–431.

Scott-Hayward, L. A. S., M. L. Mackenzie, C. R. Donovan, C. Walker, and E. Ashe (2014). Complex region spatial smoother (CReSS). *Journal of Computational and Graphical Statistics 23*(2), 340–360.

Seber, G. A. F. (1973). *The Estimation of Animal Abundance and Related Parameters*. London, UK: Charles Griffin & Company Limited.

Shono, H. (2008). Application of the Tweedie distribution to zero-catch data in CPUE analysis. *Fisheries Research 93*(1-2), 154–162.

Sibly, R. M. and J. Hone (2002). Population growth rate and its determinants: An overview. *Philosophical Transactions of the Royal Society of London. Series B: Biological Sciences 357*(1425), 1153–1170.

Sigourney, D. B., S. Chavez-Rosales, P. Conn, L. Garrison, E. Josephson, and D. Palka (2018). Development of a species distribution model for fin whales (*Balaenoptera physalus*) within a Bayesian hierarchical framework: Implications for uncertainty. *PeerJ Preprints 6:e27424v1 https://doi.org/10.7287/peerj.preprints.27424v1*.

Steen, H. and D. Haydon (2000). Can population growth rates vary with the spatial scale at which they are measured? *Journal of Animal Ecology 69*(4), 659–671.

Stoyan, D. (1982). A remark on the line transect method. *Biometrical Journal 24*(2), 191–195.

Swallow, B. (2015). *Bayesian multi-species modelling of non-negative continuous ecological data with a discrete mass at zero*. Ph. D. thesis, University of St Andrews.

Thomas, L. (1996). Monitoring long-term population change: Why are there so many analysis methods? *Ecology 77*(1), 49–58.

Thomas, L., S. T. Buckland, K. B. Newman, and J. Harwood (2005). A unified framework for modelling wildlife population dynamics. *Australian & New Zealand Journal of Statistics 47*(1), 19–34.

Thomas, L., S. T. Buckland, E. A. Rexstad, J. L. Laake, S. Strindberg, S. L. Hedley, J. R. Bishop, T. A. Marques, and K. P. Burnham (2010). Distance software: Design and analysis of distance sampling surveys for estimating population size. *Journal of Applied Ecology 47*(1), 5–14.

Thomas, L., K. Burnham, and S. Buckland (2004). Temporal inferences from distance sampling surveys. In *Advanced Distance Sampling*, pp. 71–107. Oxford, UK: Oxford University Press.

Urquhart, N. S. and T. M. Kincaid (1999). Designs for detecting trend from repeated surveys of ecological resources. *Journal of Agricultural, Biological, and Environmental Statistics 4*(4), 404–414.

USFWS, U.S. Fish and Wildlife Service (1970). Notice of proposed rule making (conservation of endangered species and other fish and wildlife). *Federal Register 35*(50 CFR Part 17), 13519–13520.

USFWS, U.S. Fish and Wildlife Service (2006). *Revised Recovery Plan for Hawaiian Forest Birds.* Region 1, Portland, Oregon, USA: U.S. Fish and Wildlife Service.

USFWS, U.S. Fish and Wildlife Service (2010). *Hakalau Forest National Wildlife Refuge Comprehensive Conservation Plan.* U.S. Department of the Interior, Fish and Wildlife Service, Pacific Region.

USGS, U.S. Geological Survey (2013). LANDFIRE Existing Vegetation Type layer. Data retrieved September 25, 2014, from http://landfire.cr.usgs.gov/viewer.

USGS, U.S. Geological Survey (2014). National elevation dataset (NED): U.S. Geological Survey database. Data retrieved September 25, 2014 from http://nationalmap.gov/elevation.html.

van Dam-Bates, P., O. Gansell, and B. Robertson (2018). Using balanced acceptance sampling as a master sample for environmental surveys. *Methods in Ecology and Evolution 9*(7), 1718–1726.

Ver Hoef, J. M. (1996). Parametric empirical Bayes methods for ecological applications. *Ecological Applications 6*(4), 1047–1055.

Vitousek, P., G. P. Asner, O. A. Chadwick, and S. Hotchkiss (2009). Landscape-level variation in forest structure and biogeochemistry across a substrate age gradient in Hawaii. *Ecology 90*(11), 3074–3086.

Walls, S. C. (2018). Coping with constraints: Achieving effective conservation with limited resources. *Frontiers in Ecology and Evolution 6*, 24.

Wang, H. and M. G. Ranalli (2007). Low-rank smoothing splines on complicated domains. *Biometrics 63*(1), 209–217.

Williams, R., S. L. Hedley, T. A. Branch, M. V. Bravington, A. N. Zerbini, and K. P. Findlay (2011). Chilean blue whales as a case study to illustrate methods to estimate abundance and evaluate conservation status of rare species. *Conservation Biology 25*(3), 526–535.

Williamson, L. T., W. D. Walter, S. R. Klinger, and D. R. Diefenbach (2018). Incorporating detection probability to estimate pheasant density. *The Journal of Wildlife Management 82*(8), 1680–1688.

Wilmshurst, J. M., T. L. Hunt, C. P. Lipo, and A. J. Anderson (2011). High-precision radiocarbon dating shows recent and rapid initial human colonization of East Polynesia. *Proceedings of the National Academy of Sciences 108*(5), 1815–1820.

Wood, S. N. (2003). Thin plate regression splines. *Journal of the Royal Statistical Society: Series B (Statistical Methodology) 65*(1), 95–114.

Wood, S. N. (2006). *Generalized Additive Models: An Introduction with R*. Boca Raton, FL, USA: CRC Press.

Wood, S. N. (2011). Fast stable restricted maximum likelihood and marginal likelihood estimation of semiparametric generalized linear models. *Journal of the Royal Statistical Society: Series B (Statistical Methodology) 73*(1), 3–36.

Wood, S. N. (2016). mgcv: Mixed GAM computation vehicle with GCV/AIC/REML smoothness estimation, version 1.8-17. The Comprehensive R Archive Network (CRAN).

Wood, S. N. (2017). *Generalized Additive Models: An Introduction with R*. Boca Raton, FL, USA: CRC press.

Wood, S. N., M. V. Bravington, and S. L. Hedley (2008). Soap film smoothing. *Journal of the Royal Statistical Society: Series B (Statistical Methodology) 70*(5), 931–955.

Wood, S. N., F. Scheipl, and J. J. Faraway (2013). Straightforward intermediate rank tensor product smoothing in mixed models. *Statistics and Computing 23*(3), 341–360.

Woodworth, B. L., J. T. Nelson, E. J. Tweed, S. G. Fancy, M. P. Moore, E. B. Cohen, and M. S. Collins (2001). Breeding productivity and survival of the endangered Hawaii creeper in a wet forest refuge on Mauna Kea, Hawai'i. *Studies in Avian Biology 22*, 164–172.

Woodworth, B. L. and T. K. Pratt (2009). Life history and demography. In T. K. Pratt, C. T. Atkinson, P. C. Banko, J. D. Jacobi, and B. L. Woodworth (Eds.), *Conservation Biology of Hawaiian Forest Birds: Implications for Island Avifauna*, Chapter 8, pp. 194–229. New Haven, CT, USA: Yale University Press.

Yuan, Y., F. E. Bachl, F. Lindgren, D. L. Borchers, J. B. Illian, S. T. Buckland, H. Rue, and T. Gerrodette (2017). Point process models for spatio-temporal distance sampling data from a large-scale survey of blue whales. *The Annals of Applied Statistics 11*(4), 2270–2297.

Zipkin, E. F., B. D. Inouye, and S. R. Beissinger (2019). Innovations in data integration for modeling populations. *Ecology 100*(6), e02713.

Zuur, A. F. (2012). *A Beginner's Guide to Generalized Additive Models with R*. Newburgh, UK: Highland Statistics Ltd.